THE FLOW
OF
FLUIDISED SOLIDS

by

RICHARD R. PUGH

A thesis submitted in fulfillment of the requirements
for the degree of Doctor of Philosophy.

Department of Mechanical Engineering,
The University of Aston in Birmingham.

October 1974.

SUMMARY.

The design and construction of a large test rig comprising an open sloping channel along which fluidised particulate materials may flow is described. A large number of experiments have been performed in this rig, aimed at establishing the rheological properties of a bed of flowing sand under a wide range of conditions, the parameters varied being channel width and slope, bed depth and fluidising velocity. The results of these experiments were analysed in terms of a comparison between the fluidised bed and a power-law non-Newtonian fluid flowing under similar conditions. Over a large range of shear rates the power law model is adequate, and it shows the bed to be substantially Newtonian at high fluidising velocities. At lower fluidising velocities, the bed becomes increasingly pseudoplastic in nature. At low shear rates, however, the behaviour of the bed is much more difficult to describe; tentative explanations for the various phenomena evident in this region are advanced, these being in terms of the interaction of two mechanisms, styled "inviscid layer dissipation" and "bubble suppression and segregated layer dissipation", by the author. The existence of these mechanisms has been established both by experimental methods and visual observations. Correlations of friction factor and modified Reynolds number show that the fluidised bed follows the liquid laminar flow correlation up to Reynolds numbers in excess of 4000; again, tentative explanations are advanced for the absence of any transition between flow regimes. Despite the limitations of the theory used throughout, the study has established the best range of operating conditions for the flow of fluidised sand, and the test rig built as part of it should be useful for a further considerable range of experiments.

ACKNOWLEDGEMENTS

The author would like to acknowledge the help of, and express his thanks to, the following:

His supervisor, Professor D.E. Elliott, whose enthusiasm has sustained this work.

His research colleagues in the Department of Mechanical Engineering, for help and advice.

His former colleague, S.J. McGuigan, in co-operation with whom the design and construction of the test rig used in this work was undertaken.

The technicians of the Department of Mechanical Engineering, from whom the author has received every assistance.

The University of Aston in Birmingham, who supported the work, and the author, financially.

CONTENTS

FIGURES

CHAPTER 1

INTRODUCTION

1. Introduction

The technique of fluidisation is one which has been known for a considerable time. It offers a unique means whereby particulate solids of many types may be handled as though they were fluids. This property may be used in many ways: gas fluidised beds are noted for their uniformity of temperature, and for the high heat transfer rates attainable within them; such beds also offer an extremely effective means of promoting gas/particle contact; fluidised beds may also be used for transporting solids, in which application they offer several important advantages over the alternative methods.

1.1 Basic concept of fluidised bed

When a bed of particles is placed over some form of porous base and fluid made to flow upwards through the system, the particles will offer a certain resistance to the flow. As the velocity of the fluid is increased, so the drag increases, and the particles will become rearranged to offer less resistance. Expansion occurs, and eventually the drag force will balance the weight of the bed of particles. In this state, the bed is said to be incipiently fluidised, and it assumes many of the characteristics of a fluid; waves will travel through it, light objects will float and heavy ones sink, and it will flow readily under the influence of a hydrostatic head.

Particles may be fluidised using gas or liquid, the patterns of fluidisation being somewhat different above the minimum fluidising velocity - that velocity necessary to create the state described above. Liquid fluidised systems will usually continue to expand uniformly until the particles begin to be

carried out of the restraining vessel. In gas fluidised systems, further increase in gas velocity is usually accompanied by the formation of gas bubbles which contain little or no solids. Such a bed is essentially a two phase system, consisting of the bubble phase, and the dense phase. The transition to aggregative fluidisation (bubbling) is not always made at or near minimum fluidising velocity; in fine particle systems it may occur at gas velocities considerably in excess of this. Conversely, the use of very heavy particles in liquid fluidised systems can create areas which contain no solids. This work is concerned only with gas fluidised systems.

1.2 Existing and possible applications

Fluidisation has certain important advantages and disadvantages, some of which were mentioned earlier. However, for clarity, these may be listed as:

1.2.1 Advantages

1) Smooth flow of particles allows continuous automatically controlled operation.
2) Rapid solids mixing leads to near isothermal conditions.
3) Circulation between two beds allows transportation of heat produced or required by large reactors.
4) The process is suited to large scale operations.
5) Heat and mass transfer rates between gas and particles are high.
6) The heat transfer from the bed to an immersed surface is high.

1.2.2 Disadvantages

1) Mixing leads to non-uniform residence time of particles.

2) Erosion of vessels may be a problem.

3) The sintering of small particles may set an upper temperature limit to operation.

The advantages of fluidised beds are so pronounced that such systems have found very wide application. A comprehensive survey of past applications is given by KUNII and LEVENSPIEL[69]; some of these are listed below, together with others, both current and projected.

1.2.3 Historical background

The first major use of fluidisation was made by Winkler in 1922 who built a large scale plant for the gasification of coal. This seems to have been the only notable use for the technique until about 1940, when there was an upsurge of interest in the use of fluidisation in the large scale cracking of hydrocarbons. Two major processes emerged, the T.C.C. (Thermofor catalytic cracking) and F.C.C. (Fluid catalytic cracking) processes; the former using two moving beds joined by a bucket elevator (later an airlift), the latter being an entirely pneumatic system of fluidised beds and pneumatic transport lines. The first commercial F.C.C. plant was built in 1942. Two further uses are worthy of note, the use of fluidised beds for the roasting of ore, first done in 1947, and their use in drying and calcination of limestone in 1948.

1.2.4 Current applications

The current field of application of fluidisation techniques is extremely wide. Flowing fluidised bed coolers are used for sugar and powdered milk, and for freezing peas. "Static" fluidised beds are used for the mixing of powders, for drying and sizing of materials, and for the recovery of oil from shale. The heat transfer properties are made use of in the cooling of solids, and in many arrangements of fluidised bed combustion systems, for steam raising.

Fluidised beds have also been used in the plastic coating of small metal objects.

1.2.5 Projected applications

Fluidised bed combustion systems offer certain advantages over conventional ones, and it is possible to foresee their wide application both commercially and domestically. Another possible use is in the recovery of waste heat from many types of plant, including diesel engines. An extremely interesting possibility is the use of solids as a heat transport and storage system. A fluidised bed boiler could heat solids, which could then be conveyed to a steam raising unit which could be part of a steam turbine. It is also envisaged that hot solids could be stored, and used for the immediate generation of power to satisfy peak demands.

1.2.6 Transport

For a number of the applications cited above, the transportation of solids is an essential. Fluidised transport is also interesting in its own right, offering useful advantages over the mechanical or lean-phase

pneumatic alternatives:

1) The air power requirement is quite low, certainly much lower than in the equivalent pneumatic system.
2) Much less erosion of plant due to the lower particle velocities involved.
3) No risk of explosion due to static electricity build-up such as that experienced in pneumatic conveying.
4) No costly tubing to convey the material.
5) Can operate at higher temperatures than mechanical systems.
6) Potentially more reliable than mechanical systems.

1.3 Observations

Although there is considerable, and growing interest in flow properties of fluidised solids, the subject is still in its infancy. The complexity of the interactions and the number of parameters involved make any theoretical study difficult, and of very limited practical use. Empirical approaches, however, although requiring the collection of much experimental data, do provide useful insights into the complex flow characteristics. Many approaches have been used (Chapter 2), their diversity perhaps reflecting the complexity of the problem. This work has been viewed as a basic, first-stage study of flow in an open channel (this being selected both because it is a simple system, and because of its possible practical uses) and some attempt has been made to describe the bed behaviour.

CHAPTER 2

SURVEY OF PUBLISHED LITERATURE

2. Survey of published literature

This survey of published literature is divided into three sections. The first presents some general notes on the properties of fluidised beds, and goes on to deal with the important parameters and characteristics of such systems, especially where these are important to flow behaviour. The second section covers work on flow behaviour; the models used by other workers to characterise fluidised beds are reviewed, with special emphasis on flowing bed studies.

Finally, a short section deals with recent applications of flow systems, and those applications which may become practical within the foreseeable future.

2.1 Behaviour of gas fluidised beds

The overall concept of a fluidised bed has already been discussed in Chapter 1. Once the bed is fluidised, the lower limit to this state being the point of incipient fluidisation mentioned earlier, its state is usually stable over a range of fluidising velocities, this range depending on the particle and fluidising gas properties. The upper limit to normal fluidisation is set by the tendency of the smallest particles in the bed to be entrained, that is, blown out of the bed by the fluidising gas.

The behaviour of normal gas fluidised beds (non-flowing systems) has been the subject of many practical and theoretical studies over a considerable period of time. However, many of these studies have been concerned with deep beds, these being of most interest to the chemical engineers who have traditionally been the main exponents of fluidised bed technology. The use of shallow beds offers many advantages for certain combustion and heat transfer processes, notably the minimising of bed pressure drop, and hence the power required to fluidise the bed. Bubble growth is also reduced in shallow beds, which can be advantageous in heat transfer applications. Thus increasing interest has been shown in shallow beds in recent years, but one must be extremely careful in using concepts developed for deep beds to describe much shallower ones; the problem of scale-up in fluidised beds is by no means fully understood.

This section will present notes on the important parameters of shallow fluidised beds, and discuss the approaches used to evaluate or describe them. It is convenient to discuss these in a series of short sub-sections.

2.1.1 Minimum fluidising velocity

The concept of the point of incipient fluidisation, at which the gas is said to have the velocity of minimum fluidisation, has already been mentioned. This minimum fluidising velocity is perhaps the most fundamental parameter, and yet it is a measure of the complexity of fluidised systems that even this is difficult to estimate, and has been the subject of many attempts at accurate evaluation.

Fluidising velocities are defined as superficial gas velocities in the empty bed, that is, as the fluid flow rate divided by the cross sectional area of the bed, and it is usual to define minimum fluidising velocity as that velocity at which the pressure drop across the bed of particles is equal to the weight of the bed per unit area of the distributor. However, although the transition from fixed to fluidised state has been described as taking place at a "point" of incipient fluidisation, this does not happen in practice; the transition takes place over a range of gas velocities, and the pressure drop may not become equal to the bed weight until well after minimum fluidising velocity has been passed, if at all. This subject of incipient fluidisation is exhaustively discussed by RICHARDSON[109].

The published literature provides many expressions for the evaluation of minimum fluidising velocity, most relying on equating bed pressure drop to the weight of the particles. This takes the form

$$\Delta P_B = (\rho s - \rho g)(1 - \epsilon_{mf}) g_c h_{mf} \qquad (2.1)$$

For fine particles, the CARMEN-KOZENY[28] equation applies:

$$U_{mf} = \frac{\epsilon_{mf}^3}{5(1-\epsilon_{mf})^2} \quad \frac{\Delta P_B}{S^2 \mu_g h_{mf}} \qquad (2.2)$$

For larger particles, the equation of ERGUN[45] is used:

$$\frac{\Delta P_B}{h_{mf}} = 150\frac{(1-\epsilon_{mf})^2}{\epsilon_{mf}^3}\frac{\mu_g U_{mf}}{(\phi_s d_p)^2} + 1.75\frac{(1-\epsilon_{mf})\rho_g U_{mf}^2}{\epsilon_{mf}^3 \phi_s d_p} \qquad (2.3)$$

By substituting (2.1) into (2.2) and (2.3) expressions for minimum fluidising velocity are obtained. However, these presuppose the knowledge of bed voidage and particle sphericity, properties which are themselves not easily evaluated. This difficulty is obviated by the use of the expression of WEN and YU[142]:

$$(Re)_{mf} = \left[(33.7)^2 + 0.0408\ Ga\right]^{\frac{1}{2}} - 33.7 \qquad (2.4)$$

where $Re = \frac{d_p \rho_g U_f}{\mu_g}$ and $Ga = d_p^3 \rho_g (\rho_s - \rho_g) g_c / \mu_g^2$

It is also possible to simplify equation (2.3) considerably, to obviate knowing the bed voidage. The first term represents viscous losses, and the second kinetic energy losses. According to KUNII and LEVENSPIEL[69], at values of Reynolds number less than 20, viscous losses may be considered dominant, and (2.3) reduces to:

$$U_{mf} = \frac{(\phi_s d_p)^2}{150}\frac{(\rho_s - \rho_g) g_c}{\mu_g}\left[\frac{\epsilon_{mf}^3}{1-\epsilon_{mf}}\right] \qquad (2.5)$$

At values of Reynolds number greater than 1000, kinetic energy dominates, and (2.3) becomes

$$U_{mf}^2 = \frac{\phi_s d_p}{1.75} \frac{(\rho_s - \rho_g)}{\rho_g} g_c \in_{mf}^3 \qquad (2.6)$$

WEN and YU found for a wide variety of conditions that:

$$\frac{1}{\phi_s \in_{mf}^3} \simeq 14 \text{ and } \frac{1 - \in_{mf}}{\phi_s^2 \in_{mf}^3} \simeq 11$$

These findings are incorporated intheir general expression equation (2.4) but two simpler equations can be obtained by inserting them into (2.5) and (2.6)

For fine particles $U_{mf} = \frac{d_p^2(\rho_s - \rho_g)g_c}{1650 \mu_g}$ $Re < 20$ (2.7)

For large particles $U_{mf}^2 = \frac{d_p(\rho_s - \rho_g)g_c}{24.5 \mu_g}$ $Re > 1000$ (2.8)

In the case of the above equations $Re = \frac{d_p \rho_g U f}{\mu_g}$

Other expression similar to (2.7) have been proposed. ROWE'S [113] uses 1240 instead of 1650, and RICHARDSON[109] suggests 1695. It is unfortunate that all these expressions are of limited accuracy. KUNII and LEVENSPIEL state that the correlation of WEN and YU predicts U_{mf} with a standard deviation of $\pm$ 34% over 284 points taken from the literature. This may be compared with a correlation due to NARSIMHAN[93] which has a standard deviation of $\pm$ 46% over 267 points.
This lack of accuracy is regrettable, but perhaps not surprising considering the approximations made and the neglection of any interparticle cohesive forces which may exist in the packed bed. In view of the limited

accuracy of the correlations available it is extremely fortunate that minimum fluidising velocity may be easily obtained experimentally. It is merely necessary to plot the pressure drop across a bed of the material in question against fluidising velocity. This should be done whilst the fluidising velocity is reduced from a value well above the minimum. Such a plot has two distinct sections, with a gradual change in slope between them. Tangents drawn to these two sections intersect at the minimum fluidising velocity. Such a method is obviously open to some error, but this should be much less than the use of any correlation would provide.

A further simple method is proposed by MOTAMEDI and JAMESON[87], who introduced bubbles into a bed which was below minimum fluidisation, and said that

U_{mf} = least total velocity (fluidising air + bubbles) necessary to allow bubbles to pass through the bed to the surface.

This method gives results which are somewhat different to those obtained from the normal pressure drop technique, but there is no reason to suppose that they are any more accurate.

Some little time has been spent on the subject of minimum fluidising velocity, because the difficulty in obtaining any accurate expression for this essential and basically simple parameter emphasises the complexity of fluidised systems and the difficulty faced in dealing with them. Other aspects will be discussed in less detail.

2.1.2 Entrainment velocity

As already stated, the entrainment velocity of the smallest particles in the bed represents the upper limit of fluidising velocity. This is so only in open beds; sometimes much higher velocities are used in closed systems, and a cyclone separator employed to extract the small particles from the exhaust air. Commercial materials often contain a proportion of very fine particles, and it may not be realistic to operate at fluidising velocities below their entrainment velocity. In such cases, solids loss from the bed must be accepted, and means incorporated in the plant to recover this material.

The entrainment velocity is usually approximately equal to the terminal, or free-fall velocity of the particles. This can be expressed as:

$$U_t = \left[\frac{4 g_c d_p (\rho s - \rho g)}{3 \rho_g C_d} \right]^{\frac{1}{2}} \qquad (2.9)$$

where C_d is an experimentally determined drag coefficient. KUNII and LEVENSPIEL present a graph of $C_d Re_p^2$ against Re_p where

$$Re_p = \frac{d_p \rho_g U_t}{\mu_g} \qquad (2.10)$$

and

$$C_d Re_p^2 = \frac{4 g_c d_p^3 \rho_g (\rho_s - \rho_g)}{3 \mu_g^2} \qquad (2.11)$$

This chart includes both spherical and non-spherical particles, and enables U_t to be found from known values of d_p, ρ_g, ρ_s and μ_g.

An alternative is the use of an analytic expression for the drag coefficient C_d. No single expression will suffice, the useful range of Reynolds numbers being covered by:

$$C_d = \frac{24}{Re_p} \qquad \text{for } Re_p < 0.4 \qquad (2.12)$$

$$C_d = \frac{10}{Re_p^{\frac{1}{2}}} \qquad \text{for } 0.4 < Re_p < 500 \qquad (2.13)$$

$$C_d = 0.43 \qquad \text{for } 500 < Re_p < 200{,}000 \qquad (2.14)$$

Inserting these values into equation (2.9) gives

$$U_t = \frac{g_c(\rho_s - \rho_g)d_p^2}{18\mu_g} \qquad \text{for } Re_p < 0.4 \qquad (2.15)$$

$$U_t = \left[\frac{4}{225}\,\frac{(\rho_s - \rho_g)^2 g_c^2}{\rho_g \mu_g}\right]^{\frac{1}{3}} d_p \qquad \text{for } 0.4 < Re_p < 500 \qquad (2.16)$$

$$U_t = \left[\frac{3.1 g_c(\rho_s - \rho_g)d_p}{\rho_g}\right]^{\frac{1}{2}} \qquad \text{for } 500 < Re_p < 200{,}000 \qquad (2.17)$$

Equations (2.12) to (2.17) apply only to spherical particles.

Terminal velocity can also be expressed in terms of Galileo Number, Stokes' law applying for low Reynolds number, the Schiller-Naumann equation for intermediate values, and Newton's law for high values.

$$Ga = 18\,Re_p \qquad \text{for } Ga < 3.6 \qquad (2.18)$$

$$Ga = 18\,Re_p + 2.7\,Re_p^{1.687} \qquad \text{for } 3.6 < Ga < 10^5 \qquad (2.19)$$

$$Ga = \frac{1}{3}\,Re_p^2 \qquad \text{for } Ga > 10^5 \qquad (2.20)$$

The range of feasible operation is described by the ratio of entrainment velocity to minimum fluidising

velocity. PINCHBECK and POPPER[105] derived an equation to estimate this ratio, and compared the equation with experimental data. A plot of the ratio against $C_d Re_p^2$ is given by KUNII and LEVENSPIEL, and one of the ratio against Galileo number is given by RICHARDSON. However, the two limits to this ratio are easily obtained.

For small particles $Re_p < 0.4$

$$\frac{U_t}{U_{mf}} = \frac{U_t \text{ by } 2.15}{U_{mf} \text{ by } 2.7} = 91.6 \qquad (2.21)$$

For large particles $Re_p > 1000$

$$\frac{U_t}{U_{mf}} = \frac{U_t \text{ by } 2.17}{U_{mf} \text{ by } 2.8} = 8.72 \qquad (2.22)$$

The practical range of operation is thus between 10:1 and 90:1, but often this range is considerably narrowed by bubbling and slugging of the bed.

2.1.3 Bubbling and slugging

Broadly speaking, liquid-solid systems exhibit smooth or particulate fluidisation, and gas-solid systems exhibit bubbling or aggregative fluidisation. This is ussually said to be due to the large density difference between the two fluids but this may be much reduced in a high pressure gas-solid system.

WILHELM and KWAUK[145] found that the Froude number distinguished between the two states.

$$Fr_{mf} < 0.13 \quad \text{smooth} \qquad (2.23)$$

$$Fr_{mf} > 1.3 \quad \text{bubbling}$$

where $$Fr_{mf} = \frac{U_{mf}^2}{d_p g_c}$$

ROMERO and JOHANSON[112] use four dimensionless groups to characterise the quality of fluidisation. These are:

$$Fr_{mf};\ Re_{p,mf};\ \frac{\rho_s - \rho_g}{\rho_g};\ \frac{h_{mf}}{d_t}$$

Note: $$Re_{p,mf} = \frac{d_p \rho_g U_{mf}}{\mu_g}$$

and their findings may be summarised as:

$$(Fr_{mf})(Re_{p,mf})\left(\frac{\rho_s - \rho_g}{\rho_g}\right)\left(\frac{h_{mf}}{d_t}\right) \begin{cases} < 100 & \text{smooth} \\ > 100 & \text{bubbling} \end{cases} \qquad (2.24)$$

Other examples of approaches to this problem are those of SIMPSON and RODGER[125] who evolved theory based on various dimensionless groups, considering the bed as a bundle of capillary tubes, and various workers[63, 88, 104] attempts at mathematical approaches based on the stability

or growth of disturbances in the bed. Other workers in this field include HARRISON et al[59] and VERLOOP and HEERTJES[137].

It is true to say that whilst these criteria will distinguish between gas and liquid fluidisation, they will not predict with any accuracy whether or not a gas fluidised bed will bubble.

Probably the simplest approach in this field is an attempt by GELDART[50] to classify powders into groups. These are:

Group A

Small particles and/or density less than $1.4 \times 10^3 kg/m^3$ which expand homogeneously before bubbling starts.

Group B

Materials having

$40 \mu_m < d_p < 500 \mu_m$, and $1.4 \times 10^3 kg/m^3 < \rho_s < 4 \times 10^3 kg/m^3$ which bubble at or near U_{mf}.

Group C

Powders having cohesive properties.

Group D

Very large and/or dense particles.

Groups A and B are the only ones which can be said to fluidise properly, and a criterion is given for minimum bubbling velocity which distinguishes between the two:

$U_{mb} = 100\, d_{sv}$ The constant 100 has units of s^{-1}

The work of GELDART, and other workers, has very recently been comprehensively reviewed by McGUIGAN[92] and thus little point is served by describing it fully here.

A reasonable overall model of the bubbling behaviour of fluidised beds is the so-called "2-phase theory" of DAVIDSON and HARRISON[34]. This states that the particulate phase of the bed is at the minimum fluidising condition, and that all excess gas passes through as bubbles. This theory is supported by experimental findings[117]. However, as stated by McGUIGAN, it is likely that in a heavily bubbling bed, some local areas of the particulate phase will have greater or lesser aeration due to the passage of bubbles, and that these areas will have a considerable effect upon the flow properties.

A phenomenon occurring in deep beds is that of slugging, where the bubbles grow until they equal the column diameter. These slugs rise through the bed, raining particles down around their periphery. ZENZ and OTHMER[148] observed slug flow in tubes up to 50 mm. diameter, and a review of the subject is given by HOVMAND and DAVIDSON[62], who point out that two types of slugging can occur, as show in Figure 2.1. Type B is that which occurs in tubes of up to 50 mm. diameter, being a breakdown of proper fluidisation. Type A can occur in much larger columns, and has in fact been observed by the author in columns of 150 mm. diameter. The phenomenon of slug flow is of little interest in shallow bed work, and will not be discussed further. However, it is likely to be of great importance in the study of vertical fluidised transport.

Figure 2.1

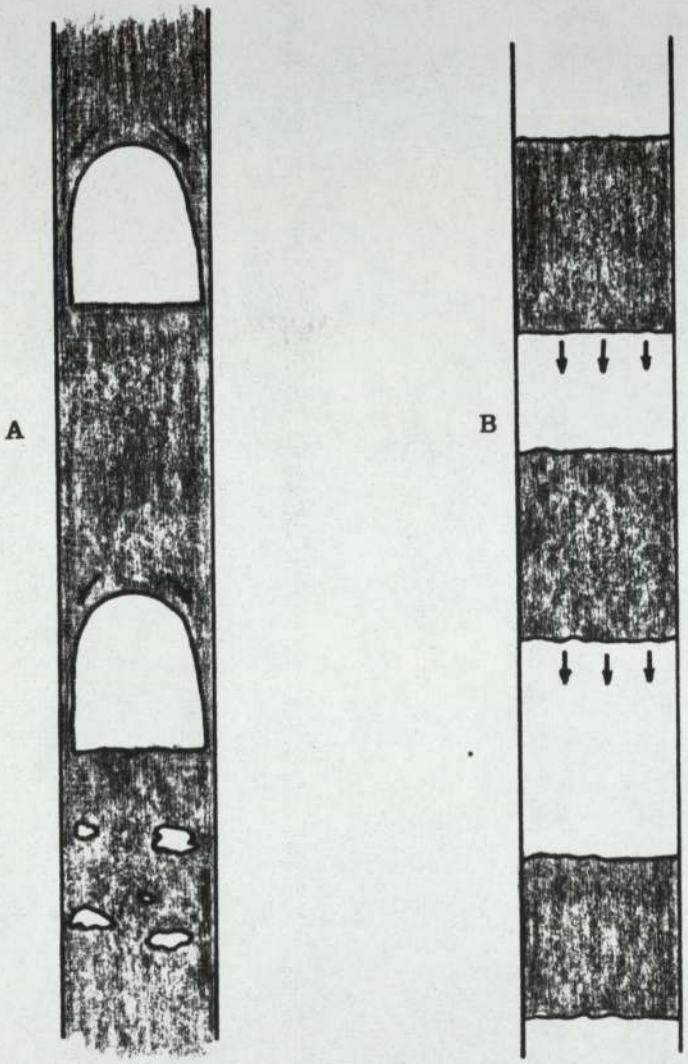

ALTERNATIVE SLUG FLOW REGIMES

The rise of single bubbles through a fluidised bed has been studied by many workers, notably DAVIDSON[32], JACKSON[63], and MURRAY[88]. DAVIDSON found that in fine particle systems gas flows upwards through the bubble, down the outside and in again at the base, causing solids to be carried upward in the wake. Several workers have obtained expressions for the rise velocity of a single bubble similar to that of DAVIES and TAYLOR[35] for the rise of a bubble in a inviscid liquid. That was:

$$U_b = 0.792\, g_c^{\frac{1}{2}} V_b^{\frac{1}{6}} = 0.711 (g_c d_b)^{\frac{1}{2}} \qquad (2.25)$$

Other workers have found different values of constant. This sort of expression may be expected to yield only approximate results, but in any case the single rising bubble is a situation so artificial that its study is of very limited value. The most useful aspects of bubble study are discussed in sections 2.2.1 and 2.2.4.1.

2.1.4 Effects of distributor and internal surfaces

It is usual to neglect the influence of the distributor plate when trying to predict bed behaviour, but in fact the characteristics of a bed may depend very much on the type of distributor used, particularly in shallow beds. The only types of distributor which it is practical to use in shallow beds are the porous and pierced plate types, the shallow bed providing insufficient depth to achieve the gas diffusion necessary for uniform fluidisation if the bubble cap, tuyere, or orifice type of distributor commonly used in deep beds were used. The characteristics required of a distributor plate are:

1) Uniform fluidisation

2) Minimum pressure drop consistent with this.

The allowable distributor pressure drop may be quite small in shallow beds; down to about 5% of the bed pressure drop.

Obviously, it is more difficult to obtain uniform fluidisation in large beds, and also in systems where solids are being added and extracted. A further difficulty is that where locally defluidised regions do occur, they will tend to grow due to the air flowing preferentially through the rest of the bed which will have alower pressure drop.

Although one might expect that distributor effects would be confined to an area quite close to the base, this may not be so. MORSE and BALLOW[86] measured the uniformity of fluidisation using capacitance probes and found distributor effects up to 16 inches from the base, although McGUIGAN and ELLIOTT[91] found little influence of the distributor more than 50 mm. above it.

Clearly, the specification of distributor type is a subject which the designer must study most carefully, especially in the case of large beds, where variations in porosity of supposedly uniform materials may add to his problems.

The effect of placing any internal surfaces in the bed will obviously depend on their size and shape, but they are virtually always deleterious to uniform fluidisation. The lower sections of an immersed object are scoured by bubbles, and thus lose effective contact with the dense phase, and the upper surfaces become covered with defluidised material. These two phenomena may have a

serious effect on, for example, the heat transfer obtained from a heat exchanger immersed in the bed. The reported effects of immersed objects are diverse. ROMERO and JOHANSON[112] report that baffles reduce bubbling, but the work of VOLK et al[139] and BOTTERILL[21] has shown that any internal surface causes dead pockets in the bed and promotes channelling. In the case of the latter, who was flowing solids horizontally past arrays of heat transfer tubes, this phenomenon prevented the expected increase in performance. Whilst the above is generally true, it may also be said that stirring will promote uniformity of fluidisation in some cases, especially that of very fine powders.

The effect of the containing walls of the bed is reported by BENENATI and BROSILOW[10] and YAGI and KUNII[146] to disappear about ten particle diameters or less from the wall, and thus it is doubtful that wall effects may be regarded as significant.

It is clear from the above discussion that the placing of any surface in a fluidised bed must be viewed with caution. It is probably true to say that the only way to determine the effect of such a move is experimentally.

2.1.5 Segregation

Segregation, that is the settling of large particles at the base of the bed to form a stagnant layer, may be a serious operational problem. WEN and YU[142] have reported that segregation was likely in a two component mixture if the ratio of their minimum fluidising velocities is greater than two. Some useful observations on the problem are made by BOLAND[14], and his assertion that the

presence of segregation can be detected from the curve of pressure drop against fluidising velocity is supported by McGUIGAN[92]. Segregation may be important in flowing bed situations, and it is discussed in this context in a later chapter.

2.1.6 Material properties

In the fluidised bed, where particles are in contact, their size distribution and shape will obviously have great importance. TRAWINSKI[133] suggests that fine material could act as a lubricant, and that the ideal two component mixture would be one in which large particles were covered by a mono-layer of fines. This concept seems rather unrealistic. ZENZ and OTHMER[148] suggest that the greatest fluidity is obtained using a normal size distribution of material in which

$$d_{p_{largest}} = 11 \times d_{p_{smallest}}$$

McGUIGAN and ELLIOTT[91] have shown that the minimum viscosity of a fluidised bed is unaffected by particle size distribution. They also point out how easy it is to fail to appreciate the way in which U_{mf} for the bed is changed as the size distribution changes. MATHESON et al[79] show that beds of spherical particles have a higher viscosity than irregular particles, and attribute this to the closer packing obtainable using spheres. The effect of using very fine particles is investigated by BAERNS[5] who used particles less than 50 μm in diameter and suggested a criterion to determine the quality of fluidisation likely using a particular material.

2.1.7 Electrostatic charging

Electrostatic charging in fluidised beds may alter their flow characteristics. Generally, its effect is to promote agglomeration and thus cause loss of uniformity of fluidisation, and the adherance of particles to the bed surfaces. Charging is caused by friction as two surfaces are brought into contact, and is thus a serious problem in pneumatic conveyors because of the high particle velocities involved. There have been instances of explosions in such systems caused by electrostatic charging. It is generally systems which are very dry which suffer this problem; the presence of even small amounts of moisture will allow the charges to dissipate. It is not thought that electrostatic charging was an important parameter in the present study, and thus it will not be discussed in detail. The published literature has several contributors[15, 16, 29, 65, 84] whose work will be most useful to those concerned with this problem. It is hoped that the foregoing section has brought out some of the important parameters which must be carefully considered by those embarking on the design of fluidised systems, and also emphasised the considerable difficulties experienced in obtaining reliable data on these parameters. It is a measure of the complexity of fluidised systems that the available data is often conflicting and confusing.

2.2 Flow behaviour of fluidised beds

Although fluidisation has been widely used by chemical engineers for many years, it is true to say that there is still little understanding of the mechanisms by which fluidised beds flow;

it may be that it is the fact that chemical engineers have been the main users of fluidised beds that has prevented this aspect being more fully investigated. Nevertheless, there have been many attempts to model the fluidised bed, some models being extremely complex, but none is really adequate. The fact that this is so is indicative of the complexity of the problem, and this is underlined by the diversity of the approaches used. These fall into several categories, and it is convenient to discuss them in this way.

2.2.1 Ideal fluid model

This approach may be summarised as the study of the motion of bubbles through the dense phase, treating this as an inviscid, incompressible fluid. The 2-phase theory of DAVIDSON and HARRISON[34] falls into this category as does other work by DAVIDSON[32]. JACKSON[63] looked at the motion of a fully developed bubble and found that the equations and boundary conditions were only satisfied if the bubble rise velocity conformed to the equation of DAVIES and TAYLOR[35]. Also worthy of note is the work of MURRAY[88] who obtained solutions describing the motion of the particulate and fluid phases in the presence of a fully developed bubble. The difficulty of all this work is that of allowing for wake and coalescence effects, and particle flow through the bubble. Bubbling in fluidised beds has been discussed also in section 2.1.3 and will not be dealt with further here.

2.2.2 Statistical model

The difficulty of any approach based on statistics is the essentially random motion of the fluidised bed which

must have a decisive influence on its properties. This approach has one consistent exponent in BUYEVICH[24-26], who has developed a theory describing the number of particles in a volume of a fluidised bed, this number being a random function of time. Although interesting, this technique seems to have little practical use.

2.2.3 Observations from a variety of approaches

In the search for a realistic model, many diverse approaches have been used. GABOR[48] studied particle trajectories and found that they were predicted only by a Bingham plastic model of the fluidised bed. MARTYUSHIN and KHARAKOZ[75] performed a theoretical analysis of the first stage of fluidisation, and also found that a Bingham plastic model fitted. GOLDSCHMIDT and LE GOFF[54] and GRAHAM and HARVEY[56] studied beds of conducting materials. The results of the latter workers show a maximum in bed resistance near U_{mf}, except very close to the distributor plate, where the resistance continues to rise with increasing fluidising velocity. They postulate current flow along contacting chains of particles, and say that if fluidisation were particulate, resistance would rise with velocity until the stage was reached where all particles were supported by gas and did not contact. This would point to the existence of particulate fluidisation only near the distributor. The authors attribute the fall in resistance beyond U_{mf} to bubbles extracting air locally from the dense phase, increasing its density and decreasing its resistance. This could also explain the dependance found of resistance on electrode position. The results

of GOLDSCHMIDT and LE GOFF show a steady increase of resistance with fluidising velocity throughout their range of experiments, and thus it would seem that their fluidisation was particulate.

SAXTON et al[119] performed a statistical thermodynamic analysis to obtain values of bed viscosity and compared these with values obtained from viscometers by FURUKAWA and OHMAE[47] and SCHUGERL et al[122], finding them to be consistently low by a factor of two.

From the above, it can be seen that the means used to shed light on the flow mechanisms of fluidised beds are extremely diverse; it is true to say that this is one of the fascinations of fluidisation. The largest amount of work in this field may be broadly grouped under the description of "liquid analogy of fluidised beds", but this covers such a range of theoretical and experimental work that it must be discussed in sub-sections.

2.2.4 Liquid analogy of fluidised beds

Because of the superficial similarity between fluidised systems and liquids, there have been many attempts to pursue this analogy, and evaluate the flow properties of fluidised beds by treating them broadly as liquids. GELPERIN and EINSTEIN[39] discuss this exhaustively, comparing the fall of viscosity with increase in temperature in liquids with the fall of fluidised bed viscosity with increase in U_f. However, they state that this fall is exponential, whereas the variation in fluidised bed viscosity with fluidising velocity is usually much more complex. Fluidised bed flow through orifices has been well studied[23, 76, 77] and some work

has been done on flow across weirs and through open channels[20, 22, 108].

The pursuit of the liquid analogy can be in two main ways:

1) Study of bubble behaviour

2) Study of bed behaviour when sheared, which may be done in 2 ways, by small scale viscometer, or by using a flowing bed.

2.2.4.1 Study of bubble behaviour

There is much evidence which compares data obtained from bubbles rising through fluidised beds with the same situation in liquids with considerable success. BLOORE and BOTTERILL[12] injected bubbles into a fluidised bed and compared their results with those of Calderbank for air bubbles in water successfully. It has already been shown that bubble rise velocities in fluidised beds are often predicted quite well by the Davies-Taylor equation (eqn. 2.25); HARRISON and LEUNG[61] found the constant to be 0.71 for a single spherical capped bubble rising in a fluidised bed. BAUMGARTEN and PIGFORD[7] have also studied bubble rise, confirming that bubble air flow agrees with the 2-phase theory, and stating that the flow corresponds to that in a liquid having a viscosity of between 1 and 10 NS/m^2 (10 - 100 poise). Further evidence of the shape of bubbles in fluidised beds is provided by ROWE and PARTRIDGE[115] who used x-ray cine photography to study bubbles

and found them to be spherical capped. Their data was used by GRACE[55] to develop a correlation for change in bubble shape as a function of viscosity. He found that spherical capped bubbles became more rounded in liquids of higher viscosity and compared his results for viscosity with those of STEWART[129] who also studied bubbling, and SCHUGERL et al[122] who used a rotating element viscometer. The results of all three are of similar magnitude, but the similarity extends no further, Stewart's work showing an effect of particle size where Grace's shows none, for example. The difficulty of the Grace approach lies in the necessityto measure bubble included angle from photographs, a measurement not easily taken with accuracy. MURRAY[88] has calculated viscosity by estimating the viscous drag on a rising bubble and found it to be a function of bubble size; clearly this approach is of limited use.

A slightly different direction was taken by ORMISTON[99] who estimated viscosities by looking at the rising velocity of slugs; his values ranged between 1.2 and 4.5 $Ns(m^2$ (12 to 45 poise). Two further methods are worthy of note. The first is the attempts of some workers to extend the analysis of Albert Einstein for the viscosity of an infinitely dilute suspension to finite concentrations; an attempt which must be said to have met with little success. The second

method is attempts by MERSMANN[81] and WEISLEHNER[141] to use heat transfer measurements as an indication of flow properties; once again an approach which is of severely limited practical use.

2.2.4.2 Shearing - viscometer studies

Several types of viscometer have been used by workers in fluidisation. The falling sphere method was used by PETERS and SCHMIDT[103], and TRAWINSKI[133], but the accuracy of this is extremely suspect due to the influence of the walls, and the tendency of the ball to be displaced by rising bubbles; certainly this method is not quantitatively accurate for a bubbling fluidised bed, and even its qualitative predictions must be viewed most carefully. HAGYARD and SACERDOTE[58] used a torsion pendulum viscometer; such an instrument is not suitable for use with non-Newtonian fluids, and their results showed considerable scatter; it is doubtful that the trends predicted can be relied upon.

All other viscometers than those mentioned above rely on a rotor of some kind. The first work on this type of viscometer was done by MATHESON et al[79] using a Stormer (falling weight) type with a paddle type rotor. However, the bed used was only 1 inch in diameter, and thus the situation within it cannot be the same as that in a much larger bed. Nevertheless, the

results obtained, although only qualitative, have been confirmed by subsequent workers. Amongst other things, the authors found that the "viscosity" of a wide particle size range was less than that of a narrow cut, and that the addition of a small proportion of fines to a bed could significantly reduce its "viscosity". TRAWINSKI developed his fine particle monolayer theory to explain this, but more recently GELDART has shown it to be due to changes in the surface mean size of the sample not considered by Matheson. Geldart has corrected the results on this basis and shown that they become consistent.

A similar Stormer apparatus, but with a "dumb-bell" type of rotor was used by KRAMERS[66], but the fact that the rotor was run at constant speed means that the true shear rate was probably not constant under non-Newtonian conditions. DIEKMAN and FORSYTHE[37] used a Brookfield viscometer without calibration; thus their results are only qualitative, but similar to those of other workers. However, it is reported by McGUIGAN[92] that the use of a Brookfield viscometer is rendered inaccurate by the disturbance of the rotor caused by bubbling: this criticism must also apply to the similar work of LIU and ORR[74] who calibrated their instrument with liquids and LEEDEN and

BOUWHUIS[70] whose findings are so much at variance with those of all other workers that they must be largely discounted.

A well known study is that of FURUKAWA and OHMAE[47] who used a Stormer viscometer, calibrating with liquids. This calibration seems to have little justification, and their results must be considered merely qualitative. One point worthy of note is that they found the shear curves to be shear thickening, in contrast to the findings of most other workers.

SHUSTER and HAAS[126] also used a Stormer viscometer and paddle type rotor. They found substantially Newtonian behaviour over the range of experiments performed and claimed very good reproducibility - a surprising claim in the light of the recent experience of others[92].

The conclusions emerging from the body of literature on viscometer studies will be discussed later, and a more comprehensive review of the subject is presented by McGUIGAN.

2.2.4.3 Shearing - flowing bed studies

Flowing fluidised beds have been studied little in comparison with static beds, due to the complexity of the problem and the comparatively sophisticated equipment usually needed. However, considerable work has been done by MASSIMILLA[76] on fluidised bed efflux from orifices, and some by TREES[134] on flow through pipes betweenfluidised beds; this type of work

obviously is of limited application. Work which is somewhat analogous to the latter was performed by ELLIOTT and GLIDDON[43] on hydraulic transport of coal, but it is unlikely that many of their findings could be useful to workers on fluidised beds.

Lean-phase pneumatic transport is widely used industrially, and has been the subject of considerable study. This work is reviewed by KUNII and LEVENSPIEL[69]. As in fluidisation, measurement techniques are often a problem: many of these are reviewed by BOOTHROYD and GOLDBERG[17].

Vertical fluidised bed transport is used to some extent industrially, but is little understood, and has been the subject of no major studies. The problem was looked at superficially by the author using two similar rigs (see figs. 3.3 and 3.4) and the principle of differential aeration, that is, using more air in the upgoing leg than in the downcoming, thus promoting circulation. It has been reported[41] that similar systems have worked extremely well using other materials, but in the sand systems used by the author, rise of solids in the upgoing leg was by means of heavy slugging which proved impossible to remove, whilst retaining a reasonable circulation rate. It is also likely that segregation would be a problem in any

system involving vertical transport. Clearly, this subject must be studied much more deeply before it is at all well understood.

The remaining aspect of fluidised bed flow is the open channel, the first published work on which is due to SIEMES and HELLMER[124]. Their equipment was a channel 2m. long and 150 mm. wide, which was variable in inclination between 1^{o} and 6^{o}. Solids feed was from a hopper, at a maximum rate of 4.0 kg/s., the rate being determined by timed weighing of the channel efflux. The material used was sand of mean particle size 210 μm and minimum fluidising velocity 0.02m/s. Fluidising air was supplied by a blower, and maintained at a very high relative humidity (80-90%). It was fed to a porous distributor.

It was assumed that the flow was laminar and Newtonian under all conditions, although this latter seems dubious, and two approaches used to evaluate the results. These were, firstly that the flow was analogous to liquid channel flow, and thatthe shear stress was the same on all "wetted" surfaces, and secondly that shear stress occurred only at the bed walls, and was absent at the distributor. Values of viscosity were calculated by the two approaches, and it was inferred that there was slip at the base. However, the calculation assumed that viscosity was independent of bed depth, an assumption

now known to be invalid. Thus whilst the results seem to show that slip is occurring, the magnitudes cannot be relied upon. The data showed that slip increased with inclination and flow velocity, and decreased with fluidising velocity.

Another inclined channel study is that of NEUZIL and TURCAJOVA[94], but so little detail of fluidising conditions and experimental methods is given as to render the work of little use to others.

QASSIM[108] carried out experiments in an inclined channel and derived equations for flow of non-Newtonian substances in ducts. He also proposes a model for the viscosity of a bubbling bed in terms of dense phase viscosity and bubble voidage. This is extremely complex and difficult to use. This latter criticism may also be levelled at the experimental results; flow curves are plotted at various fluidising velocities, and range apparently randomly between shear thinning and shear thickening behaviour. Shear rates up to $10^4 s^{-1}$ are reported, but it is difficult to comprehend how they were achieved.

A considerable amount of work has been carried out in a channel flow rig by BOTTERILL and co-workers[18, 20, 22]. Their channel arrangement was a horizontal continuous loop, through which the solids were circulated by means of

paddles. Initially, tests were carried out in a channel 292 mm. wide, using a bed depth of 240 mm. and sand of mean particle size 185 μm. This displayed Bingham plastic behaviour, especially at low fluidising velocities, and a minimum in the plot of viscosity against fluidising velocity was observed at $3U_{mf}$. Later tests using Bauxilite of mean particle size 102 μm showed behaviour ranging from shear thinning (pseudoplastic) to shear thickening (dilatant); the former type of behaviour was attributed to the flow velocity causing more air to pass through the dense phase increasing inter-particle lubrication and the latter type to a layer of gas at the distributor base being scoured away as flow velocity increased.

Further tests in the same channel were made by BESSANT[11], who used a calibrated propellor device to measure local bed velocity, and also measured wall shear stress. The velocity profiles obtained show a change from liquid-like to semi-plug flow with increasing fluidising velocity, suggesting increasing slip at the distributor.

A power law equation of the form

$$\tau = K'(\gamma)^{n'}$$ where τ = mean shear stress

γ = mean shear rate

K', n' = constants

was used to describe the flow. For a channel 140 mm. wide and 118 mm. deep the appropriate values of constants were:

$K' = 1.3N\ s^{n'} m^{-2}$

$n' = 0.55$

Using these values, velocity profiles were calculated using the approach of WHEELER and WISSLER[143] and compared with the measured ones, the agreement being good under some conditions. The wall shear stress measurements were compared with those obtained from the head loss of the flowing bed, and it was found that at high fluidising velocities the shear stress at the distributor became almost zero. Tests were also carried out in a small sloping channel using very shallow beds, and the theory of ASTARITA et al[4] for the flow of non-Newtonian liquids was modified to enable base slip velocities to be calculated.

Although it must be said that experimental difficulties must cast some doubt on the magnitudes of the quantities assessed in this work(for example, average channel velocity was obtained by timing a float, and considerable rearrangement of the channel was necessary to obtain a symmetrical profile) it is clearly of considerable value.

The most recent work on a flowing channel is that of MUSKETT et al[89] using a sloping channel 8 ft. in length and 3 in. in width.

Mass flow rate is measured by timed weighing, and a pneumatic return system is employed. However, this work is clearly in its early stages, and no tests analogous to those of other workers have yet been reported.

2.2.5 Conclusions from viscometer and flowing bed studies

Although it seems that viscometric studies produce only qualitative data about real systems, they are clearly of value. The non-Newtonian nature of a fluidised bed clearly precludes the use of any device which cannot indicate such characteristics; equally clearly, any device which uses a rotor of considerable length is made inaccurate by the considerable variation in fluidised bed viscosity with bed depth. Any immersed rotor will disturb the fluidisation to some extent, and this will probably have more effect than the disturbance caused by the walls of a flowing bed. In spite of these criticisms, it must be reiterated that viscometer studies have provided valuable qualitative data on flow behaviour, which may be summarised as follows:

1) The viscosity of a fluidised bed varies considerably with fluidising velocity, most materials displaying a minimum near U_{mf}.

2) The viscosity increases with bed depth.

3) The viscosity may be affected to varying degrees by the design of the distributor plate.

4) Particle shape and surface roughness, and also the surface roughness of the viscometer rotor have little effect on viscosity.

5) The viscosity of beds of some particles may be considerably affected by the moisture content of the fluidising air, probably due to electrostatic charge effects.

6) Mixtures of different sizes and densities of particles have markedly different viscosities, for example, that of a bed of small dense particles can be reduced by the addition of a small proportion of larger lighter particles.

Clearly, the results obtained from flowing bed studies are much more directly related to the transport of fluidised materials than are those obtained from viscometric work. The main drawback to flowing bed work is the much larger and more complex equipment necessary. A further limitation is the relative lack of sophistication in measurement techniques.

At the moment, it would seem that the non-Newtonian liquid analogy treatment used by Botterill et al is the most useful, being based on quite easily taken experimental results. It seems likely that it may be fruitful to pursue the analogy with liquid flow in open channels, and derive correlations similar to the well known ones for such situations. Due to the non-Newtonian nature of the fluidised bed, it is also clearly better to work at the sort of high shear rates likely to be acceptable in industrial use of fluidised transport. Most previous work has been of necessity carried out at much lower shear rates, and the knowledge at present available makes any extrapolation of this data to higher rates extremely hazardous.

2.3 Industrial applications of flowing beds

Some unique characteristics of fluidised bed combustion systems, especially their compactness, high heat transfer, low pollution levels and ability to burn low-grade fuels, make such systems very attractive for steam raising. The advantages are discussed by ELLIOTT[40, 42], as are some of the problems, particularly start-up, control and turn-down. Fluidised bed combustors must of necessity operate within a narrow temperature range, bounded by inefficient combustion at the lower end and sintering or metallurgical constraints at the upper. The start-up and other problems may be overcome by using separate combustor and heat exchanger units, transporting hot solids between the two. In such a system, it would be simple to provide means of storage for the hot solids to satisfy transient high load requirements.

Although the subject of fluidised bed combustion has been extensively studied, it having been shown that gas, coal and light oil can be burnt in shallow beds, and many applications having been devised, including industrial heat treatment of metal components and wire[138], and the disposal of old pneumatic tyres[3], fluidised transport has been comparatively neglected. Industrial transport of powders is usually done by pneumatic conveyor, a fact which is surprising in view of the advantages of fluidised systems already discussed in Chapter 1. The only commercial fluidised conveyors known to the author are made by Polysius Ltd., in a range of sizes capable of transporting up to 2000 m^3/h, and by Sheepbridge Equipment Limited, also in a range of sizes with a maximum capacity of 1700 m^3/h. The design of these is done, in the first case at least, purely empirically, based on pilot tests on the specific material to be handled.

A further type of fluidised conveyor has been patented by SQUIRES[127]. The top of the bed is enclosed, and thus the fluidisinggas is made to flow over the surface of the bed at high speed; this is said to cause the bed to flow, but it is not known if this has been proved experimentally. The operation of such a conveyor would obviously be confined to a very narrow range of conditions, especially regarding bed depth.

Clearly, although fluidised transport has been used with some success, and the growth potential of the applications of this technique is high, considerable further study is necessary before the mechanisms of flow are at all clearly understood. However, it is possible to progress without such knowledge by use of simple correlations, and to design systems which although not the optimum, will work satisfactorily. Much greater sophistication in both experimental technique, and mathematical modelling is obviously necessary, but at the present time, it would seem that the simple approach is the most likely one to prove useful to the practical engineer.

TABLE 2.1 - RESULTS OF REPORTED DIRECT EXPERIMENTAL INVESTIGATIONS

From Bessant[11]

Reference	Method	Material	Conditions	Findings
Botterill et al[20,22]	Open Channel	135 and 185 μm sand 102 μm bauxilite	2 - 4 U_{mf}	Viscosity 1.8 - 3 Ns/m^2 Range of non-Newtonian behaviour.
Daniels[31]	Terminal velocity of falling sphere	200 - 300 μm sand 100 μm ballotini	508 mm dia. column	Viscosity increased with d_p and ρ_s. Logarithmic drag coefficient Reynolds number relationship.
Diekman et al[37]	Brookfield viscometer	Cracking catalyst 30 to 150 μm.	102 mm dia. column	Solids which increased in viscosit more slowly on de-aeration have better flow quality.
Furukawa et al[47]	Stormer viscometer	277-755 μm vinyl acetate spheres	Up to 20 U_{mf} 152 mm dia. column	Viscosity 0.071 - 2.25 Ns/m^2 increase in viscosity with shear rate. No effect of roughened rotc
Gupalo[57]	Terminal velocity of falling sphere	100 - 420 μm sand	1 - 2.2 U_{mf} 120 mm dia. column	Viscosity 0.5 - 1.3 Ns/m^2. Assumed Newtonian behaviour.

Table 2.1 Continued

	Method	Material	Conditions	Findings
Hagyard[58] et al	Torsion viscometer	125 - 305 μm graphite coated spheres.	66 - 76 mm dia. column	Viscosity 0.25 - 25 Ns/m^2. Newtonian
Kramers[66]	Rotating dumb-bell	Sand, glass beads, silica gel. Various sizes	1 - 2.86 U_{mf}	Viscosity 1.5 - 6 Ns/m^2.
Leeden et al[70]	Brookfield viscometer	75 μm. Aluminium silicate	65 - 90 mm dia. column	Torque independent of: immersion depth, shear rate, bed cross sectional area.
Liu et al[74]	Brookfield viscometer	45 μm catalyst 349 μm polystyrene beads 14 - 123 μm glass beads all spherical.	46 mm dia. column	viscosity 0.01 - 0.46 Ns/m^2 Pseudoplastic tending to Newtonian as U_f increased.
Matheson et al[79]	Stormer viscometer	28 - 96 μm sand 45 - 450 μm cracking catalyst	25.4 mm dia. column.	Viscosity 0 - 40. Stormer gm.
McGuigan et al[91]	Brookfield viscometer	Sand of various sizes and mixtures	1 - 3 Umf	Viscosity approximately 0.2 Ns/m^2 humidity effect.

Table 2.1 Continued

Reference	Method	Material	Conditions	Findings
Neuzil et al[94]	Airslide 43 mm wide length 808 and 1200 mm.	500 μm corundum 1000 μm glass spheres 1100 μm sand	Bed height up to 25 mm.	Assumed Newtonian. Obtained friction factor/Reynolds number correlation.
Prudhoe et al[107]	Terminal velocity of falling sphere	Ballotini 210 μm	Viscous oil as dispersing medium.	No correlation between viscosity c fluidised bed and stable suspensic of comparable concentration.
Qassim[108]	Airslide	266 μm sand.	1.5 - 2.5 U_{mf} Heights up to 25mm.	Viscosity 0.002 - 0.12 Ns/m^2. Newtonian at high Uf.
Siemes et al[124]	Airslide 150 mm wide 2 m long.	1000 μm sand	Up to 5 U_{mf}.	Viscosity 0.1 - 1.2 Ns/m^2. Assumed Newtonian.
Shuster et al[126]	Stormer viscometer	glass spheres	146 mm dia. column	Viscosity 10 - 40 Stormer gm.
Schugerl et al[122]	Rotating concentric cylinders	Various	Various	0.2 - 100 Ns/m^2. Range of non-Newtonian behaviour.

CHAPTER 3

THEORETICAL AND EXPERIMENTAL

3. Theoretical and experimental

3.1 Liquid flow in an open channel

Before discussing the flow of fluidised material in an open channel, some observations on the flow of liquids in open channels are relevant, as the treatment used for the fluidised bed is based very much on that for liquids.

Consider the uniform flow of a liquid between sections 1 and 2 of the open channel shown in figure 3.1. The forces acting on the control volume ABCD are:

1) Static pressure forces F_1 and F_2.
2) The weight W, which has a component $W\sin\theta$ in the direction of flow.
3) The pressure forces exerted by the bottom and sides of the channel.
4) The resistance exerted by the sides and bottom of the channel, $Pl\tau$

As the flow is steady

$$F_1 + W\sin\theta - F_2 - Pl\tau = 0$$

Now $F_1 = F_2$

$W = Al\rho g_c$

$\sin\theta = \frac{h_1}{l}$

The slope So of the channel is $\tan\theta$, which for small angles is equal to $\sin\theta$. Substituting gives

$$= \frac{A}{P} So.\rho g_c$$

$\frac{A}{P}$ is the hydraulic radius, R_H, and so

$$\tau = R_H S_o \rho g_c$$

In pipe flow, τ is given by $\frac{f\rho U^2}{8}$

The mechanism of flow in pipes and channels is similar, and it is assumed that the use of the hydraulic radius accounts for the difference in cross-sectional shapes of a circular pipe and a channel. Thus the two expressions for τ may be equated, yielding

$$U = \sqrt{\frac{8g_c}{f}} \sqrt{R_H S_o}$$

or if $C = \sqrt{8g_c/f}$

$$U = C\sqrt{R_H S_o}$$

This is the Chezy equation, and C is the Chezy coefficient, which is related to both the Darcy friction factor (as shown above) and the Manning roughness coefficient, "n", through the equation.

$$C = 1.49\, R_H^{\frac{1}{6}} / n$$

In this equation, the values of "n" which are inserted must have the units of $ft^{\frac{1}{6}}$, a typical range being from 0.01 to 0.035.

In pipe flow, the correlation $f = \frac{64}{R_e}$ applies to the laminar flow region. In channel flow, this is defined somewhat differently by STRAUB et al[130] as $f = \frac{\bar{K}}{Re}$ where $\bar{K}$ depends only on channel shape. They develop values of $\bar{K}$ for several different channel cross sections. A graph showing the variation of $\bar{K}$ with the aspect ratio of a rectangular channel is shown in figure 3.2.

Basically, it is the foregoing approach which has been used to examine the flowing bed. The approach has been modified where appropriate to take account of the non-Newtonian character of the fluidised bed.

Figure 3.1

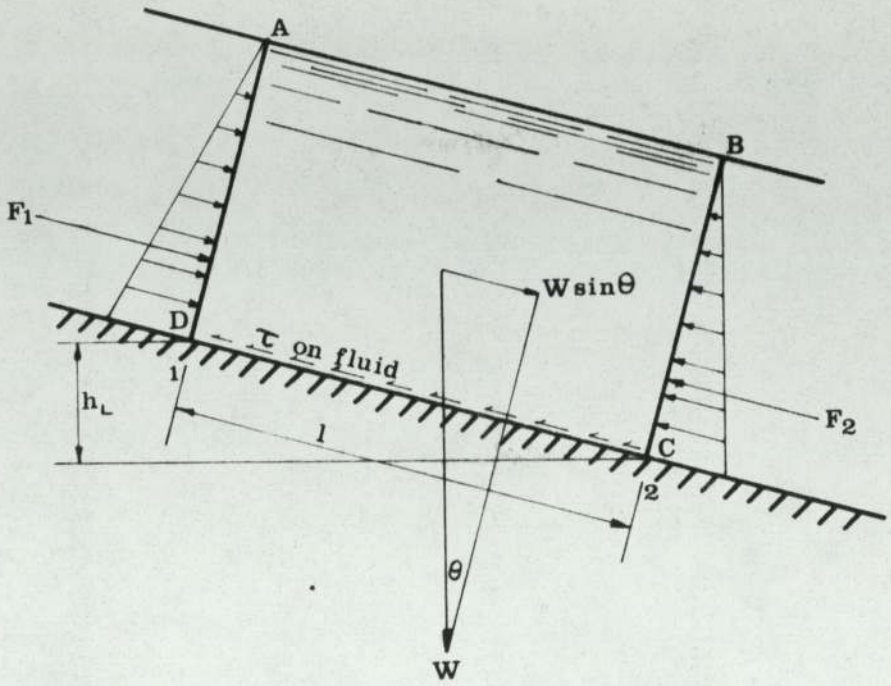

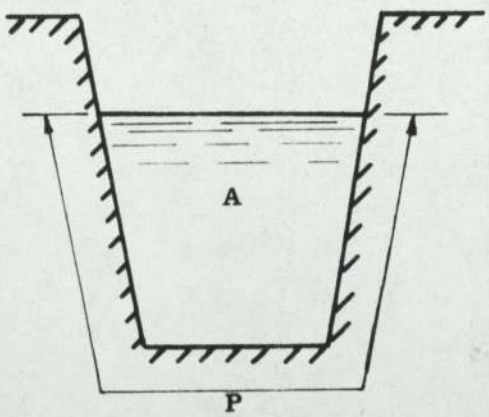

Figure 3.2

COEFFICIENT $\bar{K}$ AGAINST ASPECT RATIO $\bar{b}/d$
FROM STRAUB et al.
Ratio $\bar{b}/d$
Coefficient $\bar{K}$
95
90
85
80
75
70
65
60
55
100
60
40
20
10
6
4
2
1
p
$\bar{b}$

3.2 Choice of model

When studying fluidised transport, one of the most difficult things is to decide upon the approach to be used. As already discussed in Chapter 2 it seems that a fruitful one is to pursue the analogy between the flow of a fluidised bed in an open channel and the equivalent situation for a non-Newtonian liquid. There still remains, however, the problem of selecting a model to characterise the non-Newtonian behaviour of the fluidised bed as closely as possible.

For flow of a liquid in a circular pipe we have

$$Q = \int_0^R 2\pi r.dr.V \qquad (3.1)$$

where R = pipe radius

V = local velocity at position r.

and shear stress

$$\tau = \mu.\frac{dV}{dr} \qquad (3.2)$$

or from pressure drop considerations

$$\tau = \frac{r}{2}\frac{d(\Delta P)}{dL} \qquad (3.3)$$

thus Q becomes

$$Q = \frac{\pi R^4}{8\mu}\left(\frac{d\Delta P}{dL}\right) \qquad (3.4)$$

the well known Hagen-Poisseulle equation.

Non-Newtonian liquids do not obey equations (3.2) and (3.4) because the ratio of shear stress to shear rate varies with the shear rate. Various approaches have been used to resolve this problem. It is possible to substitute an empirical equation for (3.2), an approach used by McMILLAN[90] with some success, but the most common method is to substitute a power law, or similar model. CRAMER and MARCHELLO[30] have reviewed

many of the models available, comparing their predictions with experimental data obtained from the literature. Their findings are most illuminating, and it is relevant to discuss them further.

Some of the models examined are: REF.

Powell-Eyring 3 parameter

$$\mu = \mu_\infty + \frac{\alpha_1}{\gamma} \sinh^{-1}(\alpha_2 \gamma) \qquad 106$$

Powell-Eyring 5 parameter

$$\mu = \mu_\infty + \frac{\alpha_1}{\gamma} \sinh^{-1}(\alpha_2 \gamma) + \frac{\alpha_3}{\gamma} \sinh^{-1}(\alpha_4 \gamma)$$

Extended Williamson

$$\mu = \mu_\infty + \frac{\mu_0 - \mu_\infty}{1 + \left(\frac{\gamma}{\alpha_1}\right)^{\alpha_2}}$$

Oldroyd

$$\mu = \mu_0 \left[\frac{1 + \alpha_1(\gamma)^2}{1 + \alpha_2(\gamma)^2}\right] \qquad 97$$

Seely

$$\mu = \mu_\infty + (\mu_0 - \mu_\infty) e^{-\tau/\alpha_1} \qquad 123$$

To test the fit of each model, an error function $\in i = \frac{fi - yi}{fi}$ was used, together with the R.M.S. error expression

$$\sqrt{\frac{\sum_{i=1}^{N} \in_i^2}{N}}$$

where: μ = viscosity

μ_∞ = limiting value at infinite shear rate

μ_0 = limiting value at zero shear rate

γ = shear rate

α = system parameters

fi = experimental value of dependant variable

yi = fitted value of dependant variable

N = number of data points.

The Powell-Eyring 5 parameter and extended Williamson models were found to provide the best agreement with experimental results, the error on both being about 5%.

The Powell-Eyring 3 parameter model had an error of 14%, the Seely 20% and the Oldroyd 38%.

The main point which emerges from an examination of these models, and others which are far more complex, is that the model used is not important as long as it fits the data fairly well. Probably the simplest model which fits the available shear stress against shear rate data over most of its range is the power law

$$\tau = K'(\gamma)^{n'}$$

used by Bessant in open channel fluidised bed flow. The remaining problem is the evaluation of shear stresses and shear rates. METZNER and REED[83] have developed a correlation for flow of non-Newtonian liquids in pipes of the form

$$\frac{D\,\Delta P}{4L} = K'\left(\frac{8U}{D}\right)^{n'} \qquad (3.5)$$

where D = pipe diameter

$\frac{\Delta P}{L}$ = pressure drop/unit length

U = average pipe velocity

K', n' = constants

They have developed this further using the definition of Fanning friction factor

$$f_F = \frac{D\,\Delta P}{4L} \Big/ \frac{\rho U^2}{2} \qquad (3.6)$$

Substitution of (3.5) into (3.6) gives

$$f_F = \frac{16Z}{D^{n'} U^{2-n'} \rho} \quad \text{where } Z = K' 8^{n'-1}$$

and a generalised Reynolds number is obtained

$$N_{RE} = \frac{D^{n'} U^{2-n'} \rho}{Z}$$

Thus data for all non-Newtonian liquids reduces to the line $f = 16/N_{RE}$ using these expressions. This work is clearly of great importance in liquid flow, but its possible application to fluidised bed flow has hitherto received little attention. The main exponent has been BOTTERILL, whose channel flow experiments have confirmed these findings.

Various restrictions apply to the use of this approach. These are:

1) Pseudohomogeneous flow assumed.

2) For an open rectangular channel, the expressions must be modified by the use of the equivalent diameter concept.

$$D_E = \frac{4.w.h}{(w + 2h)}$$

where w = channel width

h = bed depth

3) Laminar flow prevails, that is viscous forces dominate, and friction is not affected by the surface roughness of the walls. Ideally, all surrounding walls should be identical to eliminate any possible effect, but clearly this is not possible, or very difficult, in practice. The normal critical Reynolds Number of approximately 2100 for transition from laminar to turbulent flow will not apply in the non-Newtonian case; the onset of turbulence in open channels has been observed[100, 130] to be delayed until Reynolds Numbers of the order of 4000 are reached.

4) Steady and uniform flow is assumed, that is, that the bed is of uniform depth throughout the test section, and free from any entrance effects. The extent of the entry zone in non-Newtonian flow is not well documented, a common form of expression used being

$L_E = C.D.R_e$ where C is a constant between 0.02 and 0.06. This is probably reasonable for liquids, but observation of fluidised beds suggests that flow becomes fully developed within much shorter lengths. Some data on entrance effects in non-Newtonian flow is presented by BOGUE[13]. This takes the form of a plot of $\frac{X/R}{N_{RE}}$ against non-Newtonian index n', where X is the distance from the entrance, and R is the pipe radius N_{RE} is defined as $\frac{D^{n'} U^{2-n'} \rho}{K' \left(\frac{3n'+1}{4n'}\right)^{n'} 8^{n'-1}}$

The plot shows that entrance length increases with N_{RE} and decreases with lower values of n'.

It also seems likely that as the velocity profile in pseudoplastic flow is flatter than that in Newtonian flow, the flow is likely to become fully developed earlier. The velocity profile is largely governed by the non-Newtonian index n', but the volumetric flow rate will be affected more by any slip present atthe walls.

For flow in open sloping channels, the BESSANT[11] development of the one-dimensional non-Newtonian flow of ASTARITA[4] is of interest. This defines a slip velocity at the distributor of

$$V_s = \left(\frac{dQ_l}{dh}\right)_{h = 0}$$

where Q_l = volumetric flow rate/unit width of channel

h = bed height.

Bessant's results on shallow bed flow down an inclined channel may be summarised as:

1) Small entry effects, attributed to the low resistance at the distributor.

2) The sand used showed increasingly Newtonian behaviour as fluidising velocity was increased up to 2.5 U_{mf}.

3) Viscosities were much lower than those obtained in the large horizontal channel, this being attributed to reduced bubbling in the shallow bed.

4) Slip velocity had a maximum at 2.0 U_{mf}.

3.3 Experimental

3.3.1 Initial work

As already reported in Chapter 2, the first stage of the author's investigation of fluidised flow concerned circulation systems having two vertical legs, circulation being promoted by differential aeration (see figure 3.3). It should be possible to obtain circulation when the bed is smoothly fluidised, but in the case of these experiments, using sand, motion in the up-going leg was by means of heavy slugging, with stick-slip flow in the down-coming leg. Although quite considerable circulation rates were attainable (regrettably no apparatus existed for determining the rates) such a mode of operation is clearly not the optimum. Although the base section was well fluidised, a large "dead"

zone existed, where motion was negligible, the particle layers shearing along the upper surface of this zone. Attempts were made to reduce slugging by placing vertical baffles of various types in the up-going leg, but these failed. It seemed that experiments could more easily be done in small apparatus, and so the rig shown in figure 3.4 was constructed. Its basic design is similar to the large one: construction is in perspex, with a 3/16" thick porous plastic distributor supported by expanded metal mesh, separate air supplies being provided for each of the vertical legs and the horizontal top section. Various air inlets into the sloping section were tried, two typical ones being shown in the figure. These were intended to promote flow along this section, and create a low pressure zone at the base of the down-coming leg. This rig worked with some success, but again, using sand, circulation was by means of slugging in the up-going leg.

Experiments with these two pieces of apparatus had really only served to emphasise the likely complexity of the problems involved in a total study of a fluidised circulation system. A practical system is likely to consist of slightly sloping sections, where movement is due to gravity, and vertical or near-vertical sections. It was felt that the complexity of the problem precluded simultaneous study of both sections using one test rig, and as the slightly sloping channel appeared to have the greatest number of potential applications, the decision was made to concentrate initially on this aspect.

Figure 3.3

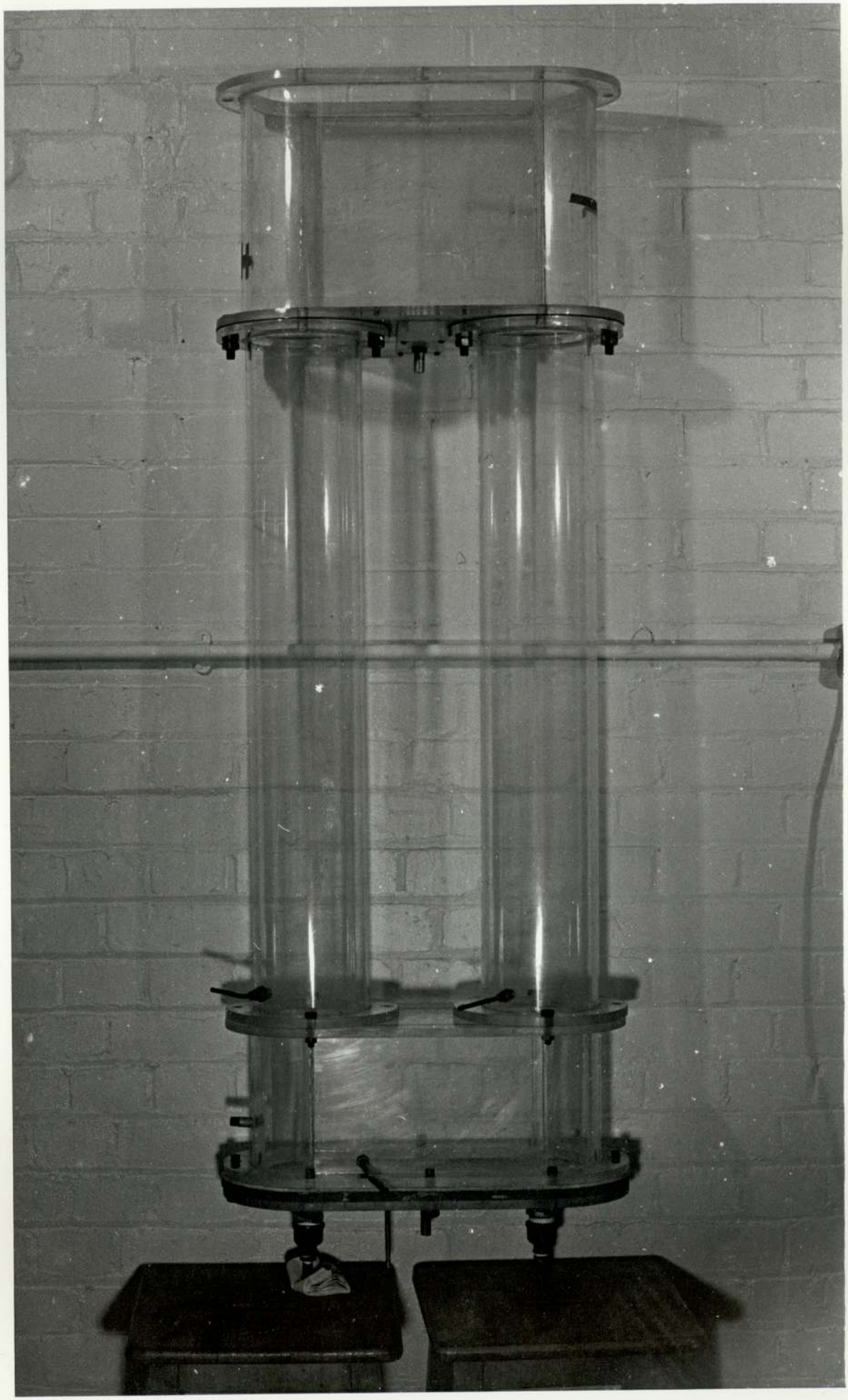

Figure 3.4

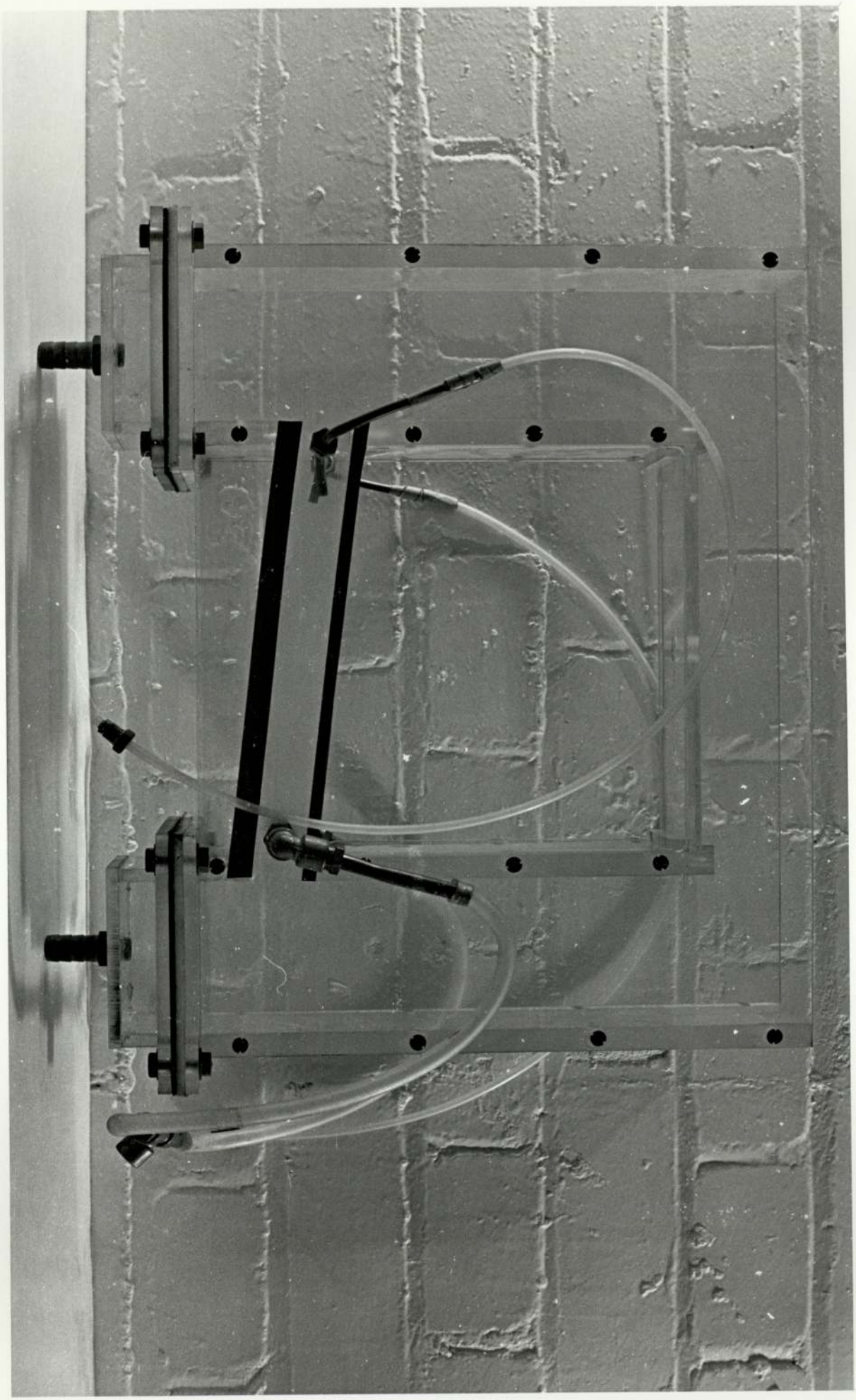

As already mentioned, most previous work on sloping or horizontal channels has of necessity been performed at relatively low shear rates (low channel linear velocities). For any industrial applications, such low rates are economically unviable. The current state of knowledge in this subject will not permit extrapolation of data from low shear rates to much higher ones, and thus it was decided that for the work to be commercially useful, it would have to be carried out at high velocities. This immediately meant high mass flow rates, and a large piece of equipment was clearly necessary. A viscometer study was in progress within the same department[92] using a circular bed 150 mm. in diameter, and it was decided to make the experimental channel of comparable size. Initial designs called for the channel to be 2 m. in length, but this was later increased to 3 m. With these basic parameters set, the author began work, with a colleague, on the design and construction of the test rig. The design is described and discussed fully in Appendix 1 and will not be discussed further here, except to state the general specification.

Channel length 3 m.

Channel width 150 mm. or 100 mm.

Maximum mass flow rate 10 kg/s.

Maximum fluidising velocity: 150 mm. channel width - 17.9cm/s

100 mm. channel width - 21.0cm/s

A general view of the rig is shown in figure 3.5.

Figure 3.5

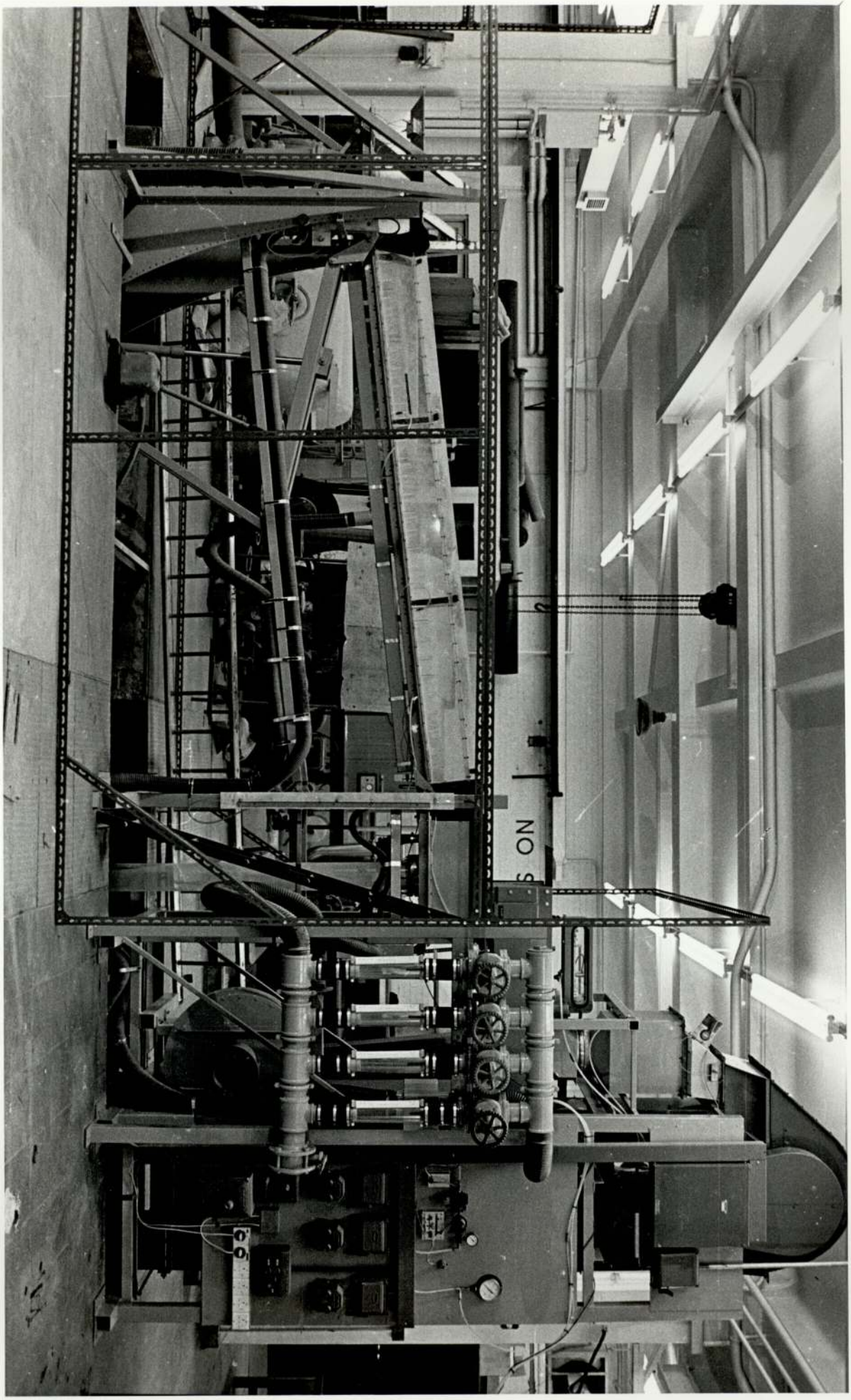

3.3.2 Experimental technique

The range of experiments undertaken may conveniently be summarised as follows:

150 mm. channel - mainly two bed depths 27.5 mm and 40 mm. Fluidising velocities from 6.3 cm/s.(1.64 U_{mf}) to 17.9 cm/s.(4.65 U_{mf})

100 mm. channel - three bed depths, 27.5, 40 and 55 mm. Fluidising velocities from 8.1 cm/s.(2.1 U_{mf}) to 21.0 cm/s.(5.45 U_{mf}).

The material used throughout the tests is a silica sand of true density 2.7047 x 10^3 kg/m^3 and surface mean particle diameter approximately 150 μm.

A notable problem with all types of pneumatic handling equipment is instrumentation. In this equipment the instrumentation used is basically simple, but one problem encountered was accurate measurement of bed height. When the bed is bubbling vigorously, it is difficult to measure its height with any accuracy. In an attempt to overcome this, experiments were performed in a small circular bed 150 mm. in diameter using packed bed heights of 10 to 100 mm. and fluidising velocities up to 31 cm/s. A pressure drop against bed depth correlation was established, and applied to the flowing channel, a reading of bed pressure drop thus being all that is necessary to obtain the bed height. The accuracy of this method was verified by comparing the results so obtained with those given by a vertically traversing pressure probe (see figure 3.6), whose readings enable the bed height to be accurately

Figure 3.6

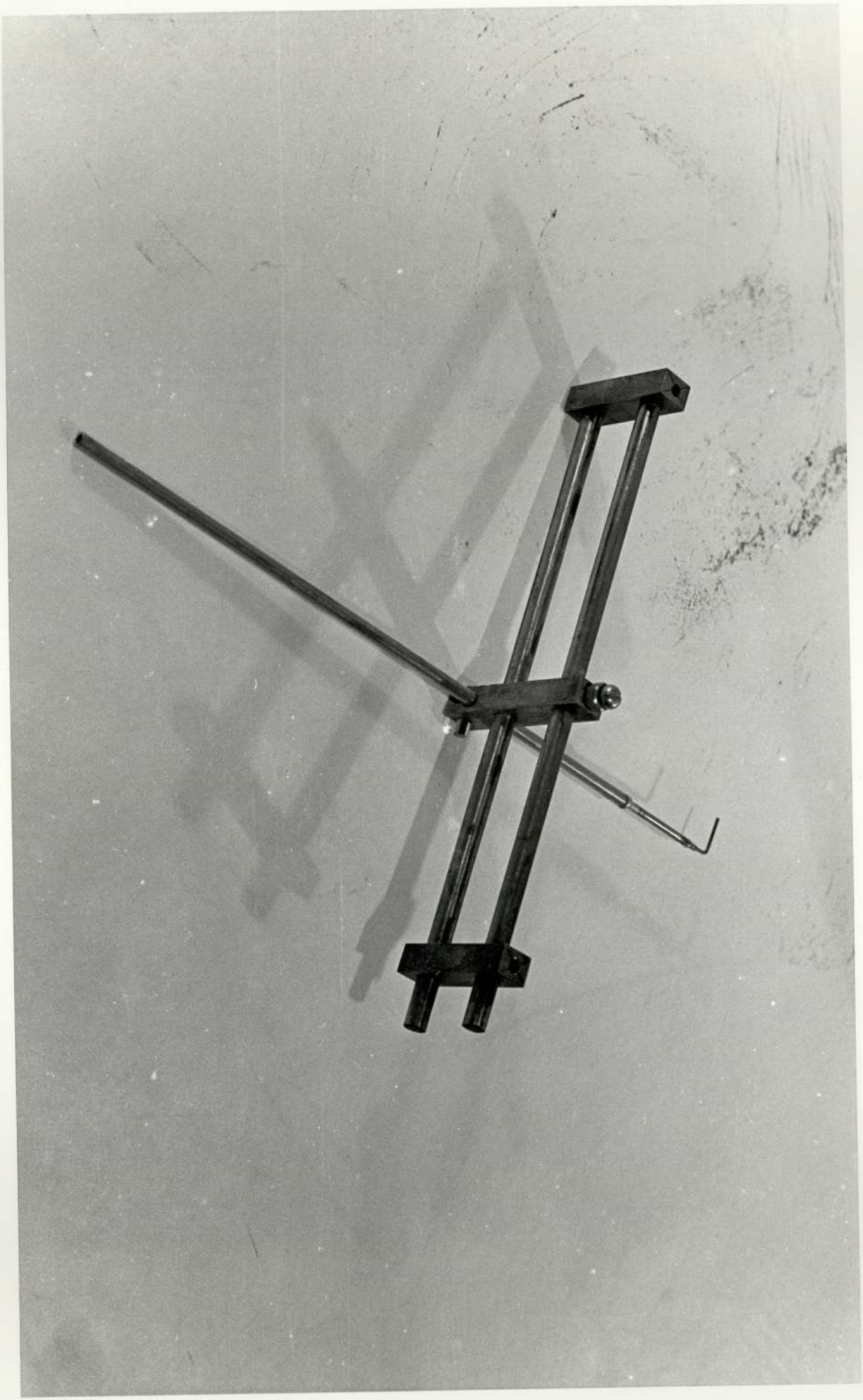

determined; the use of this probe is precluded during actual tests because of the time needed to obtain each reading. Agreement between the two sets of results was good, and the pressure drop correlation technique was used throughout the experiments.

It is essential that the flow in the test section, which comprises the central metre of the 3 m. long channel, should be uniform and fully developed. Entry effects have already been discussed in Section 3.2, and it is believed that any effects will be fully dissipated before the test section is reached. To ensure uniformity of bed depth, pressure tappings were taken at distributor level and applied to a differential manometer. Inevitably on some occasions the pressure differential (positive indicating a deepening of the bed lower down the test section, and negative the inverse) was excessive. This problem will be further discussed later, but where practical such points were neglected.

The condition of the fluidising air is obviously of paramount importance. The fan which was incorporated is not sufficiently powerful for an effective filter to be fitted to its inlet without adversely affecting the flow available to an unacceptable degree. Thus no filter of any sort is fitted and the fan inevitably ingests some dust particles, leading to these being deposited in the air lines and, more importantly, on the distributor, leading eventually to partial clogging of this, and the resultant increased pressure drop. With the present configuration of the rig this is a

problem which must be carefully monitored. Its implications are discussed later, and a solution is proposed in Appendix 1.

The temperature and relative humidity of the fluidising air were constantly monitored during the tests. Regrettably, because of the large air flow (up to 10 m^3/min.) it has not yet been possible to incorporate means whereby these properties could be controlled. Again, a possible solution to this is discussed in Appendix 1. During the programme of tests undertaken, the relative humidity has remained remarkably constant at approximately 20% and thus this cannot be regarded as a variable. However, it is sufficiently low for electrostatic charges of considerable magnitude to be generated in the equipment. The duration of a typical test session is approximately $2\frac{1}{2}$ hours, and in this time the air temperature rises typically by $5^{\circ}C$: it is not thought that this is enough variation to have any significant effect.

The other parameter which it is necessary to measure accurately is the slope of the channel. In order to do this, vertical glass tubes are set up, one fixed to the framework at the mouth of the top receiver, and the other at the same point on the bottom receiver. These tubes are interconnected, and supplied with water by a syringe. When the channel is inclined, the water level in the bottom tube is set to a mark which corresponds to the top surface of the distributor, and the level in the top tube is read against a scale.

Thus this provides a reading of the slope of the channel in millimetres. This arrangement is shown in figure A1.7.

Two types of experiments have been performed. The majority of the work has involved keeping the bed depth constant, and varying solids mass flow rate and channel inclination. The other type of experiment involved setting the channel at a constant slope, varying the mass flow rate and measuring the resultant bed depth. Samples of solids were taken at various times under differing conditions, this being done by placing a core down into the bed to rest on the distributor and removing the portion of the bed within by vacuum extraction.

3.3.3 Observations on experimental technique

In the first series of experiments using a channel width of 150 mm. (SET A in the tabulated results, Appendix 7) readings were taken whilst the mass flow rate was being increased or decreased, but not both. This set of results was taken during a short period before the perspex screening was erected around the rig; pressure was mounting for the rig to be enclosed to prevent the spread of dust, and this SET A was taken rather hurriedly. When the screening was in position, further sets of results (B, C, D and E) were taken, with readings being observed whilst the mass flow rate was being increased to a maximum and then decreased again. This procedure was naturally followed during the subsequent tests using the 100 mm. wide channel.

A difficulty arising regarding the comparison of SET A results on the 150 mm. wide channel and later sets is the distributor blockage already mentioned. The same distributor was used throughout the tests on the 150 mm. channel, and obviously it was becoming progressively dirtier. The implications of this are fully discussed in Chapter 4. Before the tests on the 100 mm. wide channel were begun, the distributor in the channel and both receivers was changed. The tests were all completed as quickly as possible so that blockage of the distributor should not be a variable. With the extractor fan installed in the rig enclosure, little dirtying takes place; the first distributor suffered most of its damage when the rig was not enclosed, and more dust was present, both rig-generated, and from other sources.

3.3.4 Processing of results

3.3.4.1 Constant depth tests

The experimental readings obtained during constant depth tests are:-

Bed depth

Fluidising velocity

and for each value of solids mass flow rate:

Channel slope

Pressure differential across test section

Fluidising air temperature and humidity.

These basic measurements are converted into values of shear stress and shear rate by use of the expressions of CALDWELL and BABBITT[27]

also used by BOTTERILL[20].

These are:

Shear stress $$\tau = \frac{R_H \Delta P}{L} \qquad (3.7)$$

Shear rate $$\gamma = \frac{2U}{R_H} \qquad (3.8)$$

The factor of 2 in equation (3.8) is strictly only applicable to the effect of drag at the wall of a circular tube, however the use of the hydraulic radius concept modifies the expressions for non-circular sections. It is also implicit in the derivation of equation (3.7) that the shear stress is equal on all "wetted" walls; evidence suggests that in a fluidised bed this is not always so. This point will be discussed in Chapter 4.

Pursuing the liquid analogy further, the conventional Darcy friction factor may be obtained thus:

Chezy coefficient for open channel flow

$$C = \frac{U}{(R_H S_o)^{\frac{1}{2}}} \qquad (3.9)$$

and Darcy friction factor

$$f = \frac{8 g_c}{C^2} \qquad (3.10)$$

The average linear flow velocity in the channel is easily obtained

$$U = \frac{\dot{M}}{\bar{\rho}.A.} \qquad (3.11)$$

Equations (3.7) and (3.8) may be plotted as the normal shear stress/shear rate curve, to which

the power law equation

$$\tau = K'(\gamma)^{n'} \qquad (3.12)$$

is easily fitted using numerical methods to obtain values of the constants. The constant K' is effectively the viscosity of the bed, having units of $Ns^{n'}m^{-2}$, and the index n' indicates the extent of the non-Newtonian behaviour, values of n' less than unity indicating pseudoplastic or shear thinning behaviour,and values of n' greater than unity indicating dilatant or shear thickening behaviour.

Given the above quantities, it is now possible to evaluate the generalised Reynolds Number

$$N_{RE} = \frac{D^{n'}U^{2-n'}\bar{\rho}}{Z} \qquad (3.13)$$

where $Z = K'8^{n'-1}$

which can then be plotted in the conventional form of friction factor/Reynolds number correlation.

3.3.4.2 Constant slope tests

During these tests, the measurements taken are:

Channel slope

Fluidising velocity

And for each value of solids mass flow rate:

Bed pressure drop (and hence height)

Pressure differential across test section

Fluidising air temperature and humidity.

To make use of these results in the manner of BESSANT, the values of mass flow rate must be

converted into volumetric terms. This is done using values of density obtained from the small bed tests mentioned earlier. The plot of density against bed height for various fluidising velocities is contained in Appendix 4. Volumetric flow rate is then plotted against bed height for various angles of inclination and fluidising velocities. Appendix 2 shows that according to the modified one-dimensional theory, the slip velocity at the base is equal to the gradient of this curve at the origin (h = 0), and that shear stresses and shear rates can also be obtained from this plot:

Shear stress $\tau = \bar{\rho} g_c h \sin\alpha$ (3.14)

Shear rate $= \dfrac{\left(\dfrac{dQ_1}{dh}\right) - Vs}{h}$ (3.15)

where Vs is the slip velocity.

Thus it should be possible to obtain shear curves from the graphs of Q_1 against h. The method used by BESSANT was to obtain a computer curve fit for the data of Q_1 against h in order to obtain local gradients which allowed the calculation of slip velocities and shear rates. This was clearly time-consuming, and in the author's opinion, not strictly necessary. In the Bessant airslide rig, a series of calibrated orifices was used to indicate mass flow rate, and thus the results must be open to some doubt due to the impossibility of maintaining a

constant head of solids over the orifice. It is also stated that the computer curve fit often did not pass through the origin on the Q_1/h curve, although the errors in this are not stated.

In view of the still largely unproven nature of the modified one-dimensional theory, the author decided to use simple numerical techniques to evaluate local gradients. The lower sections of the Q_1/h curves were drawn to a large scale to make this as accurate as possible, and the forward difference technique used to evaluate slip velocities. The central difference method was used for other points on the curves.

3.3.5 Solids sampling

The method of solids sampling has already been described (3.3.2). The samples taken were carefully sieved by hand and by placing the test sieve stack on a Endecott Model A test sieve shaker. Weighing of individual size fractions was done on an Oertling TP40 balance. Plotting of size distributions is done in conventional histogram form, and the mean particle size evaluated is the surface mean, defined as

$$\frac{\leq W}{\leq W/d}$$

where $\leq W$ is the sum of the percentages of different size fractions present in the sample, ideally 100.

d is the mean sieve size for the particular size fraction. For example, say x% of the sample is between d_1 microns and d_2 microns, the nominal sizes of the two sieves used,

then

$$d_{mean} = \sqrt{d_1 d_2}$$

and $w/d = x/d_{mean}$ for each band between two sieve sizes.

The results for all the samples taken are not presented here, but Appendix 6 tabulates the mean particle size of each sample, and the amount of each sample which is above 250 and 300 μm. This data was needed as part of the investigation of the phenomenon of segregation in the flowing bed.

CHAPTER 4

DISCUSSION

4. Discussion of results

As the results obtained fall into several different categories, it is convenient to discuss them in this way. Initial sections will describe the ranges of behaviour observed, and the magnitudes of the quantities involved, without any attempt at explanation. This is done in a later section.

4.1 Constant depth tests

4.1.1 Shear curves

Before commencing the discussion of the shear curves obtained, it is necessary to make some general observations on their form. The shear stress/shear rate data is plotted on logarithmic scales, on which the pseudoplastic, or shear thinning, type of relationship which characterises most of the shear curves appears as a straight line. The slope of this line is representative of the degree of non-Newtonian behaviour, and hence of the power law exponent n', and the position of this line is governed by the effective viscosity, the power law constant k'.

The results obtained from constant depth tests show the fluidised bed to be pseudoplastic in nature over most of the range of shear rates used. However, at the lower end of the shear rate range the behaviour is subject to some variations.

The initial set of results taken using a channel width of 150 mm (SET A) contained insufficient data for many conclusions to be drawn from it. The trends shown by this set were:

1) At the highest fluidising velocity (4.65 U_{mf})

the shear stress-shear rate relationships were substantially linear for all the bed depths used.

2) At somewhat lower fluidising velocities (3.49 and 2.56 U_{mf}) the shear curves for a bed height of 27.5 mm were shear thinning at the lower end (that is, the linear portion was approached from above, and thus the viscosity was falling) and those for a bed height of 40 mm were shear thickening at the lower end (that is, the linear portion was approached from below, and thus the viscosity was increasing).

3) At the lowest fluidising velocities (2.1 and 1.87 U_{mf}) some kind of "transition" region occurred between two substantially linear sections.

It is convenient to describe the shear thinning lower portion of the shear curves as pseudoplastic, and the shear thickening portion as dilatant. Thus, where the terms linear, pseudoplastic and dilatant occur in this discussion they will, unless otherwise stated, refer to these shapes on the logarithmic shear stress-shear rate plots.

It was obvious after the first set of results was analysed that much more data was required before conclusions could be drawn with any conviction. It was equally clear that an improved experimental technique was required. In SET A, at any given

fluidising velocity, the results for one depth were taken with the shear rate increasing, and those for the other depth were taken with the shear rate decreasing, and thus it was not possible to tell what influence this might exert on the shape of the shear curves. In later sets of results, readings were taken at each bed depth with the shear rate increasing and decreasing.

The trends which were isolated from the later sets of results (B, C, D and E) were:

1) Results taken at 4.65 U_{mf} with a bed height of 27.5 mm again showed a linear relationship, but did not compare well with set A, where the bed depths used were 14.9, 21.5 and 35.0 mm. The new, SET B results showed the bed to be more viscous than before, as demonstrated by the position of the shear curve in relation to those of SET A (figure 4.14).

2) The lower portions of the curves show a range of behaviour. At high fluidising velocities the behaviour is dilatant for both bed depths. As the fluidising velocity falls, the curve for a bed height of 27.5 mm becomes pseudoplastic, to be eventually followed by that for a bed depth of 40.0 mm as the fluidising velocity falls even further.

3) The curves exhibited "hysteresis", that is, the path of the curve when the shear rate was increasing differed considerably from that when the shear rate was decreasing. The downward path was always dilatant in shape.

4) The results taken at 2.1 and 1.87 U_{mf} again showed transition regions. Several tests were done at 1.87 U_{mf} especially, and whilst all the curves exhibited this transition, it was of varying severity, and occurred in a slightly different position each time.

5) The amount of "hysteresis" present seemed to diminish as the fluidising velocity increased.

The results obtained using a channel 100 mm wide confirmed the above observations. In this case, however, in addition to the bed depths of 27.5 and 40 mm used in earlier tests, a depth of 55 mm was also used. The behaviour apparent was:

1) At the highest fluidising velocity (5.45 U_{mf}) the curves were dilatant at the lower ends for all bed depths. As before, as the fluidising velocity was reduced, the curves reverted to pseudoplastic, starting with the lowest bed depth.

2) "Hysteresis" was again less marked at high fluidising velocities, and seemed to be less at greater bed depths.

As already stated in Chapter 3, it was found that a power law adequately described that portion of the shear stress - shear rate graphs which appeared linear on the logarithmic plot. Such a power law was fitted to each line using regression analysis and the values of k' and n' obtained, effective viscosity and non-Newtonian index respectively, are

shown in table 4.1. Clearly there is some error inherent in this process, mainly due to the selection of points to be included in the line fitting procedure; equally clearly it is very difficult to estimate this error, but it should be acceptably low. Examination of table 4.1 reveals thatwith a channel width of 150 mm, the power-law section was pseudoplastic in nature ($n' < 1$) and in fact departed relatively little from Newtonian, the minimum value of n' being 0.715, and n' falling below 0.8 in only six out of the twenty sets of conditions. The results taken using a channel width of 100 mm again show comparatively little departure from Newtonian, but in this case, dilatant behaviour ($n' > 1$) seemed to be evident at the lowest bed depth throughout the range of tests. Greater bed depths were again pseudoplastic, the lowest value of n' being 0.853.

Also contained in table 4.1 are values of apparent viscosity τ/γ, these being mean values of this ratio over the section which was linear on the logarithmic shear stress-shear rate plot. These values of apparent viscosity, in the derivation of which the assumption of Newtonian behaviour is implicit, are compared with the values of effective viscosity, obtained from the power law, by taking the ratio of the two, this ratio again being shown in table 4.1. These two quantities are not strictly comparable, as their units differ somewhat, those of τ/γ being Ns/m^2 and those of k' being $Ns^{n'}/m^2$. However, as

the total variation of n' is between 0.715 and 1.313, it was thought that the comparison between the two quantities could still prove interesting, providing that the dimensional inequality was borne in mind.

4.1.2 Relationship between effective and apparent viscosity

As expected, the relationship between effective viscosity (k') and apparent viscosity (τ / γ) depends upon the non-Newtonian index n'. Figures 4.25 and 4.26 show the variation of both with fluidising velocity. Apparent viscosity varies little with fluidising velocity, showing the slight fall with increasing fluidising velocity that one would perhaps expect, whereas effective viscosity is subject to an apparently random variation. However, it is difficult to assess whether this is a real variation, or whether it is partially or totally due to the experimental and mathematical techniques used. It should also be stated that values of k' are not strictly comparable one with another due to the corresponding values of n' being different. It is, however, not possible to tell whether the variation evident in k' is entirely due to changes in n'. In spite of this it is perhaps worth noting that figure 4.27, which shows the variation of the ratio $k'/\tau/\gamma$ with index n', is of the form expected; that the ratio diverges substantially from unity for quite small movements away from unity of n', a change in n' from 1.0 to 0.83 causing a doubling of this ratio. Thus, apparent viscosity can be extremely misleading where any degree of non-Newtonian behaviour is expected.

This effectively rules out the use of this quantity for fluidised beds, which the present study, as well as others, has shown to be almost always non-Newtonian to some extent.

When n' is less than unity, figure 4.27 shows that

$$\frac{k'}{\tau/\gamma} = \frac{1}{(n')^{3.7}}$$ fits the data obtained.

Similarly, when n' is greater than unity

$$\frac{k'}{\tau/\gamma} = \frac{1}{(n')^{5.0}}$$

The author attaches no particular significance to the figures 3.7 and 5.0, merely stating that these lines fit the data quite well.

The data obtained has shown the difficulty arising in attempts to obtain a sensible value for the viscosity of a fluidised bed. Should one use the apparent viscosity τ/γ which takes no account of non-Newtonian behaviour, or the so-called effective viscosity, values of which cannot be compared one with another due to the different values of non-Newtonian index involved each time? It would seem at the momentthat the effective viscosity k' is the best to use, but the incompatibility of the values obtained, due to the difference in units in each case, must be considered most carefully when it is used.

Table 4.1

FLOW CONSTANTS

QUANTITY	U_f	h	n′	K′	$(\tau/\gamma)_{mean}$	$\frac{K'}{\tau/\gamma}$
UNITS	cm/s	mm	-	$N s^{n'}/m^2$	Ns/m^2	$s^{n'-1}$
	17.9	14.9	0.863	0.069	0.0306	2.255
w = 150		21.5	0.819	0.128	0.0564	2.27
SET A		35.0	0.839	0.149	0.0748	1.992
	13.45	27.5	0.848	0.151	0.0781	1.953
		40.0	0.81	0.221	0.108	2.046
	9.85	27.5	0.948	0.105	0.0863	1.217
		40.0	0.80	0.283	0.1302	2.174
w = 150	17.9	27.5	0.715	0.356	0.1049	3.394
SET B	16.1	27.5	0.803	0.268	0.113	2.372
		40.0	0.75	0.361	0.139	2.597
	14.3	27.5	1.0	0.108	0.107	1.009
		40.0	0.904	0.21	0.145	1.448
	11.65	27.5	0.998	0.113	0.112	1.009
		40.0	0.926	0.202	0.153	1.32
	9.85	27.5	1.0	0.116	0.115	1.009
		40.0	0.931	0.201	0.155	1.297
	9.0	27.5	0.761	0.33	0.116	2.845
		40.0	0.751	0.39	0.15	2.60
	8.1	27.5	0.771	0.307	0.111	2.766
		40.0	0.766	0.388	0.156	2.487

Table 4.1

FLOW CONSTANTS

QUANTITY	U_f	h	n'	K'	$(\tau/\gamma)_{mean}$	$\frac{K'}{\tau/\gamma}$
UNITS	cm/s	mm	-	$N s^{n'}/m^2$	Ns/m^2	$s^{n'-1}$
w = 100	21.0	27.5	1.04	0.048	0.0574	0.836
		40.0	1.083	0.067	0.0936	0.716
		55.0	0.974	0.116	0.1502	1.105
	18.85	27.5	1.313	0.15	0.0682	0.22
		40.0	0.978	0.112	0.0918	1.22
		55.0	0.915	0.203	0.1479	1.373
	17.9	27.5	1.10	0.044	0.0701	0.628
		40.0	0.924	0.15	0.1107	1.355
		55.0	0.951	0.198	0.1655	1.196
	16.1	27.5	1.198	0.027	0.07	0.386
		40.0	0.99	0.112	0.1075	1.042
		55.0	0.857	0.274	0.1607	1.705
	14.3	27.5	1.126	0.042	0.0764	0.55
		40.0	1.00	0.115	0.1158	0.993
		55.0	0.927	0.217	0.1658	1.309
	13.45	27.5	1.053	0.068	0.0874	0.778
		40.0	0.913	0.177	0.124	1.427
		55.0	0.872	0.284	0.1774	1.60
	11.65	27.5	1.206	0.036	0.0932	0.386
		40.0	0.921	0.173	0.1256	1.377
		55.0	0.865	0.286	0.174	1.644
	9.85	27.5	1.208	0.042	0.1087	0.386
		40.0	0.896	0.206	0.1349	1.527
		55.0	0.875	0.289	0.1858	1.555
	9.0	27.5	1.088	0.076	0.1134	0.67

Table 4.1

FLOW CONSTANTS

QUANTITY	U_f	h	n′	K′	$(\tau/\dot{\gamma})_{mean}$	$\frac{K'}{\tau/\dot{\gamma}}$
UNITS	cm/s	mm	–	$N s^{n'}/m^2$	Ns/m^2	$s^{n'-1}$
		40.0	0.983	0.153	0.1428	1.071
		55.0	0.928	0.257	0.199	1.291
	8.1	27.5	1.113	0.075	0.128	0.586
		40.0	0.864	0.27	0.1558	1.733
		55.0	0.853	0.357	0.2117	1.686

4.1.3 Friction factor data

The procedure used to evaluate Darcy friction factors was described in Chapter 3. Initially curves of friction factor against channel flow velocity were plotted for each combination of fluidising velocity and bed depth. However, it seemed that all these lines were tending towards a common one at high channel velocities, and accordingly, all data was plotted on one set of axes, the resultant graphs for the two channel widths being figures 4.28 and 4.29. There is considerable scatter on these graphs at low velocities, but the data does tend quite well to a common line above a channel velocity of about 0.2 m/s. Regression analysis was used to fit straight lines through the data for each channel width, points which were some distance away from the visually best line being neglected for this purpose. The equations resulting were:

150 mm wide channel

$$f = \frac{0.0715}{U^{1.24}}$$ for 460 data points (462 total)

100 mm wide channel

$$f = \frac{0.077}{U^{1.1}}$$ for 426 data points (485 total)

If it is considered that the difference between these is sufficiently small for all data to be fitted to one line, the resultant equation is:

$$f = \frac{0.073}{U^{1.2}}$$ for 886 data points (947 total)

Again the author attaches no particular significance to the values of the constants, although it is clear that the lines are almost at 45° on the logarithmic friction factor - velocity plot, that is, that friction factor is very close to being inversely proportional to flow velocity.

In spite of the scatter evident, these plots of friction factor against velocity would seem to have some usefulness to anyone contemplating the design of a system similar to the one used in this study. A commercial system is likely to operate at fairly high velocities, and in this region the correlation established will predict the friction factor to within about $\pm$ 25%. This seems a large margin, but the use of this correlation will at least show the designer the region of friction factors in which he is working.

A well known relationship in liquid flow is the laminar flow region one between friction factor and Reynolds number. As already stated, for the non-Newtonian fluidised bed, the modified Reynolds number of Metzner and Reed was used, as it has been by other workers, notably Botterill in his channel flow experiments. The graphs of friction factor against modified Reynolds number are shown in figures 4.30 and 4.31. The agreement with the well known relationship $f = 64/Re$ is good.

To evaluate modified Reynolds number, values of n' and k' are required for each point. For the linear portions of the shear stress - shear rate

relationship single values can be used for all points on the line, but for the curving sections individual values must be evaluated for each point from the tangent to the curve at that point.

The good agreement of the data with the laminar flow liquid relationship $f = 64/Re$, also found by Botterill, must surely be a powerful argument in favour of the liquid analogy approach to the study of flowing fluidised beds. This agreement would also seem to suggest that the use of the relationship suggested by Straub, $f = \frac{\bar{K}}{Re}$ where $\bar{K}$ is given as a function of aspect ratio in figure 3.2, is not strictly necessary for correlation of the data. It should be said, however, that the aspect ratios used in this study are not sufficiently wide ranging to cause much variation in $\bar{K}$, the limiting values of which are 66.8 and 57 for the great majority of the data. Only for the lowest bed depth used, 14.9 mm, does the corresponding value of $\bar{K}$ differ greatly from 64, being 76.5 in this case. As the values are not, except in this one case, greatly different from 64 it is not possible to state categorically whether the use of the Straub relation is necessary in flowing fluidised beds or not; however, it would certainly appear that its use is not necessary to establish correlation of data unless the bed is very wide and shallow, the correlation $f = 64/N_{RE}$ being simpler, and acceptably accurate elsewhere.

The relationship between friction factor and Reynolds number is linear up to the maximum Reynolds number

used of approximately 4400, showing no tendency towards another flow regime. Thus it would seem that the flow throughout the present study was analogous to laminar flow. It is doubtful that the descriptions "laminar" and "turbulent" can be applied with any real meaning to a fluidised bed, and although this study does not offer definite proof, it seems likely that the fluidised bed has only one regime of flow. Certainly, it should ease the designer's task to know that friction factor can be reliably predicted up to Reynolds numbers of the order of 5000. Single regime Reynolds numbers of this magnitude are highly unusual. The fact that the flowing fluidised bed follows the laminar flow correlation up to such high values clearly suggests that the flow resistance mechanism of the fluidised bed is fundamentally different to that of a liquid. In liquid flow, when the transition from laminar to turbulent flow takes place, the flow moves from a viscous friction dominated regime to an inertia loss dominated one. It would seem that in a flowing fluidised bed this does not occur; certainly it does not occur within the range ofReynolds numbers used in this study, a range which one would expect to include the laminar/turbulent transition in any more normal non-Newtonian flow. It would seem that viscous friction losses, composed of shearing at the containing walls and inter-particle friction, continue to dominate the fluidised bed up to extremely high Reynolds numbers.

In an attempt to explain this, it is necessary to briefly examine turbulence in liquid flow. When turbulence, swirling and eddying, occurs in liquid flow, local areas of turbulence interact and a good deal of kinetic energy is dissipated. Areas of liquid will be alternately accelerated and decelerated, requiring energy, and where liquid instantaneously contacts a wall, it will be brought to rest, requiring further energy to accelerate when it leaves the wall. It may be reasoned that this process is totally different in a fluidised bed. It seems possible that when particles are thrown into contact with each other, or with a wall, they will "bounce" and retain much of their kinetic energy,and thus the flowing bed will require less energy to keep it moving at high speed. This explanation does not suggest that kinetic energy losses will never attain sufficient proportions to result in a transition to another flow regime, merely that this may be delayed until Reynolds numbers of the order of eight to ten thousand are reached. If this is so, then the resultant friction factor will be very much lower than that apparent in a liquid at the same Reynolds number. This would mean that the power required to drive a fluidised bed would be lower than that necessary to pump liquid at the same Reynolds number, which could make the use of fluidised solids as a heat transport medium very attractive.

This particle "bounce" theory is partly supported by evidence obtained during a study of the pressure drop

characteristics of beds of a variety of materials[104a]. If bed pressure drop is plotted against fluidising velocity, one would normally expect it to approach quite closely to the weight of the bed of particles. Some experiments, especially a series using steel shot, have shown that the pressure drop falls well short of the bed weight, that is, that less energy is expended in fluidising the bed than one would expect. The suggestion that particles may "bounce" on the distributor could explain this, as less energy is required to keep an object bouncing off a horizontal surface than is required to hold it suspended. As yet, this is only a tentative suggestion, but it seems at least a partial explanation for the characteristics observed, both regarding the static and flowing beds.

4.1.4 Solids samples

It was thought that a possible explanation for the "hysteresis" effect apparent in the shear stress - shear rate curves was a restructuring of the bed as the channel flow velocity increased. Visual observations suggested that this was associated with considerable segregation at low fluidising velocities, that is, larger particles settling out on the distributor. Attempts were made to confirm this by taking samples from the bed as described in Chapter 3. The relevant results of the size analyses of these samples are tabulated in Appendix 6, and the analyses of three samples, one from the channel, and one from each receiver are shown compared with a sample of

unused sand in figures 4.32, 4.33 and 4.34. All samples taken from the channel at low fluidising velocity contain many more large particles (above 250 μm) than the unused sand, this being sufficient in most cases to raise the mean particle size somewhat, as shown in figure 4.32. Samples taken from the channel at high fluidising and channel flow velocities show no such trend, having size distributions close to that of the unused sand. Samples taken from the two receivers show that there is a marked tendency for large particles to collect in these components; figures 4.33 and 4.34 show this clearly. It seems likely that the segregation apparent in the channel would be even more marked but for the build-up of large material in the receivers. When the rig is stopped after a test, a layer of large particles remains in the receivers. Clearly this is a design problem of some magnitude as well as an experimental one. In a system where the material flows only once through, the problem should not be large, although it seems likely that large particles will still collect in the receivers regardless of the fluidising and flow velocities used. In circulating systems, the problem is serious, and it can change the size distribution of the material circulating over a period. This was confirmed by taking samples ofthe circulating sand at the weighfeeder exit after the rig had been running for some time at high and low fluidising velocities. These results are shown in

figure 4.35, sample CI_1 being that taken after high fluidising velocity running. This sample contains more large material, 14.3% being above 250 μm against 10.5% in sample CI_2. Whilst not conclusive, this would seem to at least partially confirm that more large material is kept in circulation at high fluidising velocities.

The technique used to obtain samples from the channel is simple, and far from ideal. It would be preferable to take samples at various levels in the bed, but it is difficult to see how this could be accomplished. However, the samples taken do seem to confirm the visual observation that large particles settle on the distributor at low fluidising velocities,and that this effect is much less marked, or totally absent, at higher fluidising velocities. The deposition of this layer is also dependent on the channel flow velocity, the effect again being much less when this is high. If the fluidising velocity is such that this layer exists at low channel velocities, it is progressively swept away as the velocity increases. However, if the velocity is decreased again, the layer will very soon re-establish itself. Obviously, in designing a flowing system, this must be borne in mind when operating conditions are being chosen.

It is also true to say that under conditions of very high fluidising velocity, significant amounts of small particles can be lost from the rig. This loss takes place from the channel itself, and at other points in the circuit, notably at the base of the

hopper at the lower end of the channel where the material falls onto the conveyor belt. Some loss also takes place at the weighfeeder, where very fine particles adhere to the belt, probably because of electrostatic charge, and are scraped off the lower run by a blade provided by the manufacturers for this purpose; obviously this loss is not a function of fluidising velocity unless the charges generated are some function of this, which seems a possibility. The results of this loss of fine material, when taken to extreme, are shown by samples CI_3 to CI_6 (Appendix 6) where the mean particle size is raised by the loss of fines after an extended period of running at very high fluidising and flow velocities.

The conclusions drawn from the materials samples and observation of the channel may be summarised as:

1) Considerable segregation of large particles takes place at low fluidising and flow velocities. Increase in either quantity will cause dispersion of this layer which will, however, soon re-establish itself upon reduction in fluidising or flow velocity.

2) Layers of large particles are deposited in both receivers under all conditions.

3) Loss of small particles may be significant at very high fluidising velocities.

4.1.5 Discussion of data

The experiments performed have shown that the flowing fluidised bed can exhibit a range of rheological behaviour depending upon the operating conditions.

Under operating conditions must be included fluidising velocity, channel flow velocity, bed depth and bed width. Other parameters which may affect the flow are the humidity and temperature of the fluidising air, and the size distribution, shape and density of the particles used, although the influence of these is outside the scope of the present study.

The key to the understanding of the flow of a fluidised bed such as that used here lies in the interpretation of the shear curves. The questions which must be answered concerning these are:

1) What governs the nature of the main section of the curve (that which is linear on the logarithmic plot).

2) How does this section change with changes in bed height and width.

3) What governs the shape of the lower sections of the curves (shear thinning or shear thickening).

4) What is the cause of the "hysteresis" apparent in the curves.

5) What is the cause of the "transition" regions evident at low fluidising velocities.

Firm answers to these questions are difficult, if not impossible, to find at the present time. In some cases, it is clear that further work will be necessary before the present tentative explanations can be proved or disproved.

The main section of the typical shear curve appears linear on the logarithmic plot. Its slope determines the nature of the flow in this region, whether pseudoplastic ($n' < 1$), Newtonian ($n' = 1$) or dilatant ($n' > 1$). There seems little reason to suppose that the bed is other than quite Newtonian at high fluidising velocities and shear rates. Although the values of n' would seem to suggest otherwise, comparison on this basis can be slightly misleading. Although, for reasons of space and to avoid unnecessary repetition, shear curves are not presented plotted on linear axes such plots do show the shear stress - shear rate relationship to be substantially linear in its upper range. This is so throughout the range of fluidising velocities and bed aspect ratios. The values of n' obtained suggest that the bed may be pseudoplastic (most of the range of results) or dilatant (the lowest bed depth and narrowest channel for all fluidising velocities) butthe departures from Newtonian are not large, the values of n' mostly ranging between 0.8 and 1.2, except for one or two results which it seems reasonable to regard as exceptions. Evidence from other sources would suggest that the fluidised bed tends towards Newtonian at high fluidising velocities and shear rates, and the data obtained in this study seems to confirm this. As the fluidising velocity falls, the bed tends to assume increasingly pseudoplastic nature, increases in bed depth also tending to increase this. This is no doubt due to the inferior

quality of fluidisation in deeper beds, with more bubbling, allied to the obvious decrease in particle mobility and interparticle lubrication caused by a decrease in air flow. This deterioration in quality happens at low shear rates, but it has been suggested that increasing shear rate can improve fluidisation by suppressing bubbling, causing more air to pass through the dense phase, with an associated increase in interparticle lubrication. This could explain the shear thinning behaviour, and this explanation is reinforced by the author's observations that the bed does indeed appear to bubble less, and flow more smoothly at higher shear rates, in most cases (see section 4.3).

Thus it seems reasonable to conclude that at high shear rates the flowing bed is substantially Newtonian or slightly shear thinning, depending on fluidising velocity. At first sight, the values of viscosity do not compare well between the two channel widths under the same conditions. However, comparison of the values of k' is misleading here, as they cannot strictly be compared unlessthe value of n' is the same in the two cases. The best way to compare results from the two channel widths is to plot the shear curves on the same axes. Here again, comparison of the later results from the 150 mm wide channel with those from the 100 mm wide channel shows surprising differences, the bed being considerably more viscous in the wider channel. However, there is evidence that the blockage of the distributor due

to dust in the fluidising air is a factor in the later results on the 150 mm channel (SETS B, C, D and E). Only SET A, taken when the distributor was clean, is directly comparable with the 100 mm channel results, also taken when a new, clean distributor had been installed. Unfortunately, it is only possible to compare a few results due to the lack of data in SET A. However, these results are quite comparable, as shown in figures 4.42 and 4.43, the differences probably being attributable to differences in experimental technique, and experimental error. This comparison seems to confirm the observation of other workers that fluidised bed flow is much more affected by changes in bed depth than by changes in bed width. This seems to suggest that under most conditions wall friction is considerably greater than base friction.

The blockage of the distributor, with its adverse effect on the quality of fluidisation, accounts for the discrepancy between SET A and later results on the 150 mm channel, highlighted by figure 4.14, a comparison between the shear curves taken at three bed depths (SET A) and later at an intermediate depth (SET B). This shows that the bed is much more viscous in the later sets of results, and serves to illustrate the serious effects of allowing dustto be carried by the fluidising air. As mentioned elsewhere this problem is, happily, not now of such large magnitude as it once was.

The shape of the lower sections of the shear curves

is open to a great deal of interpretation, and it is not possible at this stage to put forward firm explanations for the rangeof behaviour observed.

At high fluidising velocity, especially at low bed depth, the bed behaves in a shear thickening way. At least one viscometer study[92] has detected the presence of an inviscid layer close to the distributor, when this is of the porous type. It seems likely that this will exist also in the channel used in these experiments, at least under some conditions. This layer will be gradually swept away as the channel velocity increases, thus increasing the base resistance, and giving rise to shear thickening. As the fluidising velocity is decreased, this type of flow gives way first to substantially Newtonian behaviour throughout the range of shear rates,and then to shear thinning behaviour as the fluidising velocity is further decreased. This is consistent with the inviscid layer explanation, as considerable air flow is likely to be necessary to establish this inviscid layer. If this is not present, then the bed reverts to high drag at low shear rates, the bed thinning as shear rate increases due to the bubble suppression, with associated expansion, decrease in density and increase in interparticle lubrication, mentioned earlier.

It is, however, slightly more difficult to explain why this changeover in mechanisms as fluidising velocity is reduced begins with the shallowest bed. This suggests that the inviscid layer is lost more

easily in the shallowest bed, and remains lower in the range of fluidising velocity in the deepest bed. It is possible that the increased pressure drop and inferior fluidisation of the deeper bed allows the retention of sufficient air close to the distributor to create this inviscid layer even at quite low fluidising velocities, but clearly, more work on this aspect is necessary before it can be explained really satisfactorily.

As already mentioned, the shear curves display some "hysteresis" between the upward and downward paths. The above discussion of the shape of the lower sections of the curves applies mainly to the upward path, the downward one almost always curving down in a shear thickening way. It seems likely that this "hysteresis" is due to a restructuring of the bed which takes place as shear rate increases. The behaviour of thelower sections of the shear curves as shear rate increases has already been dealt with. From data obtained from solids sampling (see Section 4.1.4) it is clear that this behaviour is further complicated by the presence of a segregated layer of large particles, especially at low fluidising velocities and shear rates. This is dissipated to a large extent by increase in fluidising velocity, and is progressively swept away as shear rate increases. This phenomenon is again consistent with shear thinning behaviour at low fluidising velocities and shear rates.

However, whether the mechanism of flow at low shear rate is that of the "inviscid layer" or a combination of the "bubble suppression", and "dispersion of segregated layer" mechanisms, the end result is the same. A total reorganisation of the bed as shear rate increases leads to free-flowing, low viscosity, substantially Newtonian behaviour at high shear rate. Once the bed has achieved this state, mobile, with low drag and a good deal of air passing through the dense phase, it is reluctant to give it up. As the shear rate is decreased once again, it loses its free-flowing character only slowly, continuing to behave in a substantially Newtonian way, or the viscosity may even fall slightly. It is possible that at very low shear rates the bed will revert quite quickly to its initial state,that is, that it will suddenly "jump back" to the upward-going path, but no evidence of this is apparent in these tests. It is difficult to explain this restructuring in more concrete terms, but there seems little doubt of its existence in the light of the results obtained. The "hysteresis" is less pronounced at high fluidising velocities, tending to reinforce this hypothesis; at high fluidising velocities the segregated layer will be smaller, or altogether absent, and the bed will already be quite mobile so that less alteration in its structure takes place as shear rate increases. The"transition" regions of the shear curves at low fluidising velocity can also be explained in similar

terms. When these were first encountered, it was thought that they might indicate a movement between two flow regimes analogous to laminar and turbulent, but, as already mentioned, it now seems likely that a fluidised bed has only one regime of flow, certainly up to the limiting value of Reynolds number used in these tests of approximately 4400, and that the "transition" in fact occurs between two qualities of flow. At low fluidising velocity and shear rate, segregation of large particles is severe; sufficiently so for the layer to act as a secondary distributor, disturbing the air flow and having a deleterious effect on fluidisation quality. At low fluidising velocity, the bed would not flow freely in any event, but this additional effect means that flow is very poor at low shear rates. As this is increased, the segregated layer begins to be swept away, and more air begins to be trapped in the bed, these two leading to a dramatic improvement in the flow. In several cases, the bed has been observed making this "transition". At constant slope and mass flow rate, the bed depth is initially stable, and then suddenly begins to fall quite rapidly, before again becoming stable atthe lower value. The inclination of the channel must then be reduced to bring the bed depth back to its original value. When observed, this is quite remarkable, and is accompanied by a visually discernible improvement in the quality of the flow. It seems that it can only be due to the dispersal of the segregated layer, with its attendant dramatic improvement in bed uniformity and fluidisation

quality. The fact that the "transition" occurs at slightly different points on the shear curve and is of somewhat different magnitude in each test (figure 4.1) is attributable to the difference in initial structure of the bed in each case, and the differing severity of the segregation present. This would suggest that at low fluidising velocity, the initial flow depends on such things as the way in which the bed was collapsed at the end of the previous test, and the length of time which the bed has been defluidised between the tests. Clearly, this further complicates the analysis of the flowing bed at low fluidising velocity and shear rate, adding a further factor to the numerous ones already present, and making the job of the designer of a system intended to operate in this region even more difficult. It can truly be said that, at the moment, it is only possible to predict with any hope of accuracy the behaviour of a flowing fluidised bed when the fluidising velocity is high (in excess of 2.5 U_{mf}) and the shear rate is also quite high, the necessary value of the latter depending on the bed depth.

4.2 Constant slope tests

The technique proposed by Bessant, outlined in Chapter 3, was used to obtain slip velocities for the three fluidising velocities and three channel slopes used. The results of these tests are presented as plots of volumetric flow rate per unit width of channel against bed height in figures 4.36 to 4.38. As already mentioned, it was thought

sufficiently accurate in the first instance to evaluate local gradients on these curves by numerical methods. In order to evaluate slip velocities, the lower section of the curve was drawn to a large scale, and forward difference equations were used to obtain the gradient at the origin.

1st forward difference $y_i' = \dfrac{y_{i+1} - y_i}{\Delta x}$

2nd forward difference $y_i' = \dfrac{-y_{i+2} + 4y_{i+1} - 3y_i}{2\Delta x}$

where: y_i' = gradient at origin.

y_{i+1} = Value of $\dot{Q}/w$ after an interval Δx.

y_{i+2} = Value of $\dot{Q}/w$ after two intervals

y_i = Value of $\dot{Q}/w$ at origin = 0.

The slip velocities thus obtained are shown in table 4.2. To evaluate gradients at points on the curve, to enable shear rates to be calculated, the more accurate second central difference equation could be used.

$$y_i' = \frac{-y_{i+2} + 8y_{i+1} - 8y_{i-1} + y_{i-2}}{12\Delta x}$$

TABLE 4.2.

U_f cm/s	S_o mm.	w mm.	V_s mm/s.
11.65	50	150	81.3
	100		112.5
	150		150
9.85	50		86.3
	100		137.5
	150		151.3
9.0	50		60
	100		105
	150		140
11.65	50	100	96.3
	100		125
	150		176.3
9.85	50		150
	100		160
	150		175
9.0	50		76.3
	100		142.5
	150		175

This procedure was undertaken, using the expressions in Appendix 2 for shear stress and shear rate, initially for the set of results U_f = 11.65 cm/s., w = 100 mm. The result is shown in figure 4.39, and amply illustrates the breakdown of the theory for bed depths greater than about 20 mm. The calculations were thereafter restricted to depths of 15 mm. or less, the results for all three channel slopes being shown in figure 4.40.

The slip velocities obtained are somewhat higher than those of Bessant. He computes a slip velocity of 51.9 mm/s for sand at 2.0 U_{mf}, using a channel width of 135 mm. and an inclination of 0.0375 radians, whereas a roughly comparable set of conditions in the present study, 2.34 U_{mf} and 0.032 radians, yields slip velocities of 105 mm/s. with a 150 mm wide channel, and 142.5 mm/s with a 100 mm wide channel. However, the shear curves of figure 4.40 bear little similarity to Bessant's, exhibiting a completely different relationship for each channel slope, whereas he obtained a single curve embracing data taken at several angles of inclination. The calculations were repeated for other conditions, but the shear stresses and shear rates obtained had no meaning, some showing falling shear rates as shear stress and velocity were increasing. The lower portions of some of the curves of $\dot{Q}/w$ against h are shown in figure 4.41, and examination of these explains this. The lack of data at bed depths below 10 mm. is obvious and regrettable, but the difficulty in taking accurate measurements here is also clear; it is difficult to believe that Bessant did not encounter similar difficulties, and indeed his curves stop well short of the origin. The

results obtained here show that there is not likely to be a great change in the gradient of the curve between the origin and h = 10 mm. This being so, and the shear rate being given by

$$\gamma = \frac{\text{slope} - V_s}{h}$$

then this must fall as h is increased, the slope and slip velocities being substantially constant.

The shape of the curves also explains the breakdown in the theory above bed depths of 20 mm. In this region also, the local gradient of the curve is changing little, again causing the shear rate to fall as the shear stress is increased. Thus it would seem that the above expression for shear rate can only produce results which are at all sensible when the local gradient of the $\dot{Q}/w$ against h curve is changing rapidly.

In the light of the results obtained in this study, Bessant's ability to produce good shear curves from similar data is remarkable; certainly the author has been unable to duplicate this. Although the numerical techniques used must call into question the accuracy of the results, it seems unlikely that sufficient error would arise from this quarter to explain the differences. It is the author's opinion that the technique used can at least be said to be so restricted in application as to be almost useless. The simplifying assumptions made in extending the work of Astarita seem now to be unjustified. The most major of these is that slip velocity does not change with bed height, that is, that a plug-like flow prevails. There seems little real

justification for this assumption, especially when a range of operating conditions is being considered. It seems likely that slip velocity will be some function of both fluidising velocity and bed depth, this latter variation being included in the theory of Astarita. Although this makes the analysis much more complex, it seems that this must be included before the validity of applying the theory to a flowing fluidised bed can be proven or otherwise.

A further puzzling point concerning the work of Bessant is the form of the equation which he states that he fitted through the data of $\dot{Q}/w$ against h. He gives this as:

$$\dot{Q}/w = A + B(R)^h$$

where A, B and R are constants.

This must pass through the origin, and thus A and B must be equal in magnitude, with opposite signs, but the values given do not support this.

The conclusion which must be drawn from the constant slope tests performed in this study is that the slip velocities obtained must be viewed with some doubt, due in part to the techniques used to obtain them from the experimental data. The author has found it impossible to obtain useful shear rate data using the simple theory presented here, and thus it would seem that the only part of the work which is to be relied on is the original flow rate per unit width against bed depth data. The comparison of data from the two channel widths appears to show that the velocity in the wider channel is initially lower than in the narrow one, suggesting a higher resistance to flow, and later becomes higher than in the narrow one, suggesting a lower resistance to flow. It is difficult to see why this should be so, and

it may be due in part to experimental error. The data obtained in the wide channel was, regrettably, taken whilst the bed was adversely affected by the distributor choking mentioned earlier in this chapter. This could well account for the apparently greater resistance to flow in the wider channel lower in the range. It may be that the greater drag in the narrower channel higher in the mass flow range is due to some kind of wall effect, but this must clearly be looked at in greater detail before useful conclusions can be drawn.

It must be reluctantly concluded that very little useful information has been obtained from the constant slope tests performed in this study. The author is not certain whether useful data can be obtained from such experiments or not; certainly it is his opinion that a much closer look at the theory is required before this is possible.

4.3 Visual observations

Several points of interest have arisen from visual observation of the bed during the programme of tests. Some of these are to a large extent unexplained at the moment, whilst it seems likely that others are what might be called rig effects, that is, they occur because of some physical characteristic of the rig, and are not general phenomena encountered in flowing fluidised beds. Nevertheless, an appraisal of the visual observations taken demonstrates, at least, the complexity of a flowing fluidised bed.

The first, and perhaps most interesting, of these phenomena is that which the author and his colleagues style the "hydraulic jump". Although not strictly appropriate, this term describes well enough the character of this phenomenon.

In the programme of tests described here, it occurs always at quite low fluidising velocities ($2U_{mf}$ or less) and usually only if the channel outlet is restricted in some way, although this latter condition is not essential. When this "jump" occurs, the sequence of events is as follows. Initially, the bed begins to deepen at the downstream end where the channel flows into the lower receiver. This discontinuity can reach quite large proportions, and it travels upstream, often as far as one metre. On some occasions this "jump" can remain stationary and stable for some time, whilst on others it is continually being dissipated and re-forming. Once a discontinuity is established, of course, the fluidising air will flow preferentially through the rest of the bed, where the pressure drop is lower, and this will help the discontinuity to stabilise and grow. At some stage, the lower end of the discontinuity will slump forward into the receiver. This lessening of bed height here will cause more air to pass through this part of the bed, and the discontinuity will disperse from the downstream end. Under certain conditions it will almost immediately begin to re-form. As already stated, restriction of the receiver outlet makes discontinuities much more likely to form, due to the resulting increase in bed height in the receiver, but the process can occasionally take place under low fluidising velocity conditions when the outlet is not restricted. It is possible that this is caused by a minor disturbance or discontinuity at the lower end of the channel: perhaps a local build up of large particles on the distributor restricting the air flow at that point, the disturbance gradually growing. This

could be helped by the local defluidisation inevitably caused by the metal strip which covers the join between the channel and receiver distributors. A hydraulic jump is shown in the photographs, figure 4.44, and this phenomenon should repay further study as to its exact cause.

During the course of the tests, occasionally smaller discontinuities would occur between the bed pressure drop probes,that is, in the middle of the test section. These took the form of small "humps" in the bed, again presumably caused by some local disturbance in the fluidisation pattern, possibly caused by a patch of large particles on the distributor. It is also possible that this was partly due to a disturbance of the uniformity of porosity of the distributor due to dust clogging the pores from the underside.

A certain amount of work was done during the course of the experiments using a tracer material. This was sand of the same type used throughout the study, and was dyed blue. Photographs taken whilst the tracer was in use form figure 4.45 (1) and (2). These were taken when the bed was fluidised at 1.64 U_{mf}, and the channel velocity was 0.104 m/s. They clearly show that under these low fluidising velocity conditions there is little discernible bubbling of the bed, and thus little mixing, in either the horizontal or vertical directions. This is demonstrated by the fact that the line of tracer is quite straight along the channel, and varies little in intensity. Clearly, such conditions represent the closest analogy with laminar flow. These

photographs also provide further evidence of the segregation of large particles at low fluidising velocity, due to the lack of vertical mixing.

Photograph 4.45 (3), taken when the bed was still fluidised at 1.64 U_{mf}, but now flowing at 0.655 m/s, shows the development of a "boundary layer" at the channel wall. Although the centre is still "laminar,"as witnessed by the tracer, it is clear that quite a steep velocity gradient exists at and close to the wall. Most of the shearing seems to be taking place in this layer, and it is interesting to note that tracer dropped in very close to the wall moves out to the line apparent in the photograph, and travels stably along this line. It is often the case in fluidised beds that slightly more air flows up close to the walls, and it seems possible that this causes a layer close to the wall to be slightly better fluidised, and thus allows it to flow more easily. Under conditions of even lower fluidising velocity very strange velocity profiles have been observed, having a maximum on the line close to the wall shown in photograph 4.45 (3) and decreasing both towardsthe wall and towards the centre of the channel. This is difficult to explain, but is undoubtedly a function of airflow at the wall, segregation, and the attendant secondary distributor effect, and possibly blocking of the distributor.

If the fluidising velocity is increased to the order of 2.5 U_{mf}, much more bubbling occurs, the bed shows considerable "turbulence", and vertical mixing is good. As shown in photograph 4, figure 4.45, the tracer is dispersed immediately. When fluidised at this sort of level, the bed shows no evidence of any "shearing layer" close to the wall.

One set of photographs, figure 4.46, taken when the bed was fluidised at 2.56 U_{mf} seems to show an increase in bubble size with increasing flow velocity. At low velocity there are many small bubbles, but at higher velocity the bubbles are fewer and much larger. This seems at variance with the main body of the results, where bubblesuppression with increasing flow velocity was noted, as it has also been by Botterill. Here, as the flow velocity increased, the bubbling bed became much smoother in appearance, and it was inferred that the increase in velocity was promoting an improvement in the quality of fluidisation by causing more air to pass through the dense phase and scouring away bubblesfrom the distributor before they had time to grow. It may be that in the case of the photographs which show larger bubbles at higher flow velocities some segregation was taking place, but this seems unlikely at fluidising velocities of this order. It would seem that for some reason the increased velocity was increasing the time taken for the bubbles to rise through the bed, thus giving them time to grow by coalescence. Whether this was accompanied by an increase in the amount of air in the dense phase cannot be assessed. It would seem that the conditions prevailing whilst the photographs were taken were in some way exceptional; the body of observations confirms that the fluidised bed becomes smoother and bubbles less at high flow velocities (figure 4.47).

Visual observation has also highlighted some characteristics of the rig itself. The first of these is that it would seem that the receivers are unnecessarily large, especially the upper one. Thesection of this above the valve, that is,

opposite to the outlet into the channel, plays little useful role and could well be much smaller. The same criticism applies to the lower end of the bottom receiver. The receivers were intended, especially the top one, to stabilise and smooth the flow, but smaller components could do this equally well. It has also become clear that the corners of the receivers form stagnant pockets of material, especially large material, contributing to the build up of this in the receivers. These corners could well be rounded off.

With the narrower channel it was found to be impossible to perform experiments at fluidising velocities of less than 2.1 U_{mf}. This was due to the formation of a discontinuity at the lower end of the channel which could only be dispersed by the use of large channel inclinations. As the wider channel had always operated satisfactorily at fluidising velocities well below this, it can only be concluded that this discontinuity was somehow caused by the divergent section which joined the 100 mm wide channel to the 150 mm wide "neck" of the receiver, although it is difficult to see why this should be so. A possible explanation is that the drop in bed depth in the divergent section and lower receiver in reducing the pressure drop here disturbed the air-flow pattern. Previous experience has shown that at fairly low fluidising velocities small disturbances can have disproportionately large effects. Thus, the observations made during the course of the experiments have helped to reinforce some theories concerning the bed behaviour, and have also brought to light other interesting phenomena which must be studied in greater depth before they are satisfactorily explained.

Figure 4.1

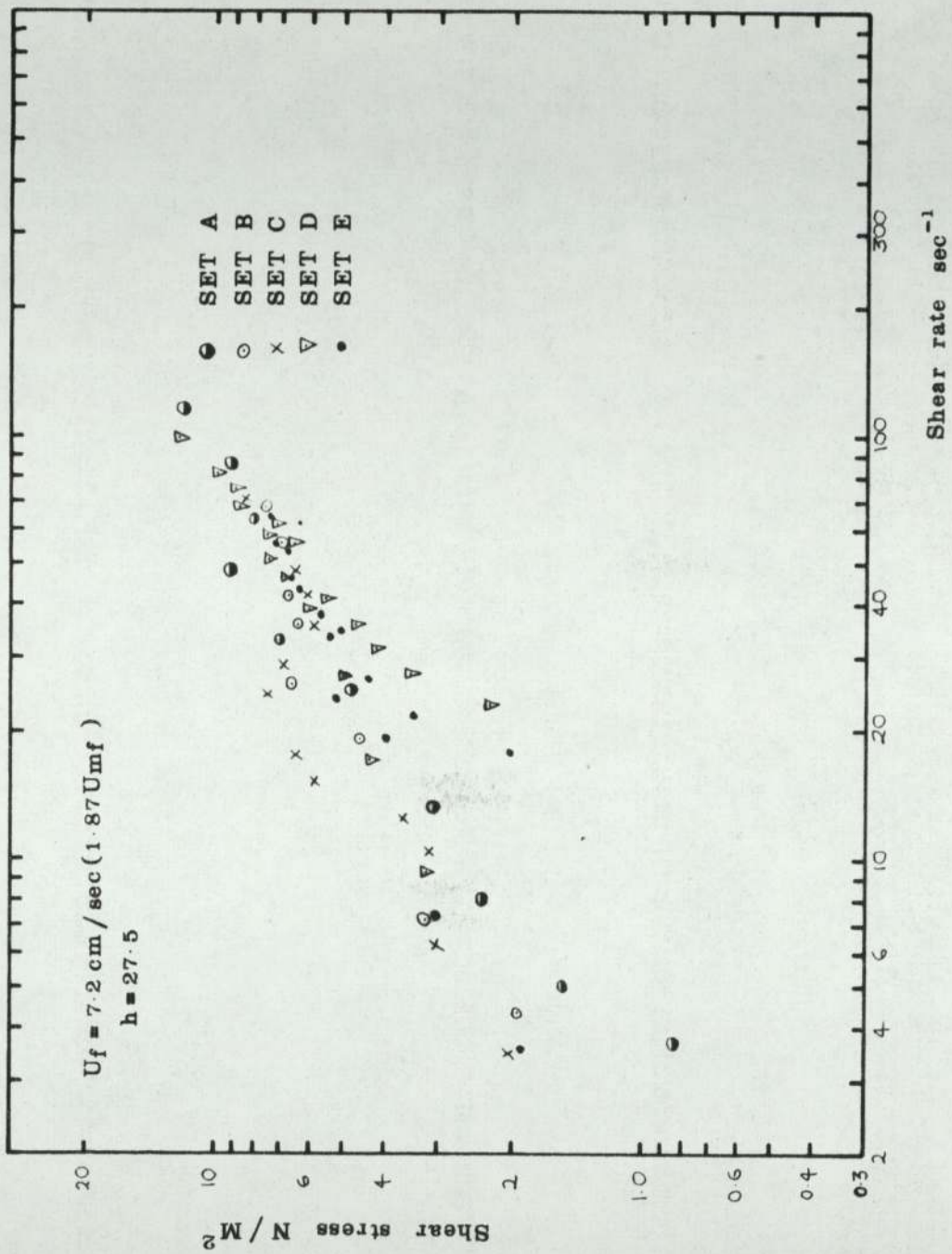
SET A
SET B
SET C
SET D
SET E
Uf = 7·2 cm/sec(1·87Umf)
h = 27·5
Shear stress N/M²
Shear rate sec⁻¹
20
10
6
4
2
1·0
0·6
0·4
0·3
2
4
6
10
20
40
100
300

Figure 4.2

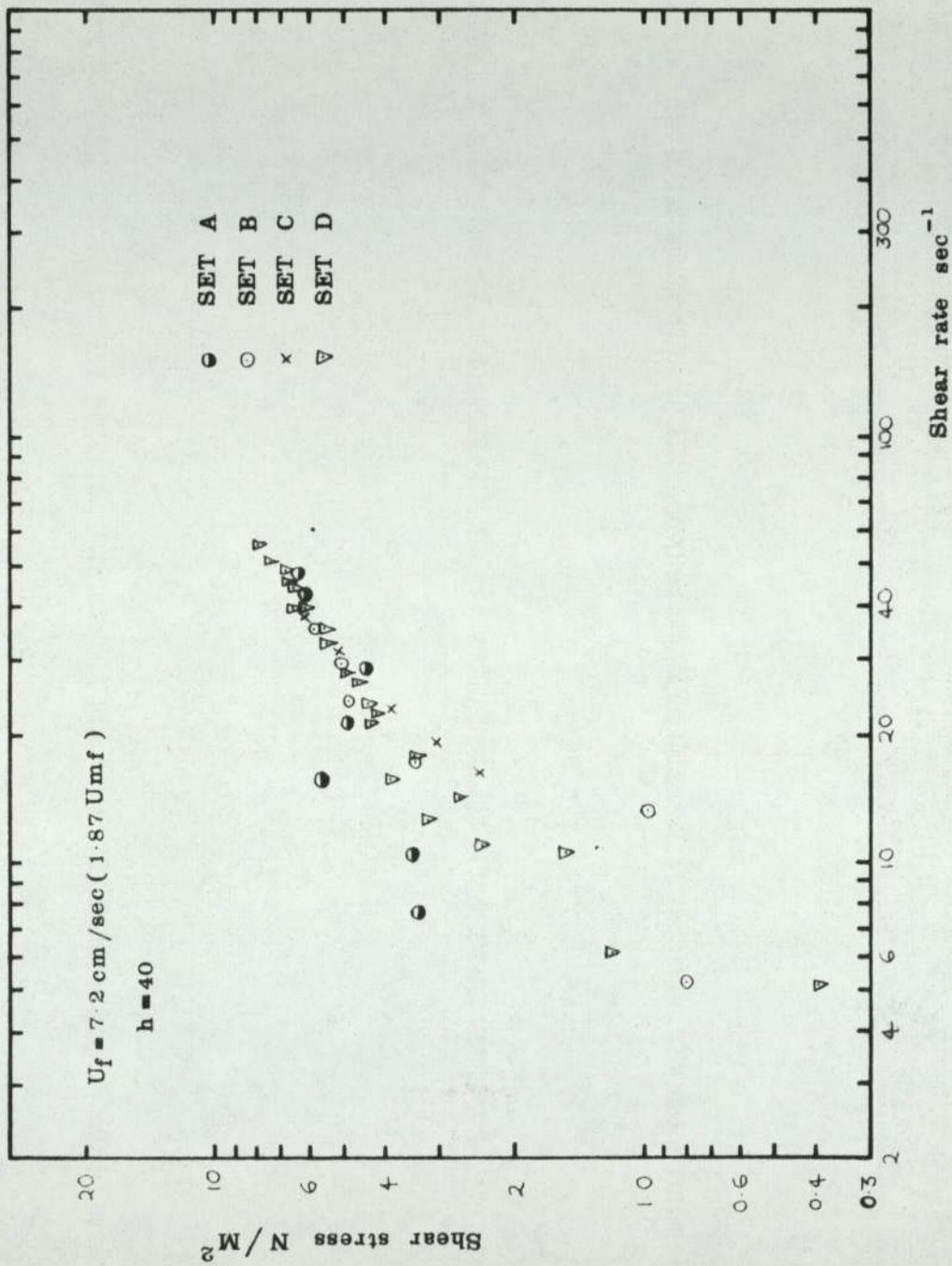
SET A
SET B
SET C
SET D
U_f = 7·2 cm/sec (1·87 Umf)
h = 40
Shear stress N/M²
Shear rate sec⁻¹
20
10
6
4
2
1
0·6
0·4
0·3
2
4
6
10
20
40
100
300

Figure 4.3

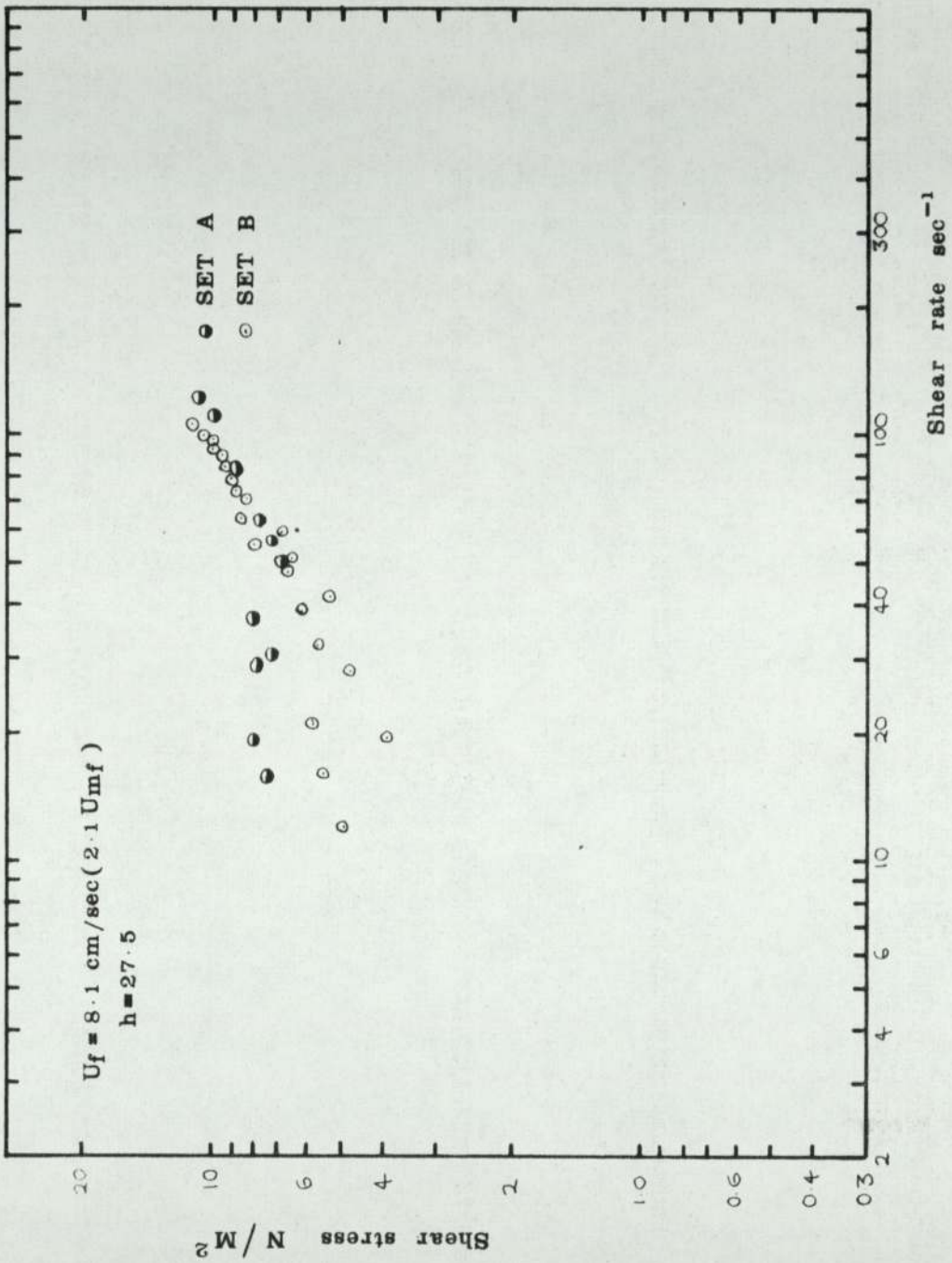
● SET A
⊙ SET B
U_f = 8·1 cm/sec(2·1 Umf)
h = 27·5
Shear stress N / M²
Shear rate sec⁻¹
20
10
6
4
2
1·0
0·6
0·4
0·3
2
4
6
10
20
40
100
300

Figure 4.4

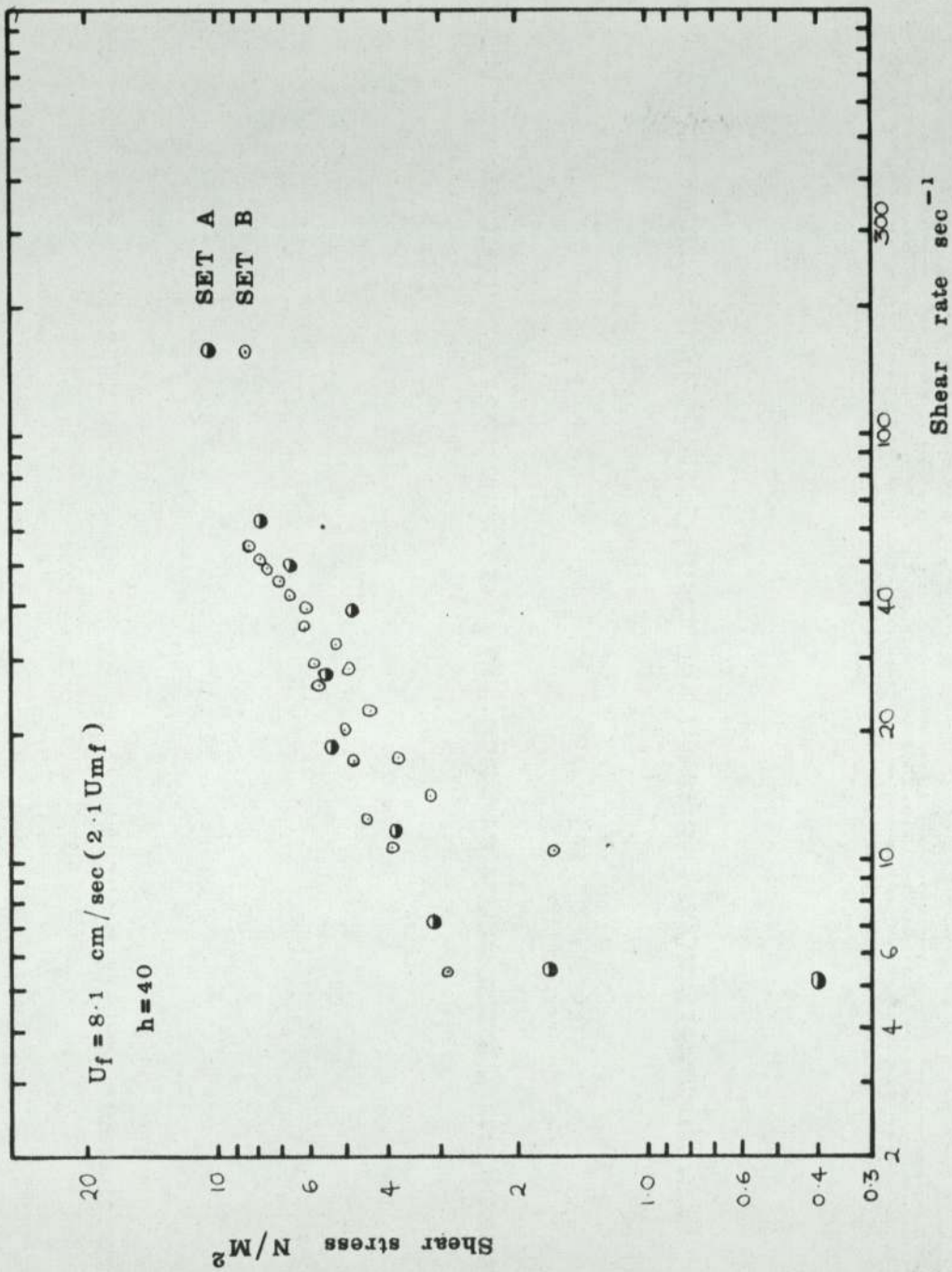
SET A
SET B
$U_f = 8{\cdot}1$ cm/sec ($2{\cdot}1 U_{mf}$)
h = 40
Shear stress N/M²
Shear rate sec⁻¹
20
10
6
4
2
1·0
0·6
0·4
0·3
2
4
6
10
20
40
100
300

Figure 4.5

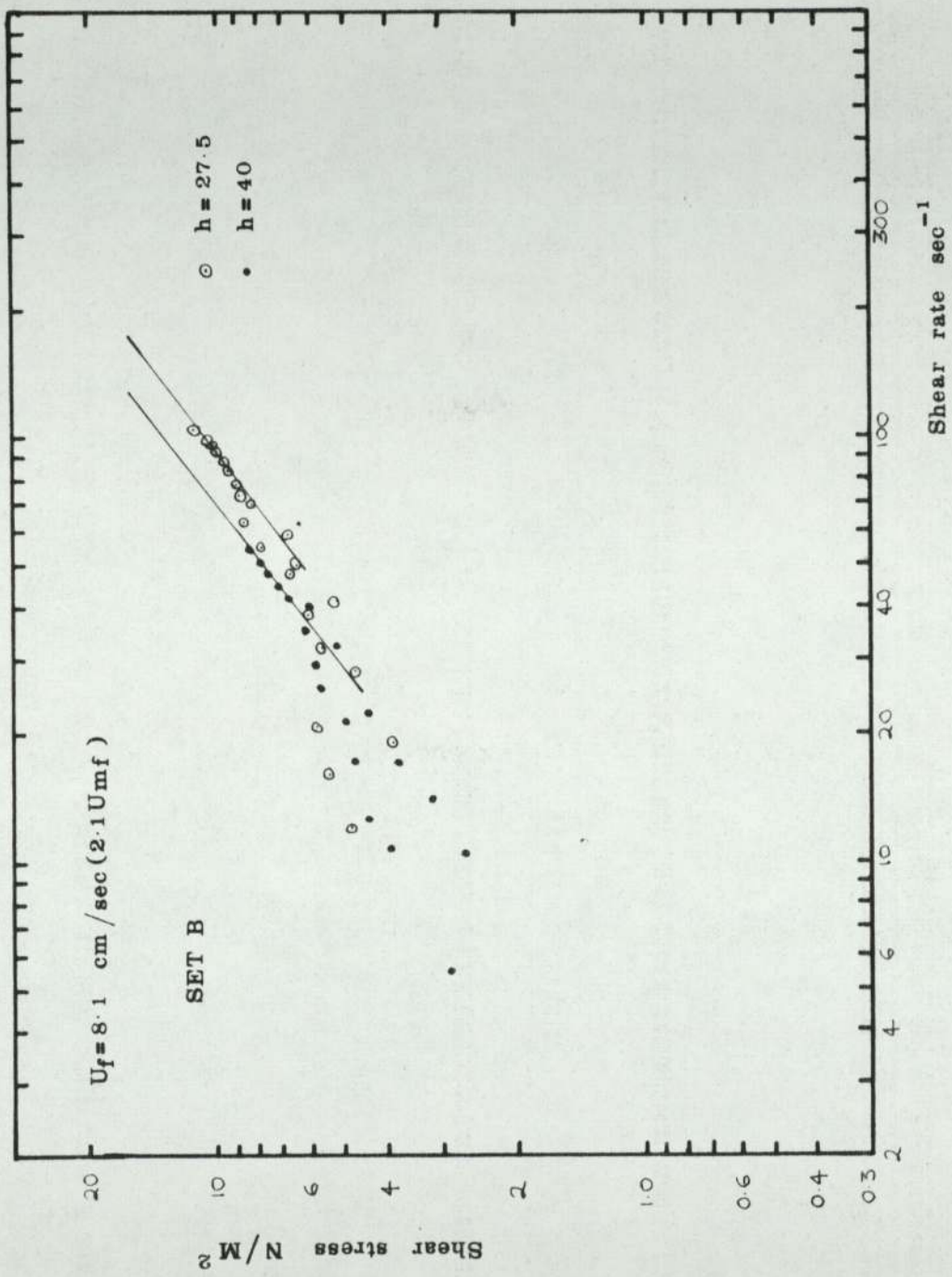
Shear stress N/M²
20
10
6
4
2
1.0
0.6
0.4
0.3
2
4
6
10
20
40
100
300
Shear rate sec⁻¹
SET B
Uf = 8·1 cm/sec (2·1 Umf)
⊙ h = 27·5
• h = 40

Figure 4.6

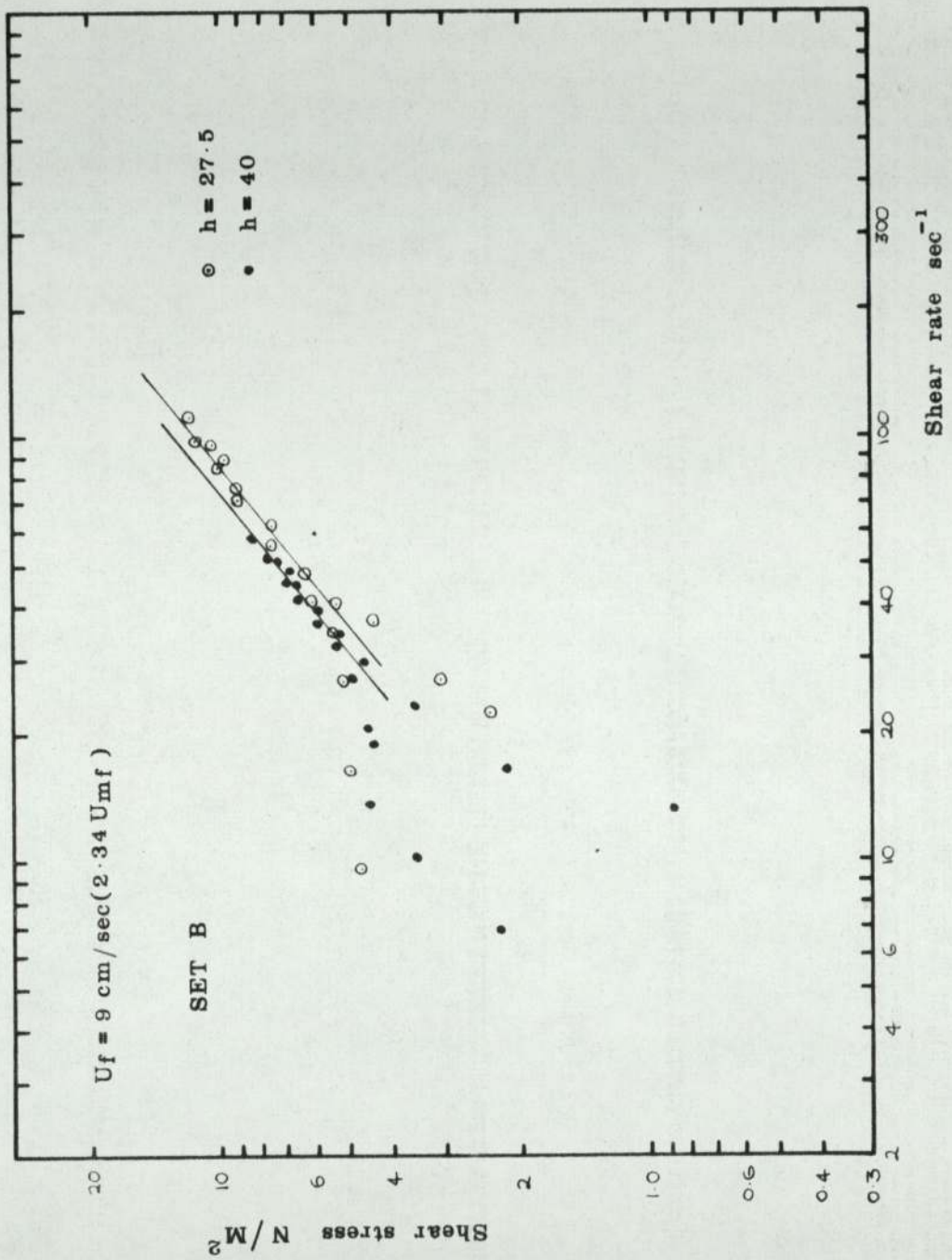
Shear stress N/M²
Shear rate sec⁻¹
Uf = 9 cm/sec(2·34 Umf)
SET B
⊙ h = 27·5
• h = 40
20
10
6
4
2
1·0
0·6
0·4
0·3
2
4
6
10
20
40
100
300

Figure 4.7

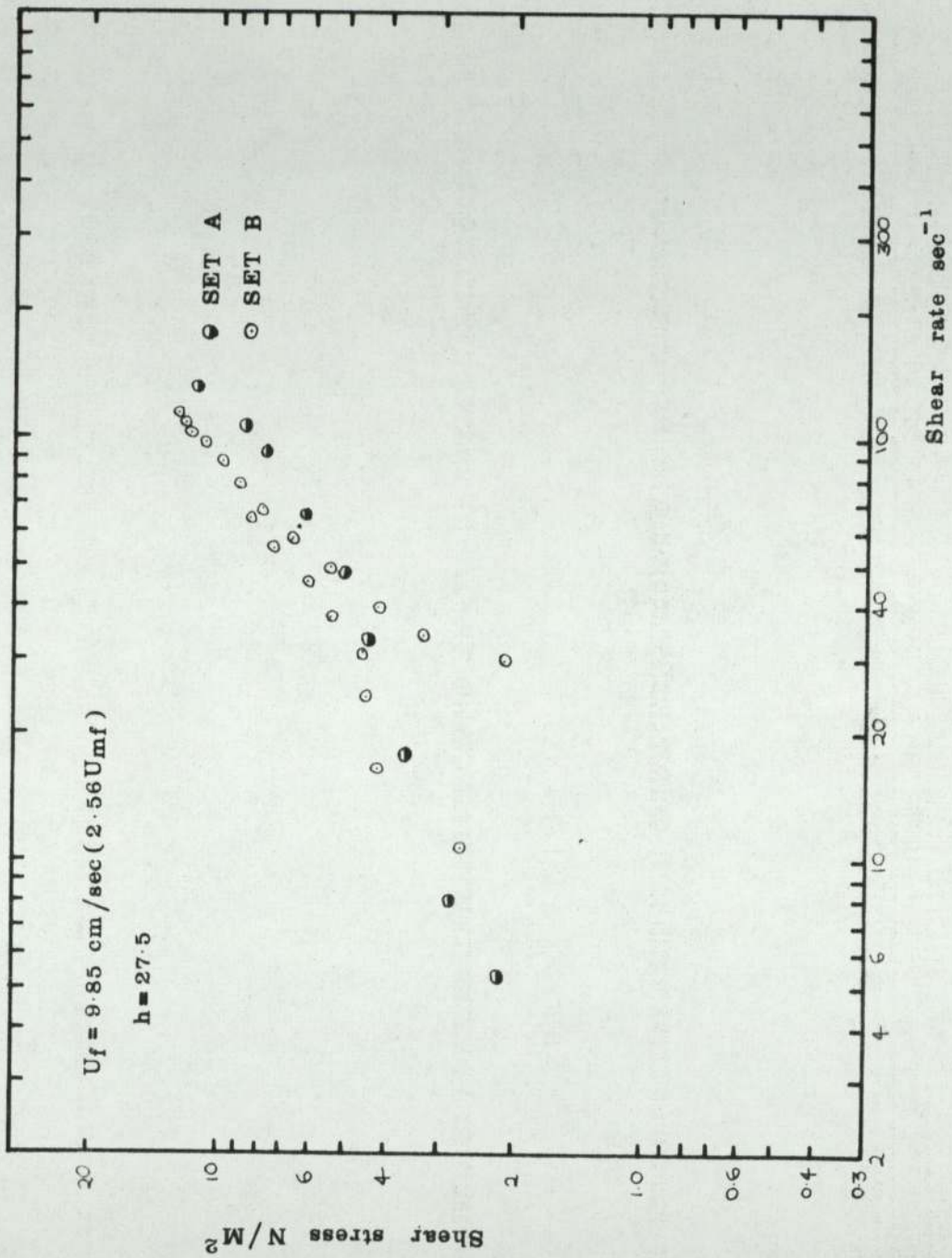
SET A
SET B
U_f = 9.85 cm/sec (2.56U_{mf})
h = 27.5
Shear stress N/M²
Shear rate sec⁻¹
20
10
6
4
2
1.0
0.6
0.4
0.3
2
4
6
10
20
40
100
300

Figure 4.8

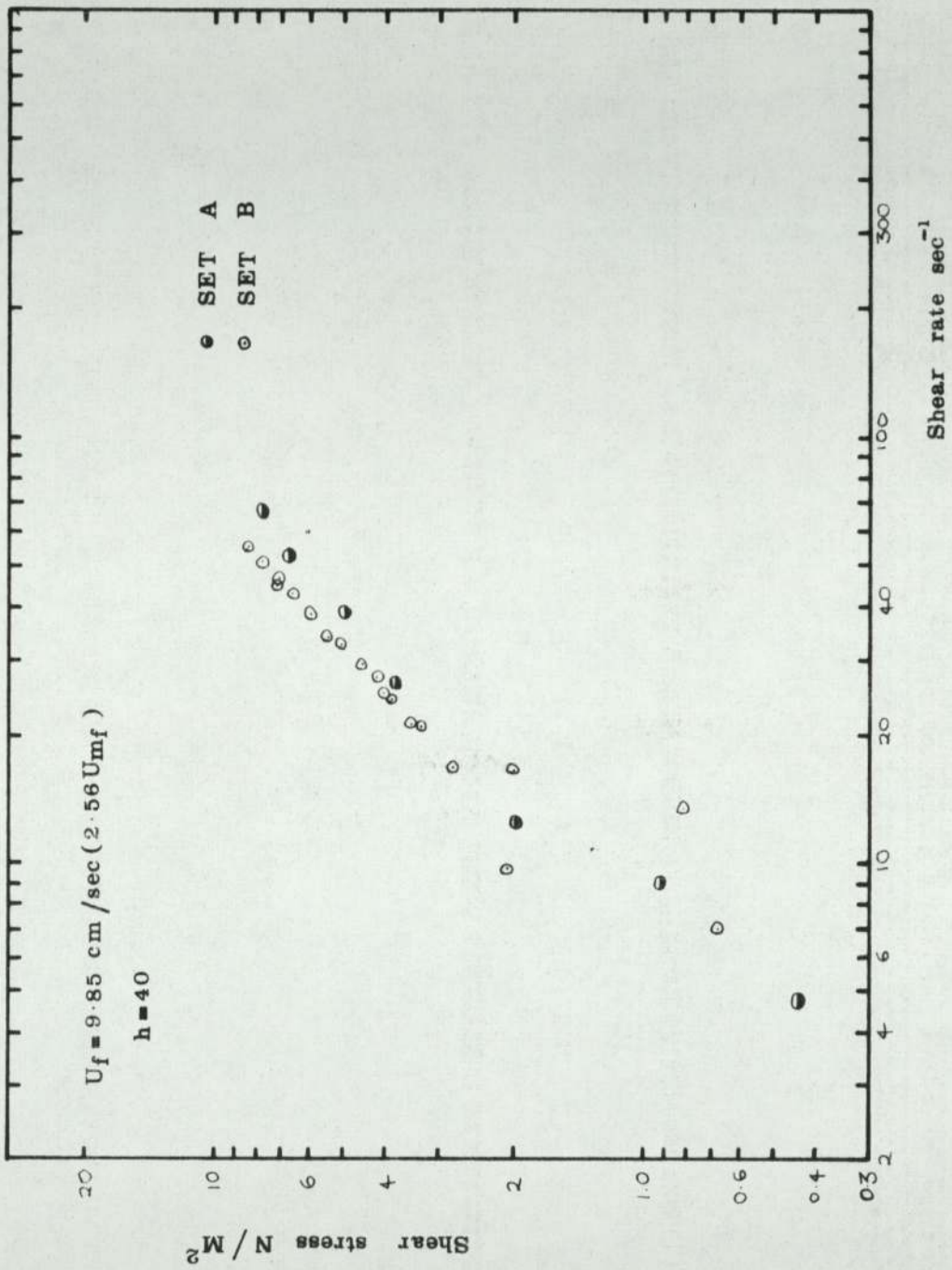
Shear stress N / M²
Shear rate sec⁻¹
● SET A
○ SET B
Uf = 9·85 cm /sec (2·56 Umf)
h = 40
20
10
6
4
2
1·0
0·6
0·4
0·3
2
4
6
10
20
40
100
300

Figure 4.9

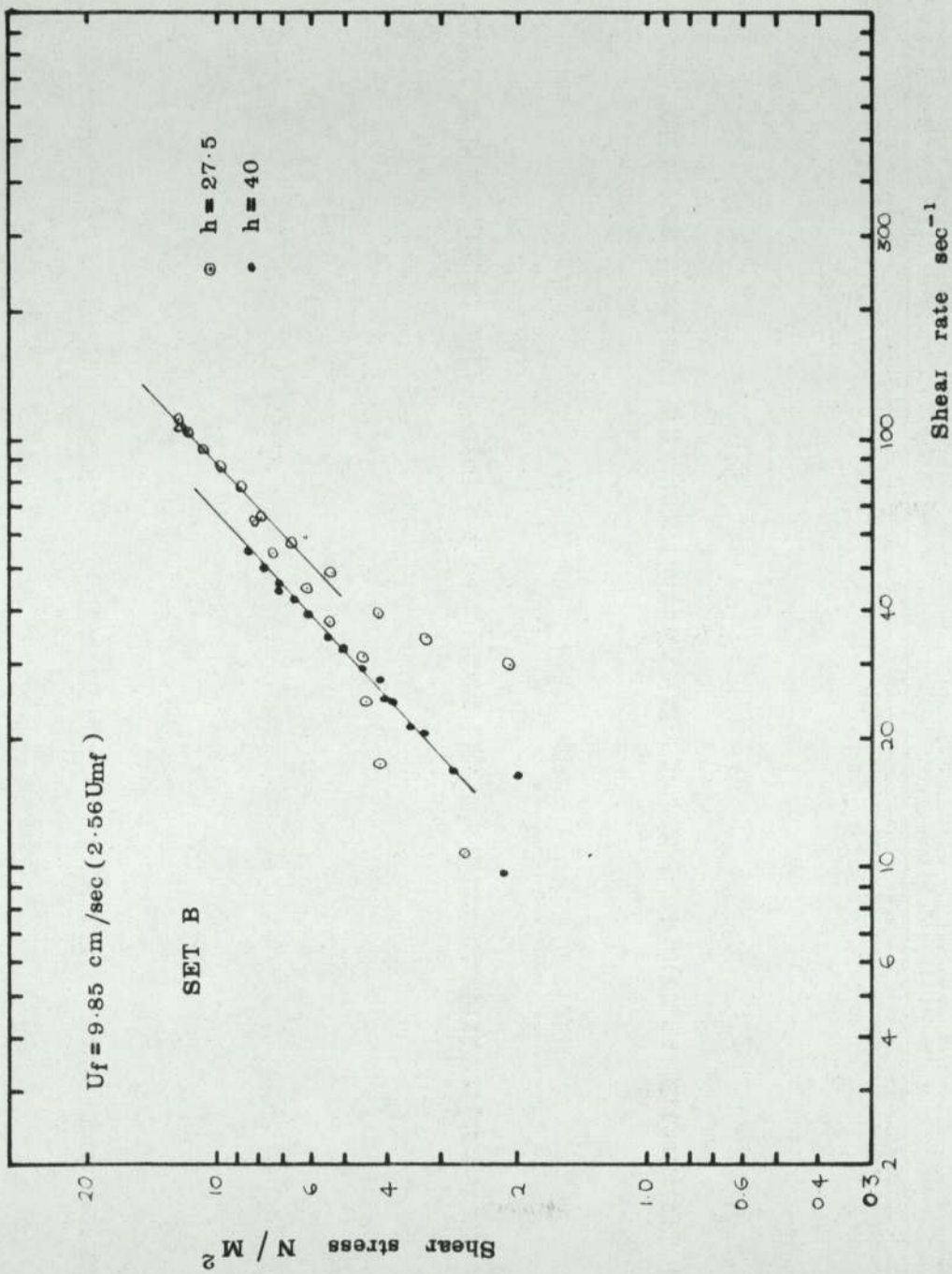
Shear stress N / M²
Shear rate sec⁻¹
Uf = 9·85 cm/sec (2·56Umf)
SET B
h = 27·5
h = 40
20
10
6
4
2
1·0
0·6
0·4
0·3
2
4
6
10
20
40
100
300

Figure 4.10

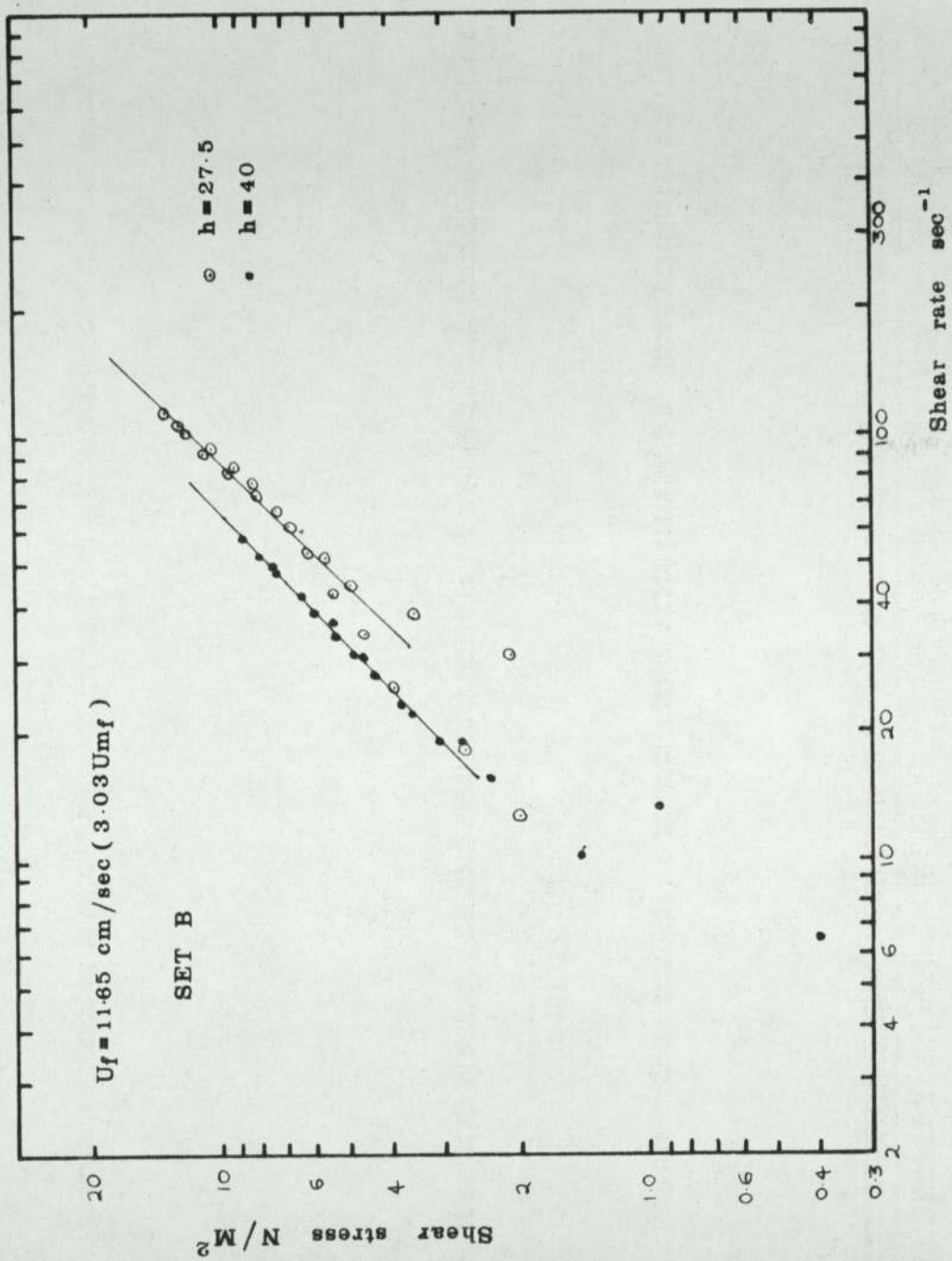
Shear stress N/M²
Shear rate sec⁻¹
Uf = 11·65 cm/sec (3·03 Umf)
SET B
h = 27·5
h = 40
20
10
6
4
2
1·0
0·6
0·4
0·3
2
4
6
10
20
40
100
300

Figure 4.11

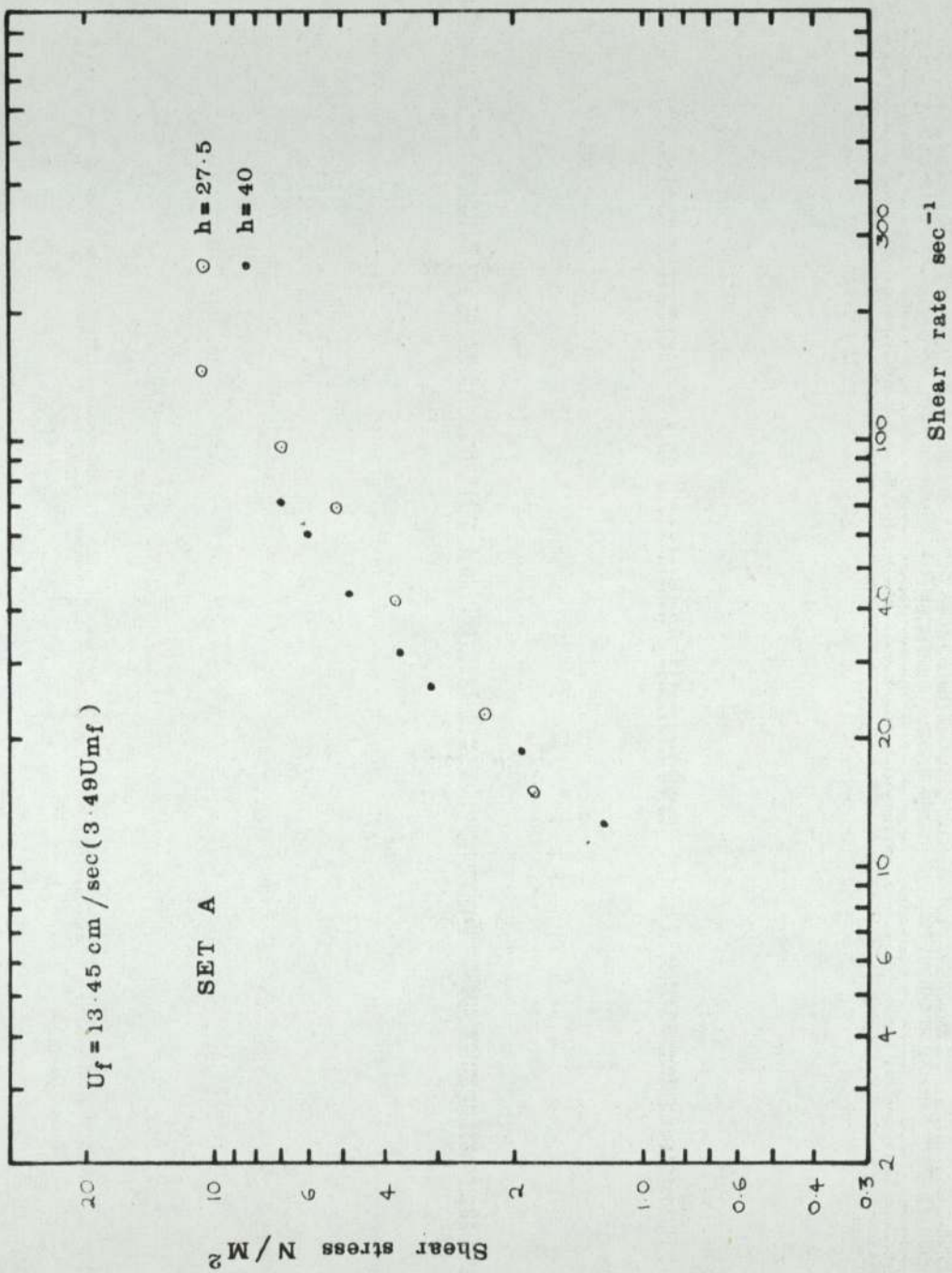
h = 27·5
h = 40
SET A
U_f = 13·45 cm / sec (3·49 U_{mf})
Shear stress N / M²
Shear rate sec⁻¹
20
10
6
4
2
1·0
0·6
0·4
0·3
2
4
6
10
20
40
100
300

Figure 4.12

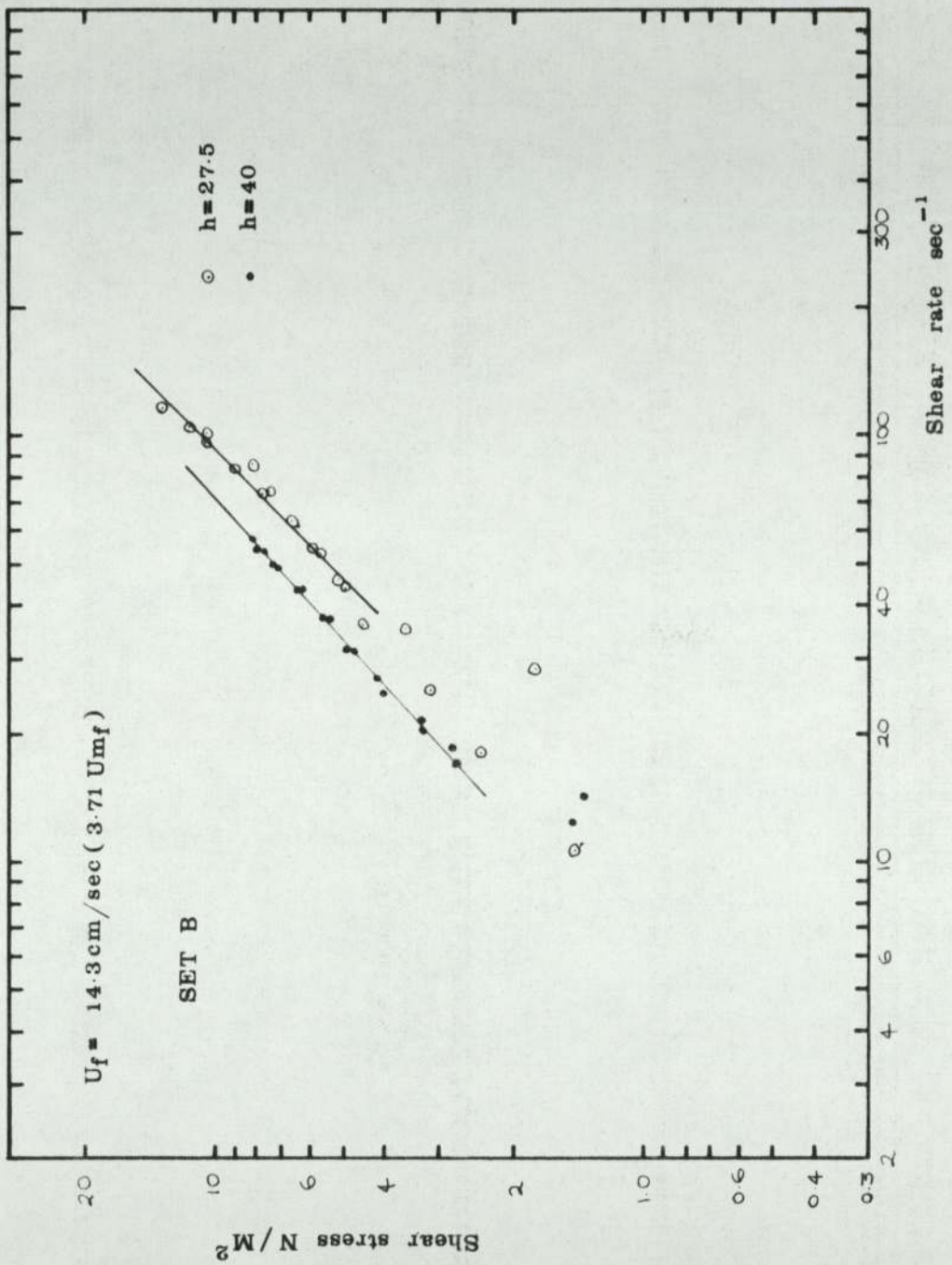
h=27.5
h=40
Uf= 14.3 cm/sec (3.71 Umf)
SET B
Shear stress N/M²
Shear rate sec⁻¹
20
10
6
4
2
1.0
0.6
0.4
0.3
2
4
6
10
20
40
100
300

Figure 4.13

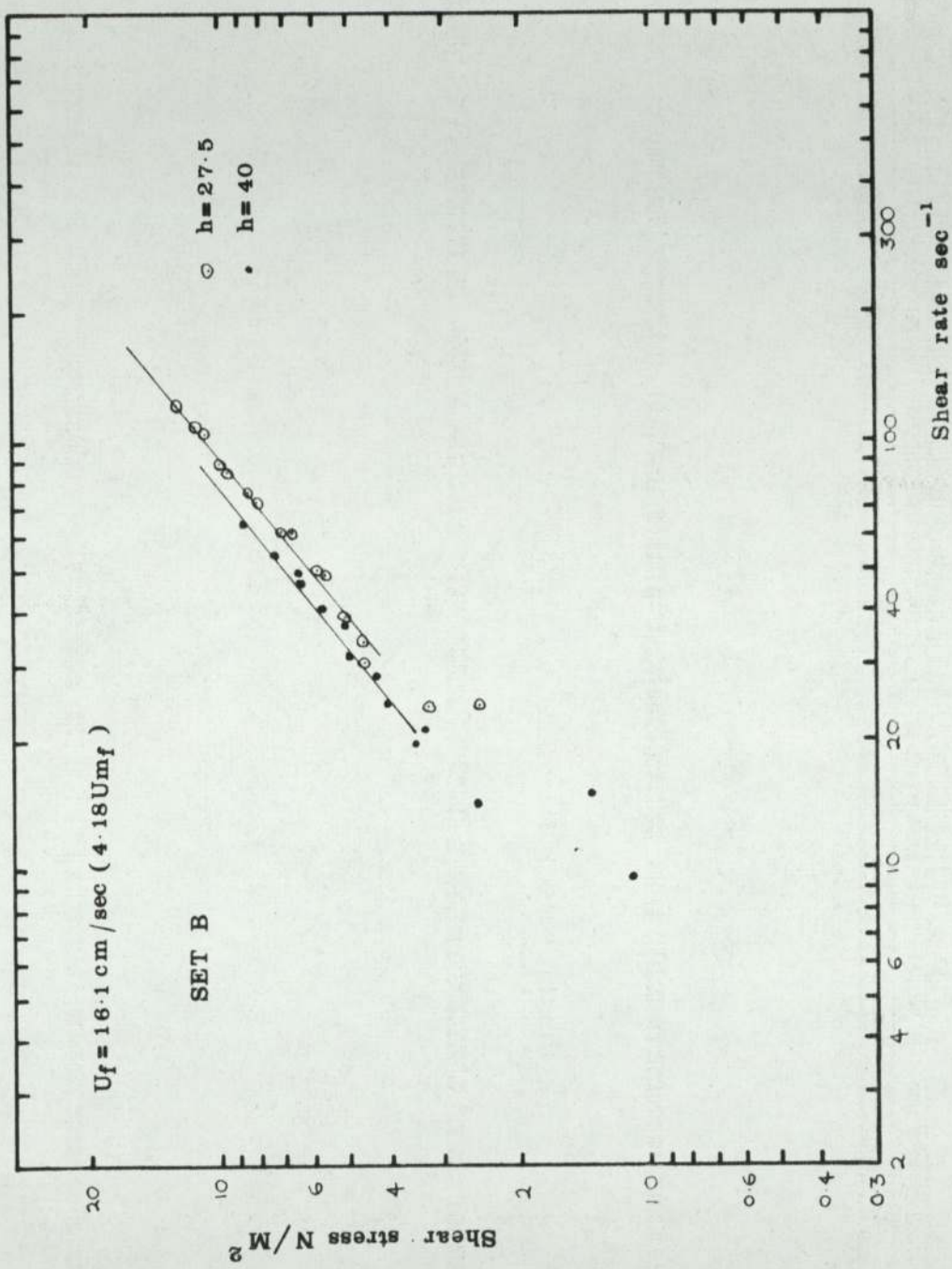
Shear stress N/M²
Shear rate sec⁻¹
Uf = 16·1 cm/sec (4·18Umf)
SET B
h = 27·5
h = 40
20
10
6
4
2
1
0·6
0·4
0·3
2
4
6
10
20
40
100
300

Figure 4.14

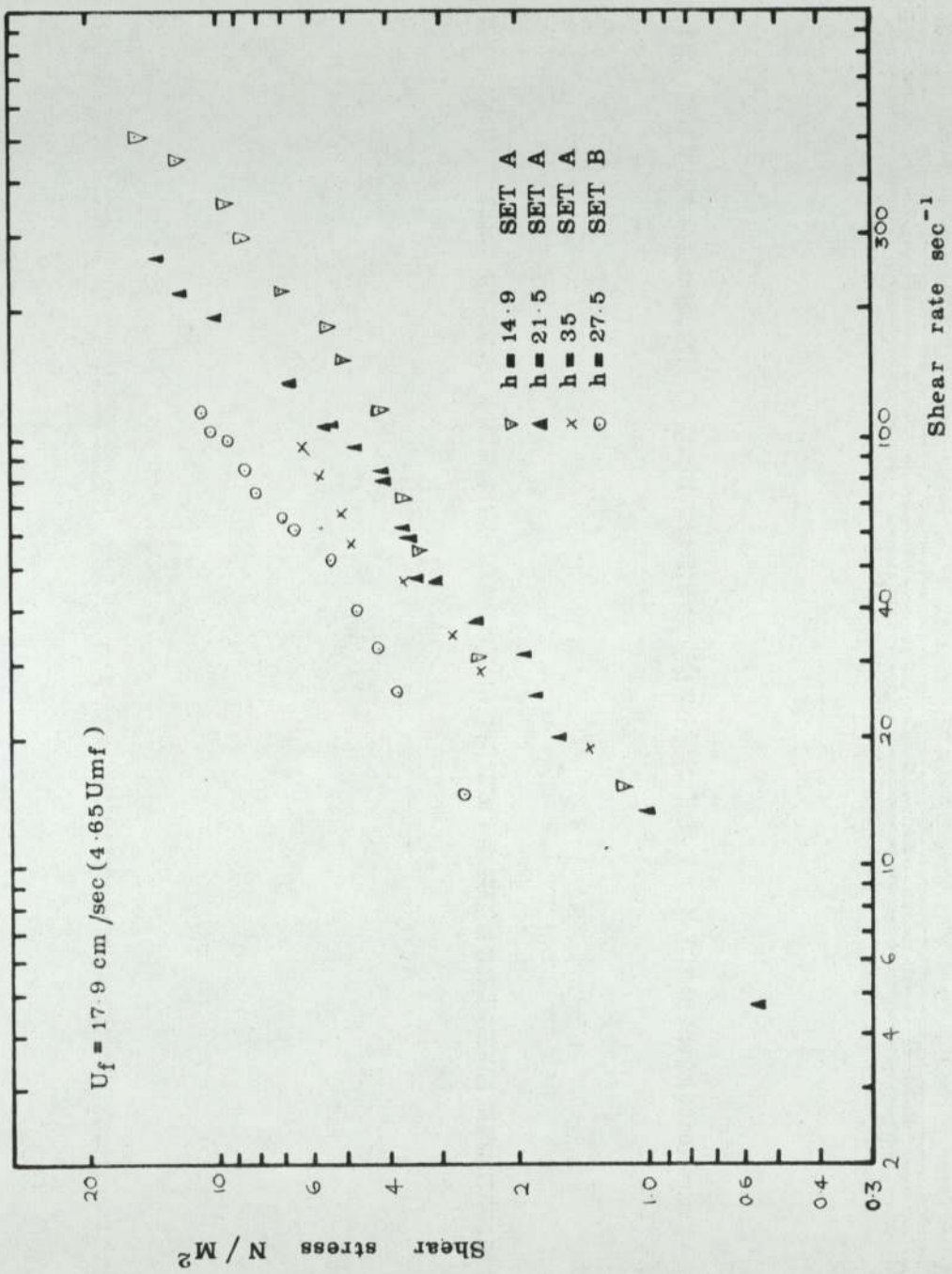
Shear stress N / M²
Shear rate sec⁻¹
Uf = 17·9 cm /sec (4·65 Umf)
h = 14·9 SET A
h = 21·5 SET A
h = 35 SET A
h = 27·5 SET B
20
10
6
4
2
1·0
0·6
0·4
0·3
2
4
6
10
20
40
100
300

Figure 4.15

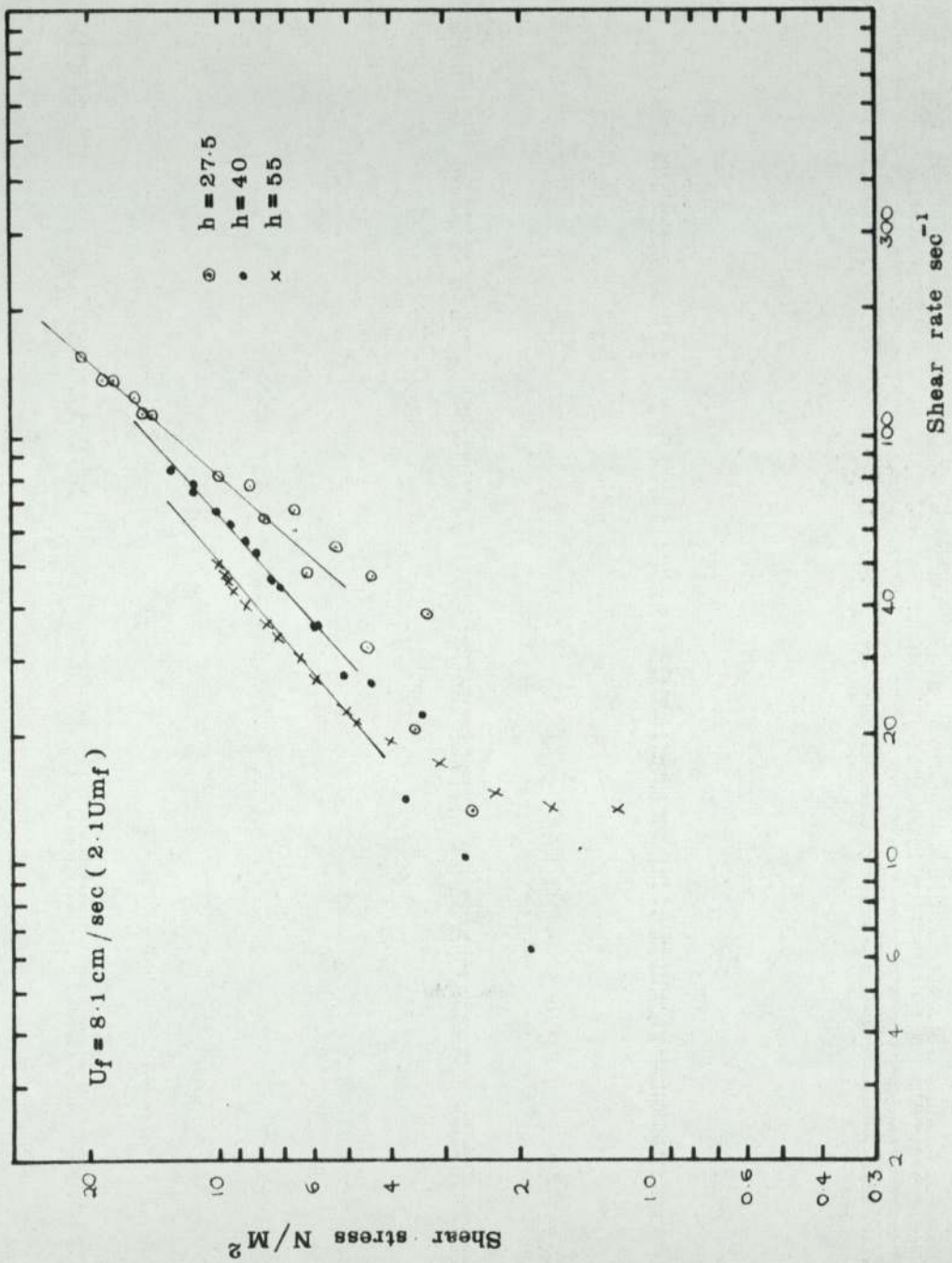
h = 27·5
h = 40
h = 55
U_f = 8·1 cm / sec (2·1Umf)
Shear stress N/M²
Shear rate sec⁻¹
20
10
6
4
2
1·0
0·6
0·4
0·3
2
4
6
10
20
40
100
300

Figure 4.16

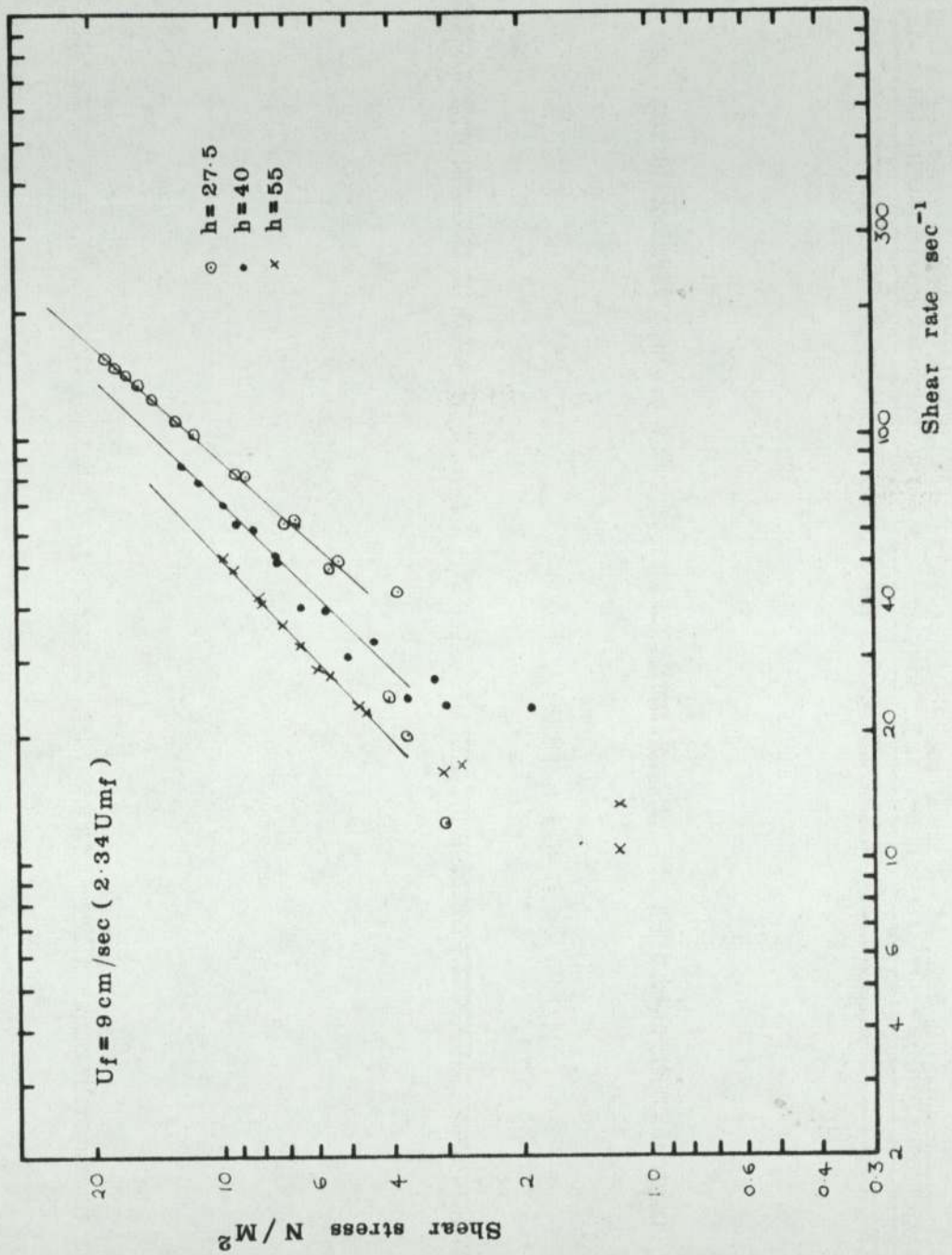
Uf = 9 cm/sec (2·34 Umf)
h = 27·5
h = 40
h = 55
Shear stress N / M²
Shear rate sec⁻¹
20
10
6
4
2
1·0
0·6
0·4
0·3
2
4
6
10
20
40
100
300

Figure 4.17

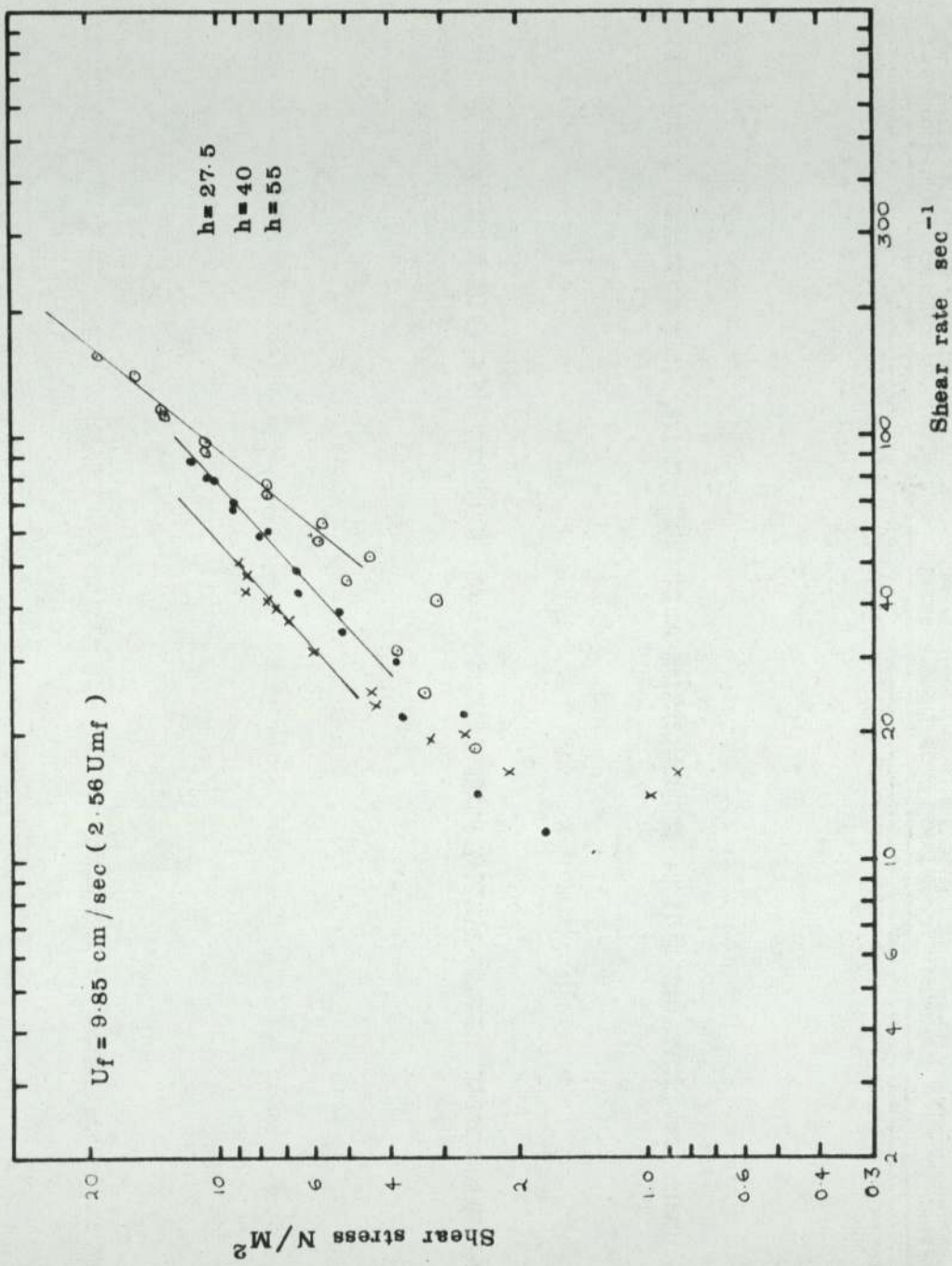
h=27.5
h=40
h=55
U_f = 9.85 cm/sec (2.56 Umf)
Shear stress N/M²
Shear rate sec⁻¹
20
10
6
4
2
1.0
0.6
0.4
0.3
2
4
6
10
20
40
100
300

Figure 4.18

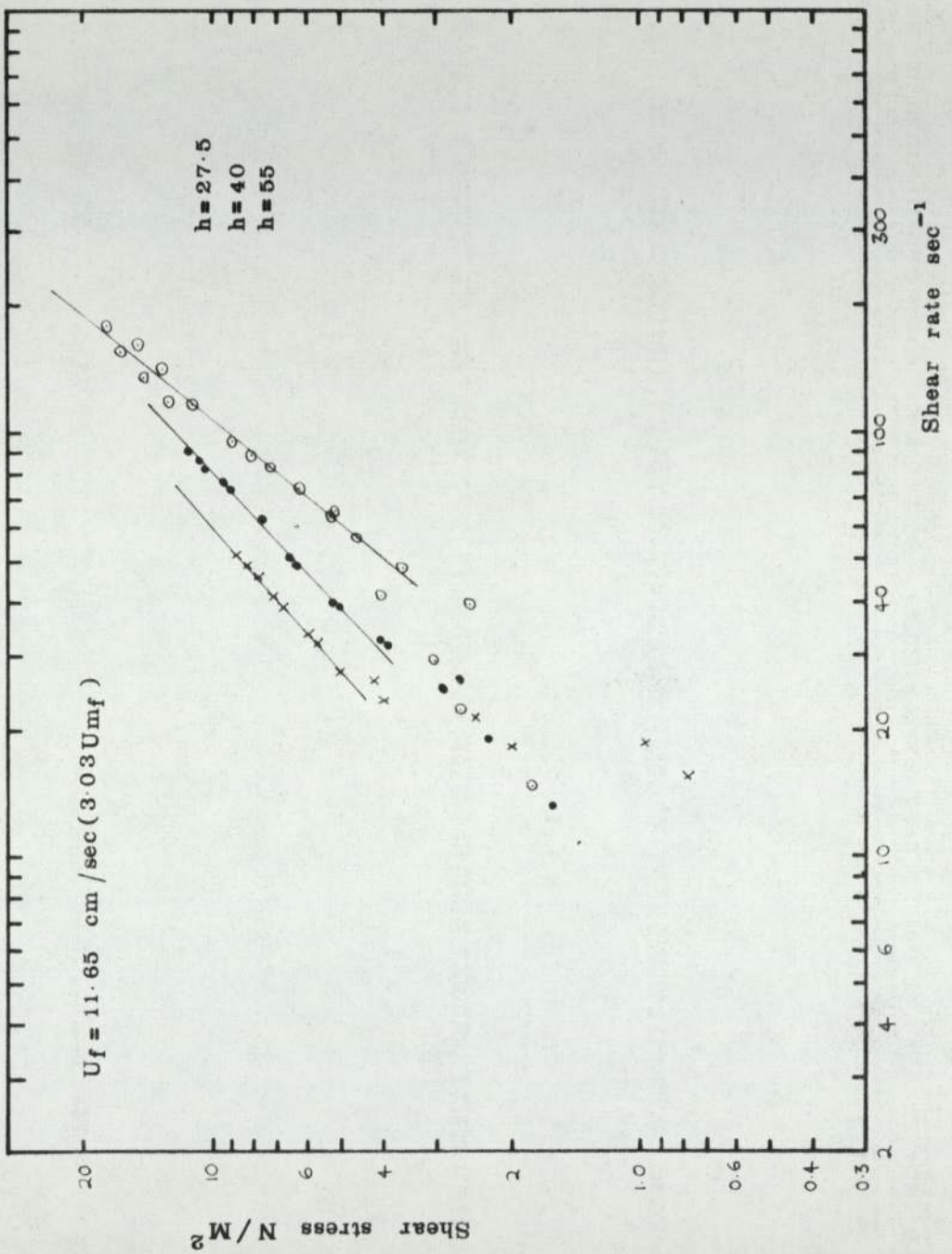
h=27·5
h=40
h=55
U_f = 11·65 cm /sec (3·03 U_{mf})
Shear stress N / M²
Shear rate sec⁻¹
20
10
6
4
2
1·0
0·6
0·4
0·3
2
4
6
10
20
40
100
300

Figure 4.19

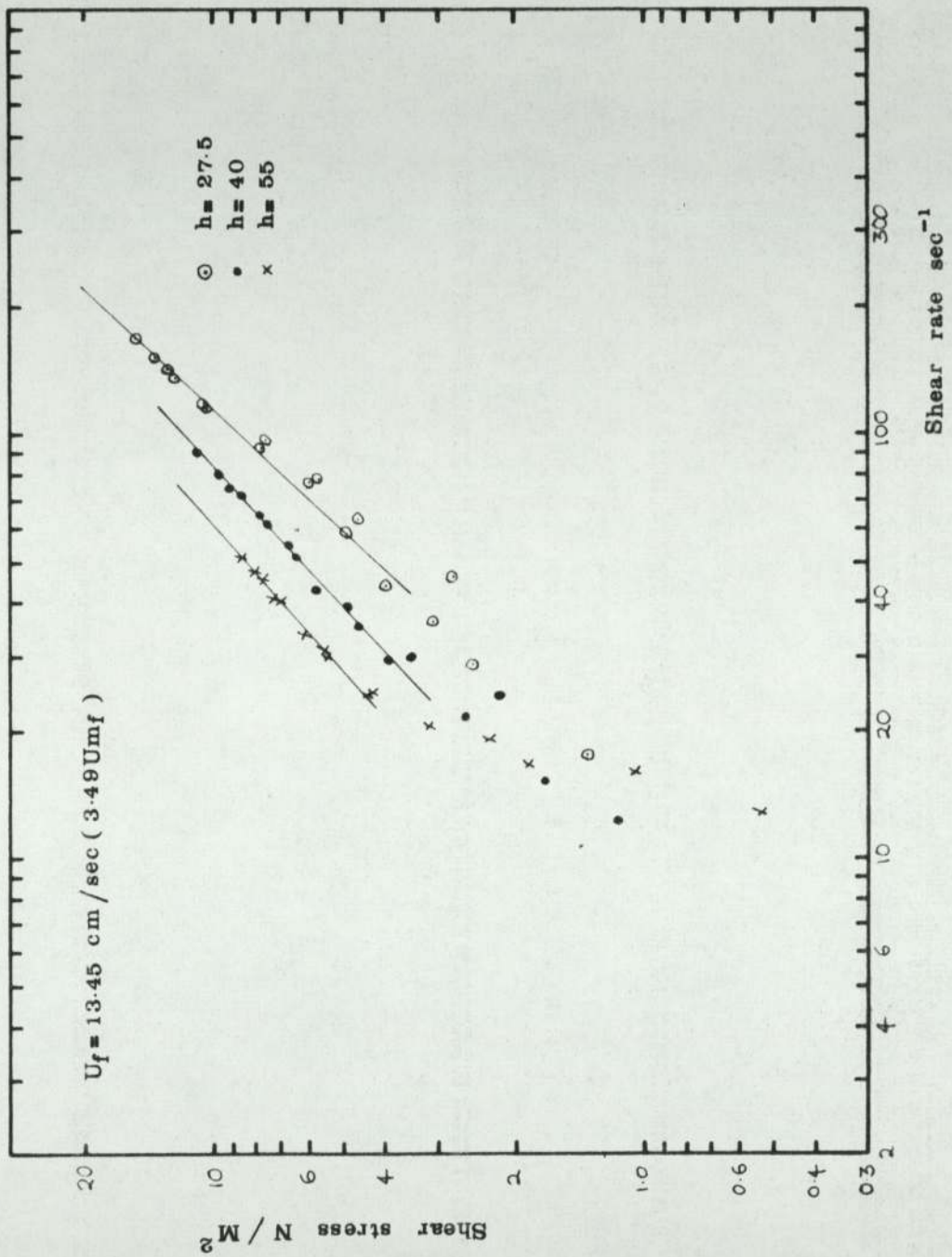
h= 27·5
h= 40
h= 55
U_f = 13·45 cm/sec (3·49Umf)
Shear stress N / M²
Shear rate sec⁻¹
20
10
6
4
2
1·0
0·6
0·4
0·3
2
4
6
10
20
40
100
300

Figure 4.20

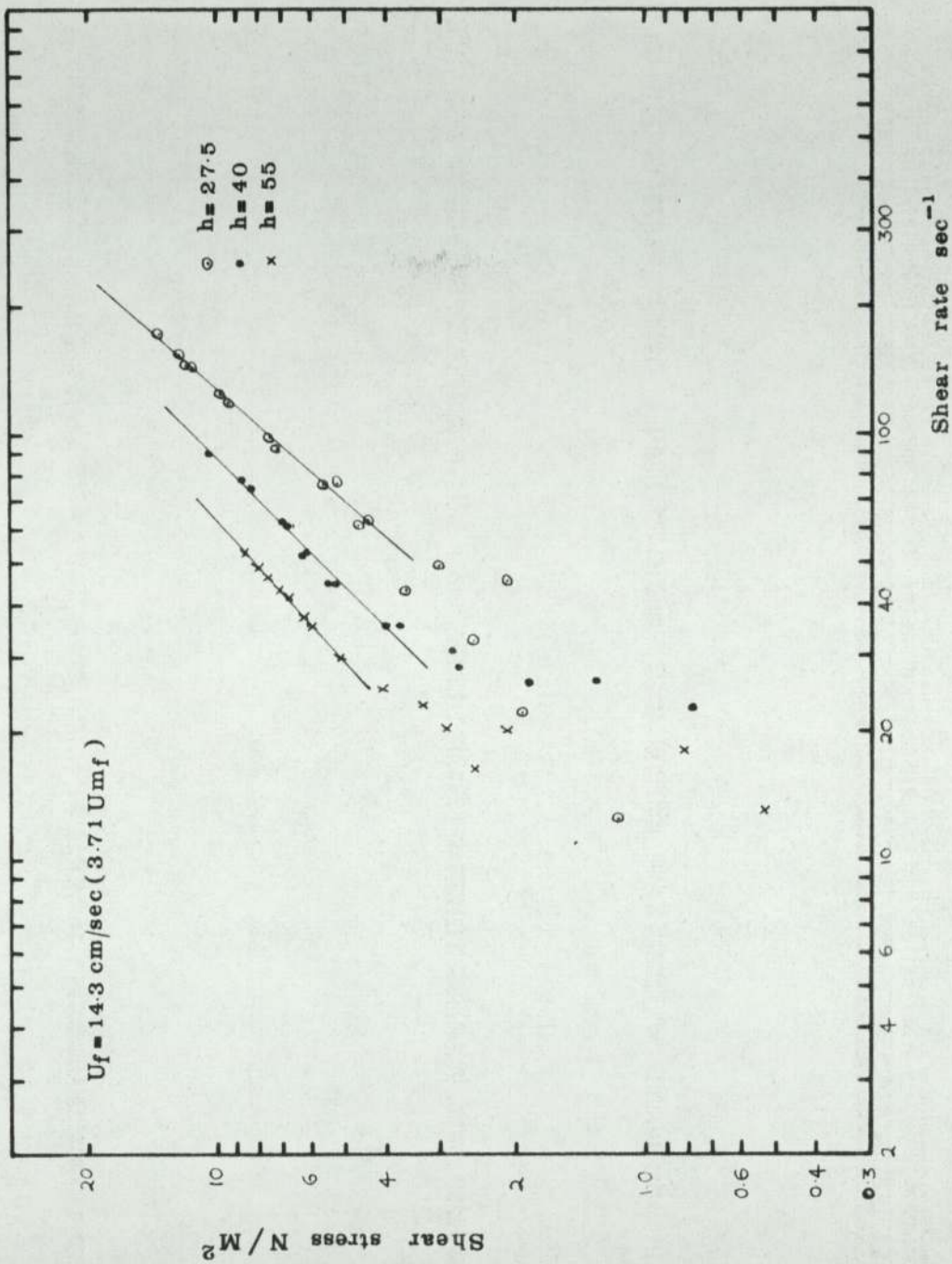
Shear stress N/M²
Shear rate sec⁻¹
Uf = 14·3 cm/sec (3·71 Umf)
h = 27·5
h = 40
h = 55
20
10
6
4
2
1·0
0·6
0·4
0·3
2
4
6
10
20
40
100
300

Figure 4.21

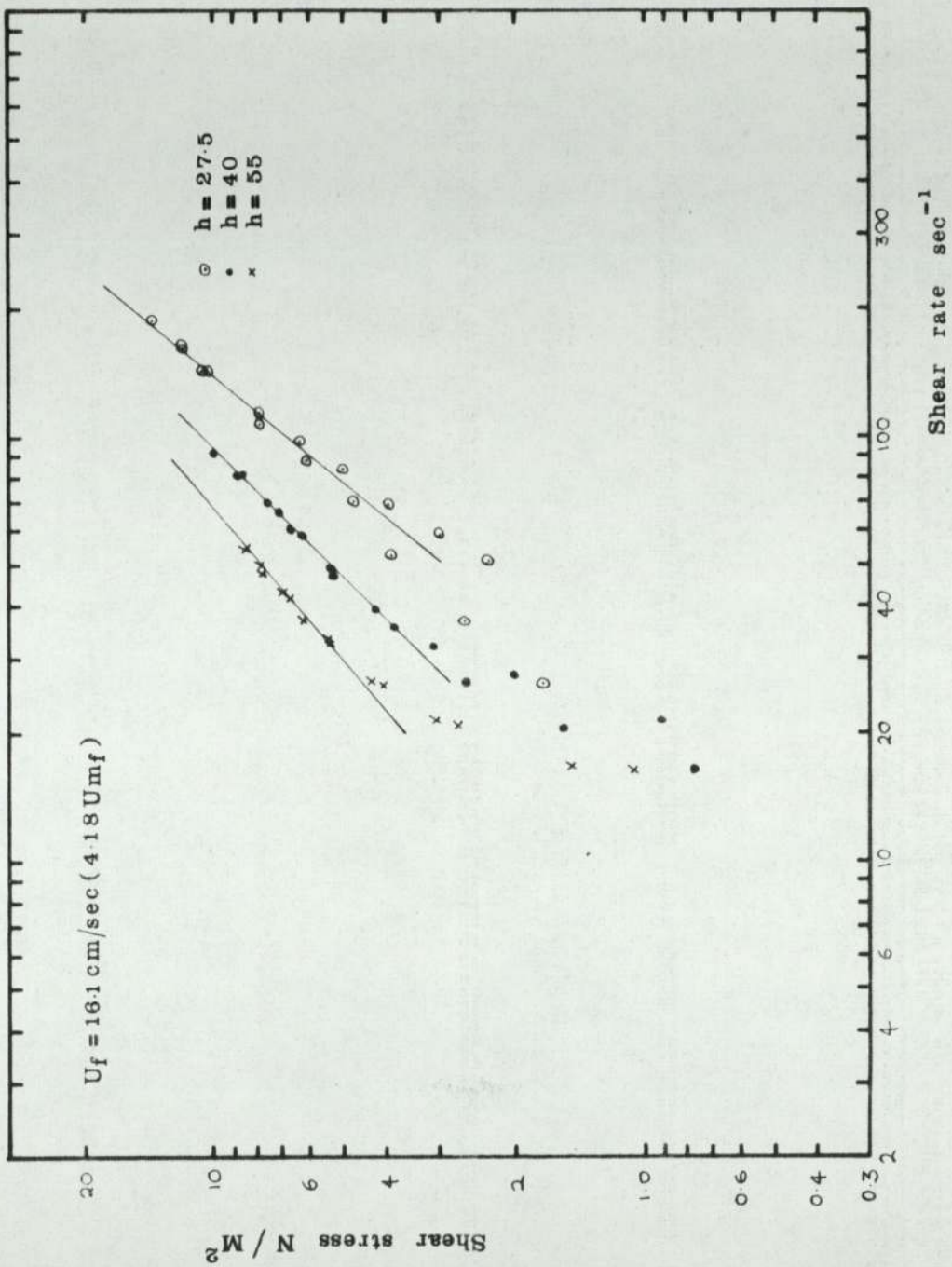
Shear stress N / M²
Shear rate sec⁻¹
Uf = 16·1 cm/sec (4·18 Umf)
h = 27·5
h = 40
h = 55
20
10
6
4
2
1·0
0·6
0·4
0·3
2
4
6
10
20
40
100
300

Figure 4.22

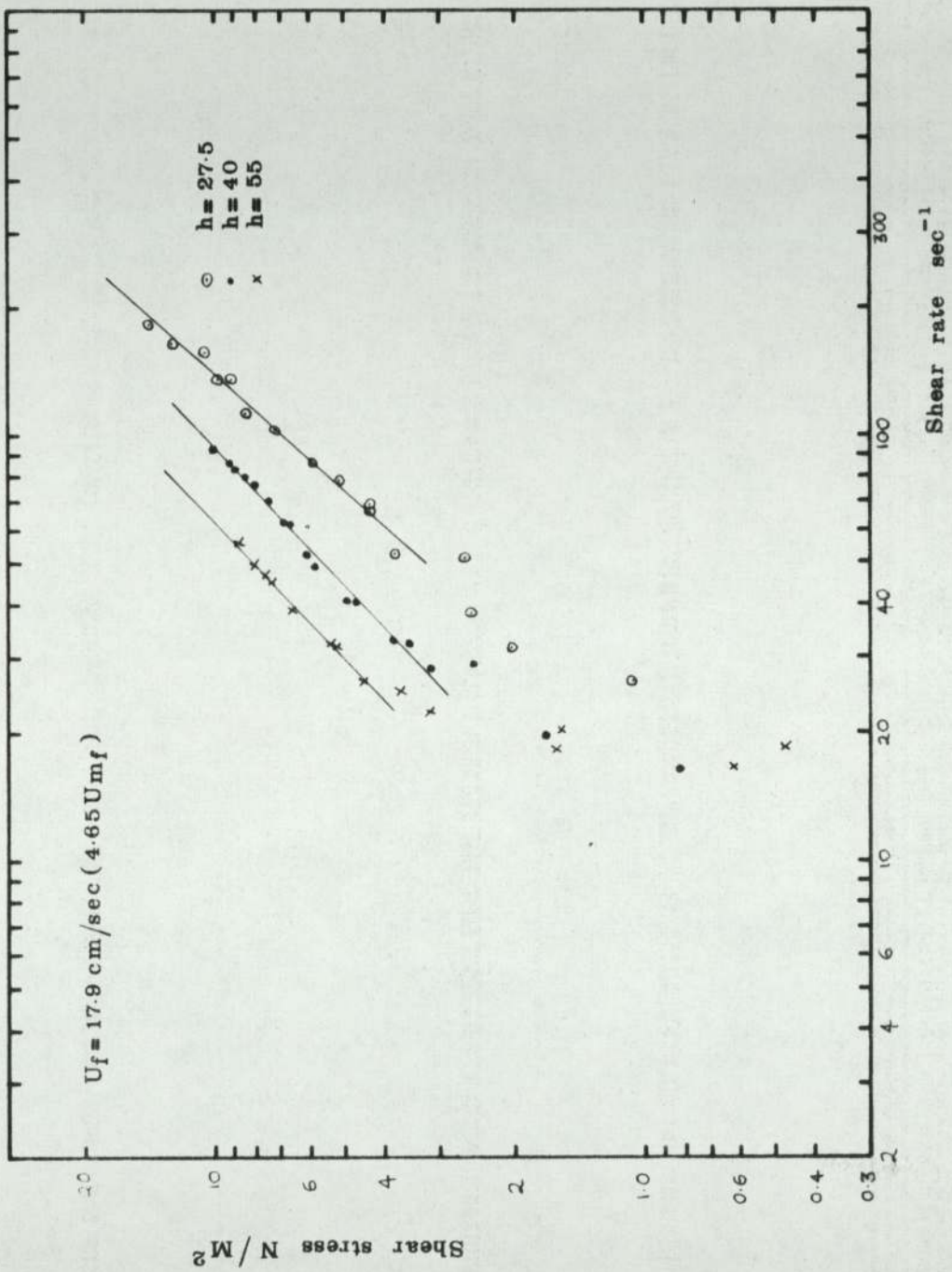
h= 27·5
h= 40
h= 55
Uf = 17·9 cm/sec (4·65 Umf)
Shear stress N/M²
Shear rate sec⁻¹
0·3
0·4
0·6
1·0
2
4
6
10
20
40
100
300

Figure 4.23

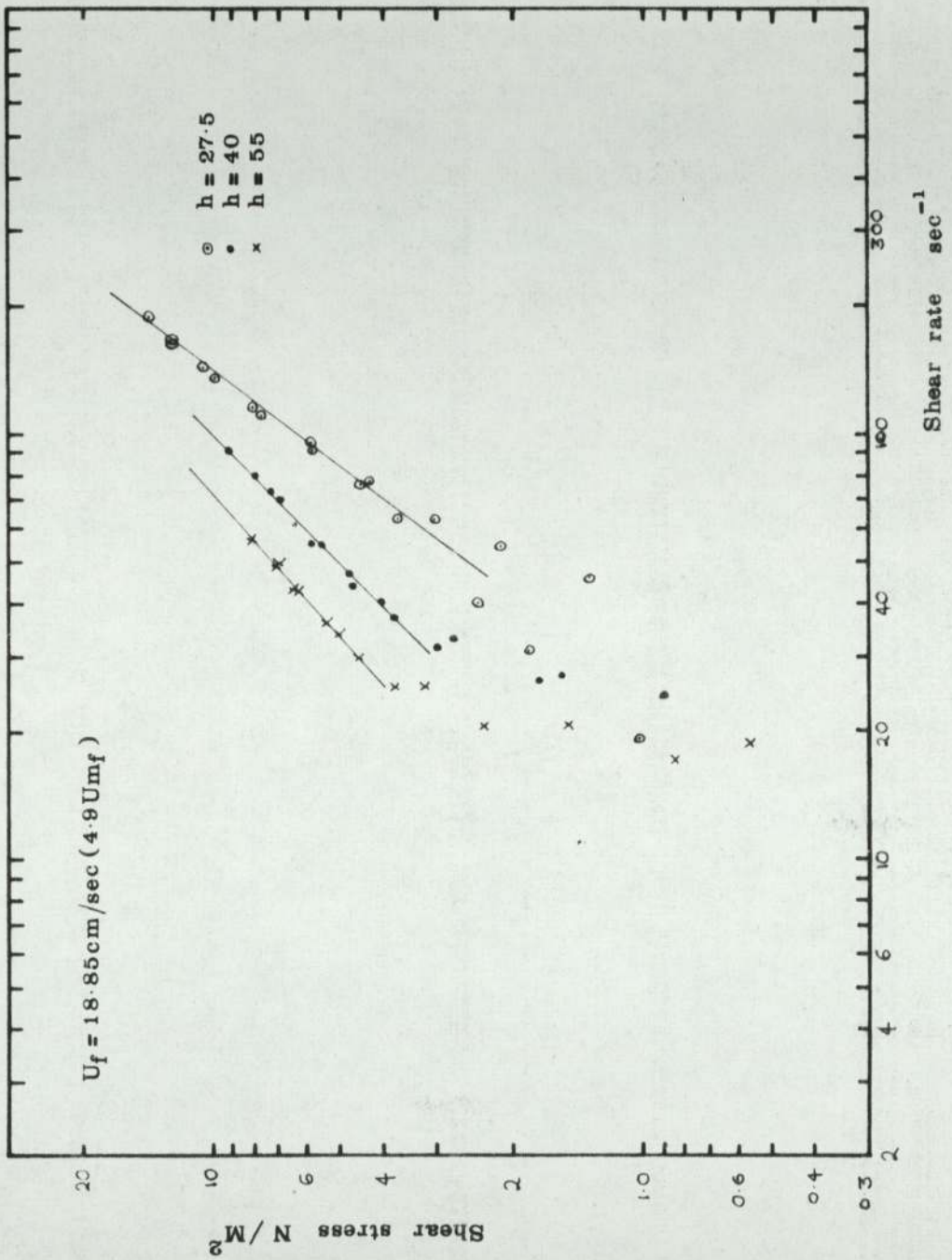
h = 27·5
h = 40
h = 55
U_f = 18·85cm/sec (4·9U_{mf})
Shear stress N/M²
Shear rate sec⁻¹
20
10
6
4
2
1·0
0·6
0·4
0·3
2
4
6
10
20
40
100
300

Figure 4.24

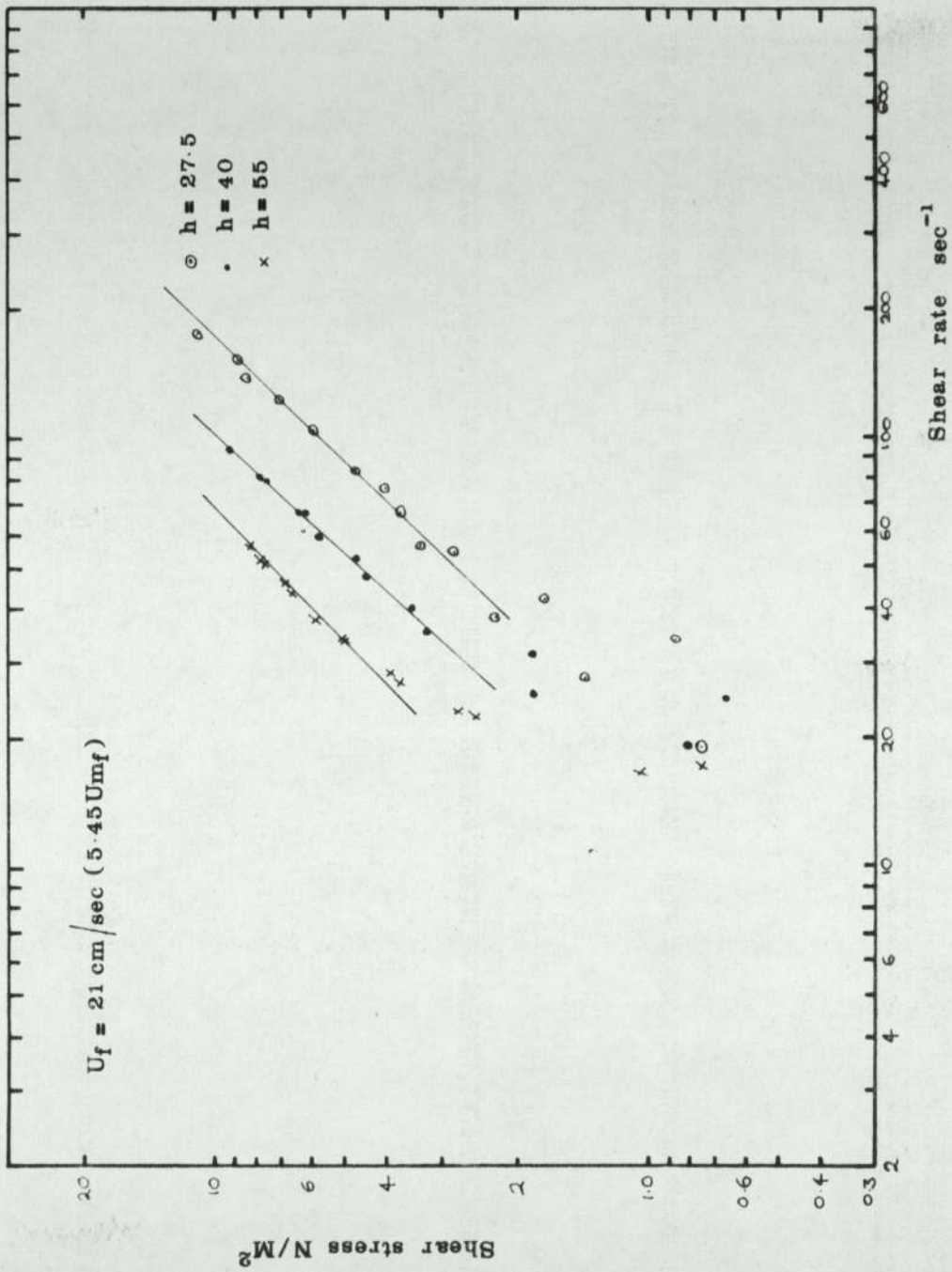
Shear stress N/M²
Shear rate sec⁻¹
Uf = 21 cm/sec (5·45Umf)
⊙ h = 27·5
• h = 40
× h = 55
0·3
0·4
0·6
1·0
2
4
6
10
20
40
60
100
200
400
800
2·0
4
6
10

Figure 4.25

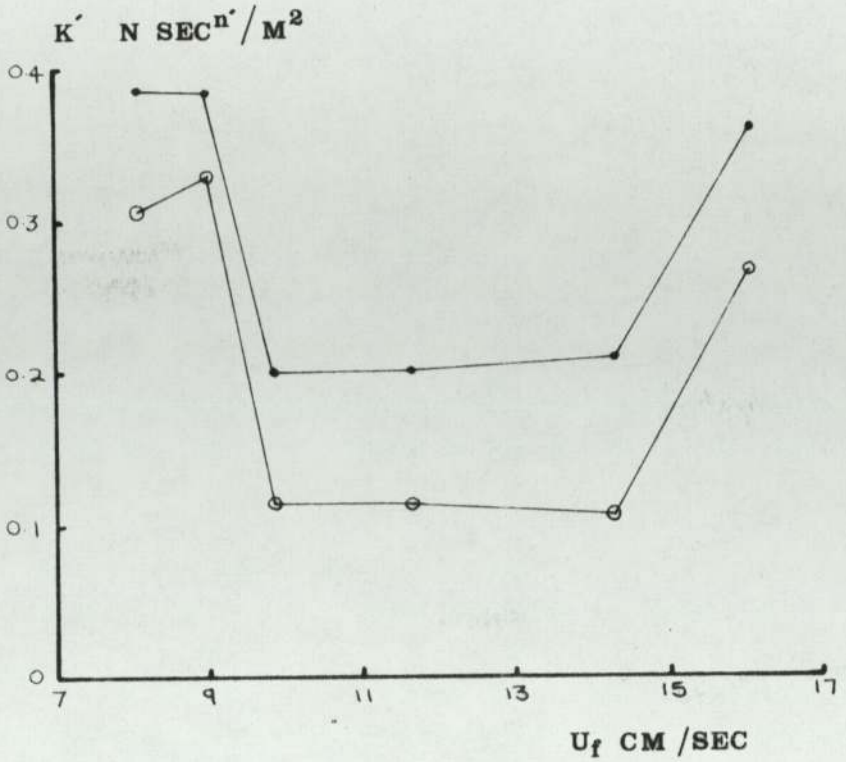

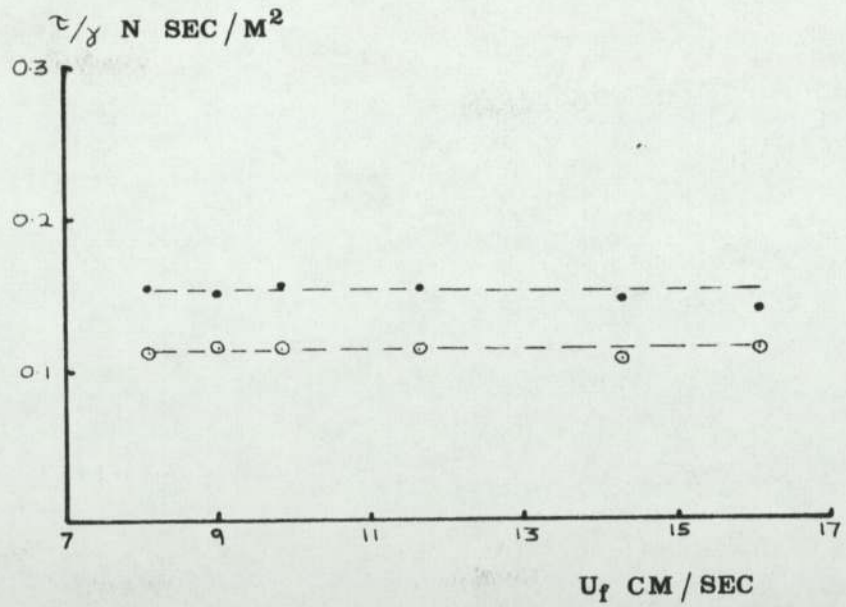

CHANNEL WIDTH = 150 mm

VARIATION OF K´ AND τ/γ WITH FLUIDISING VELOCITY FOR WIDE CHANNEL

Figure 4.26

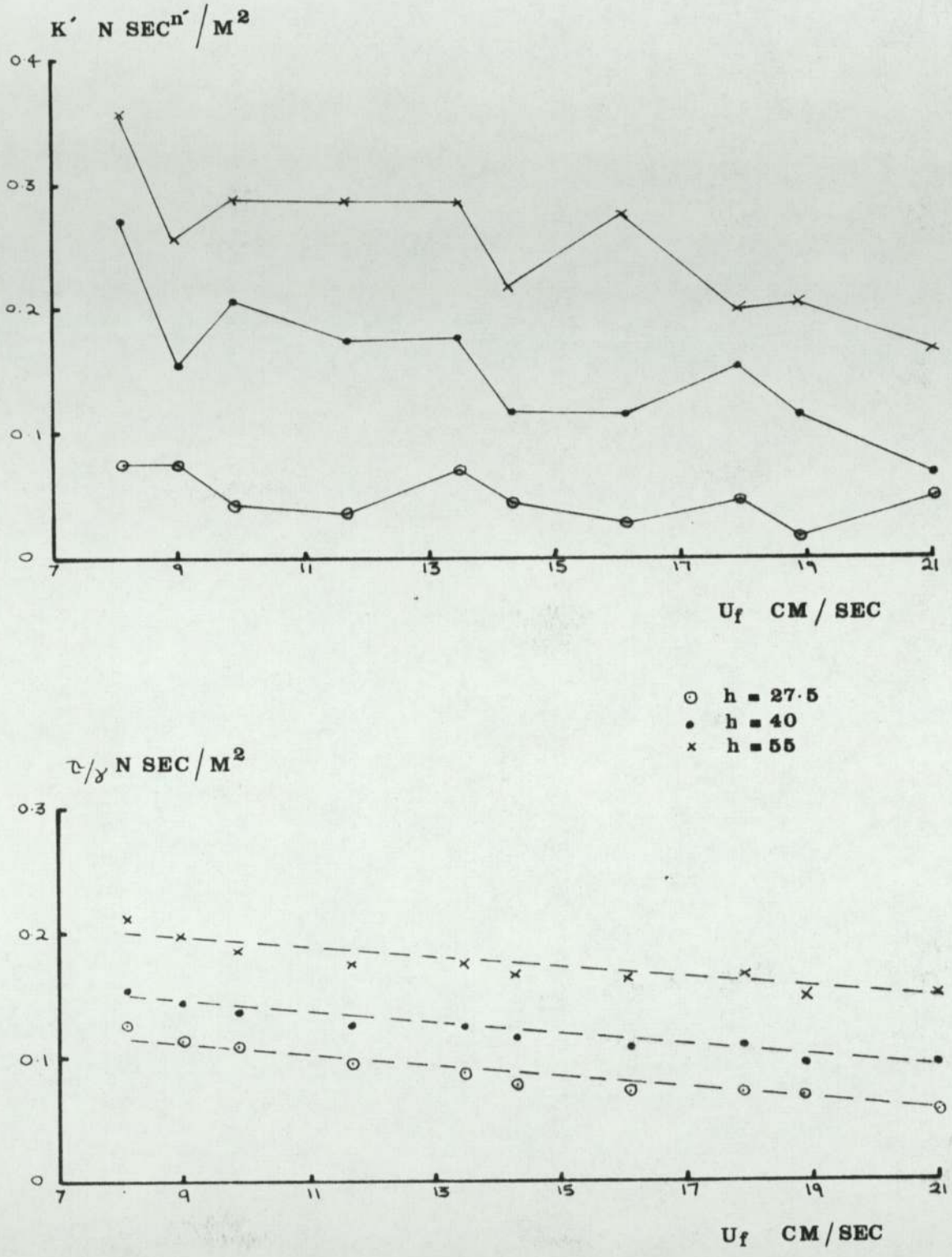

CHANNEL WIDTH = 100 mm

VARIATION OF K′ AND τ/γ WITH FLUIDISING VELOCITY FOR NARROW CHANNEL

THE RATIO $\frac{K'}{\tau/\dot{\gamma}}$ AGAINST NEWTONIAN INDEX

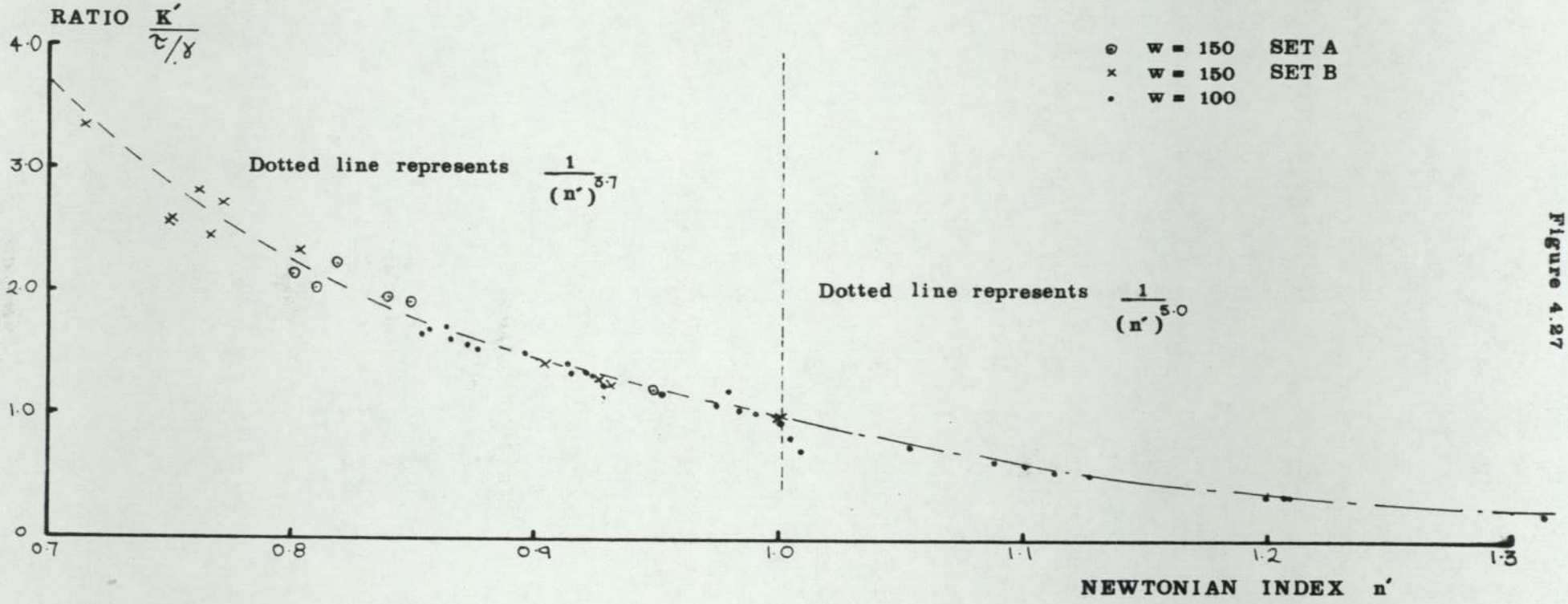

Figure 4.27

Figure 4.28

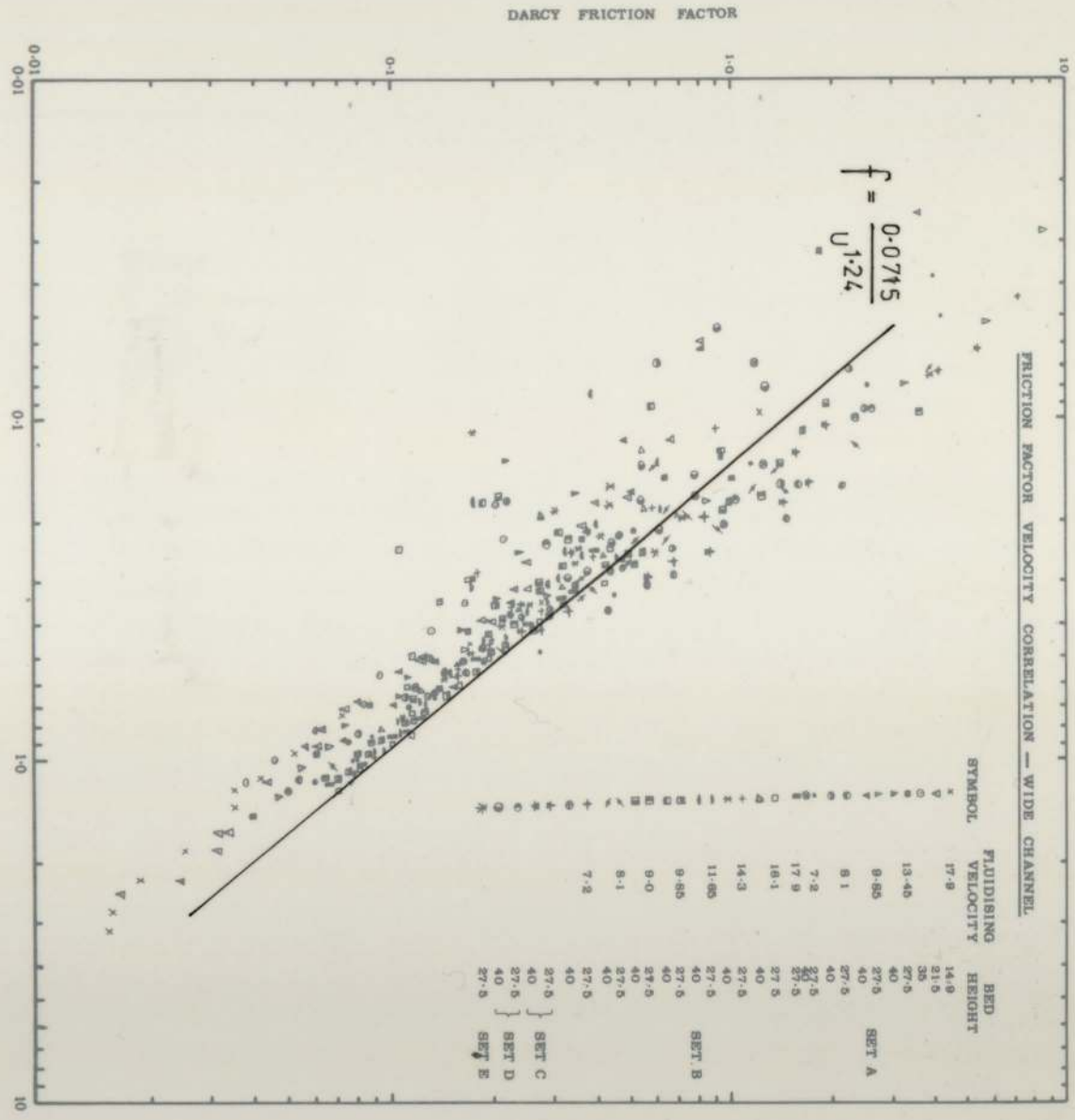
DARCY FRICTION FACTOR
CHANNEL FLOW VELOCITY
FRICTION FACTOR VELOCITY CORRELATION — WIDE CHANNEL
f = 0·0715 / U^1·24
SYMBOL
FLUIDISING VELOCITY
BED HEIGHT
SET A
SET B
SET C
SET D
SET E

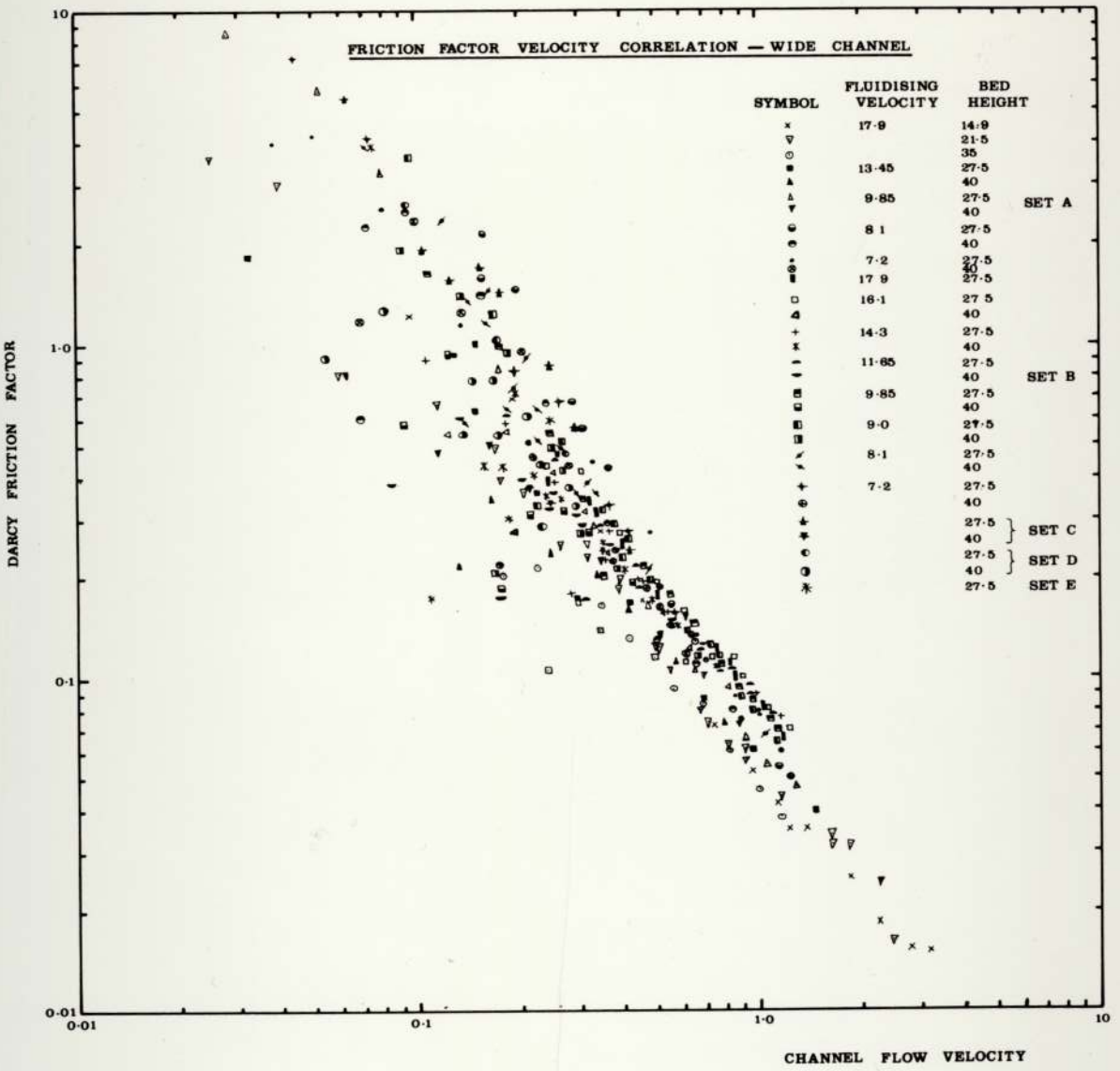
FRICTION FACTOR VELOCITY CORRELATION — WIDE CHANNEL
SYMBOL
FLUIDISING VELOCITY
BED HEIGHT
17·9
14·9
21·5
35
13·45
27·5
40
9·85
27·5
40
SET A
8·1
27·5
40
7·2
27·5
40
17·9
27·5
16·1
27·5
40
14·3
27·5
40
11·65
27·5
40
SET B
9·85
27·5
40
9·0
27·5
40
8·1
27·5
40
7·2
27·5
40
27·5
40
SET C
27·5
40
SET D
27·5
SET E
DARCY FRICTION FACTOR
CHANNEL FLOW VELOCITY
10
1·0
0·1
0·01
0·01
0·1
1·0
10

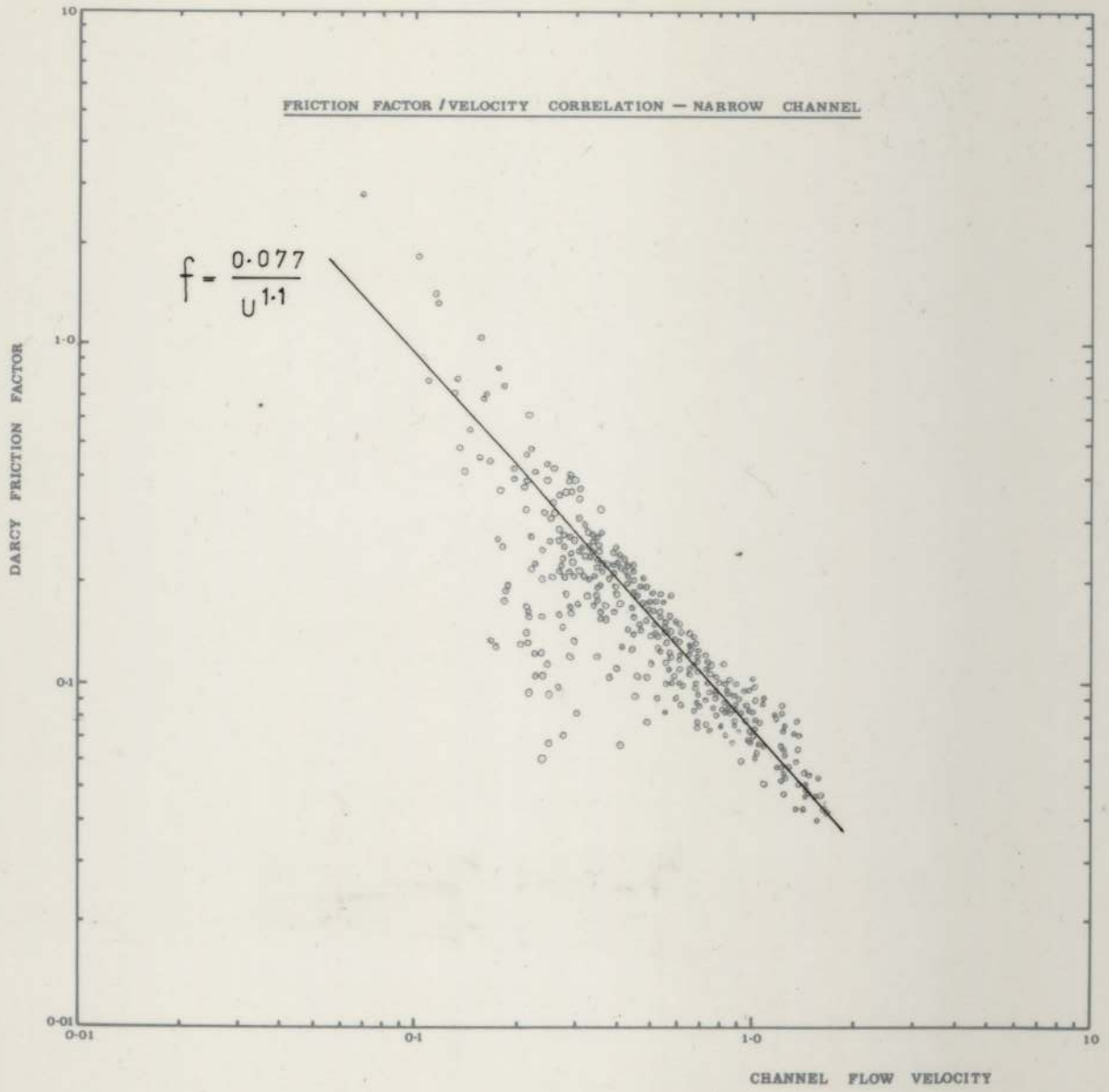
FRICTION FACTOR / VELOCITY CORRELATION — NARROW CHANNEL
f = 0·077 / U^1·1
DARCY FRICTION FACTOR
CHANNEL FLOW VELOCITY
10
1·0
0·1
0·01
0·01
0·1
1·0
10

Figure 4.29

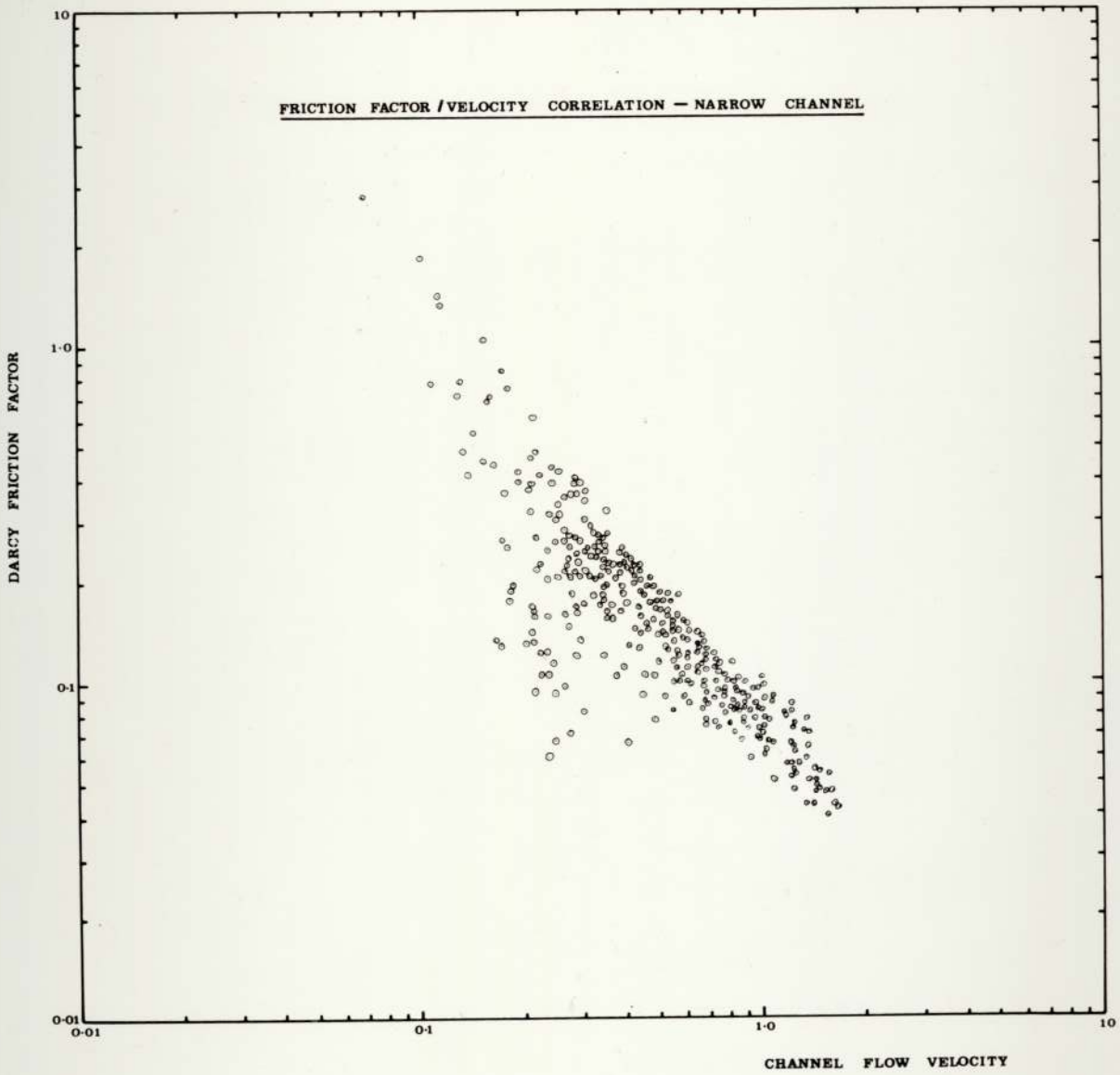
FRICTION FACTOR / VELOCITY CORRELATION — NARROW CHANNEL
DARCY FRICTION FACTOR
10
1·0
0·1
0·01
0·01
0·1
1·0
10
CHANNEL FLOW VELOCITY

Figure 4.30

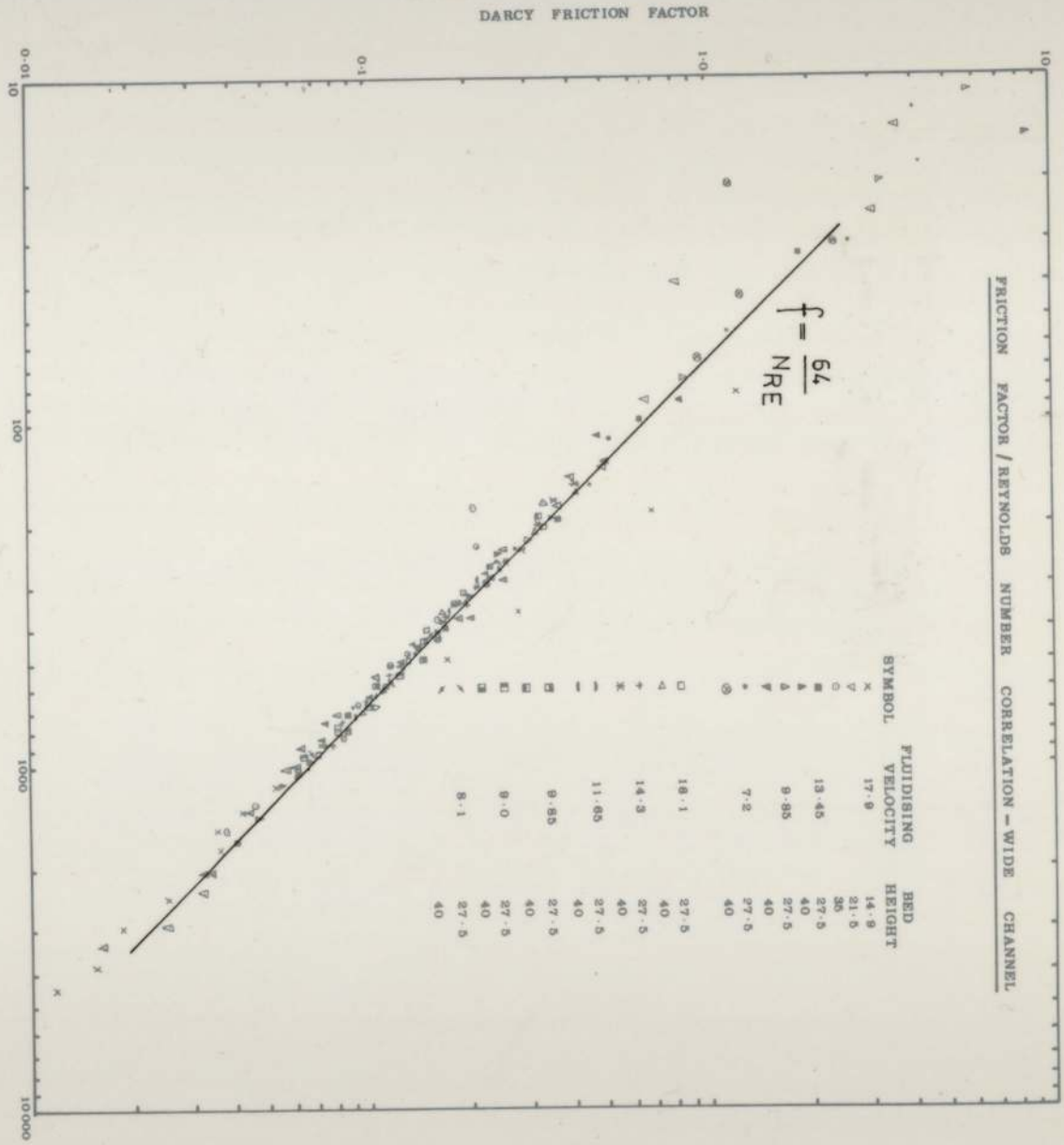
FRICTION FACTOR / REYNOLDS NUMBER CORRELATION – WIDE CHANNEL
SYMBOL
FLUIDISING VELOCITY
BED HEIGHT
17·9
14·9
21·5
35
13·45
27·5
40
9·85
27·5
40
7·2
27·5
40
18·1
27·5
40
14·3
27·5
40
11·65
27·5
40
9·85
27·5
40
9·0
27·5
40
8·1
27·5
40
$f = \frac{64}{NRE}$
DARCY FRICTION FACTOR
MODIFIED REYNOLDS NUMBER
10
1·0
0·1
0·01
10
100
1000
10000

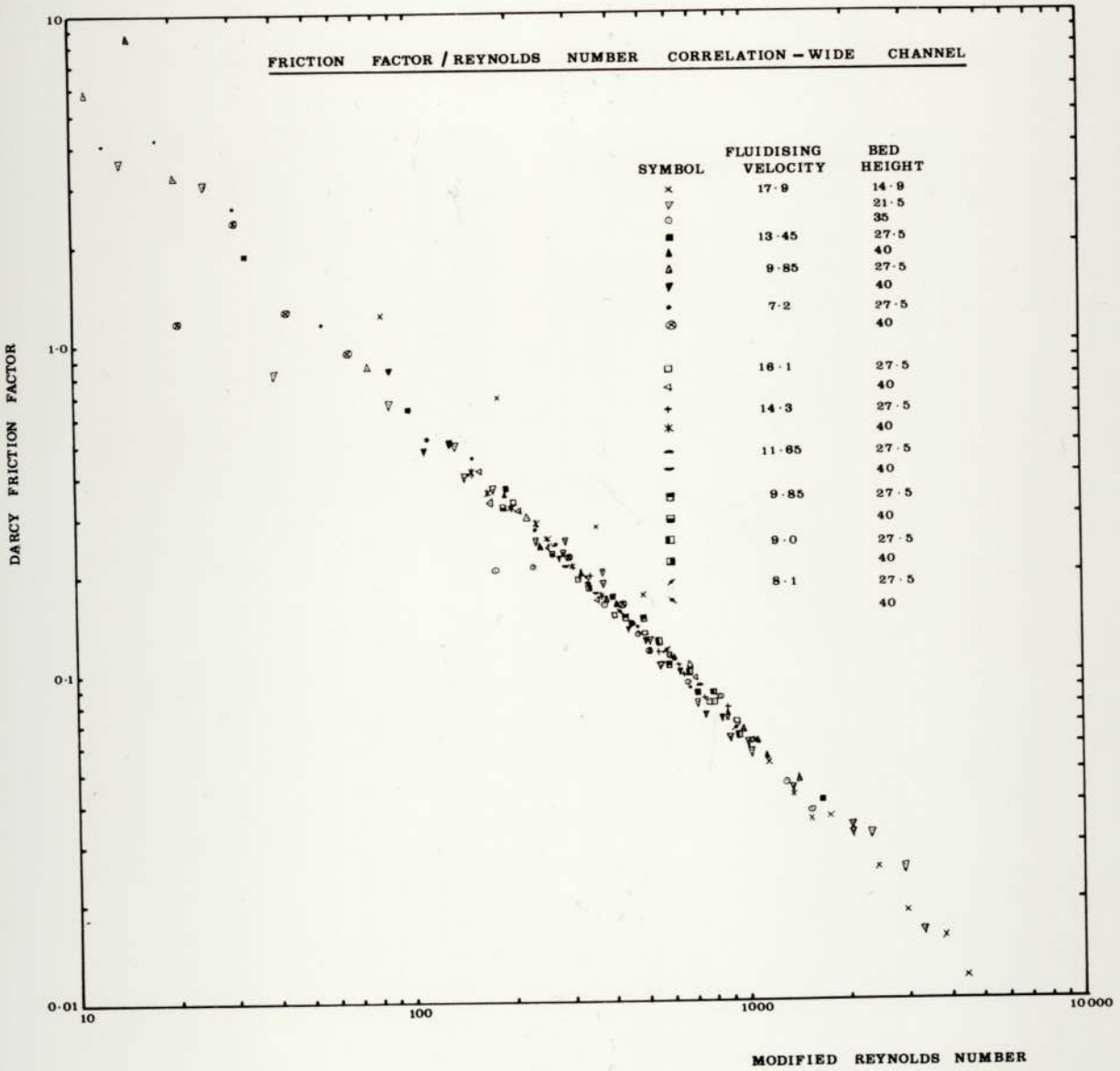
FRICTION FACTOR / REYNOLDS NUMBER CORRELATION – WIDE CHANNEL
SYMBOL
FLUIDISING VELOCITY
BED HEIGHT
17·9
14·9
21·5
35
13·45
27·5
40
9·85
27·5
40
7·2
27·5
40
16·1
27·5
40
14·3
27·5
40
11·65
27·5
40
9·85
27·5
40
9·0
27·5
40
8·1
27·5
40
DARCY FRICTION FACTOR
10
1·0
0·1
0·01
10
100
1000
10000
MODIFIED REYNOLDS NUMBER

Figure 4.31

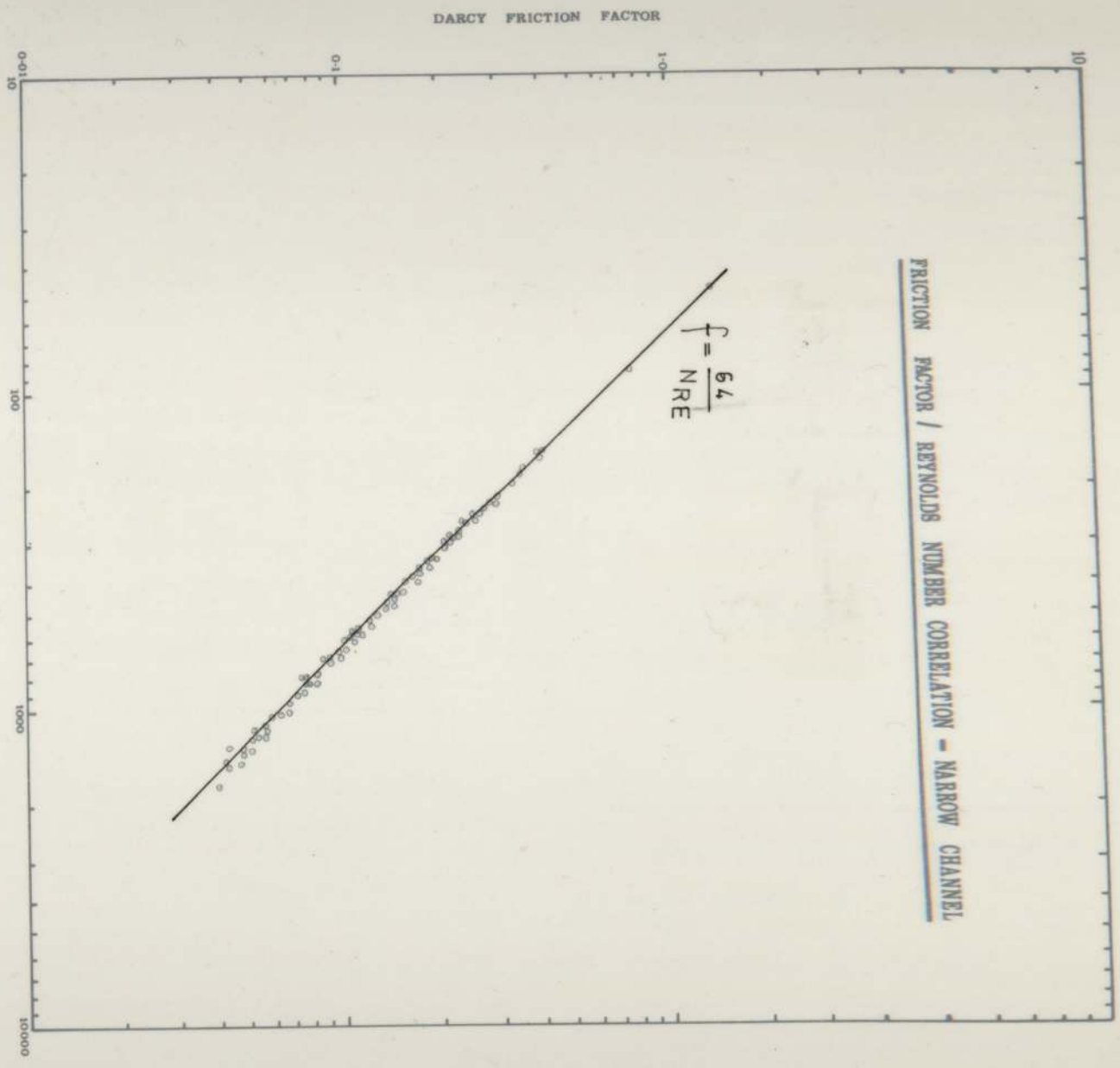
DARCY FRICTION FACTOR
0·01
0·1
1·0
10
10
100
1000
10000
MODIFIED REYNOLDS NUMBER
FRICTION FACTOR / REYNOLDS NUMBER CORRELATION - NARROW CHANNEL
f = 64/NRE

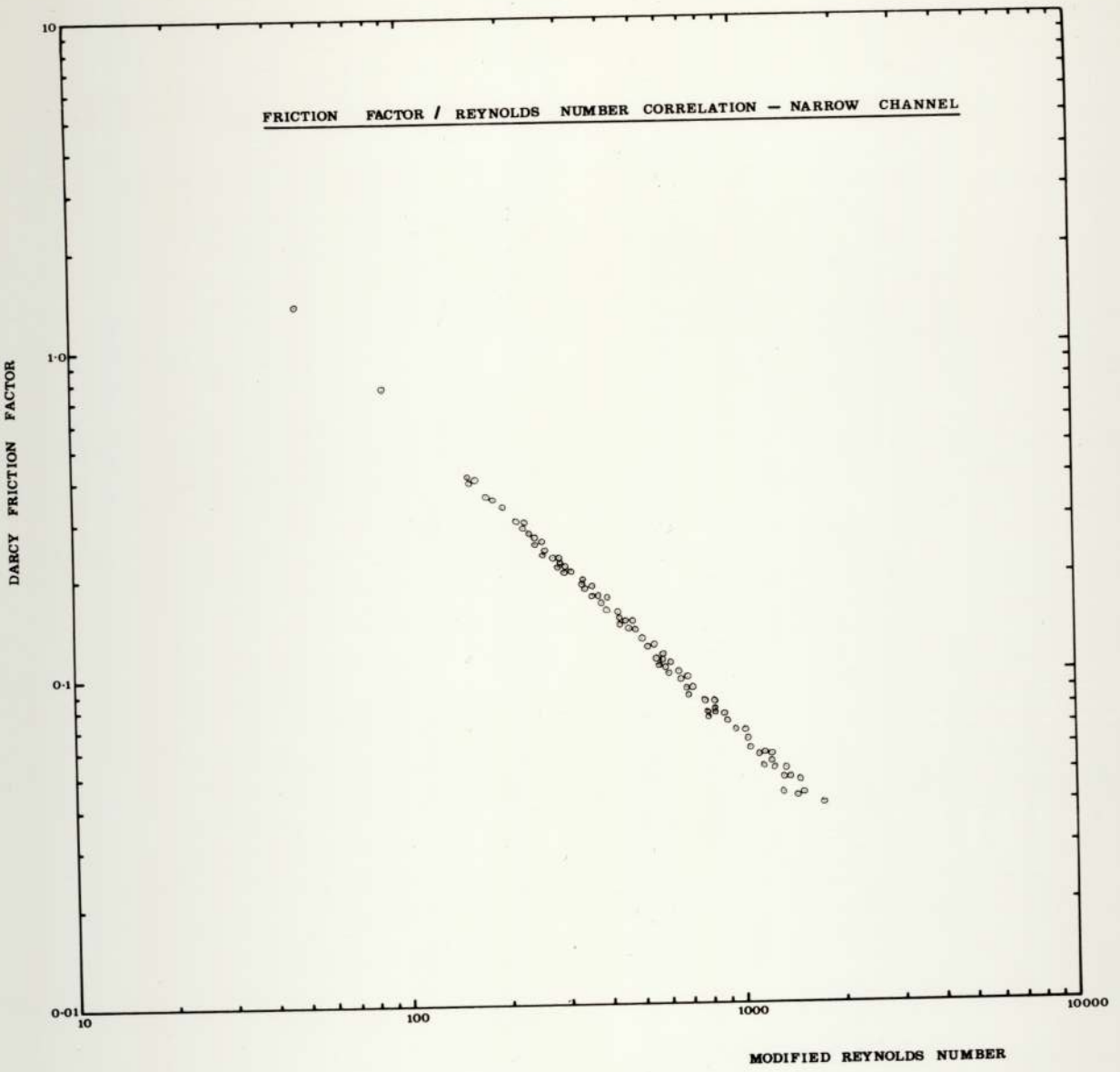
FRICTION FACTOR / REYNOLDS NUMBER CORRELATION — NARROW CHANNEL
DARCY FRICTION FACTOR
10
1·0
0·1
0·01
10
100
1000
10000
MODIFIED REYNOLDS NUMBER

Figure 4.32

SIEVE ANALYSES — SAMPLES C_1 AND S_3

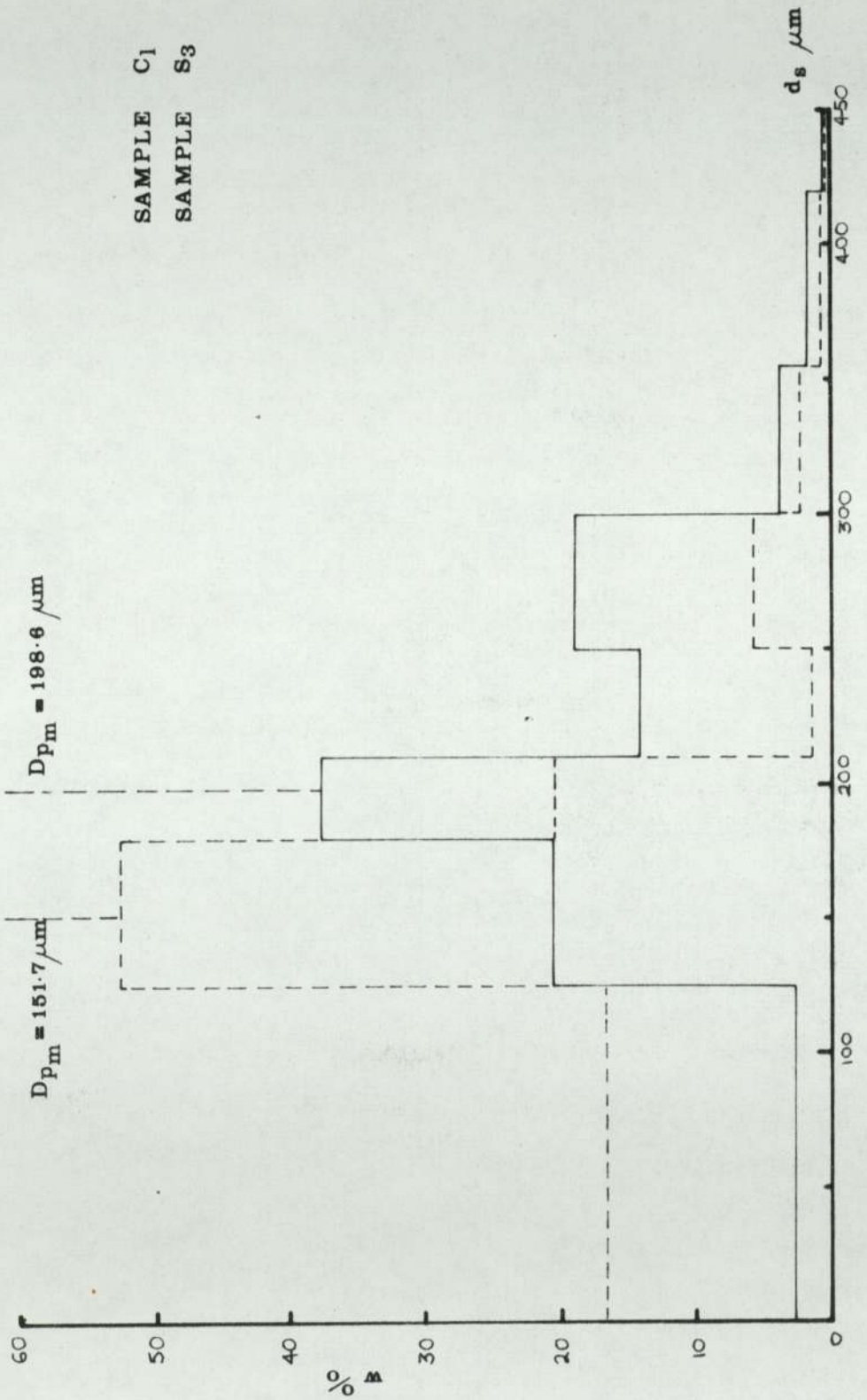

Figure 4.33

SIEVE ANALYSES — SAMPLES UR_4 AND S_3

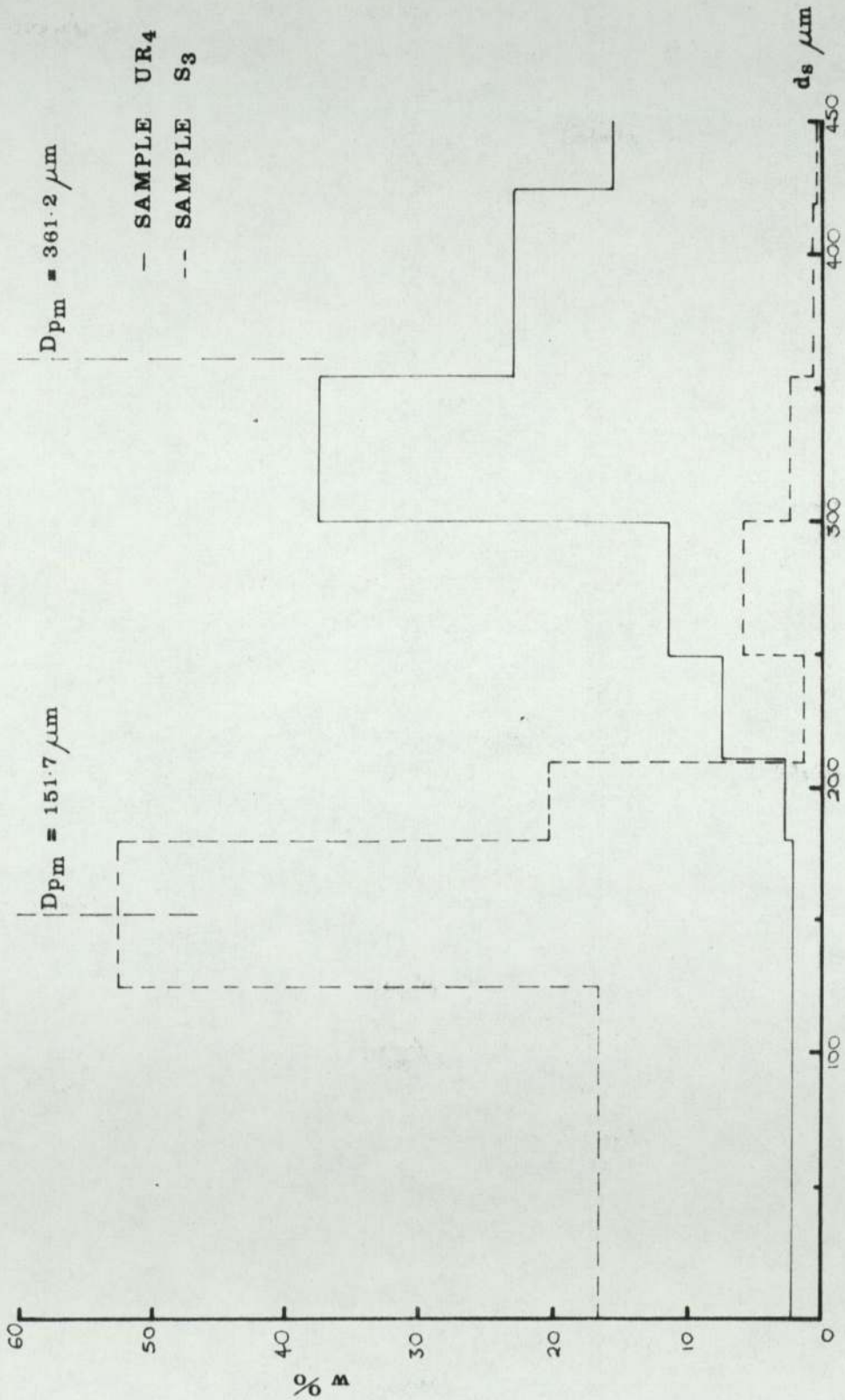

Figure 4.34

SIEVE ANALYSES — SAMPLES LR_1 AND S_3

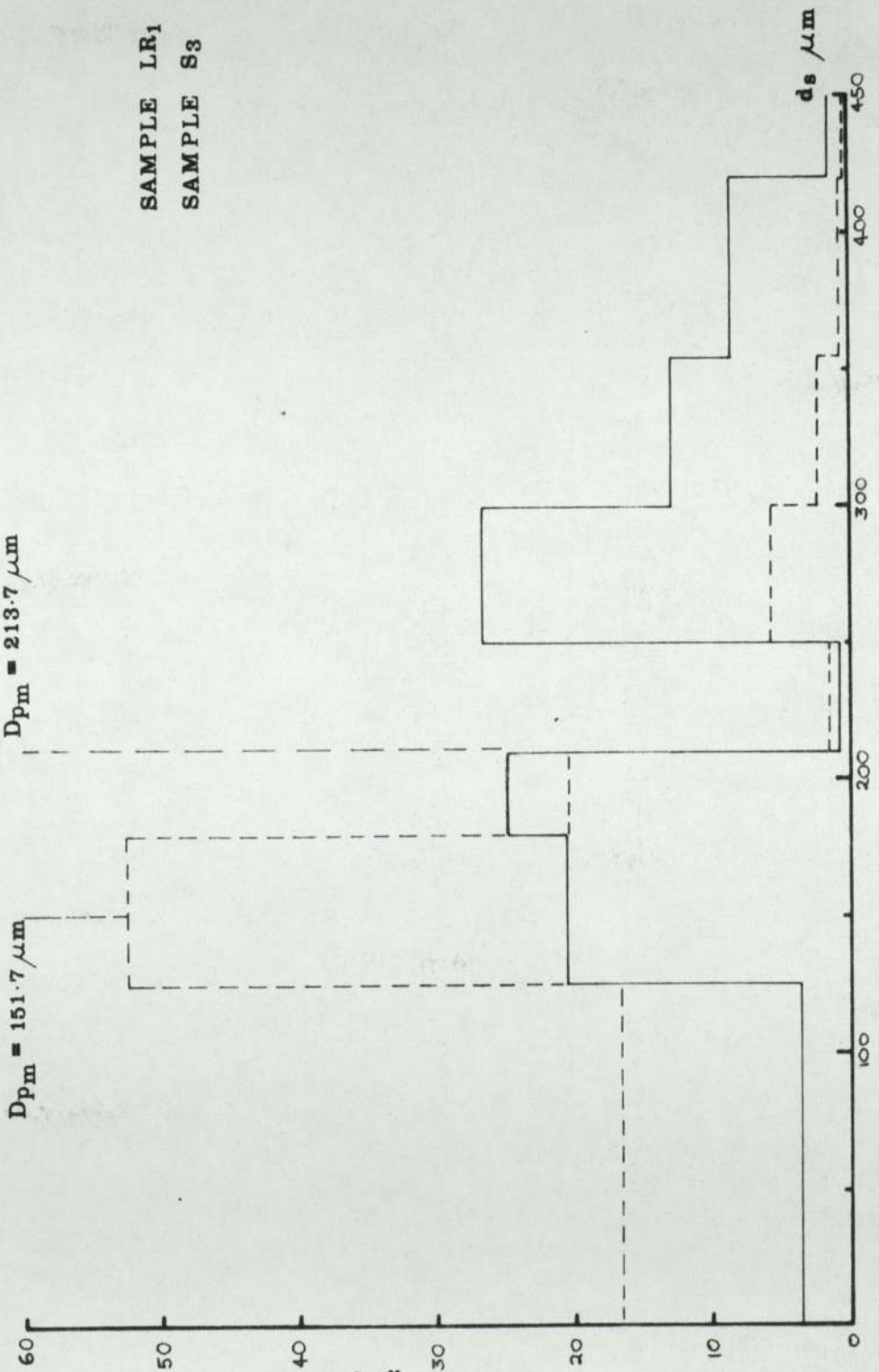

Figure 4.35

SIEVE ANALYSES — SAMPLES CI_1 AND CI_2

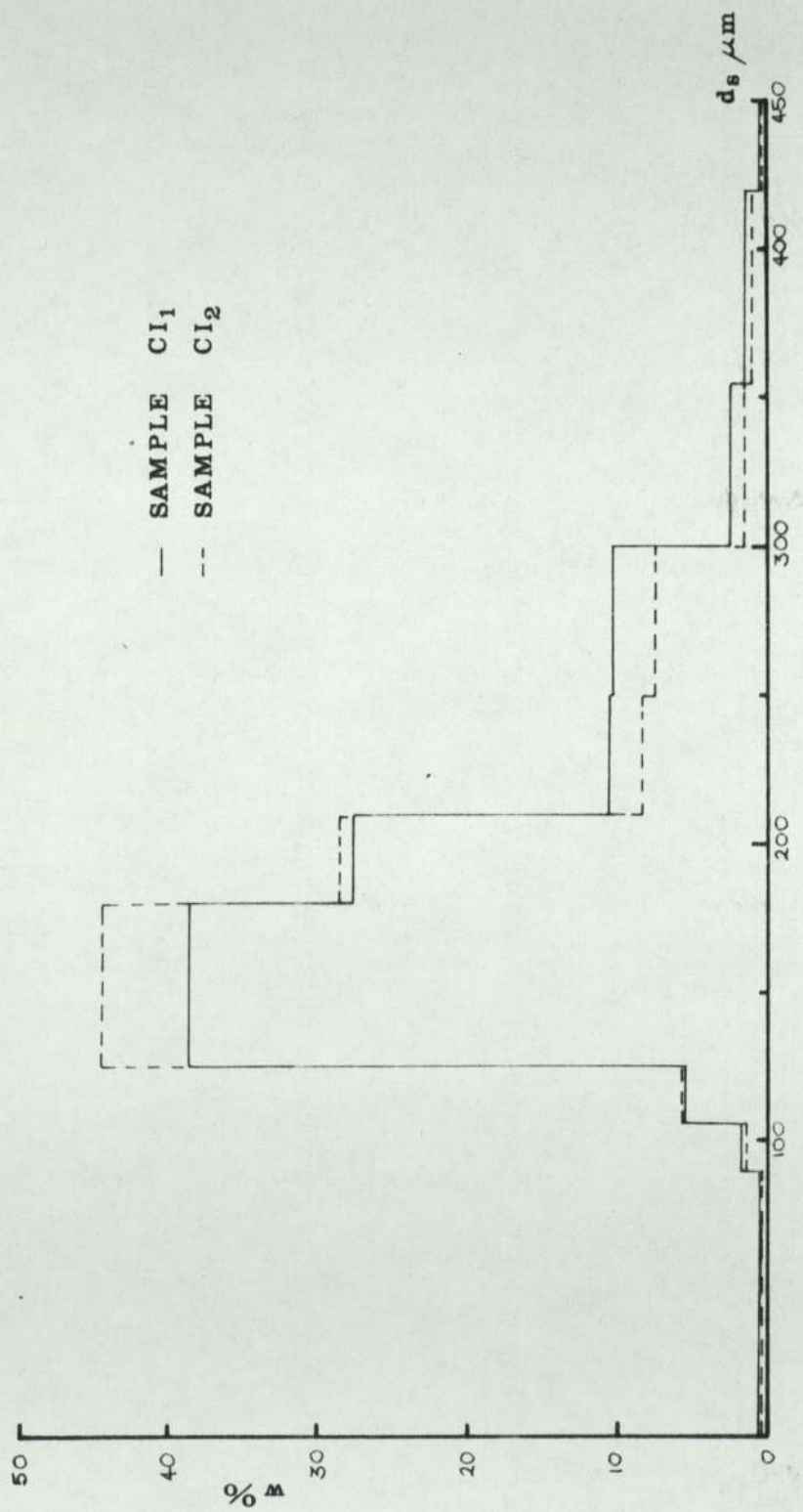

Figure 4.36

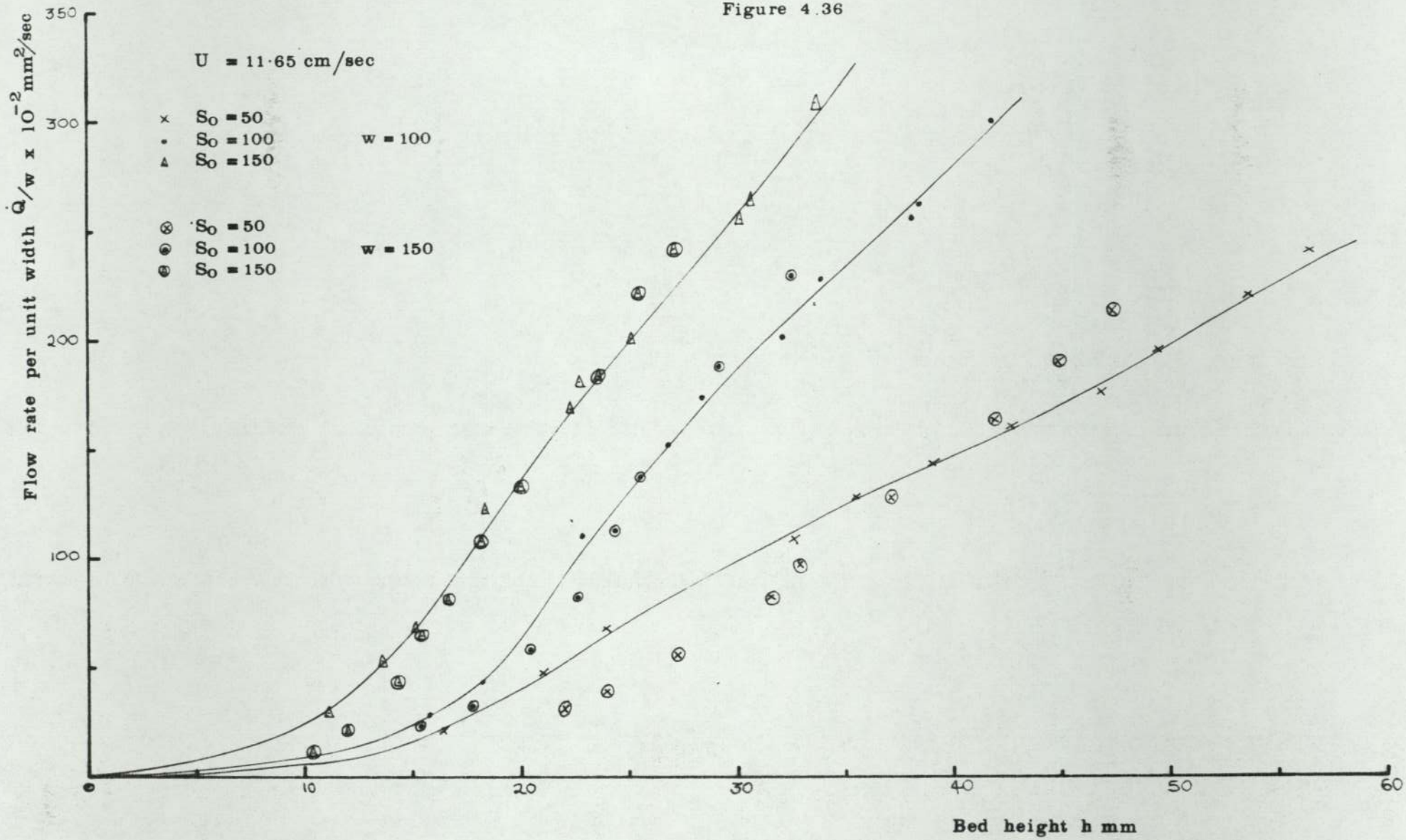
U = 11·65 cm/sec
× So = 50
• So = 100
▲ So = 150
w = 100
⊗ So = 50
◉ So = 100
◉ So = 150
w = 150
Flow rate per unit width Q̇/w x 10⁻² mm²/sec
350
300
200
100
0
10
20
30
40
50
60
Bed height h mm

Figure 4.37

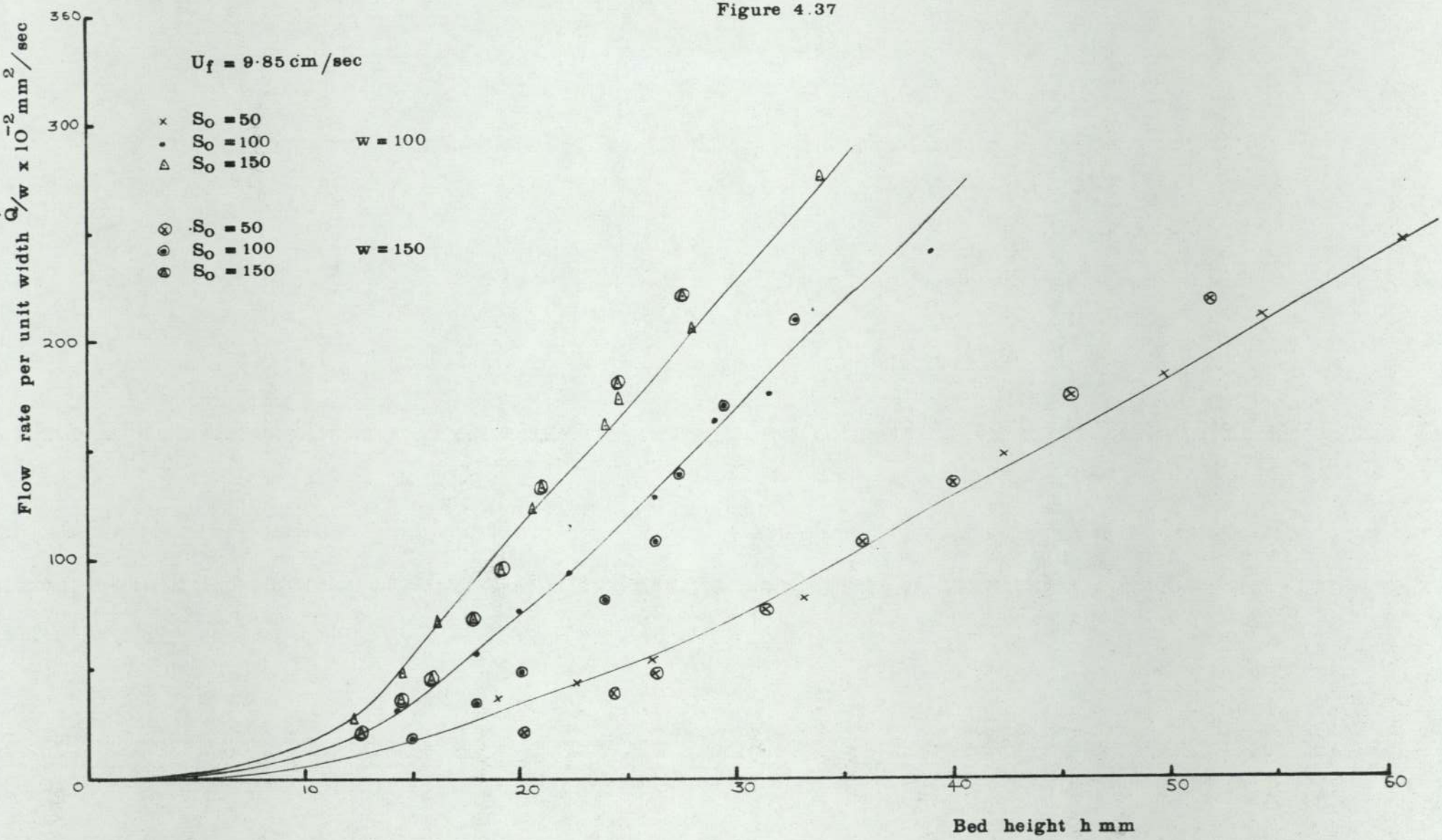
U_f = 9·85 cm/sec
× S_o = 50
• S_o = 100
△ S_o = 150
w = 100
⊗ S_o = 50
◉ S_o = 100
⊛ S_o = 150
w = 150
Flow rate per unit width $\dot{Q}/w \times 10^{-2}$ mm²/sec
Bed height h mm
0
100
200
300
360
10
20
30
40
50
60

Figure 4.38

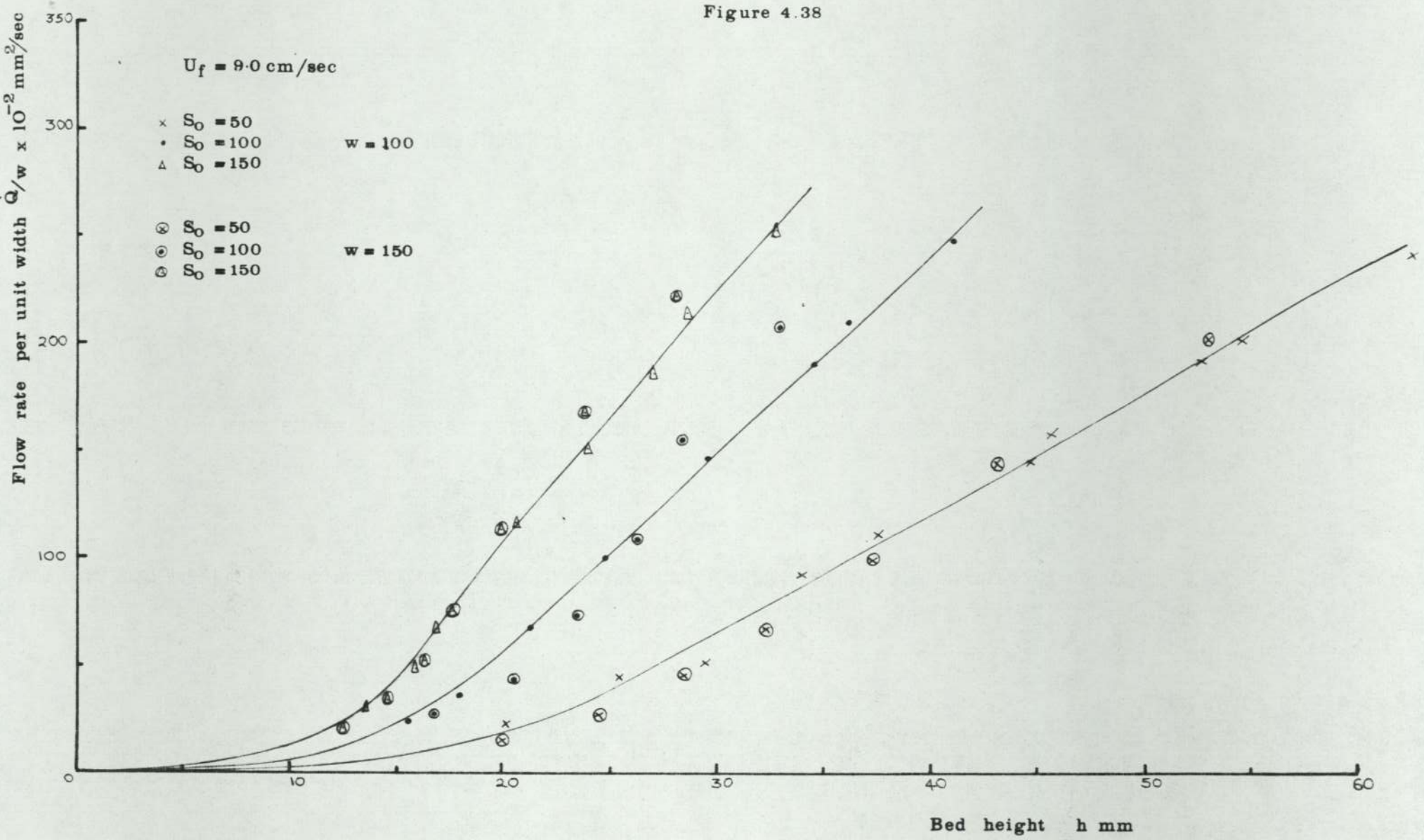
U_f = 9·0 cm/sec
× S_0 = 50
• S_0 = 100
△ S_0 = 150
w = 100
⊗ S_0 = 50
⊙ S_0 = 100
◎ S_0 = 150
w = 150
Flow rate per unit width $\dot{Q}/w \times 10^{-2}$ mm²/sec
350
300
200
100
0
10
20
30
40
50
60
Bed height h mm

Figure 4.39

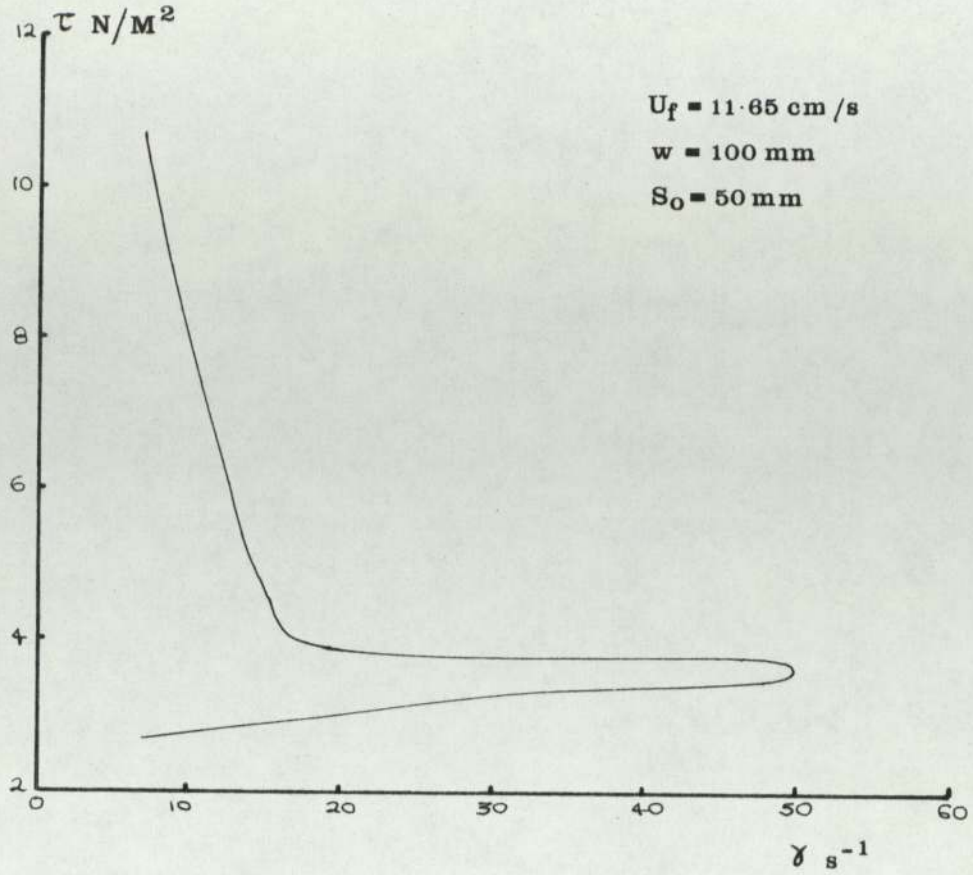

Figure 4.40

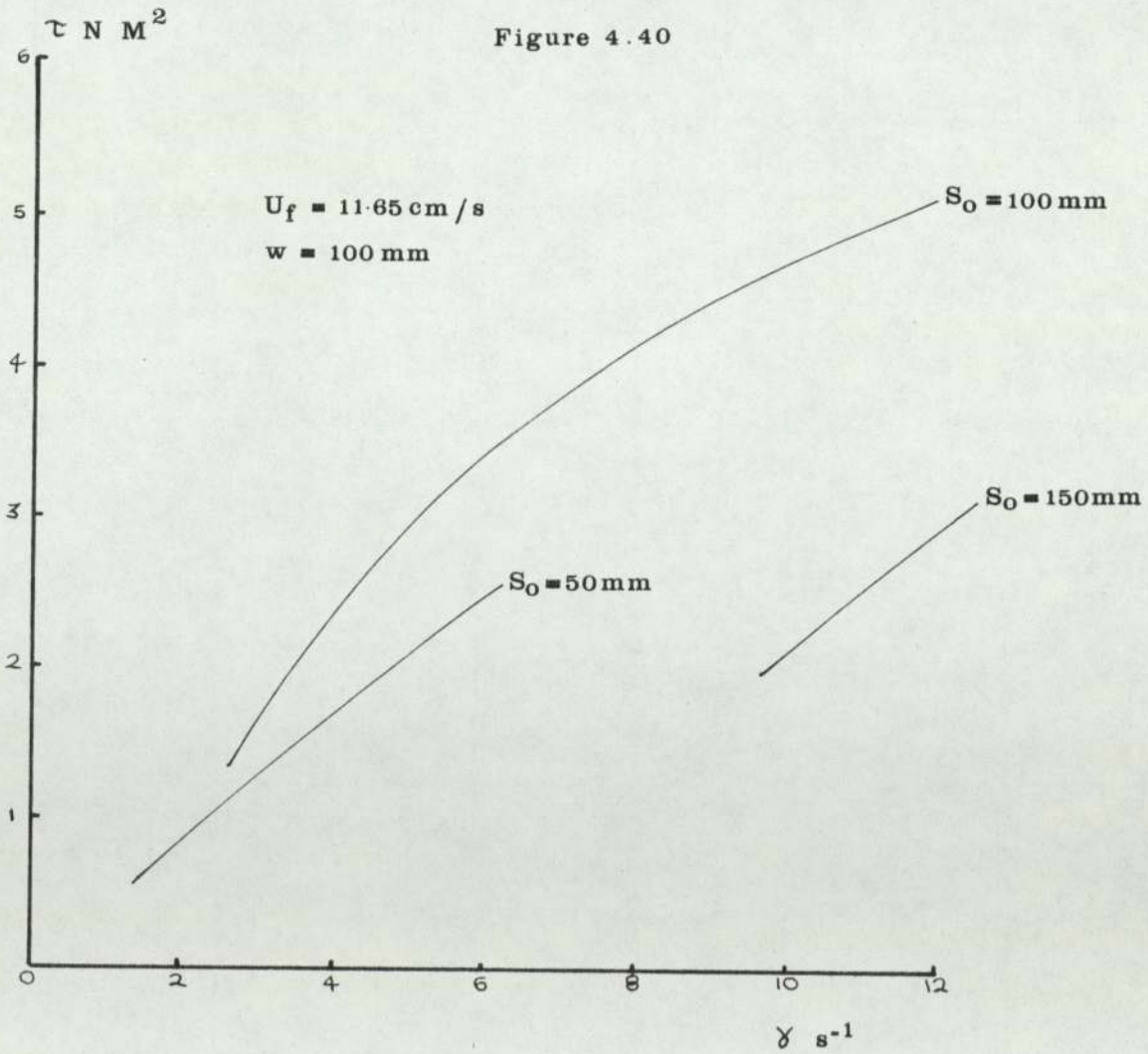

Figure 4.41

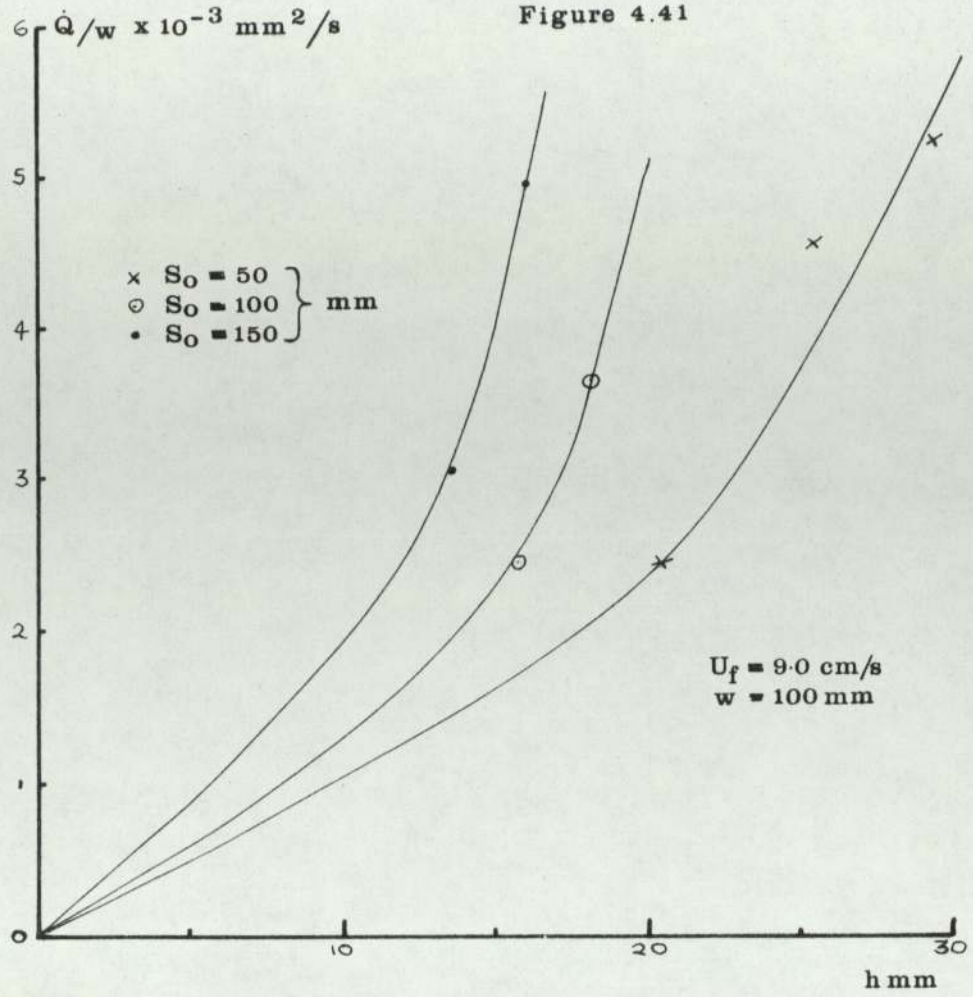
$\dot{Q}/w \times 10^{-3}$ mm^2/s
× S_o = 50
⊙ S_o = 100
• S_o = 150
} mm
U_f = 9·0 cm/s
w = 100 mm
h mm

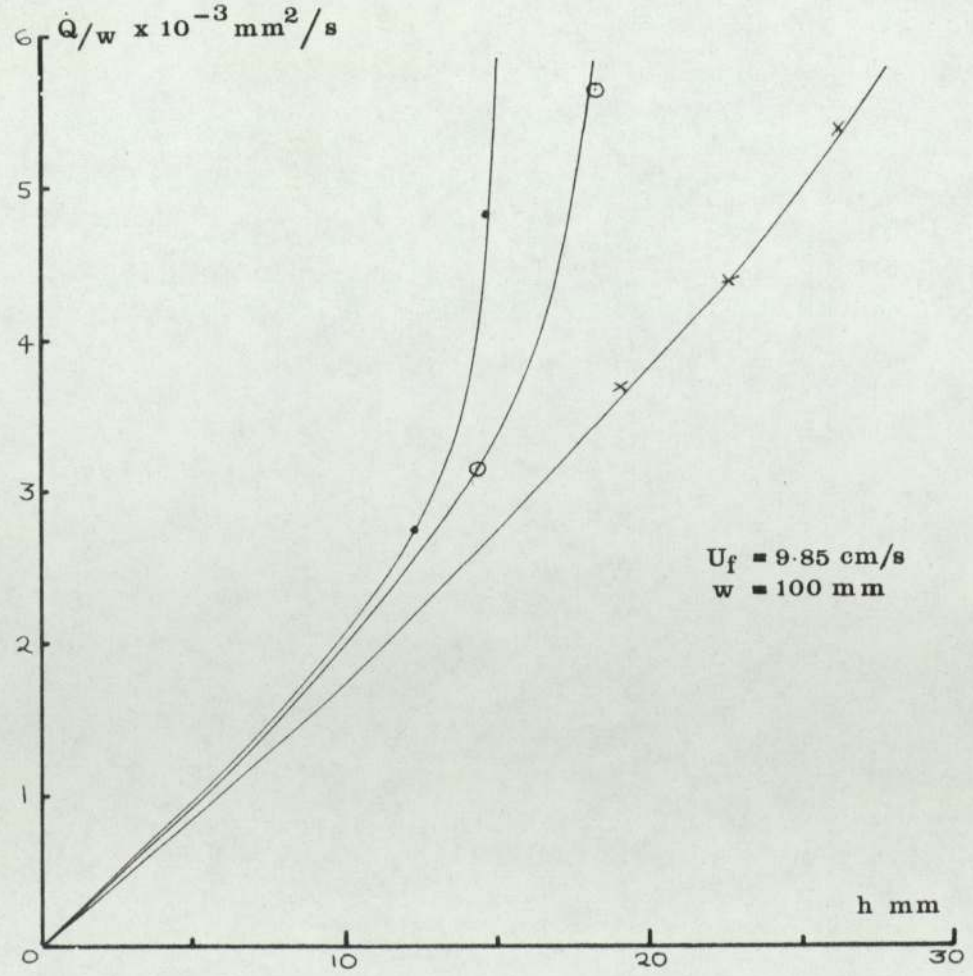
$\dot{Q}/w \times 10^{-3}$ mm^2/s
U_f = 9·85 cm/s
w = 100 mm
h mm

Figure 4.42

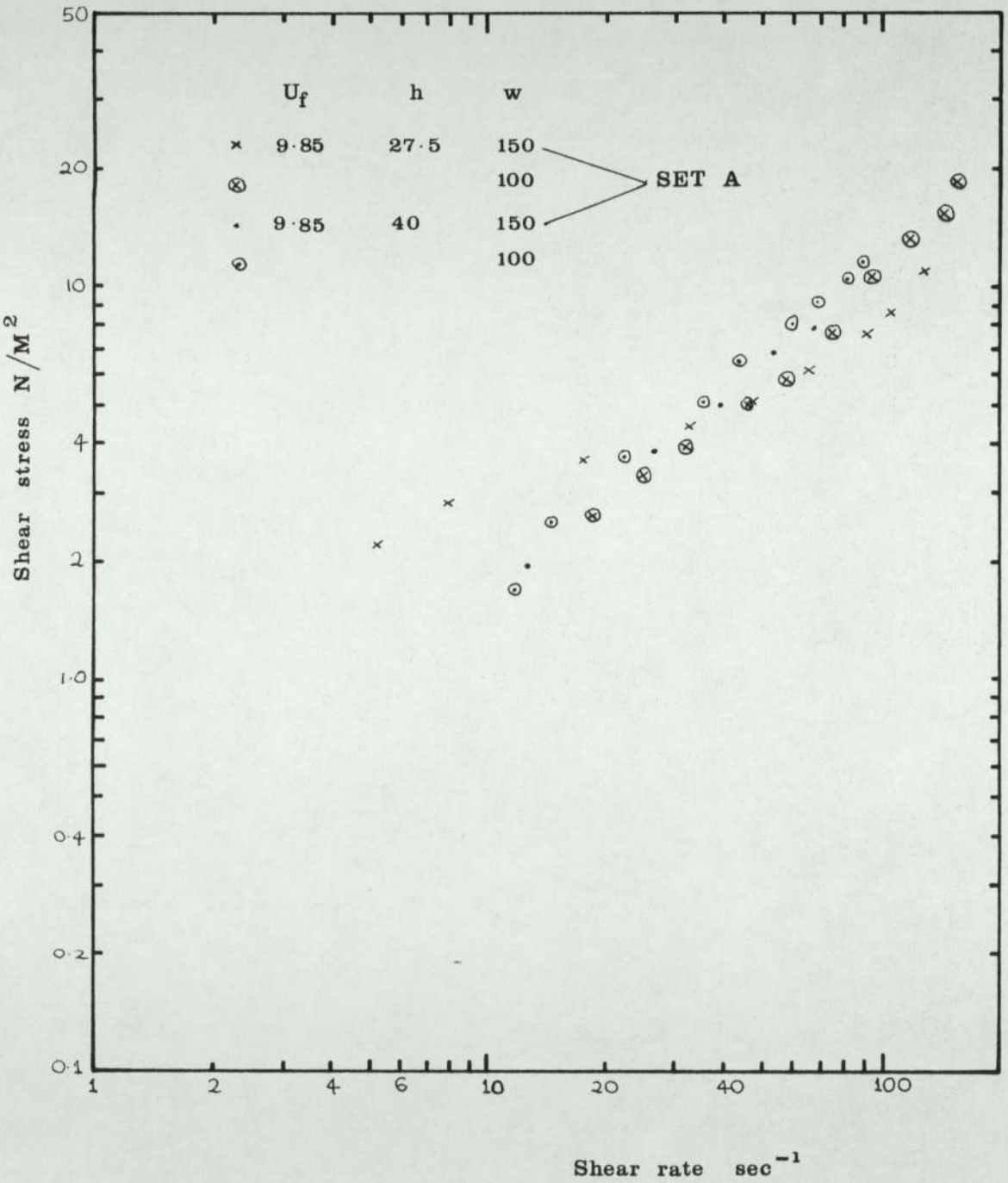
50
20
10
4
2
1.0
0.4
0.2
0.1
1
2
4
6
10
20
40
100
U_f
h
w
9·85
27·5
150
100
SET A
9·85
40
150
100
Shear stress N/M^2
Shear rate sec^{-1}

Figure 4.43

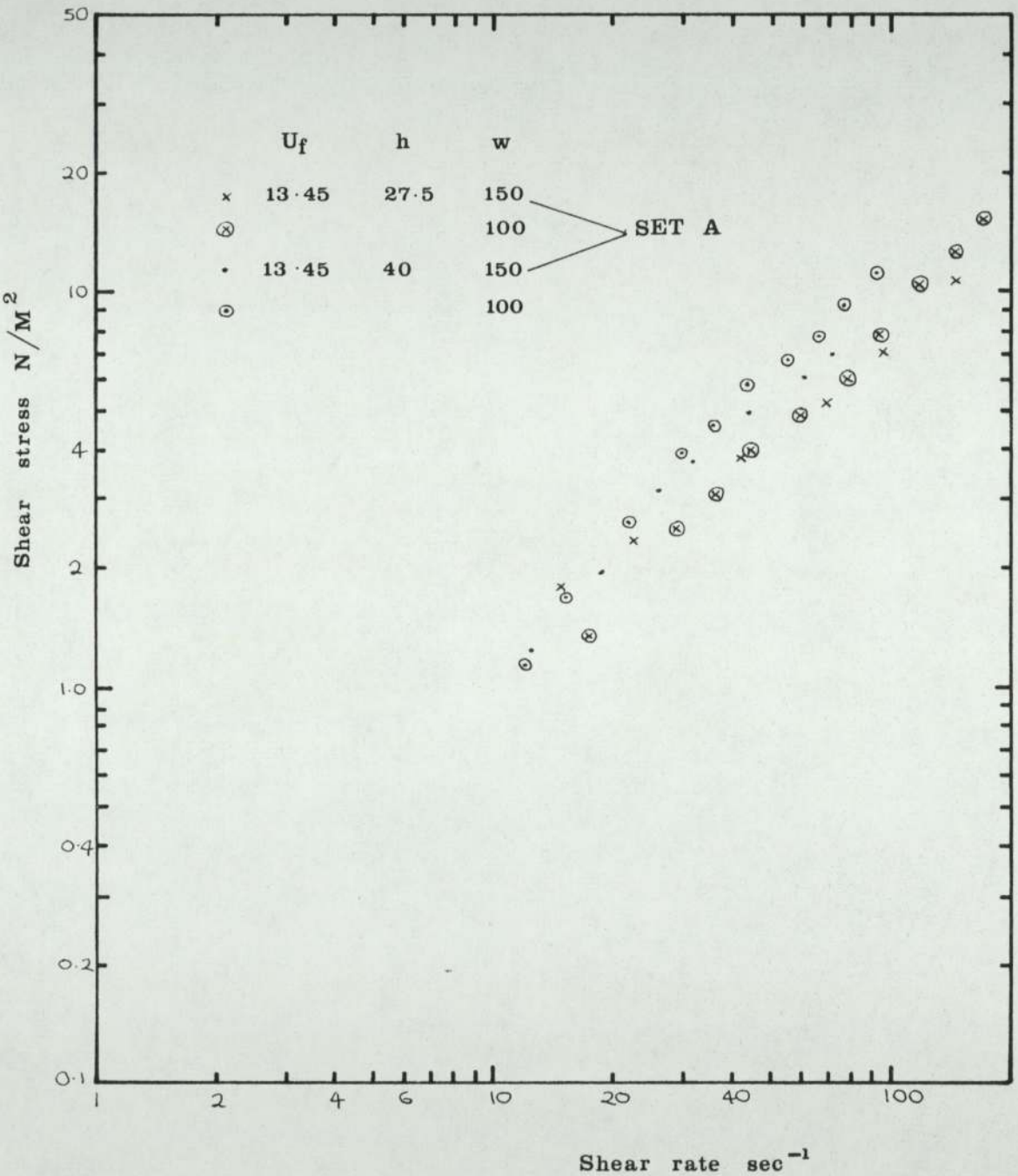
Uf h w
13·45 27·5 150
100
SET A
13·45 40 150
100
Shear stress N/M²
Shear rate sec⁻¹
50
20
10
4
2
1·0
0·4
0·2
0·1
1
2
4
6
10
20
40
100

Figure 4.44

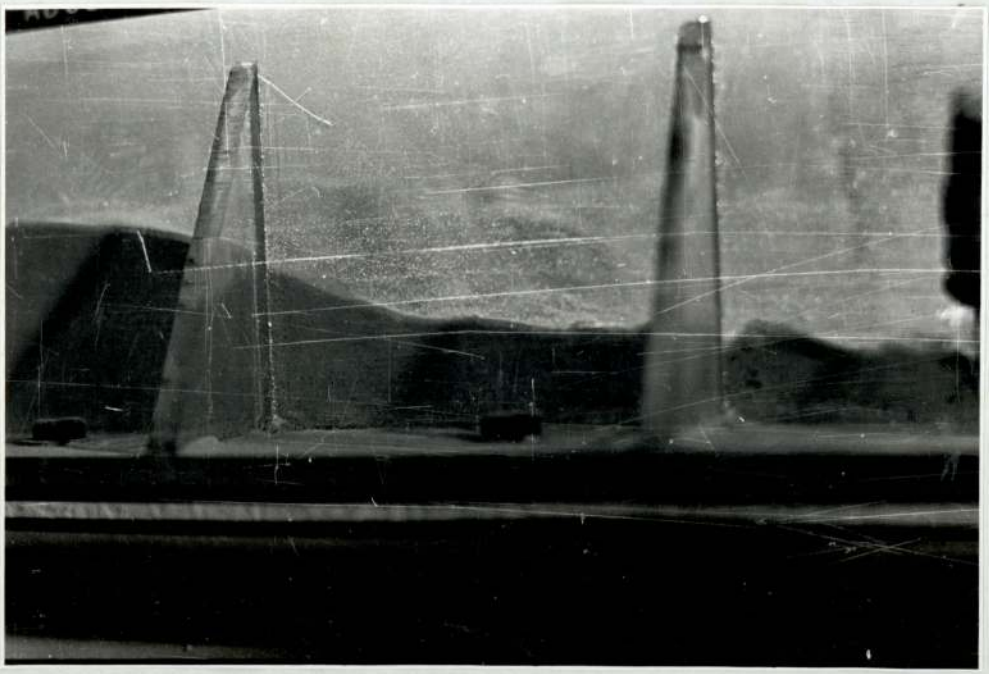

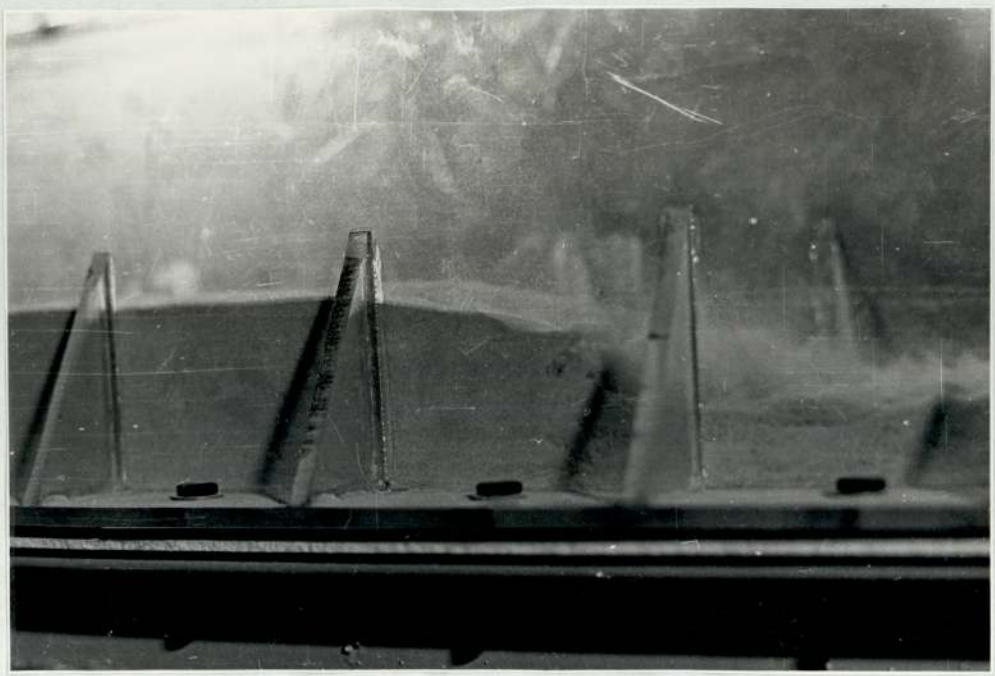

Figure 4.44

Figure 4.45

1

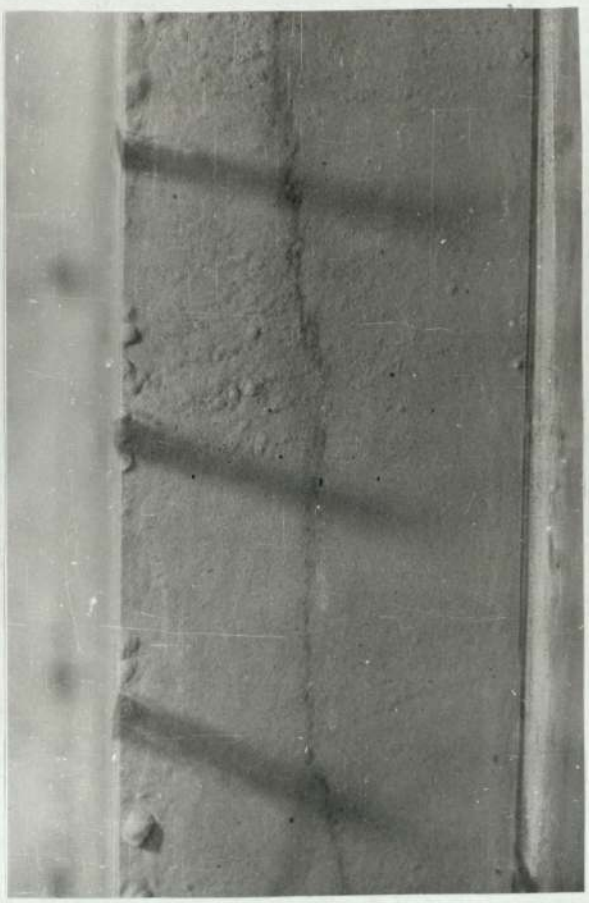

2

3

4

Figure 4.46

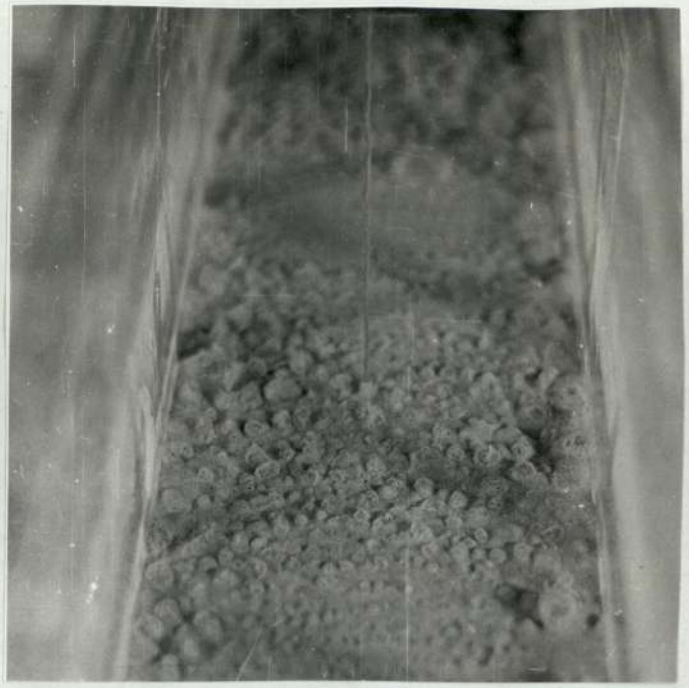

U = 0.052

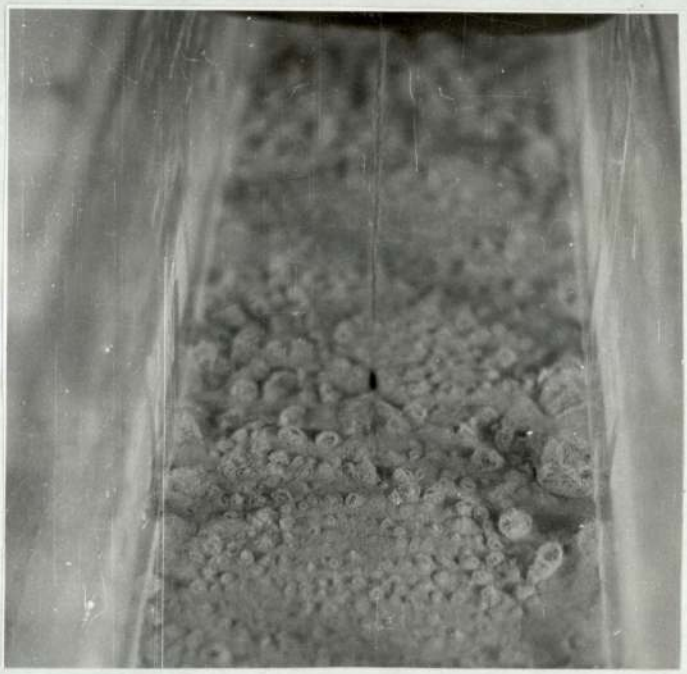

U = 0.079

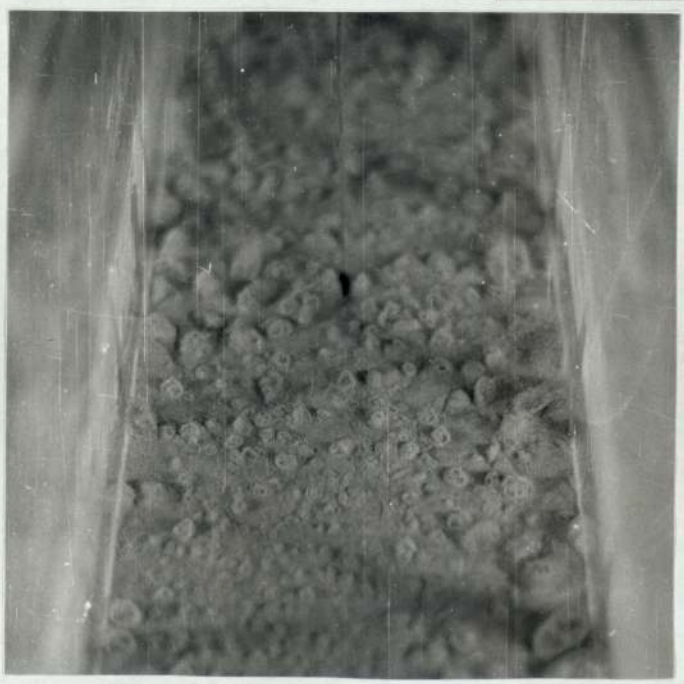

U = 0.175

Figure 4.46

U = 0.328

U = 0.469

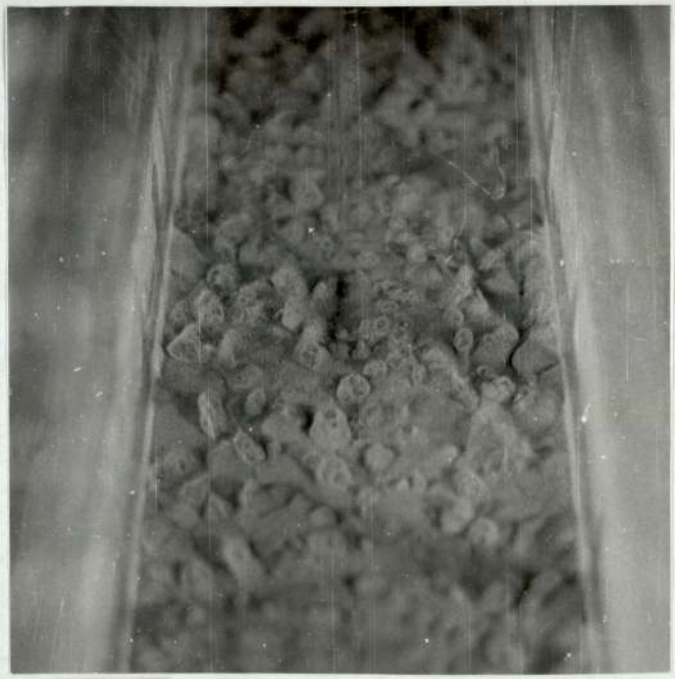

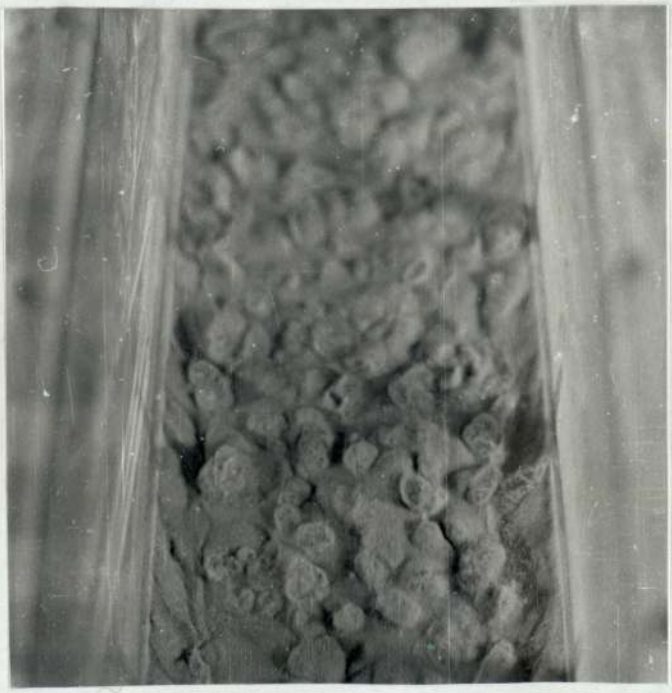

U = 1.066

Figure 4.47

U = 0.324

$4.65 U_{mf}$

U= 0.961

CHAPTER 5.

CONCLUSIONS

5. Conclusions

The experiments performed in the channel-flow test rig have shown that the rheological properties of the flowing fluidised bed may be described over most of the range of shear rates used by a simple power-law equation. At high shear rates and fluidising velocities the flowing bed is very close to Newtonian in character, becoming increasingly pseudoplastic as the fluidising velocity is reduced. At low shear rates, it is postulated that the flow is influenced by three mechanisms. The first of these is that of "bubble suppression", whereby as shear rate increases, more air passes through the dense phase, leaving less present in the form of bubbles. The bed expands more, its density is lower, and inter-particle lubrication is increased. This mechanism produces shear thinning characteristics. The second mechanism is one of segregation. Large particles settle on the distributor, effectively acting as a secondary distributor for the rest of the bed, having a deleterious effect on the quality of fluidisation, and resulting in high base drag. This segregated layer is swept away as the shear rate increases, reducing the drag, and thus this mechanism results in basically shear thinning behaviour also.

It seems likely that under at least some conditions an inviscid layer exists close to the distributor. This would result in low drag at low shear rates. As the shear rate is increased, this layer is progressively swept away, causing increased base drag, resulting in shear thickening characteristics.

It is believed that the behaviour of the flowing fluidised bed at low shear rates is the result of either the "inviscid layer dissipation" mechanism, or a combination of the "bubble suppression" and "segregated layer dissipation" mechanisms. The actual behaviour resulting is the product of a complex interaction of these, this interaction being a function of fluidising velocity and bed depth.

It is also thought that the shear history of the bed could be a further variable under conditions of low shear rates and fluidising velocities.

Whatever the mechanism prevailing at low shear rates, a re-arrangement of the bed takes place as shear rate is increased to produce a low viscosity, easily flowing bed at high shear rates. As shear rate is decreased once more, the bed is reluctant to give up its character, and continues to flow quite easily. This results in the "hysteresis" apparent in the shear curves. Clearly, the amount of re-arrangement taking place is dependent on fluidising velocity, the greater particle mobility produced at high fluidising velocities meaning that less re-arrangement is necessary to produce the free-flowing nature. Thus the reduction in "hysteresis" at high fluidising velocities is explained. Although the existence of this "hysteresis", which produces low drag at low shear rates, would appear to make it desirable to operate on the downward-coming path of the shear curve, this may not, in fact, be desirable. It seems possible that this section is unstable, and that at some time the flow may "jump back" to the upward-going curve, resulting in a sudden increase in drag which would surely cause serious problems if it took place in a commercial system.

The re-arrangement of the bed with increasing shear rate is especially pronounced at low fluidising velocities, of the order of 1.8 U_{mf}, where it is associated with sharp "transitions" from poor, heavily segregated flow to much better flow.

Samples taken from the bed have, together with visual observations confirmed the existence of the "bubble suppression" and "segregated layer" mechanisms.

The dependence of fluidised bed viscosity on bed depth, already noted

by other workers from experiments using viscometers, has been confirmed.

Experiments performed to attempt to establish the existence of slip at the distributor, and to obtain shear curves from graphs of flow rate against bed height at a constant slope met with little success due to the limitations and simplifications introduced by the theory used. Other workers have claimed that slip exists, but the present study has not absolutely confirmed this, although it does seem possible that this is present under some conditions.

The pursuit of the liquid analogy has proved to be quite fruitful in establishing the general rheological behaviour of the fluidised bed. It has been established that the flowing bed conforms to the laminar flow liquid correlation of friction factor and Reynolds number, and that it shows no evidence of more than one regime of flow up to Reynolds numbers in excess of 4000. The absence of any transition from viscous drag dominated laminar flow to inertia loss dominated turbulent flow seems to suggest that inertia losses continue to be low. A tentative explanation for this suggests that whereas turbulent areas in liquid flow interact and dissipate kinetic energy, and liquid is brought to rest on touching a containing wall, in fluidised beds particles may "bounce" off each other, and the containing walls, thus retaining most of their kinetic energy, and requiring less additional energy to accelerate them to their former velocity. If further experiments confirmed that the fluidised bed continued to follow the laminar correlation up to even higher Reynolds numbers, this would mean that the energy expended in moving fluidised materials would be extremely low. At the Reynolds numbers already reached, the friction factor is very much lower than that of a liquid at the same Reynolds number. The "bounce" theory would also suggest that the use of spherical particles

would reduce friction still further due to the increased coefficient of restitution.

Although, as already stated, a simple power-law will describe the flowing bed over a considerable range of shear rates, it is the author's opinion that to develop a model to describe the bed behaviour at low shear rates would be very difficult, if not impossible, due to interaction of mechanisms producing the characteristics of the bed, and the number of parameters relevant to this interaction. However, this study has shown the area in which it is best to operate. The fluidising velocity should be moderately high, certainly in excess of 2.5 U_{mf}, and the bed should be shallow. The data obtained suggests that a Reynolds number as high as possible should be selected. Given these sort of conditions, a flowing system should experience none of the problems which manifest themselves at low velocities, and there seems no reason why it should not operate successfully.

Clearly, however, the full understanding of the flow of a fluidised bed requires much more work, for a good deal of which the test rig designed and built during this study is well suited.

CHAPTER 6.

FUTURE WORK.

6. Future work

Clearly, the channel flow test rig is suitable for a great deal more work. It is the author's opinion that the usefulness of the type of work described in this thesis is not yet exhausted. Further similar experiments could be carried out, extending the range of channel aspect ratios, fluidising velocities and most especially, Reynolds numbers used. However, it is clear that to gain further benefit from the pursuit of the liquid analogy more sophisticated treatment of the experimental results is called for. The present study has shown that it is not adequate to assume that the shear stress is the same on all "wetted" surfaces in the channel, and thus the investigation of the relative contributions to the overall drag of the walls and the distributor under a wide range of operating conditions must be one of the first objectives of any future study. It is also clear that whilst a simple power law will adequately describe the shear curves over most of their range, something much more complex is necessary to describe the lower sections. As already discussed in Chapter 4, it seems likely that the shape of these sections is a complex function of fluidising velocity, bed depth and shear rate, with bed width having a lesser effect. Obviously, the development of a model which will describe these curves over a range of conditions is a formidable task; so much so that it may not be feasible. However, any future investigations must surely be aimed at least at establishing the feasibility of this.

There are several other types of work to which the test rig is well suited. The one-dimensional flow approach looked at in this study may repay further work, but again, this must clearly be of a more comprehensive nature than that undertaken here. The further development of the liquid analogy will involve experiments to

determine velocity profiles. Point velocities in a fluidised bed are difficult to measure. Various methods could be used: the propellor device favoured by Bessant, drag on some small immersed body, heat transfer from an immersed body, and so on. The difficulty with all these methods is that the probe used must be calibrated; here, the rotating annular bed approach of Bessant could be useful. Any of the above methods will also require some complex mathematical modelling.

All the tests performed in this study have used sand of one type. Other workers have shown that the properties of a fluidised bed are greatly affected by particle size distribution and density. Here then is another fruitful avenue for investigation; the effect of using various narrow cuts of sand and other materials, of very wide size distributions, and of mixtures of various materials in different proportions. A practical difficulty with this type of work is the cleaning out of the various components of the rig, notably the elevator. This problem is by no means insuperable, but it necessitates a great deal of work.

At first sight, it would seem that forcing fluidised material past a heat transfer surface should bring higher heat transfer rates than those attainable in a static (non-flowing) bed. Work by Botterill has shown that this is not necessarily so, due to the surfaces causing local de-fluidisation. However, it may be possible by careful selection of the configuration of the heat transfer surfaces to obtain improvements in performance due to the high rate of movement of particles around the surface, and consequent low particle residence times at the surface.

When the test rig was built, provision was incorporated for the study of the flow of fluidised solids over notches and weirs. Vertical slots are provided in the channel walls near the top for

the insertion of plates which would form such obstacles, and it would be a simple matter to make similar provision in the middle of the channel where the flow is fully developed. Such a study would also further the liquid analogy approach.

A phenomenon sometimes observed in the channel which should prove most interesting to investigate is that of the so-called "hydraulic jump" described in Chapter 4.

It can be seen from the fore-going that the test rig constructed is well-suited to the performing of further work of many types, both along the lines suggested here and, no doubt, others.

CHAPTER 7.

NOMENCLATURE

Nomenclature

A	Flow area.
B_s	Width of settling chamber (Al.)
B_6	$\left[\frac{4g_c\mu_g(\rho_s - \rho_g)}{3\rho_g^2}\right]^{\frac{1}{3}}$ (Al.)
B_7	$\left[\frac{3\mu_g^2}{4g_c\rho_g(\rho_s - \rho_g)}\right]^{\frac{1}{3}}$ (Al.)
$\bar{b}$	Half channel width (see figure 3.2)
C	Chezy coefficient.
C_d	Drag coefficient.
D	Pipe diameter
D	Cyclone dimension (Al.)
D_E	Equivalent diameter.
d	Diameter of pneumatic conveying line.
d_b	Bubble diameter.
d_{mean}	Mean of two sieve sizes $\sqrt{d_1.d_2}$
d_p	Particle diameter.
d_{pm}	Mean size of sample.
d_{sv}	Surface to volume diameter of particle.
d_t	Bed or tube diameter (Eqn.2.24).
d_1, d_2	Sieve diameters.
F_r	Froude Number $\frac{U_f^2}{d_p g_c}$
$F_{r_{mf}}$	Froude Number at incipient fluidisation point $\frac{U_{mf}^2}{d_p g_c}$

f	Darcy friction factor.
f_b	Bend friction coefficient (Al.)
f_F	Fanning friction factor.
f_g	Friction coefficient (Al.)
f_i	Experimental value of dependant variable (CH.3)
f_p	Friction coefficient (Al.)
f_1, f_2	See Appendix 6.
Ga	Galileo Number $\frac{\rho_g(\rho_s - \rho_g)g_c d_p^3}{\mu_g^2}$
$\underline{G_s}$	Air loading in pneumatic line (Al.)
G	
g_c	Gravitational constant.
h	Bed height
h_{mf}	Bed height at point of incipient fluidisation.
H_s	Height of settling chamber (Al.)
K'	Constant in power law.
$\bar{K}$	Constant (CH.3).
L	Length of pipe or channel.
L_E	Entrance length.
L_s	Length of settling chamber (Al.)
l	Length of side of square pneumatic return duct (Al.).
$\dot{M}$	Mass flow rate of solids.
N	Number of data points (CH.3).
N_{RE}	Generalised Reynolds Number.
n	See Appendix 6.
n'	Exponent in power law.
Q	Liquid flow rate (CH.3).
$\dot{Q}$	Volumetric flow rate of solids.

Q_A	Air volumetric flow rate (A4.).
Q_l	Flow rate per unit channel width Q/w.
q	Air flow rate.
R	Pipe radius (CH.3).
Re	Reynolds Number $\frac{\rho U d}{\mu}$
Re_p	Particle Reynolds Number, generally $\frac{d_p \rho_g U_f}{\mu_g}$
$Re_{p,mf}$	Particle Reynolds Number at point of incipient fluidisation.
	N.B. Other variations of Reynolds Number are defined as they occur, notably in Chapter 2.
R_H	Hydraulic Radius.
S	Specific surface of solids.
S_o	Channel slope.
U	Channel flow velocity.
U_b	Bubble rise velocity.
U_{ch}	Choking velocity (A1.)
U_{cs}	Saltation velocity.
$U_{cs,m}$	Saltation velocity corresponding to maximum particle size.
U_f	Fluidising velocity.
U_g	Gas velocity in pneumatic line (A1.).
U_{mb}	Minimum bubbling velocity
U_{mf}	Minimum fluidising velocity.
U_o	Air velocity if airalone flowing in pneumatic line(A1.
U_s	Solids velocity (A1.).
U_t	Particle terminal velocity.
V_b	Bubble volume.

V_s	Slip velocity.
w	Channel width.
Z	$K'8^{n'-1}$

α	Angle of inclination.
$\alpha_1, \alpha_2, \alpha_3, \alpha_4$	System parameters (CH.3).
γ	Shear rate.
ΔP	Pressure drop along channel.
ΔP_a	Pressure drops (Al.).
ΔP_b	
ΔP_{fg}	
ΔP_{fs}	
ΔP_h	
ΔP_{horiz}	
ΔP_{vert}	
$\Delta P_{f_{vert}}$	
ΔP_B	Pressure drop across fluidised bed.
ϵ	Bed voidage.
ϵ_{mf}	Bed voidage at point of incipient fluidisation.
ϵ_i	Error function (CH.3).
η	Settling chamber efficency (Al.).
μ	Viscosity. (suffix g if gas viscosity).
ρ	Liquid density.
ρ_g	Gas density.
ρ_s	Solids density.
$\bar{\rho}$	Density of fluidised bed.
τ	Shear stress.
ϕ_s	Sphericity.

CHAPTER 8.

REFERENCES.

References

1.	Alves G.E.	Chem.Eng.Sci. 56, 107, 1949.
2.	Alves G.E., Boucher D.F. and Pigford R.L.	Chem.Eng.Prog. 48, 385, 1952.
3.	Anon.	Engineer, 27 June 1974.
4.	Astarita G., Marrucci and Palumbo G.	Ind. & Eng.Chem.Fund. 3, 333, 1964
5.	Baerns M.	Ind. & Eng.Chem.Fund. 5,508,1966.
6.	Baeyens J. and Geldart D.	Chem.Eng.Sci. 29, 1974.
7.	Baumgarten P.K. and Pigford R.L.	A.I.Ch.E.J. 6, 115, 1960.
8.	Baskakov A.P.	In "Fluidisation" Edited by J.F. Davidson and D. Harrison. Academic Press. 1971.
9.	Baskakov A., Malykh G.A., Shisko I.I. and Usmanova L.G.	Int.Chem.Eng. 13, 1973.
10.	Benenati R.F. and Brosilow C.B.	A.I.Ch.E.J. 8, 359, 1962.
11.	Bessant D.J.	Ph.D. thesis, Univ. of Birm.1973.
12.	Bloore P.D. and Botterill J.S.M.	Nature 190, 250, 1961.
13.	Bogue D.C.	Ind. & Eng.Chem. 51, 874, 1959.
14.	Boland D.	Ph.D. Thesis, Bradford, 1972.
15.	Boland D., Al-Salim Q.A.W. and Geldart D.	Chem.Eng.Sci. 24, 1389, 1969.
16.	Boland D. and Geldart D.	Pow.Tech. 5, 289, 1971/72.
17.	Boothroyd R.G. and Goldberg A.S.	Brit.Chem.Eng. 14, 1705, 1969 15, 357, 1970.
18.	Botterill J.S.M. and Bessant D.J.	"Powtech" conf. Harrogate 1973.
19.	Botterill J.S.M. and Elliott D.E.	Engineering 198, 146, 1964.
20.	Botterill J.S.M. and Van der Kolk M.	A.I.Ch.E. Symp. Ser. 67, No.116 70, 1971.
21.	Botterill J.S.M., Chandrasekhar R. and Van der Kolk M.	Brit.Chem.Eng. 15, 769, 1970.

22. Botterill J.S.M., Elliott D.E., Van der Kolk M. and McGuigan S.J. — Pow.Tech. 6, 334, 1972.

23. Burkett R.J., Chalmers-Dixon P., Morris P.J. and Pyle D.L. — Chem.Eng.Sci. 26, 405, 1971.

24. Buyevich Y.A. — J.Appl.Math.Mech. 32, 382, 1968.

25. Buyevich Y.A. — Chem.Eng.Sci. 26, 1195, 1971.

26. Buyevich Y.A. — J.Fl.Mech. 52, 345, 1972.

27. Caldwell D.H. and Babbitt H.E. — Ind.&Eng.Chem. 33, 249, 1941.

28. Carmen P.C. — Trans.Inst.Chem.Eng. 15,150,1937

29. Ciborowski J. and Wlodarski A. — Chem.Eng.Sci. 17, 1962.

30. Cramer S.D. and Marchello J.M. — A.I.Ch.E.J. 14, 980, 1968.

31. Daniels T.C. — J.Mech.Eng.Sci. 4, 103, 1962.

32. Davidson J.F. — Trans.Inst.Chem.Eng. 39,230,1961

33. Davidson J.F. and Harrison D. — Chem.Eng.Sci. 21, 731, 1966.

34. Davidson J.F. and Harrison D. — "Fluidised Particles" Camb. Univ. Press.

35. Davies R.M. and Taylor G.I. — Proc.Roy.Soc. A200, 375.

36. Dickey B.R., Grimmett E.S. and Kilian D.C. — Chem.Eng.Prog. 70, 1974.

37. Diekman R. and Forsythe W.L. — Ind. & Eng.Chem. 45, 1174, 1953.

38. Dodge D.W. and Metzner A.B. — A.I.Ch.E.J. 5, 189, 1959.

39. Einstein V. and Gelperin N. — In "Fluidisation" Davidson and Harrison.

40. Elliott D.E. — Inst. of Fuel total energy conference paper 23. Brighton 19

41. Elliott D.E. — Priv. Comm.

42. Elliott D.E. — C.M.E. July 1970.

43. Elliott D.E. and Gliddon B.J. — Paper presented at "Hydrotransport 1" 1970.

44. Ergun S. — Chem.Eng.Prog. 48, 89, 1952.

45.	Ergun S.and Orning A.A.	Ind. & Eng.Chem. 41, 1179, 1949.
46.	Eyring H.	J.Chem.Phys. 4, 283, 1936.
47.	Furukawa J. and Ohmae T.	Ind. & Eng.Chem. 50, 821, 1958.
48.	Gabor J.D.	Chem.Eng.Jnl. 4, 118, 1972.
49.	Geldart D.	Pow.Tech. 7, 285, 1973.
50.	Geldart D.	Pow.Tech. 6, 201, 1972.
51.	Geldart D.	Pow.Tech. 1, 355, 1967/68.
52.	Gliddon B.J.	C.E.G.B. research report RD/M/N283.
53	Godard K. and Richardson J.F.	Chem.Eng.Sci. 24, 363, 1969.
54.	Goldschmidt D. and LeGoff P.	Chem.Eng.Sci. 18, 805, 1963.
55.	Grace J.R.	Can.J.Chem.Eng. 48, 30, 1970.
56.	Graham W. and Harvey E.A.	Can.J.Chem.Eng. 43, 146, 1965.
57.	Gupalo Yu. P.	Int.Chem.Eng. 2, 376, 1962.
58.	Hagyard T. and Sacerdote A.H.	Ind. & Eng.Chem.Fund. 5,500,1966.
59.	Harrison D, Davidson J.F. and de Kock J.	Trans.Inst.Chem.Eng. 39, 202, 1961.
60.	Harrison D. and Grace J.R.	In "Fluidisation" Davidson and Harrison.
61.	Harrison D. and Leung L.S.	Trans.Inst.Chem.Eng. 40, 146, 1962.
62.	Hovmand S. and Davidson J.F.	In "Fluidisation" Davidson and Harrison.
63.	Jackson R.	Trans.Inst.Chem.Eng. 41, 13,1963.
64.	De Jong J.A.H. and Nomden J.F.	Pow.Tech. 9, 1974.
65.	Kiselnikov V.N., Vyalkov V.V. and Filatov V.M.	Int.Chem.Eng. 7, 428, 1967.
66.	Kramers H.	Chem.Eng.Sci. 1, 35, 1952.
67.	Kreiger I.M. and Elrod H.	J.App.Phys. 24, 134, 1953.
68.	Kreiger I.M. and Maron S.H.	J.Appl.Phys. 25, 72, 1954. 23, 147, 1952.

69. Kunii D. and Levenspiel O. "Fluidisation Engineering" J. Wiley N.Y. 1968.

70. Leeden P.v.d. and Bouwhuis G.J. App.Sci.Res. A10, 78, 1961.

71. Leva M. Chem.Eng.Prog. 47, 39, 1951.

72. Leva M. Chem.Eng.Prog. 44, 511, 1948. 44, 619, 1948.

73. Leva M. "Fluidisation" McGraw Hill N.Y. 1959.

74. Liu F. Fa-Keh and Orr C. J.Chem.Eng.Data 5, 430, 1960.

75. Martyushin I.G. and Kharakoz V.V. Int.Chem.Eng. 7, 255, 1967.

76. Massimilla L. In "Fluidisation". Davidson and Harrison.

77. Massimilla L., Betta V. and Della Rocca C. A.I.Ch.E.J. 7, 502, 1961.

78. Massimilla L., Volpicelli G. and Zenz F. Ind. and Eng.Chem.Fund. 2, 194, 1963.

79. Matheson G.L., Herbst W.A. and Holt P.H. Ind. and Eng. Chem. 41, 1099, 1949.

80. Matsen J.M. Pow.Tech. 7, 93, 1973.

81. Mersmann A. Chemie.Ing.Techhk. 38,1095,1966.

82. Metzner A.B. Chem.Eng.Prog. 50, 27, 1954.

83. Metzner A.B. and Reed J.C. A.I.Ch.E.J. 1, 434, 1955.

84. Morrison F.A. Ind. and Eng. Chem.Fund. 8, 594, 1969.

85. Morse R.D. Ind. and Eng.Chem 46,1117,1949.

86. Morse R.D. and Ballow C.O. Chem.Eng.Prog. 47, 199, 1951.

87. Motamedi M. and Jameson G.J. Chem.Eng.Sci. 23, 791, 1968.

88. Murray J.D. J.Fl.Mech. 21, 337, 1965. 22, 57, 1965.

89. Muskett W.J., Leicester A.R. and Mason J.S. Paper presented at "Pneumotransport 2". Sept. 1973.

90.	McMillan E.L.	Chem.Eng.Prog. 44, 537, 1948.
91.	McGuigan S.J. and Elliott D.E.	Paper presented at 4th Chisa conference. Prague Sept. 1972.
92.	McGuigan S.J.	Ph.D. thesis in preparation.
93.	Narsimhan G.	A.I.Ch.E.J. 11, 550, 1965.
94.	Neuzil L. and Turcajova M.	Coll.Cz.Chem.Comm. 34, 3652, 1969.
95.	Nicodemo L., Nicolais L. and Landel R.F.	Chem.Eng.Sci. 29, 729, 1974.
96.	Oldroyd J. G.	Proc.Roy.Soc. A200, 523, 1950.
97.	Oldroyd J.G.	Proc.Roy.Soc.A245, 278, 1958.
98.	Omarov S.M., Maslovskiy M.F. and Budkov V.A.	Sov. Chem.Ind. No.2. 131, 1971.
99.	Ormiston R.M.	Ph.D. Thesis, Cambridge, 1966.
100.	Owen W.M.	Trans.Am.Soc.Civ.Eng. 119, 1157, 1954.
101.	Parent J.D., Yagol N. and Steiner C.S.	Chem.Eng.Prog. 43, 429, 1947.
102.	Perry R.H.	Chemical Engineers Handbook McGraw_Hill 1963.
103.	Peters K. and Schmidt A.	Oesterreich Chemiker Zeitung, 54, 253, 1953.
104.	Pigford R.L. and Barron T.	Ind. and Eng.Chem.Fund. 4, 81, 1965.
104a.	Pillai K.K.	Priv.Comm.
105.	Pinchbeck P. and Popper F.	Chem.Eng.Sci. 6, 57, 1956.
106.	Powell H.E. and Eyring H.J.	Nature 154, 427, 1944.
107.	Prudhoe J. and Whitmore R.L.	Brit.Chem.Eng. 9, 371, 1964.

108.	Qassim R.Y.	Ph.D. thesis. London 1970.
109.	Richardson J.F.	In "Fluidisation" Davidson and Harrison.
110.	Ritzmann H. and Schugerl K.	Chem.Eng.Sci. 29, 427, 1974.
111.	Romero J.B. and Smith D.	A.I.Ch.E.J. 11, 595, 1965.
112.	Romero J.B. and Johanson L.N.	Chem.Eng.Prog.Symp.Series, 58, 28, 1962.
113.	Rowe P.N.	Trans.Inst.Chem.Eng. 39,175,1961.
114.	Rowe P.N. and Stapleton W.M.	Trans.Inst.Chem.Eng. 39,180,1961.
115.	Rowe P.N. and Partridge B.A.	Trans.Inst.Chem.Eng. 43,157,1965.
116.	Rowe P.N. and Sutherland K.S.	Trans.Inst.Chem.Eng. 42,55,1964.
117.	Rowe P.N.	In "Fluidisation". Davidson and Harrison.
118.	Sandy C.W., Daubert T.E. and Jones J.H.	Chem.Eng.Prog.Symp.Series. Vol.66 No.105.
119.	Saxton J.A., Fitton J.B. and Vermeulen T.	A.I.Ch.E.J. 16, 120, 1970.
120.	Schechter R.S.	A.I.Ch.E.J. 7, 445, 1961.
121.	Schugerl K.	In "Fluidisation" Davidson and Harrison.
122.	Schugerl K., Merz M. and Fetting F.	Chem.Eng.Sci. 15, 39 & 75, 1961.
123.	Seely G.R.	A.I.Ch.E.J. 10, 56, 1964.
124.	Siemes W. and Hellmer M.	Chem.Eng.Sci. 17, 555, 1962.
125.	Simpson H.C. and Rodger B.N.	Chem.Eng.Sci. 16, 153, 1961.
126.	Shuster W.W. and Haas F.C.	J.Chem.Eng.Data. 5, 525, 1960.
127.	Squires A.M.	U.S.Patent 3, 268, 264.
128.	Stairmand C.J.	Trans.Inst.Chem.Eng. 29, 356, 1951.
129.	Stewart P.S.B.	Trans.Inst.Chem.Eng. 46, 60, 1968.

130.	Straub L.G., Silberman E. and Nelson H.C.	American Soc. Civil Eng. Paper 2935.
131.	Toomey R. and Johnstone H.F.	Chem.Eng.Prog. 48, 220, 1952.
132.	Tuot J. and Clift R.	A.I.Ch.E.Symp. 69, 78, 1973.
133.	Trawinski H.	Chemie.Ing.Techn. 23,416,1951. 25,201,1953.
134.	Trees J.	Trans.Inst.Chem.Eng. 40,286,1962.
135.	Trevedi R.C. and Rice W.J.	Chem.Eng.Prog.Symp.Ser. 62, 57, 1966.
136.	Vakhrushev I.A. and Basov V.A.	Int.Chem.Eng. 12, 319, 1972.
137.	Verloop J. and Heertjes P.M.	Chem.Eng.Sci. 25, 825, 1970.
138.	Virr M. and Reynoldson R.	Ind.Process Heating Dec.1972.
139.	Volk W., Johnson C.A. and Stotler H.H.	Chem.Eng.Prog.Symp.Series 58, 38, 1962.
140.	Van Wazer J., Lyons J., Kim K. and Colwell R.	"Viscosity and Flow Measurement" J. Wiley N.Y. 1963.
141.	Weislehner G.	Chemie.Ing.Techn. 42,524,1970.
142.	Wen C.Y. and Yu Y.H.	A.I.Ch.E.J. 12, 610, 1966.
143.	Wheeler J.A. and Wissler E.H.	A.I.Ch.E.J. 11, 207, 1965.
144.	Whitehead A.B.	In "Fluidisation" Davidson and Harrison.
145.	Wilhelm R.H. and Kwauk M.	Chem.Eng.Prog. 44, 201, 1948.
146.	Yagi S. and Kunii D.	Chem.Eng.Sci. 16, 364, 1961.
147.	Yasui G. and Johanson L.	A.I.Ch.E.J. 4, 445, 1958.
148.	Zenz F.A. and Othmer D.F.	"Fluidisation and fluid-particle systems". Reinhold N.Y. 1960.

APPENDICES

APPENDICES

APPENDIX 1

THE TEST RIG

The Test Rig

The channel flow test rig is of considerable overall size, measuring 7m. in length and 6.1m. in height. It incorporates a test channel 3m. in length, along which solids flow at a maximum rate of 10 kg/s. A full drawing of the rig is shown in figure A.1.1.

A1.1 Channel and auxiliaries

A drawing of part of the test channel is shown in figure A1.2 and a cross section in figure A1.3. The channel has a steel base section which acts as a plenum chamber for the fluidising air. The sides of the channel are constructed in 6 mm. perspex in three separate 1m. lengths, the middle one forming the actual test section. At each end of the channel is mounted a receiver which acts as a stabilising reservoir for the flow. The "neck" section of one of these receivers is shown in figure A1.4. These receivers have similar steel base sections/plenum chambers, but their top sections are also made of steel. Each receiver has a "neck" of 150 mm. internal width which matches the width of the channel ends. In the case of the 100 mm. wide channel sections, these 150 mm. end pieces are joined to the body of the channel by tapering sections as shown in figure A1.5. The channel and both receivers are fluidised, the distributor being effectively continuous; joins between channel and receiver distributors are effected by narrow metal strips clamping the two ends onto a fixed strip beneath the distributor.

The distributor used is a 3 mm. thick porous plastic material which accepts the flexing necessary when the channel is inclined. The inclination of the channel is infinitely variable between horizontal and 30° downwards, movement being by means of a hydraulic ram acting through the linkage shown in figure A1.6. This latter was necessary because a ram of the required stroke

fitted at the end of the channel had a closed length too great to be accommodated in the available space. When the desired inclination is achieved, the end of the channel is supported on pairs of eccentric discs which bolt into holes in the leading edges of the large curved plates shown in figure A1.7. Sideways location is by means of clamping screws onto the sides of these plates, an arrangement clearly shown in figure A1.7.

The plastic distributor has rubber gaskets on either side, the ones below being of thin (1.5 mm.) material, but the upper ones, between distributor and perspex channel section, are thicker (3.5 mm.) aerated soft rubber to prevent cracking of the perspex as the assembly is tightened. It is only necessary to "nip" the perspex sections down onto this soft rubber to effect the seal. As these gasket strips are made in several sections, the joins between their ends take the form of labyrinths to minimise the possibility of air or solids leakage. The joints between the channel ends and the receiver "necks" are again sealed by rubber gaskets both below the distributor, between plenum chamber sections, and above it, between wall sections. Both top and bottom gaskets also incorporate the appropriate section of distributor upper or lower gasket, and thus are of quite complex shape. They have a "concertina" form to allow for the inclination of the channel, and the receiver "necks" are in two separate sections to allow easier assembly of the gasket system. Where appropriate the gaskets are fixed to the steel sections with "PANG" rubber adhesive; any small gaps remaining after assembly are filled with silicon rubber.

Efflux from the bottom receiver is controlled by a manually operated valve of a type which incorporates a nylon "iris" diaphragm. From this valve,solids drop through a short steel tube and finally through a flexible tube which allows for the channel movement into

a hopper which opens at its base onto the conveyor belt. There is a gap of approximately 40 mm. between the hopper and the belt, and this is partially closed by rubber flaps to minimise solids loss due to "splashing" onto the belt.

Having passed through the conveyor/elevator return system, solids are discharged at the top of the rig into a hopper which is again provided with the same type of valve. This controls the flow of solids into the weighfeeder mechanism, which discharges into the upper receiver. A third valve is fitted in the centre of this component, controlling flow into a long vertical 150 mm. diameter perspex tube, at the base of which is a large hopper with a final control valve at its outlet. This tube and hopper provide most of the solids storage in the system, the smaller hopper above the weighfeeder mechanism providing the remainder.

A1.2 Solids return system

Initial designs for the rig called for the provision of a lean-phase pneumatic return system. The design for this was fully evaluated (see A1.8) and appeared on several of the initial rig design drawings. After a time, however, this system was discarded because of the high air-power requirement, anticipated problems with electrostatic charge build-up, and perhaps most serious, the difficulty anticipated in cleaning the conveying air adequately. This latter problem had already necessitated the incorporation in the design of a cyclone and large settling chamber in series, but it was thought that even this system would allow some dust to be carried by the air exhausting from the system. The test rig is constructed in a location where the discharge of large quantities of air, albeit carrying only comparatively small amounts of dust, is unacceptable, and this consideration alone was sufficient to

force the abandonment of the pneumatic return system. The return system chosen consists of a conventional belt conveyor and bucket elevator. The conveyor belt is a type having raised sides to prevent solids loss, and the elevator is a dredger type (inlet and outlet on the same side of the equipment).

A1.3 Solids metering

Solids flowing from the top hopper fall through a chute supplied by the weighfeeder manufacturers onto the belt of a Wallace and Tiernan "Superweigh" pneumatic gravimetric meter, shown in figure A1.8. This consists basically of a continuously moving rubber belt, a section of which is supported on load cells which when supplied with air at 20 lbf/in^2 provide a pressure signal proportional to the weight on the belt section, this being indicated on a mercury manometer. The normal belt speed is 72 ft/min., but for continuous work at low flow rates, this may be reduced to 36 or 18 ft/min. by appropriate alterations to the drive gearing. Provided care is taken to ensure an even feed of solids onto the belt, the weighfeeder has proved to be reliable and accurate. The manometer pressure indicated varies between 3 lbf/in^2 (155.17 mm.Hg) at zero mass flow rate and 15 lbf/in^2 (775.86 mm.Hg) at a flow rate of 9.984 kg/s., the calibration being linear. The mass flow rate indicated is also directly proportional to the belt speed.

A1.4 Air supplies

The air supply needed for the weighfeeder comes from a small compressor which feeds a reservoir maintained at approximately 60 lbf/in^2. The air is then regulated down to the 20 lbf/in^2 needed for the meter.

All fluidising air is supplied by a single fan,whose output is regulated by a butterfly valve at its inlet. The air passes

to a manifold which splits the flow into four for metering by a bank of rotameters consisting of three type 65K instruments and one type 65A. This bank of rotameters is shown, together with the electrical controls, in figure A1.9. The manifold incorporates a quick-action emergency blow-off valve exhausting to atmosphere. From the common outlet to the rotameter bank the air passes to a manifold which splits the supply into three, one for each receiver and the other forthe channel. The receiver supplies are fed to manifolds which split them into the appropriate number of individual supplies for the inlets to the receivers; in the case of the upper receiver five, and in the case of the somewhat smaller lower receiver three. One air inlet is located in the narrow "neck" of each receiver. The air supply to the channel is fed into a long manifold located directly below the channel plenum chamber. From this manifold, air is supplied to the plenum chamber through eight short pipes. All air inlets are baffled to prevent air jetting onto the lower face of the distributor, these baffles mainly taking the form of "top-hats" placed over the inlet pipes.

The fluidising air supply system has worked well, fluidisation being visually uniform, but it has certain restrictions. These, together with solutions, are discussed later (section A1.7).

A1.5 Instrumentation

Most of the instrumentation fitted, for monitoring bed height and uniformity, channel slope and fluidising air conditions, has already been described in Chapter 3, and is shown in figure A1.11. That remaining consists of light sensitive cells which are inserted into the hopper above the weighfeeder, the lower receiver, and the storage hopper. These provide a signal if the light supply to them is interrupted (electric lights provide this) and thus

indicate, both audibly and visibly, when the solids level reaches them. This system is a useful safety device.

A1.6 General

Because of its overall size, it was necessary to construct the rig in a location where much of it was below ground level. This introduces few problems, apart from the relatively poor access to the control valve at the base of the storage hopper. A platform next to this hopper had to be provided, reached by a short ladder. A further ladder is provided to enable access to the valve above the weighfeeder to be gained (see figure A1.12).

Initial testing showed that the rig generateda certain amount of dust, mainly due to the entrainment of very small particles. Because of this, it was decided to enclose the rig completely; this was done using a "Dexion" framework clad in perspex sheet. The enclosure is provided with a large extractor, sucking through two outlets in the roof. The air passes through a series of bag filters before being discharged to atmosphere. The perspex sheeting is treated with anti-static solution to minimise the adherance of fine particles to it.

A1.7 Operational problems and suggested modifications

One of the major operational problems encountered during testing has been the distributor blockage discussed in earlier chapters. Fine particles suspended in the air are sucked into the fan, and although many adhere to the flexible pipes carrying the air, some find their way through into the channel and receiver plenum chambers leading to considerable dirtying of the distributor over a period. This inevitably causes disturbance of the fluidisation patterns, together with greatly increased distributor pressure drop which can lead to a decrease in fan output. This problem is much less pronounced now that the rig is enclosed and fitted with

an extractor, but it still exists, mainly due to the lack of a filter on the fan inlet. An extremely fine filter would be necessary to remove the very small particles (only a few μm in diameter) which cause the problem, but such a filter would inevitably have a high pressure drop, and would restrict the output of the existing fan to an unacceptable extent, as even with a new distributor fitted, the fan capacity is only just sufficient to fulfill the design requirement. The ideal solution would be to utilise a new fan of increased capacity. This should be placed in a sound insulated enclosure outside the normal rig enclosure.A very fine filter would no longer be necessary, and the noise level inside the enclosure would be considerably reduced, improving the working environment. Ideally, this change of fan location should be done as part of an overall revision of the fluidising air system. Although fluidisation is visually quite uniform in all three components, it would be an advantage for them to be fluidised separately; as an aid to dissipating an increase in downstream bed height for example. To accomplish this, the air flow should be split into three immediately downstream of the fan, taking care to ensure that all three supplies are equal, and additional rotameters incorporated. Obviously, the plenum chambers of the three components would have to be divided from one-another by airtight partitions. Should any such revision of the air supply system take place, it would be extremely useful to incorporate provision for control of the air temperature and humidity. Ideally this will involve provision of both a heater and cooler, together with means of increasing or decreasing the moisture content of the air. Clearly, because of the large air flow used ($10m^3$/min. maximum) such pieces of equipment will of necessity be large and expensive. The moisture content could be increased simply by spraying water under pressure into a chamber through which

the air passes, but the solutions to the heating, cooling and drying parts of the treatment are much more complex. It is probable, at this stage, that the improvement in versatility of the rig brought about by such changes to the sir supply system would not be sufficient to justify the expenditure incurred.

As a further small point on the air supply system, tests have shown that the metal strips on the "necks" of the receivers which cover the joins between channel and receiver distributors do cause a slight "dead" spot in the fluidised bed. Although apparently of little importance, this could obviously be avoided by cutting the entire distributor from a single sheet of porous material.

Most of the dust at present generated by the rig comes from two sources, the weighfeeder belt and the point where the solids fall into the hopper at the base of the bottom receiver. Dust from the first source is due to particles adhering to the rubber belt of the weighfeeder and being scraped off by a blade just below the bottom run of the belt provided for this purpose. The particles then fall into the airstream created by the fan motor which is directly beneath. Should the fan be moved out of the rig enclosure, obviously the problem would become much less severe, but a simple solution in the short term would be to enclose the base of the weighfeeder to catch the particles before they can fall into the airstream. Two simple trays are already provided for this purpose, but gaps still exist which allow particles through; a more comprehensive tray arrangement should be installed.

Dust from the second source is generated by solids from the lower receiver falling a varying distance into the hopper beneath. The dust could be prevented from leaving the hopper by means of a simple shroud, of polythene or similar material, fitted between the

flexible tube and the top of the hopper. It is essential, however, to retain means whereby a visual check can be kept upon the level of solid material in the hopper. To allow this, a perspex section across the top of the hopper should be provided together with internal illumination. This latter would also allow provision of a level-sensing photocell similar to those used elsewhere on the rig as a safety measure.

The relative difficulty of access to the control valves located above the weighfeeder and below the storage hopper has already been mentioned. Operation of the rig by a single person would be made considerably easier by the installation of remote control mechanisms at these two points. The type of valve used can be operated either mechanically (through "Teleflex" cables) electrically or pneumatically; probably the simple and quite inexpensive mechanical alternative is adequate for this application. With such controls installed, it would be unnecessary for the operator to move from ground level during testing except for occasional checking of the carpet of material being deposited on the weighfeeder belt. Clearly, the operator could then devote more of his time and energy to the experimental work, something which would be particularly important in the likely event of much more sophisticated experimental and measurement techniques being used on the rig at some future date.

Perhaps the most serious operational shortcoming of the rig at present is the fact that the photocell installed in the top hopper (above the weighfeeder) provides the only measure of solids level in that hopper. Initially, visual checking of the level was possible, but the perspex enclosure now fitted has rendered this impossible. Obviously, it is advantageous from the point of view of supplying the weighfeeder with an even carpet of material that the solids level in this hopper should be kept constant. This is

extremely difficult to do at present. As internal illumination is already provided, two alternative means of checking the solids level suggest themselves. The simplest would be the provision of a clear window in the hopper, but checking the internal level would again require ascending to the platform alongside the weighfeeder. To avoid this, it should be possible to provide remote indication of level by means of an array of photocells. A possible system is shown schematically in figure A1.13.

The range of experiments so far performed has used only two channel widths. It is likely that in the future it will be desirable to use many aspect ratios and hence several widths of channel. The two widths currently used are achieved by means of two completely separate perspex channels, but obviously the construction of many channel sections is to be avoided if possible. It should be feasible to construct one universal channel having wide slotted flanges which would allow the width to be varied without time-consuming stripping and re-building of the channel. Clearly, such an arrangement would make effective gasketing a much more complex problem, but it should not prove to be insoluble.

In conclusion, it must be said that the test rig has fulfilled its design objectives, and has generally performed well throughout the programme of tests. The modifications suggested are comparatively minor ones, and none are made essential by anyshortcoming in the rig as it now stands.

A1.8 Pneumatic return system design calculations

The calculations performed during the design of the pneumatic return system are based, unless otherwise stated, on procedures fully described by KUNII and LEVENSPIEL[69]; only an outline is presented here.

Necessary data:

Channel width = 150 mm.

Projected maximum bed height = 150 mm.

Projected maximum velocity at this depth = 0.3 m/s.

True density of sand, measured = 2.7047×10^3 kg/m^3.

Density when just fluidised, calculated from experimental results = 1.3×10^3 kg/m^3.

Density of air at 27°C. = 1.18 kg/m^3.

Viscosity of air at 27°C. = 1.846×10^{-5} Ns/m^2 or kgm/s.

Sand mean particle size approximately 150 μm.

Sand maximum particle size approximately 400 μm.

Horizontal section total length = 8 m.

Vertical section total length = 3 m.

The first calculations are designed to find the required conveying pipe size and air velocity.

Mass flow rate of sand for 150 mm. square bed travelling at 0.3 m/s is 8.78 kg/s.

It is now necessary to assume a value for air loading, that is, the ratio of solid to gas mass flow rates. Both information given in the above reference, and the author's previous experience, indicated that a value between 5 and 20 would be reasonable; 15 was chosen.

Thus air flow rate = $\frac{8.78}{15}$ = 0.585 kg/s. = 0.496 m^3/s.

Finding the correct pipe size and air velocity requires an iterative process.

Initially, choose an air velocity which is certain to keep all solids in suspension, say 9 m/s.

Flow area required = $\frac{0.496}{9}$ = 0.055 m^2.

If a circular pipe is used d = 0.265 m.

If a square duct is used l = 0.235 m.

We now calculate the saltation velocity using the procedure of Zenz.

$$\frac{d_p}{B_7} = d_p \Big/ \left[\frac{3\mu_g^2}{4 g_c \rho_g (\rho_s - \rho_g)} \right]^{\frac{1}{3}}$$

Insertion of the data gives $(B_7)^3 = 8.16 \times 10^{-9}$

$$B_7 = 2.01 \times 10^{-3}$$

The maximum particle size to be conveyed is 400 μm.

therefore $\left(\frac{d_p}{B_7} \right)_{MAX}$ = 19.9 which is the controlling parameter.

From the graph, figure A1.14, we obtain

$$\frac{U_{cs,m}}{B_6} = 3.6$$

$$B_6 = \left[\frac{4 g_c \mu_g (\rho_s - \rho_g)}{3 \rho_g^2} \right]^{\frac{1}{3}}$$

Insertion of the data yields:

$B_6 = 77.7$

therefore $U_{cs,m}$ = 3.6 x 77.7 cm/s. or <u>2.797 m/s.</u>

This is correct only for a pipe 0.0635 m. in diameter as used by Zenz.

Correcting for a pipe 0.265min diameter

$$\frac{2.797}{U_{cs,m}} = \left[\frac{0.0635}{0.265} \right]^{0.4} \text{ giving } U_{cs,m} = 4.95 \text{ m/s.}$$

Clearly the air velocity chosen is much too high.

Try an air velocity of 5 m/s.

Flow area = $\frac{0.496}{5}$ = 0.0992 m^2, d = 0.355 m.

$$\frac{2.797}{U_{cs,m}} = \left[\frac{0.0635}{0.355} \right]^{0.4} \qquad U_{cs,m} = 5.57$$

Try an air velocity of 6 m/s.

Flow area = $\frac{0.496}{6}$ = 0.0827 m^2, d = 0.324 m.

$$\frac{2.797}{U_{cs,m}} = \left[\frac{0.0635}{0.324}\right]^{0.4} \qquad U_{cs,m} = 5.37$$

Try an air velocity of 5.5 m/s.

Flow area = $\frac{0.496}{5.5}$ = 0.0902 m^2, d = 0.339 m.

$$\frac{2.797}{U_{cs,m}} = \left[\frac{0.0635}{0.339}\right]^{0.4} \qquad U_{cs,m} = 5.47 \text{ m/s.}$$

Clearly, these now match well, minimising the power requirements.

Pipe diameter = 0.339 m.

Air velocity = 5.5 m/s.

The minimum gas velocity required for vertical flow or choking velocity U_{ch} can be taken as

$U_{ch} \simeq \frac{1}{3}$ to $\frac{1}{5}$ U_{cs} so this is no cause for concern.

To calculate the likely pressure drop in the pneumatic system, it is necessary to calculate the terminal velocity of the particles

$$U_t = \left[\frac{4 g_c d_p (\rho_s - \rho_g)}{3 \rho_g C_d}\right]^{\frac{1}{2}}$$

where C_d is an experimentally determined drag coefficient.

A chart is given by KUNII and LEVENSPIEL relating

$$C_d Re_p^2 = \frac{4 g_c d_p^3 \rho_g (\rho_s - \rho_g)}{3 \mu_g^2}$$

to $Re_p = \frac{d_p \rho_g U_t}{\mu_g}$

Insertion of the required data gives $C_d Re_p^2 = 413$.

It is necessary to assume a value of shape factor, and a reasonable one is 0.8.

From the chart we obtain $Re_p = 4$, giving a value of U_t of 0.417 m/s.

Rose and Barnacle suggest that the pressure drop in a horizontal section is given by:

$$\Delta P_{horiz} = \Delta P_a + \Delta P_{fg} + \Delta P_{fs}$$

ΔP_a is the acceleration term.

ΔP_{fg} is the frictional pressure drop due to air only.

ΔP_{fs} is the frictional pressure drop due to solids only.

$$\Delta P_a = \frac{U_s}{g_c} \rho_g U_o \left(\frac{G_s}{G}\right)$$

where solids velocity $U_s \simeq U_g - U_t = (5.5 - 0.417)$

$= 5.083$ m/s

giving $\underline{\Delta P_a = 5.04 \text{ g/cm}^2.}$

$$\Delta P_{fg} = \frac{2 f_g \rho_g U_g^2 l}{g_c d_t}$$

the friction coefficient f_g depends on $Re_t = \frac{\rho_g U_g d_t}{\mu_g}$

which has a value of 11.81×10^4.

Two expressions are given for f_g

$$f_g = 0.0791 \left[\frac{\rho_g U_g d_t}{\mu_g}\right]^{-0.25} \quad \text{for } 3 \times 10^3 < Re < 10^5$$

$$f_g = 0.0008 + 0.0552 \left[\frac{\rho_g U_g d_t}{\mu_g}\right]^{-0.237} \quad \text{for } 10^5 < Re < 10^8$$

Using the latter expression, yields

$f_g = 0.0043$

and $\underline{\Delta Pf_g = 0.075 \text{ g/cm}^2}$

$$\Delta P_{fs} = \frac{\pi}{8}\left(\frac{f_p}{f_g}\right)\left(\frac{\rho_s}{\rho_g}\right)^{\frac{1}{3}}\frac{G_s}{G}\,\Delta P_{fg}$$

The value of f_p is obtained from figure A1.15 as 0.65×10^{-4}.

thus $\Delta P_{fs} = 4.26\ \Delta P_{fg}$

$= \underline{0.319\ g/cm^2}$

Thus the total horizontal section pressure drop is

$\underline{\Delta P_{horiz} = 5.43\ g/cm^2}$

The pressure drop in a bend is given by

$$\Delta P_b = 2f_b \bar{\rho} \frac{U_g^2}{g_c}$$

where $\bar{\rho}$ is the mean density of the gas/solid mixture, which may be approximated by

$$\bar{\rho} = \frac{G_s}{G}\frac{U_g}{U_s}\rho_g = 19.15\ kg/m^3.$$

The value of the coefficient f_b depends on the ratio of bend radius to tube diameter, for a ratio of 4, $f_b = 0.188$.

ΔP_b for 2 bends is $\underline{4.44\ g/cm^2}$

The pressure drop in the vertical section is

$$\Delta P_{vert} = \Delta P_h + \Delta P_{f_{vert}}$$

where ΔP_h is the static head $\bar{\rho}\,(h_2 - h_1)$

$\Delta P_{f_{vert}}$ is the friction drop, obtained in a similar way to that in the horizontal section.

The values are $\Delta P_h = 5.75\ g/cm^2$.

$\Delta P_{f_{vert}} = 0.197\ g/cm^2$

$\therefore\ \underline{\Delta P_{vert} = 5.947\ g/cm^2.}$

Thus the total pressure drop is $\Delta P_{horiz} + \Delta P_b + \Delta P_{vert}$

$= 15.82\ g/cm^2.$

or 0.16 m. water.

Total system pressure drop = 0.16 m. water

To extract the solids from the conveying air it was decided to use a settling chamber and cyclone separator in series.

Settling chamber

According to information given by PERRY[102], settling chamber efficiency

$$\eta = \frac{U_t L_s}{H_s V_s} = \frac{U_t B_s L_s}{q}$$

If we say that the velocity in the chamber $V_s = 1.5$ m/s.

the flow area $= \frac{0.496}{1.5} = 0.331\ m^2.$

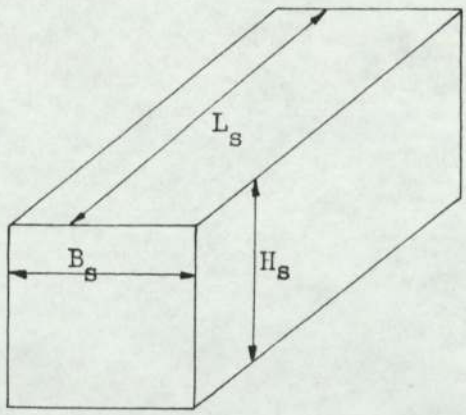

Assume initially that $H_s = 2B_s$

$$2B_s^2 = 0.331$$

$$B_s = 0.407 \text{ m.}$$

Assuming 100% efficiency

$$\frac{q}{U_t} = B_s L_s$$

$$\frac{0.496}{0.417} = 0.407 . L_s$$

$$L_s = 2.92 \text{ m.}$$

This seems rather excessive, so make $B_s = 0.5$ m., giving $L_s = 2.38$ m.

Now $B_s H_s = 0.331$, so H_s is now 0.662 m.

Thus a suitable size would be

$H_s = 0.66$ m.

$B_s = 0.5$ m.

$L_s = 2.38$ m.

Settling chambers are usually incapable of separating out particles smaller than 40 μm in diameter, and so clearly a cyclone separator

is also needed.

Cyclone

The design of the cyclone follows the procedure laid down by STAIRMAND[128]. The type chosen is the high-throughput type, the proportions of which are shown in figure A1.16.

Gas rate = $1500\ D^2\ m^3/hr$ where D is in feet.

Thus D = 1.091 ft = 0.333 m.

Inlet area = $0.75 \times 0.375\ D^2$ = $0.031\ m^2$.

Velocity in inlet = $\frac{0.496}{0.031}$ = 16 m/s or 52.5 ft/s.

This agrees well with Stairmand's data on pressure drop which is based on an inlet velocity of 50 ft/s.; thus it seems reasonable to use the figure he gives for cyclone pressure drop, that is, 4 in. water or 0.102 m. water.

Thus the total system pressure drop is 0.16 + 0.102

= 0.262 m. water.

This neglects the settling chamber, and allowing a safety factor, the conveying air fan capacity should be at least 0.6 m^3/s against a head of 0.4 m. water.

To feed the solids into the pneumatic line, it was decided to use a cylindrical rotary feeder.

The feeder must supply 8.78 kg/s of material at a density of say $2 \times 10^3\ kg/m^3$.

Let the feeder be 0.3 m. long.

Information given by PERRY suggests that a rotational speed of 30 rev/min be regarded as the upper limit, and that it is reasonable to assume that the feeder would run 70% full.

Volumetric flow rate = $\frac{8.78}{2 \times 10^3}$ = $4.39 \times 10^{-3}\ m^3/s$.

using the above figures yields a feeder diameter of 0.23 m.

Thus a feeder 0.3 m x 0.3 m would seem about the correct size.

KEY TO FIGURES APPENDIX 1

A1.1.	Overall drawing of rig.
A1.2.	The top end of the channel
A1.3.	Cross-section of the channel
A1.4.	The narrow "neck" of the top receiver.
A1.5.	Top view of the end of the 100 mm. wide channel.
A1.6.	Shows the hydraulic ram and associated linkage.
A1.7.	The water level system which indicates channel slope.
A1.8.	Shows the weighfeeder with the control valve above.
A1.9.	The rig controls.
A1.10.	A top view of the channel.
A1.11.	The instrumentation.
A1.12.	An end view of the rig.
A1.13.	Suggested solids level indication system.
A1.14.	Saltation velocity in 63.5 mm. tube.
A1.15.	Particle friction factor against Reynolds number.
A1.16.	Proportions of high throughput cyclone.

Figure A1.1

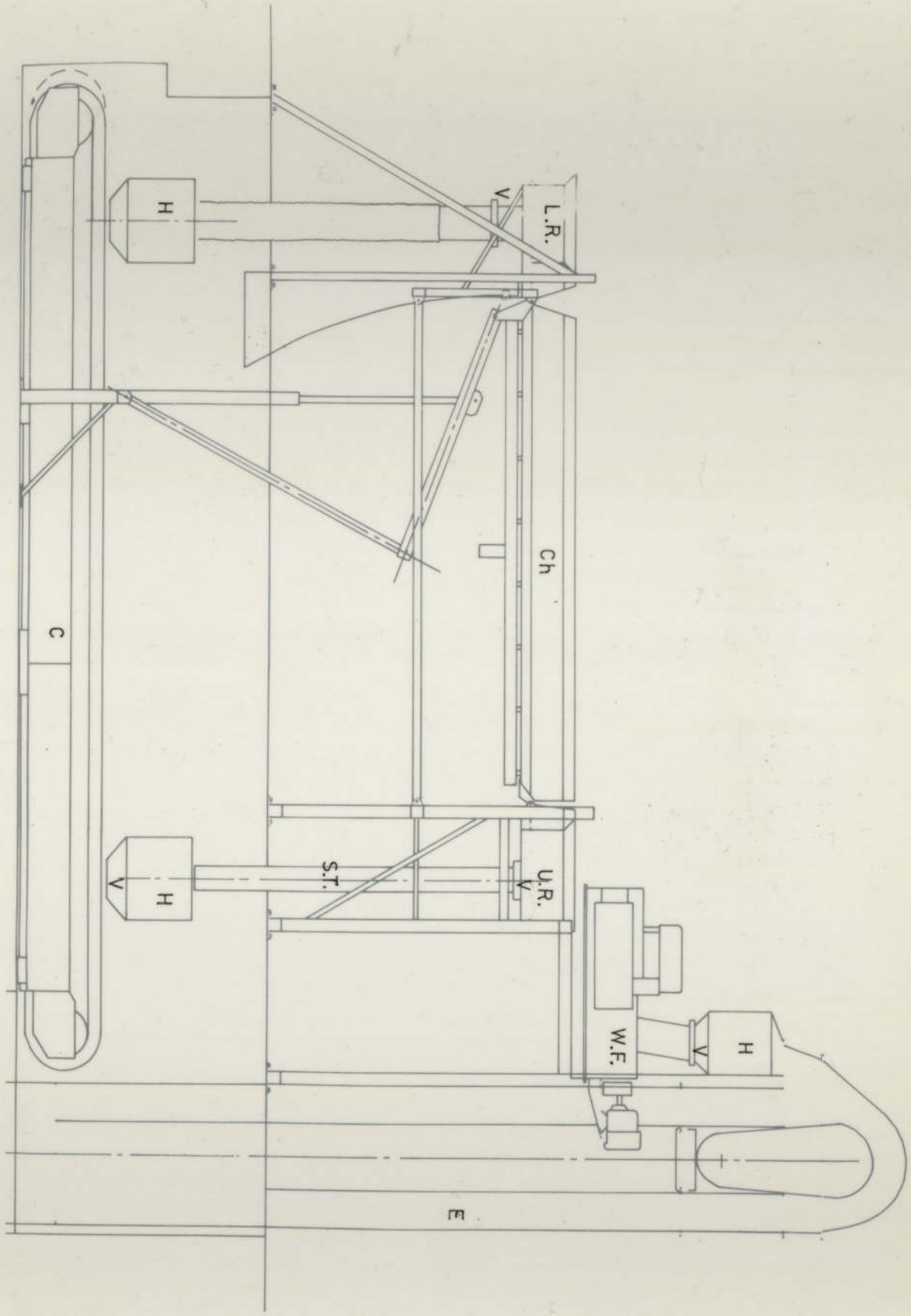

Figure A1.1

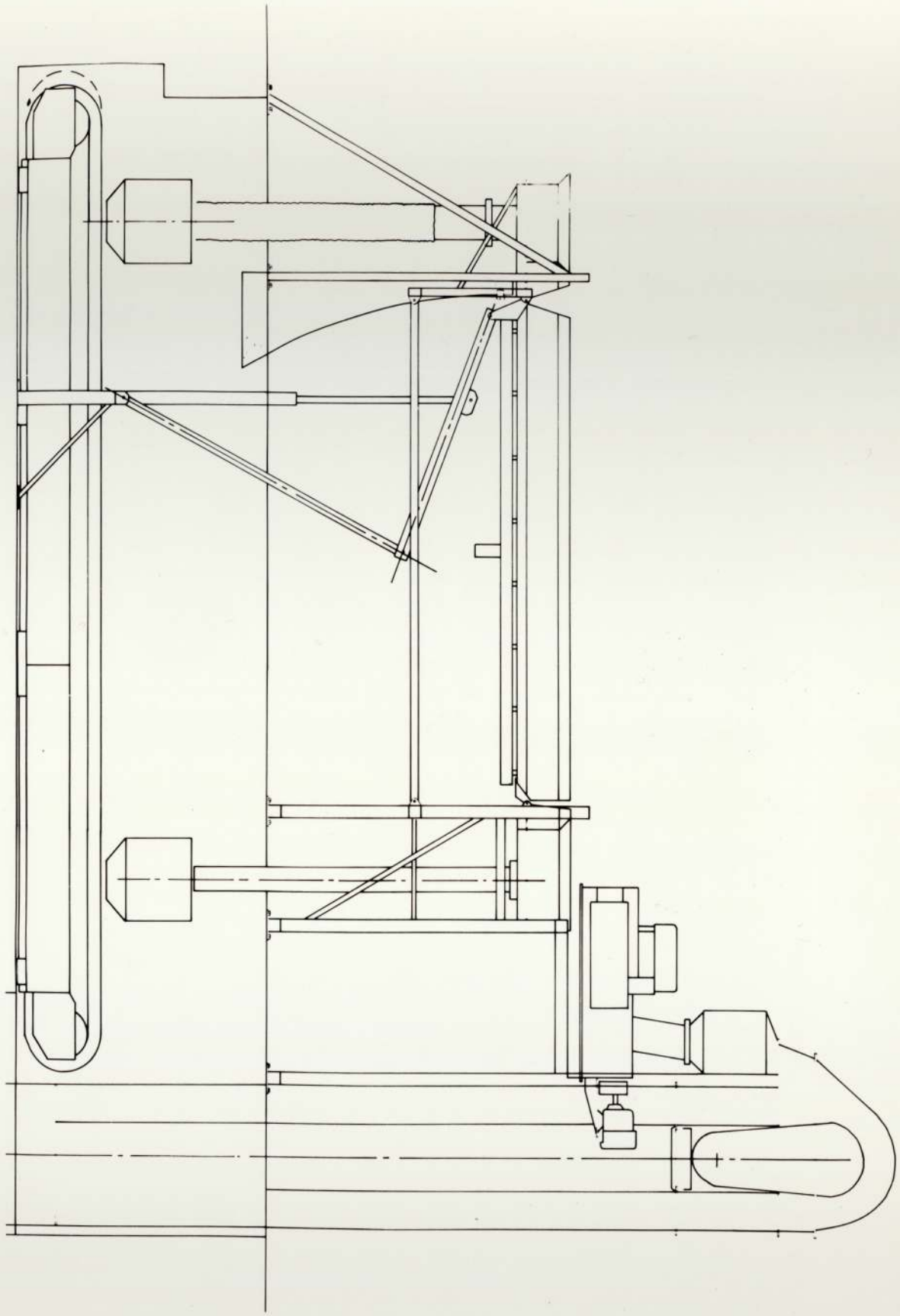

KEY TO FIGURE A1.1.

Ch.	Channel
U.R.	Upper receiver
L.R.	Lower receiver
H	Hopper
C	Conveyor
E	Elevator
S.T.	Storage tube
W.F.	Weighfeeder
V.	Valve

Figure A1.2

CHANNEL END

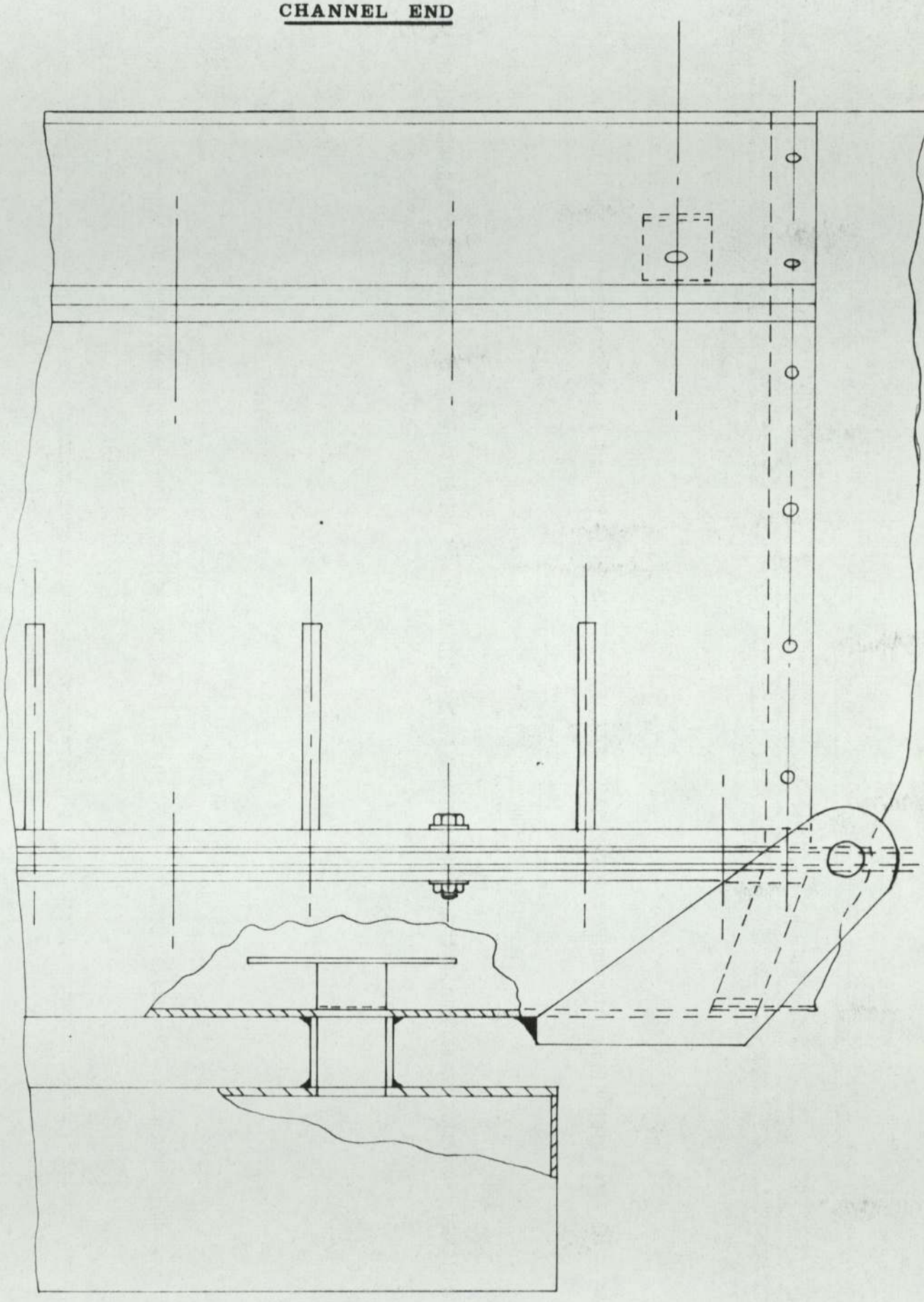

Figure A1.3

CHANNEL CROSS-SECTION

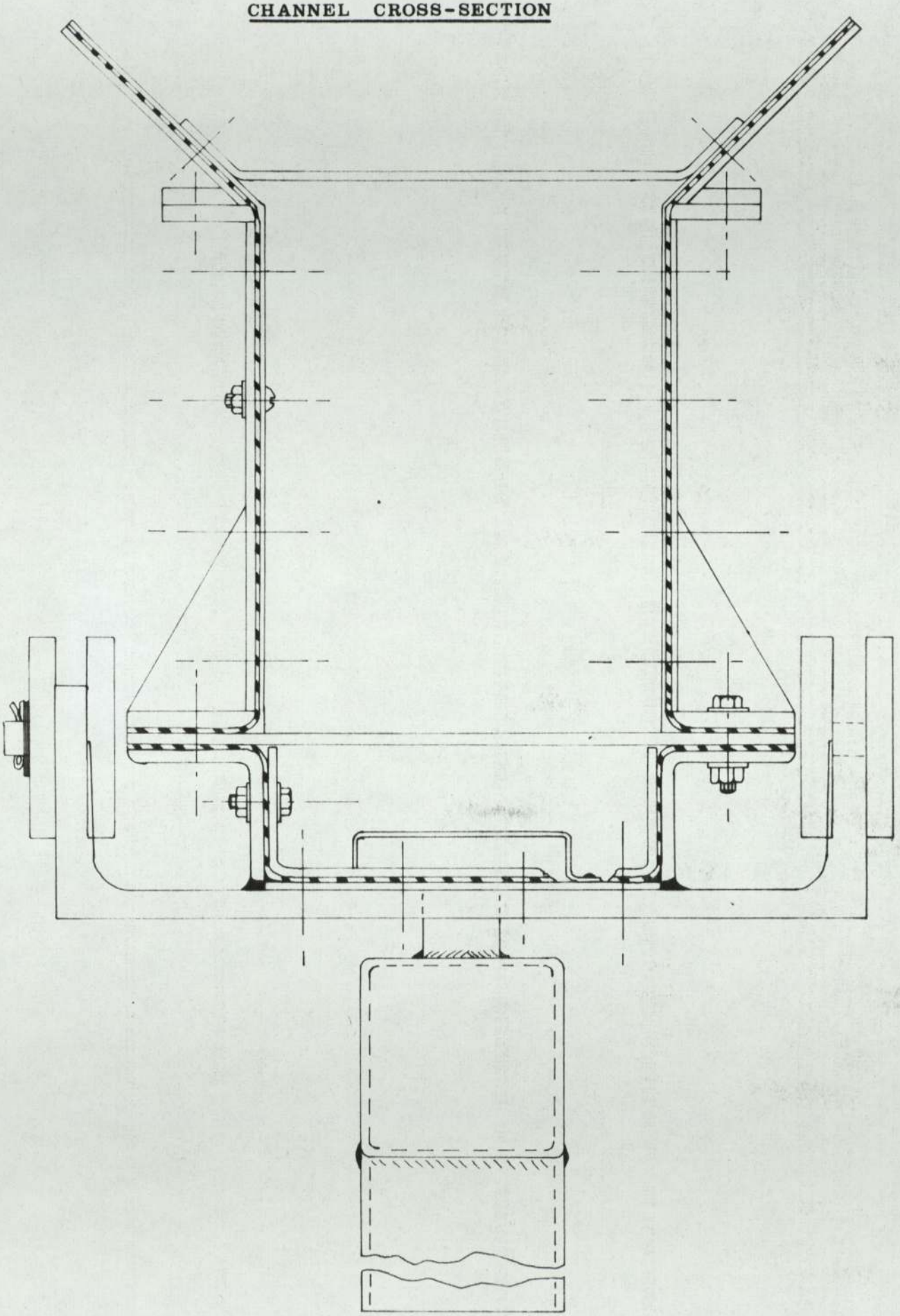

Figure A1.4

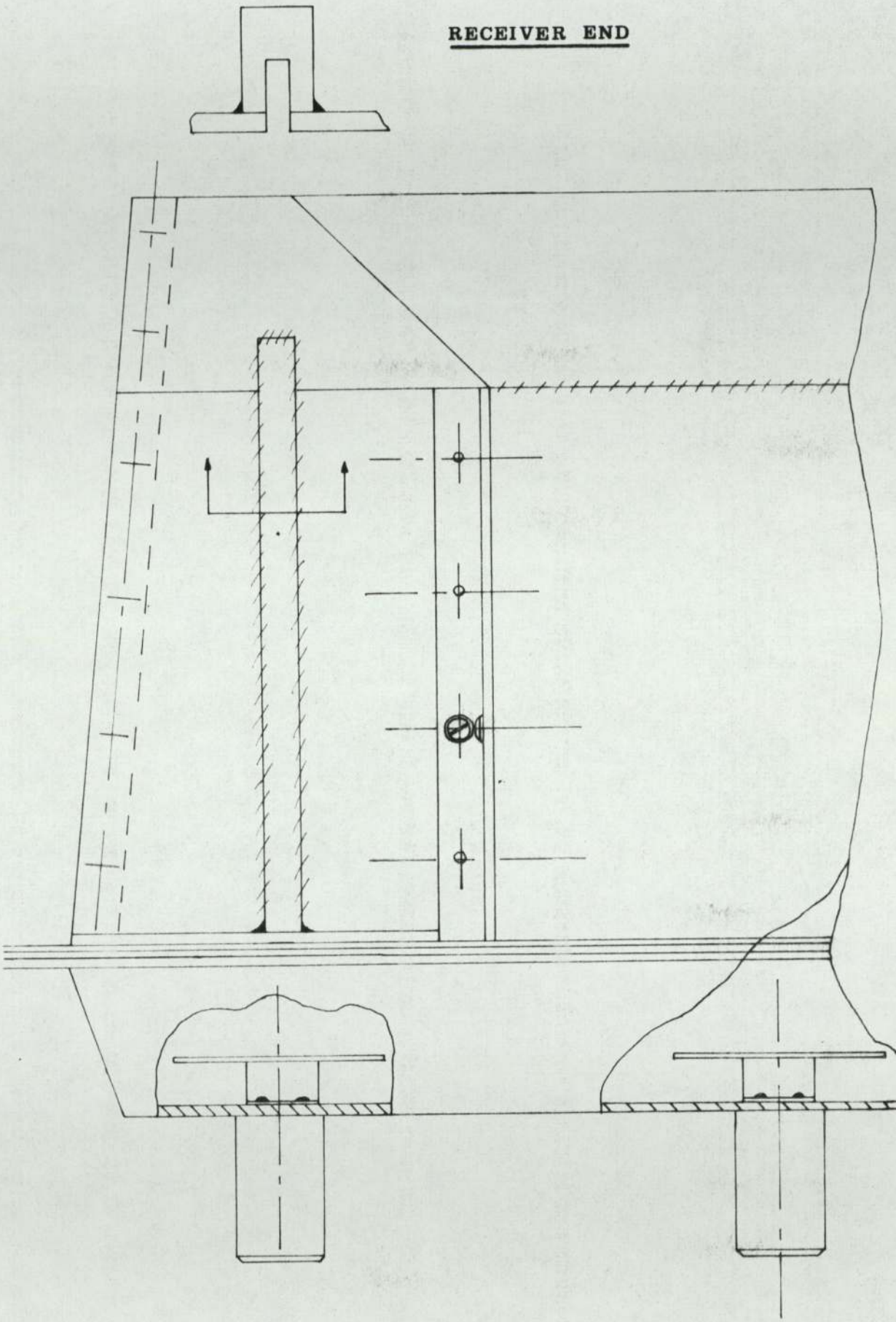

Figure A1.5

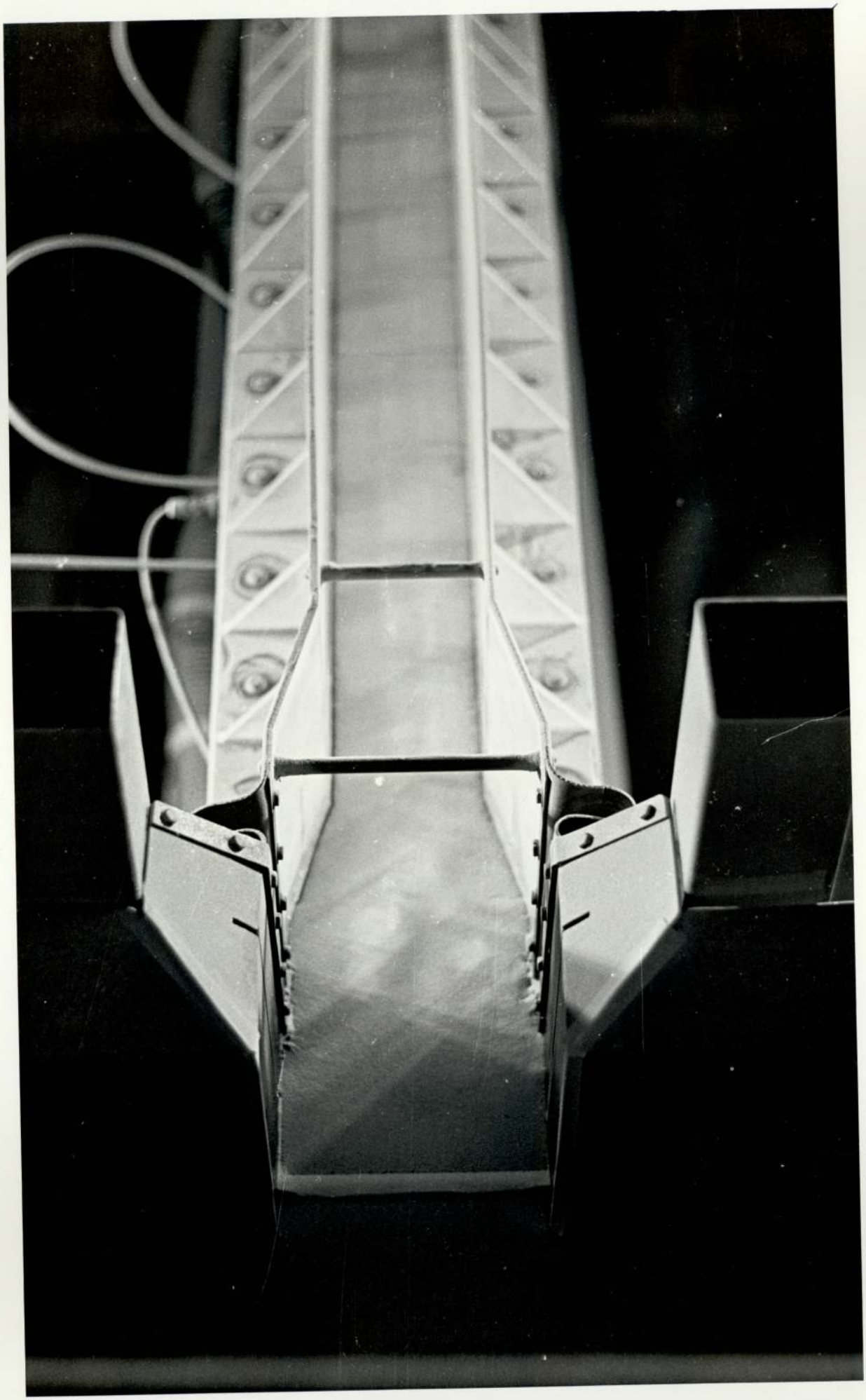

Figure A1.6

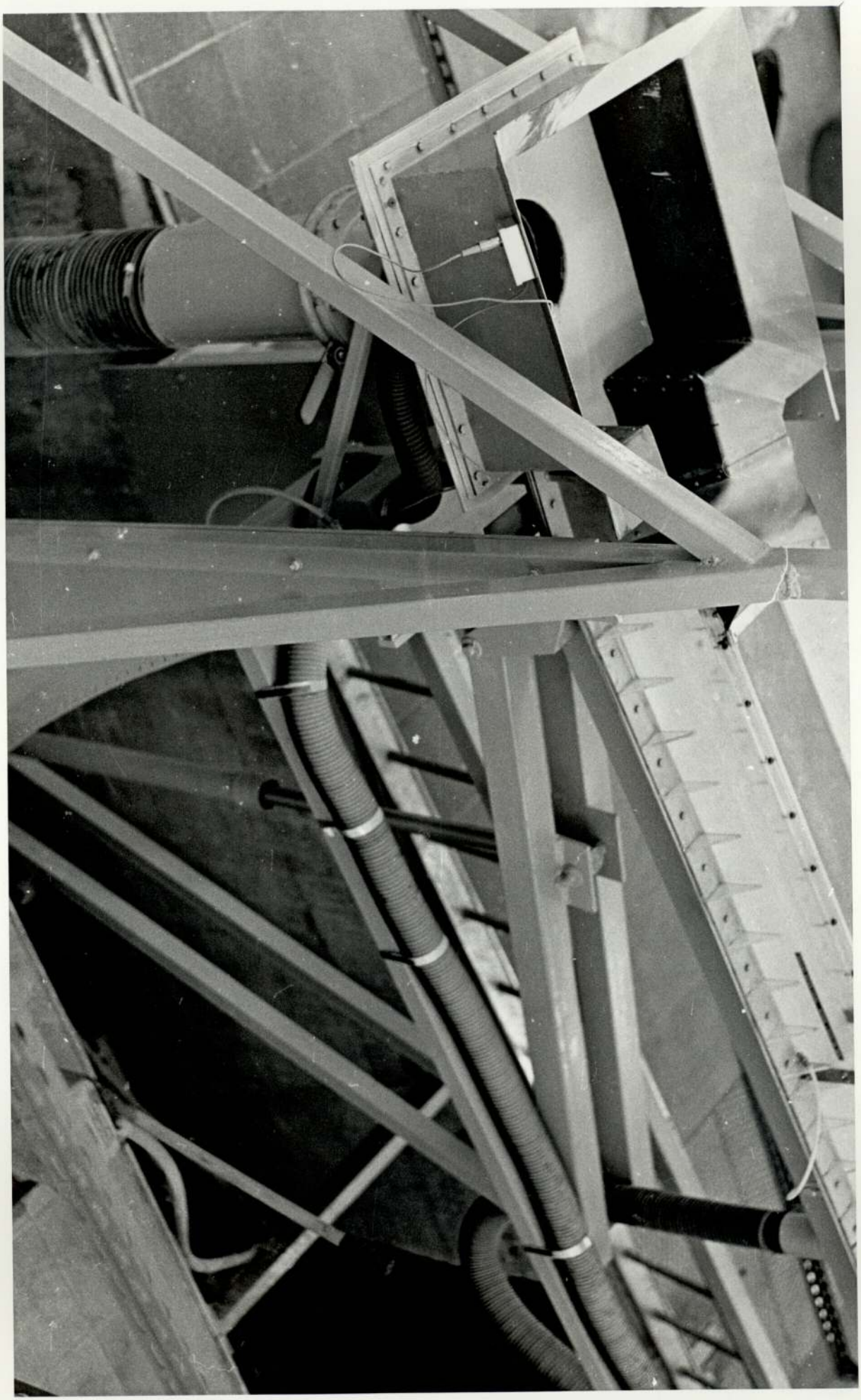

Figure A1.7

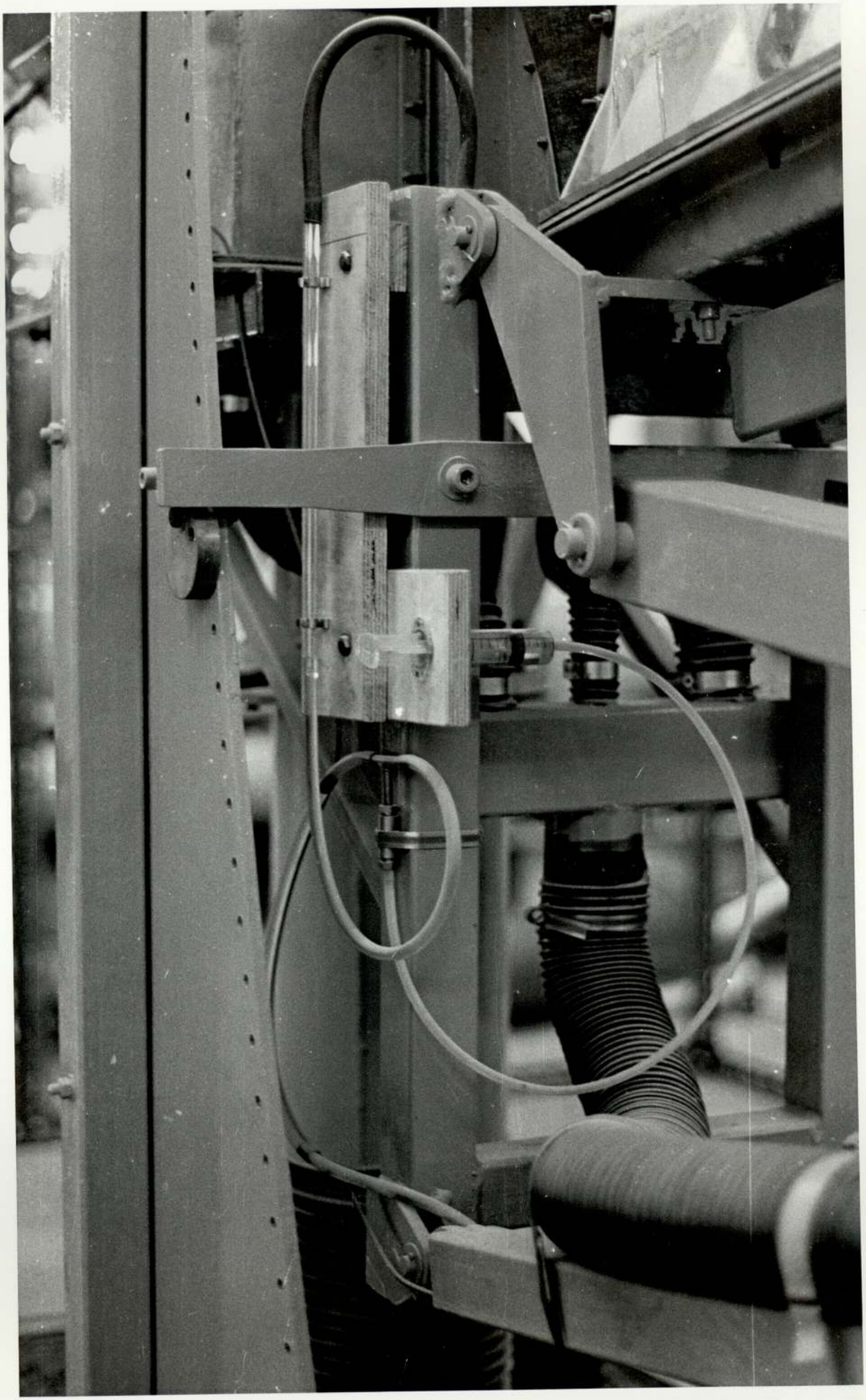

Figure A1.8

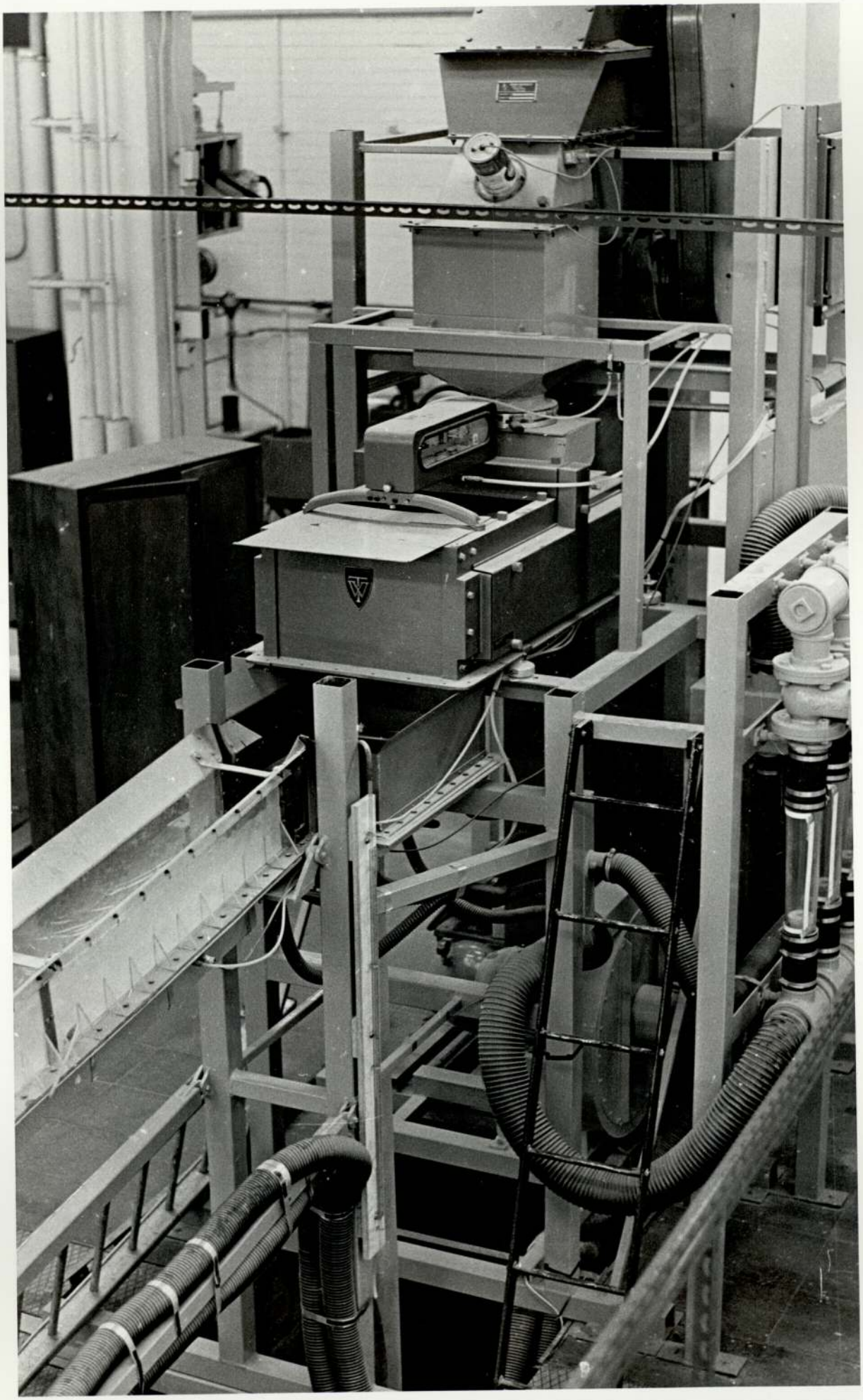

Figure A1.9

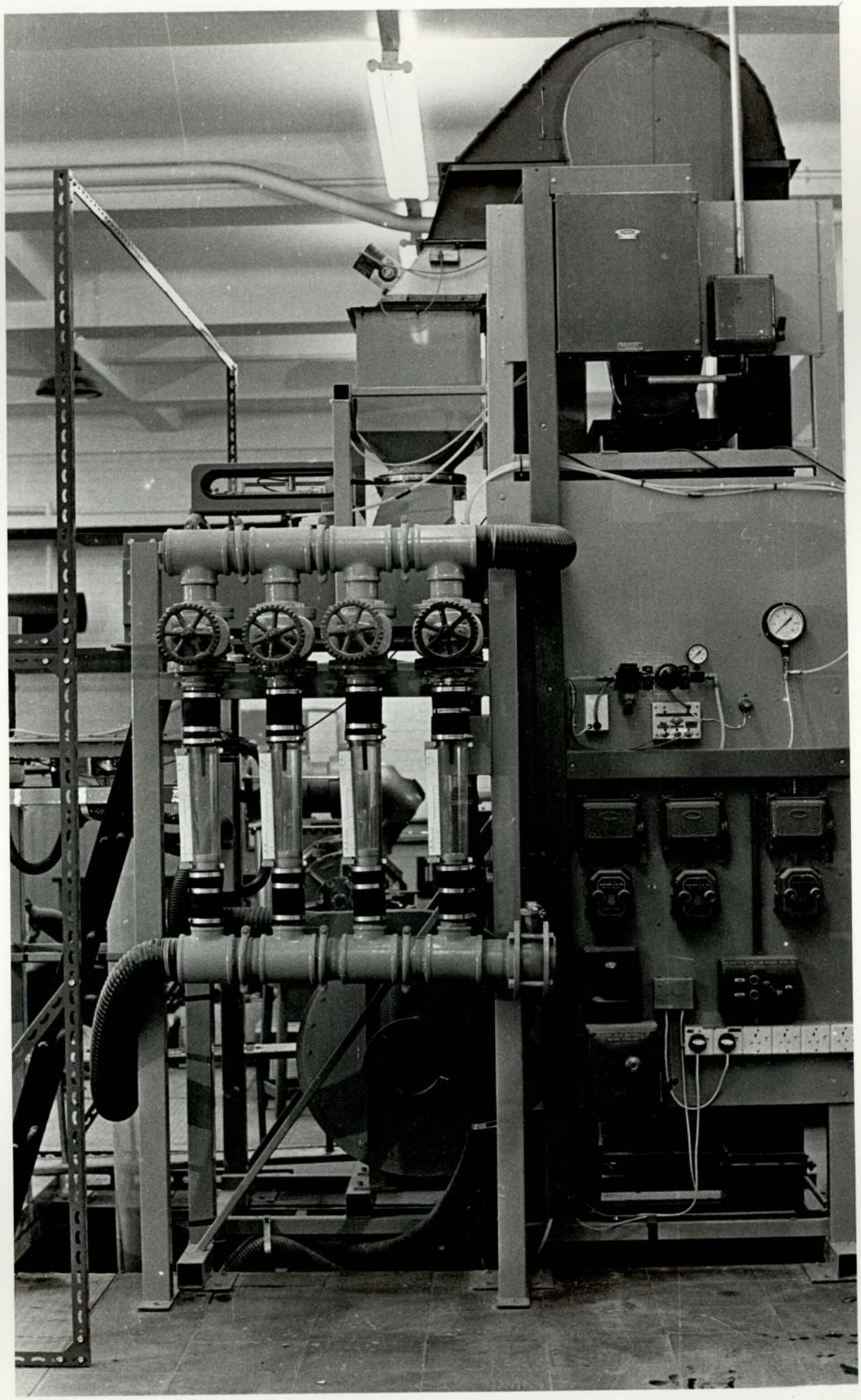

Figure A1.10

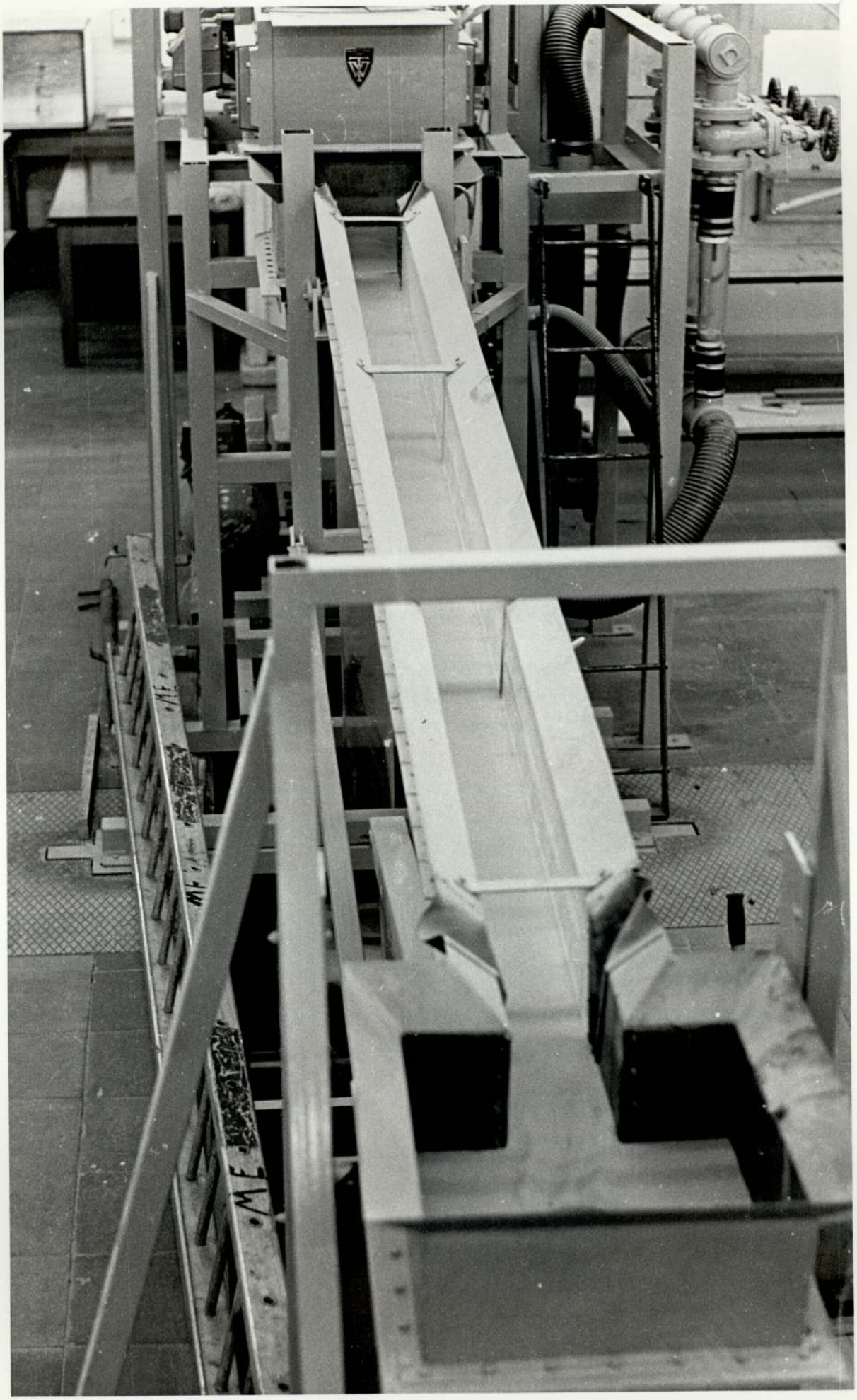

Figure A1.11

Figure A1.12

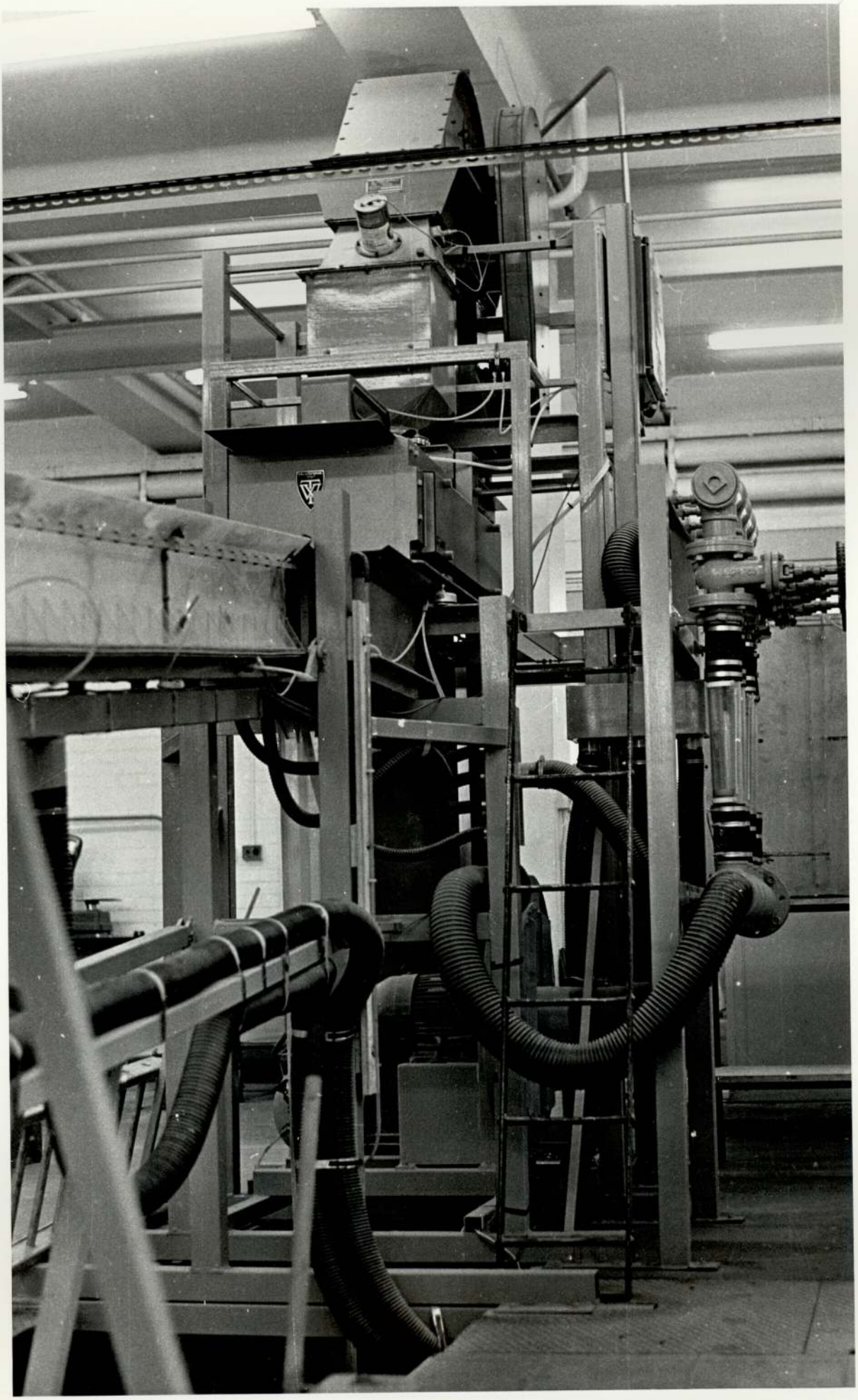

Figure A1.13

SUGGESTED SOLIDS LEVEL INDICATION SYSTEM

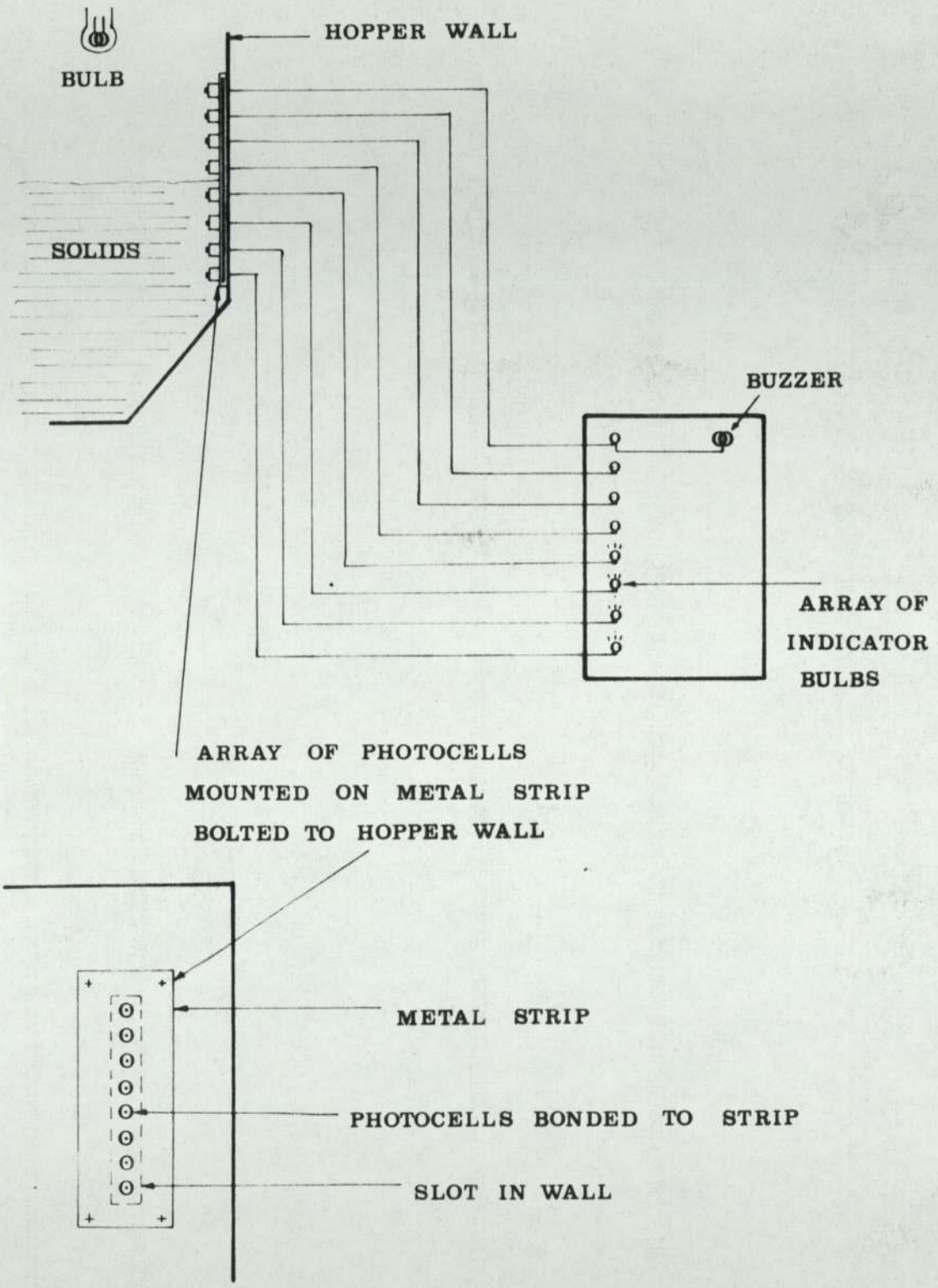

Figure A1.14

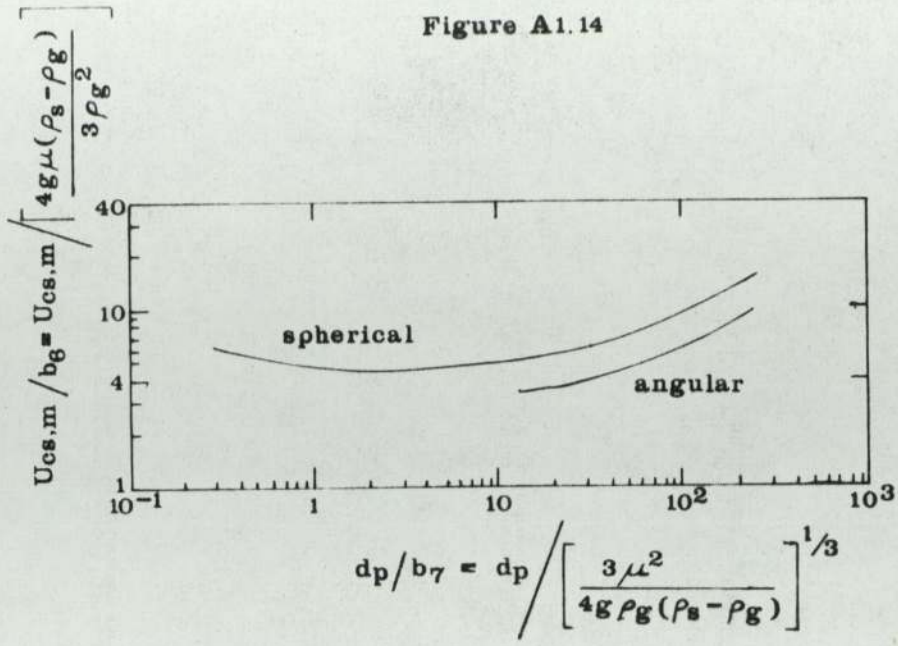

SALTATION VELOCITY $U_{cs,m}$ IN 63·5 mm TUBE

From Zenz

Figure A1.15

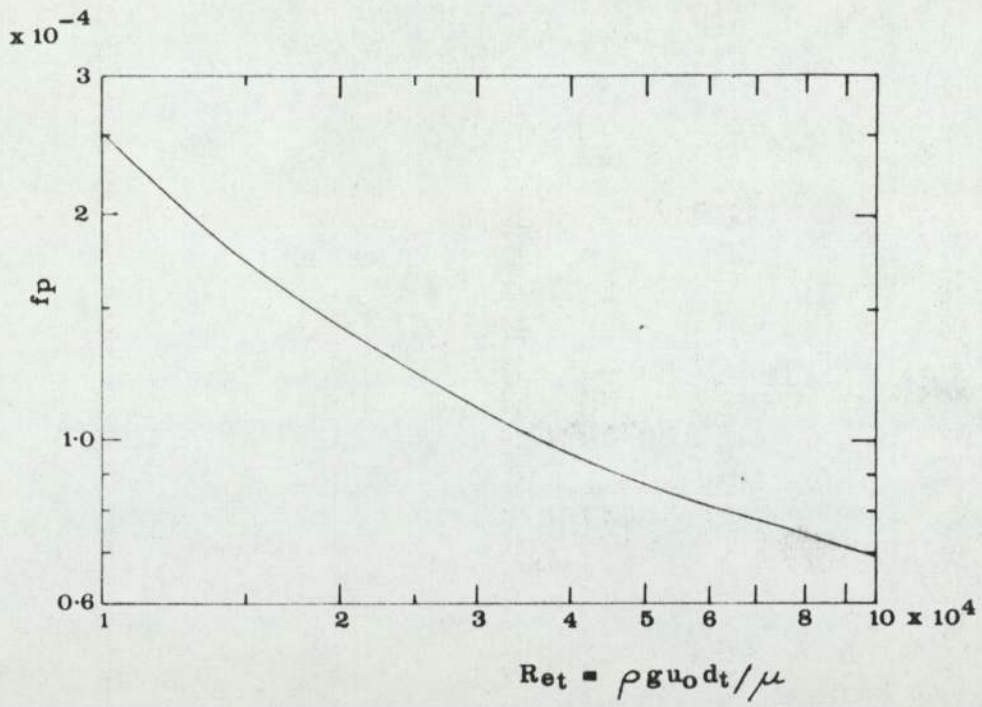

PARTICLE FRICTION FACTOR f_p AGAINST REYNOLDS NUMBER

From Rose and Barnacle

Figure A1.16

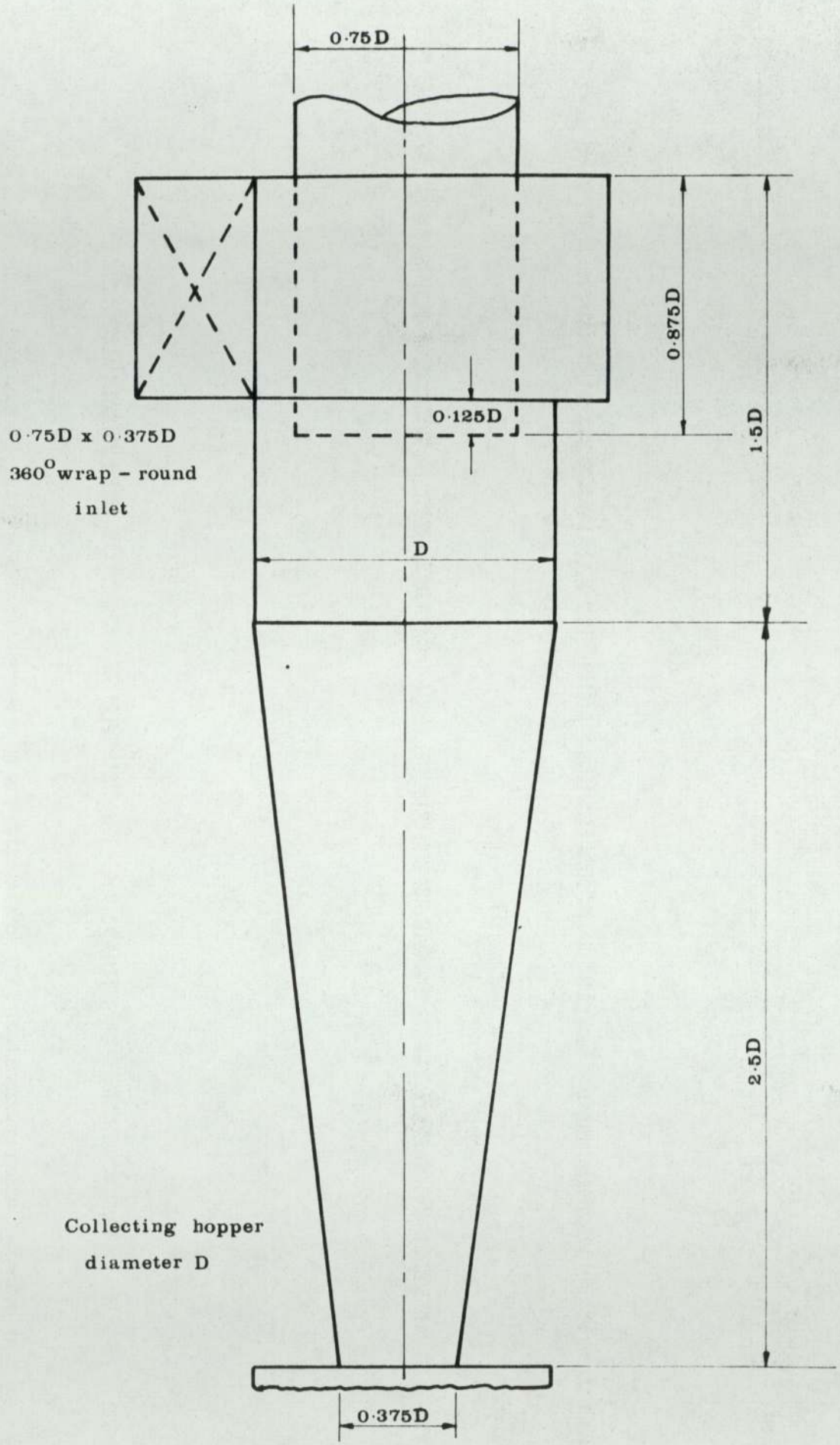

HIGH THROUGHPUT CYCLONE DESIGN

APPENDIX 2

NON-NEWTONIAN GRAVITY FLOW

DOWN INCLINED PLANE

This approach is based on work by ASTARITA et al [4] for a non-Newtonian liquid, extended by BESSANT [11].

The following assumptions are made:

1) That steady, one-dimensional laminar flow takes place; shear stress is some function of shear rate.

2) The velocity at the distributor is zero or a function of shear stress.

3) The velocity gradient at the free surface is zero.

4) No waves form at the free surface.

Referring to figure 2.1:

The velocity at a distance y from the free surface is given by

$$V = Vs + \int_{y=0}^{y=H} \left(\frac{-dv}{dy}\right) dy \qquad (1)$$

Integration of this yields the flow rate per unit width of surface

$$Q_1 = VsH + \int_{0}^{H} y \left(\frac{-dv}{dy}\right) dy \qquad (2)$$

Partial derivation at constant α gives

$$\left(\frac{\partial Q_1}{\partial H}\right)_\alpha = Vs + \left(\frac{\partial Vs}{\partial H}\right)_\alpha H + H \left(\frac{-dV}{dy}\right)_{y=H} \qquad (3)$$

If it is assumed that Vs changes little with H then this reduces to:

$$\left(\frac{\partial Q_1}{\partial H}\right)_\alpha = Vs + H \left(\frac{-dV}{dy}\right)_{y=H} \qquad (4)$$

The approach used by Bessant is to plot Q_1 against H at a constant angle of inclination, the slope of this curve at H = 0 being the slip velocity Vs (from eqn. 4).

The shear rate is $$\left(\frac{-dv}{dy}\right)_{y = H} = \frac{\frac{dQ_1}{dH} - Vs}{H} \qquad (5)$$

From figure 2.1

From simple force balance

Force down plane on element = $\rho HB\delta l g_e \sin\alpha$

Shear force resisting = $\tau B \delta l$ (assuming one dimensional flow).

$$\therefore \qquad \tau = \rho g_e H \sin\alpha \qquad (6)$$

Thus, using equations (5) and (6) it is possible to evaluate shear stresses and shear rates from the plot of Q_1 against H at constant angle.

Figure A2.1

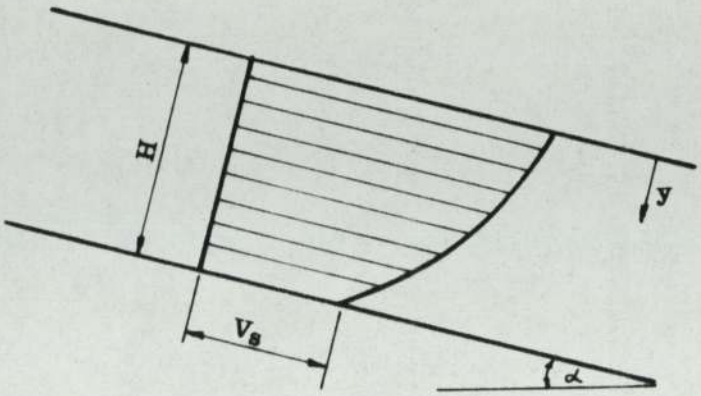

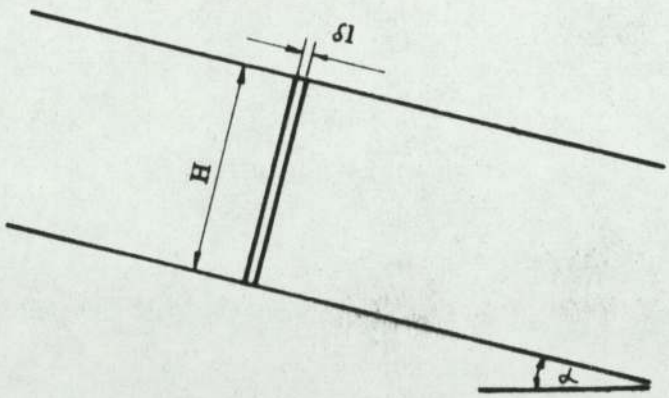

Element width B

APPENDIX 3

RIG OPERATING SEQUENCE

The following sequence was adopted when starting the rig.

1) Switch on compressor and wait until this cuts off.

2) Check that gauge indicating pressure of weighfeeder air supply shows 20 lbf/in^2.

3) Switch on weighfeeder and check that operation is correct. Energise photocell system and lamps.

4) Switch on elevator and conveyor, wait for a few minutes to check that they are operating correctly.

5) Manometer indicating weighfeeder output should have settled by now: check zero reading on this.

6) See that both inclined manometers are level and indicating zero.

7) Check that blow-off valve at right hand end of rotameter bottom connection is closed.

8) Close butterfly valve on fan inlet.

9) Check that at least two rotameter flow control valves are well open.

10) Start fan, and when up to speed open inlet butterfly.

11) Open valve in bottom receiver fully, and check that the one in the top receiver is closed.

12) Shut valve on hydraulic ram pump and pump up until channel is supported by ram at a moderate angle of inclination.

13) Open top solids control valve (above weighfeeder) a little.

14) Allow system to stabilise, ensuring that an even layer of material is deposited onto the weighfeeder belt, i.e. that the top hopper does not empty.

The rig is now ready for use. During testing, the following further sequence is adopted.

15) Set mass flow rate to the minimum which can be reliably measured. For working at very low flows the speed of the belt may be reduced. (see A.1).

16) Adjust position of channel until the upstream channel pressure tapping shows the desired reading. (This is related to bed height through a correlation discussed in chapter 3).

17) Read: Mass flow rate
Upstream pressure
Upstream/downstream differential
Channel inclination
Humidity of fluidising air
Temperature of fluidising air.

18) Increase mass flow rate and repeat until maximum mass flow reached. During this period it will be necessary to release more solids into the circuit from the storage tube and hopper to maintain the level in the top hopper.

19) Decrease mass flow and repeat back to minimum. During this period it will be necessary to remove solids from circulation into storage to avoid the rise of the solids level in the top hopper past acceptable limits.

20) Close solids control valve and check weighfeeder zero after a few minutes.

On shutting down the rig the following sequence should be followed.

21) Open valve in top receiver and allow solids to flow until storage tube and hopper are full. Close valve.

22) Close solids control valve on top hopper.

23) Allow rig to run until almost empty of solids.

24) Close valve in lower receiver.

25) Shut off fan.

26) Allow rig to run until conveyor is cleared.

27) Shut off conveyor and elevator.

28) Switch off weighfeeder, photocell system and lamps.

29) Switch off compressor.

30) Position eccentric disc channel supports appropriately and allow Channel to rest on them. Open valve in hydraulic ram pump.

APPENDIX 4

CALIBRATIONS

Figure A4.1

FLUIDISING VELOCITY CHART

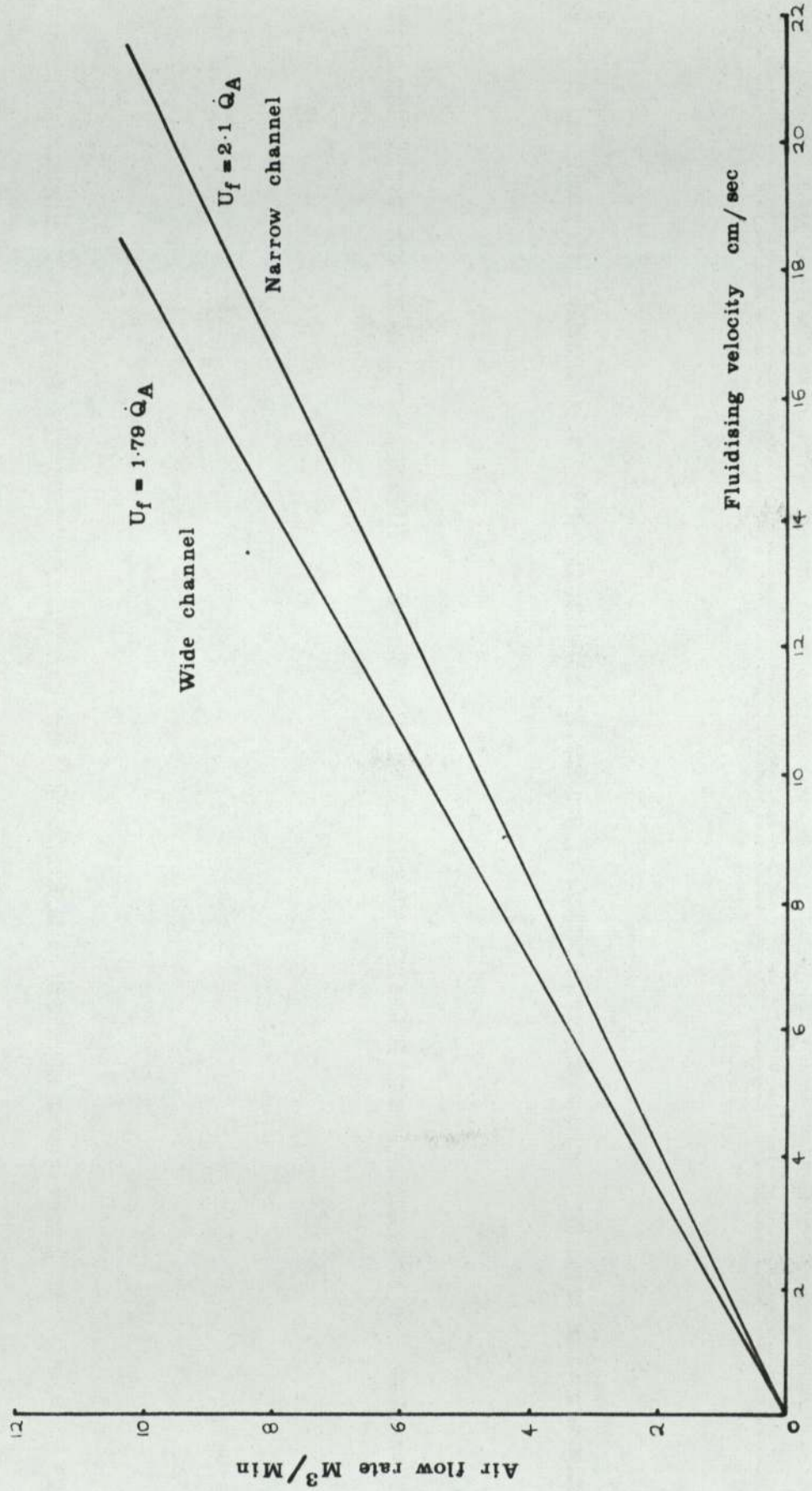

Figure A4.2

WEIGHFEEDER CALIBRATION

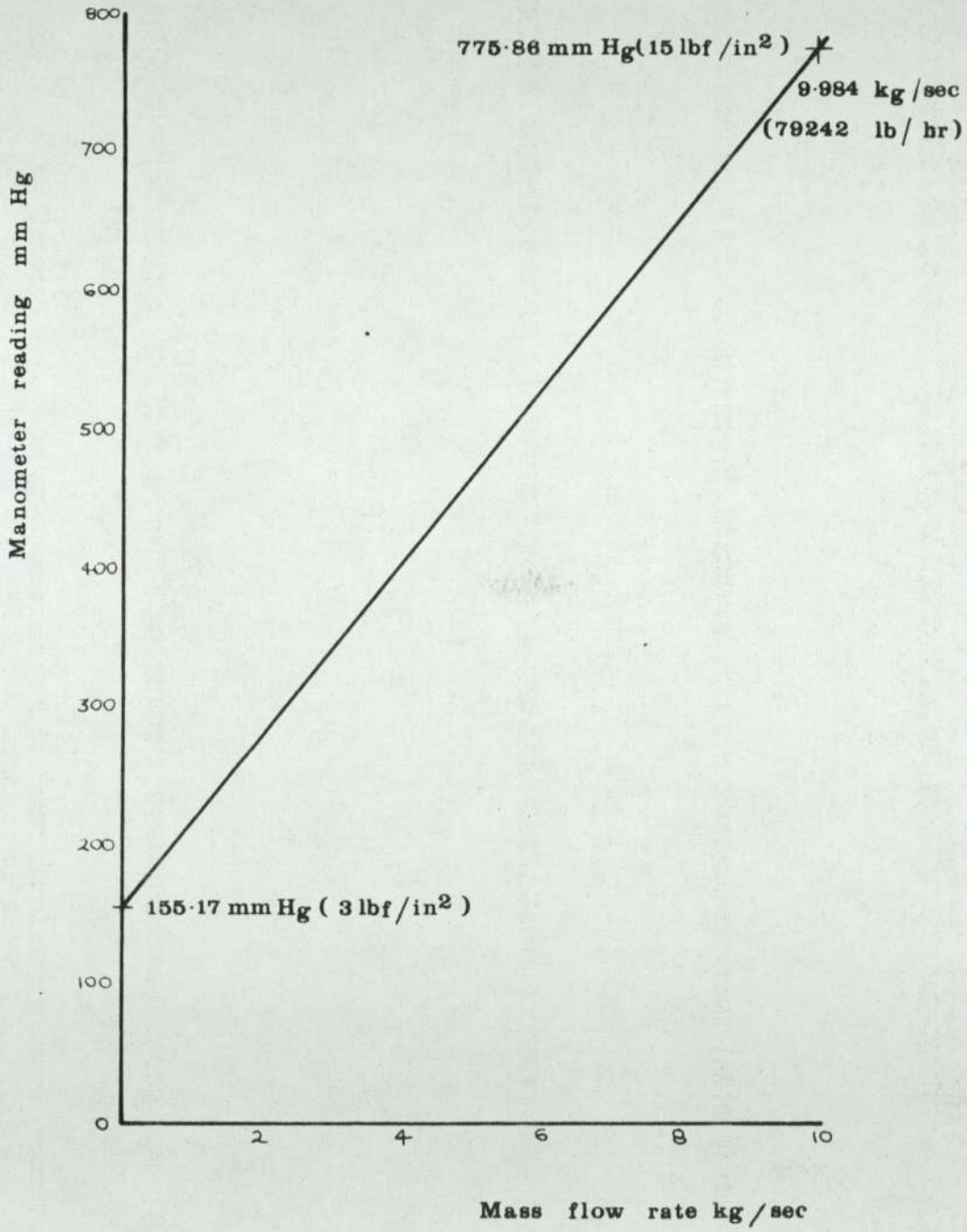

Figure A4.3

SMALL BED RESULTS BED PRESSURE DROP AGAINST FLUIDISING VELOCITY

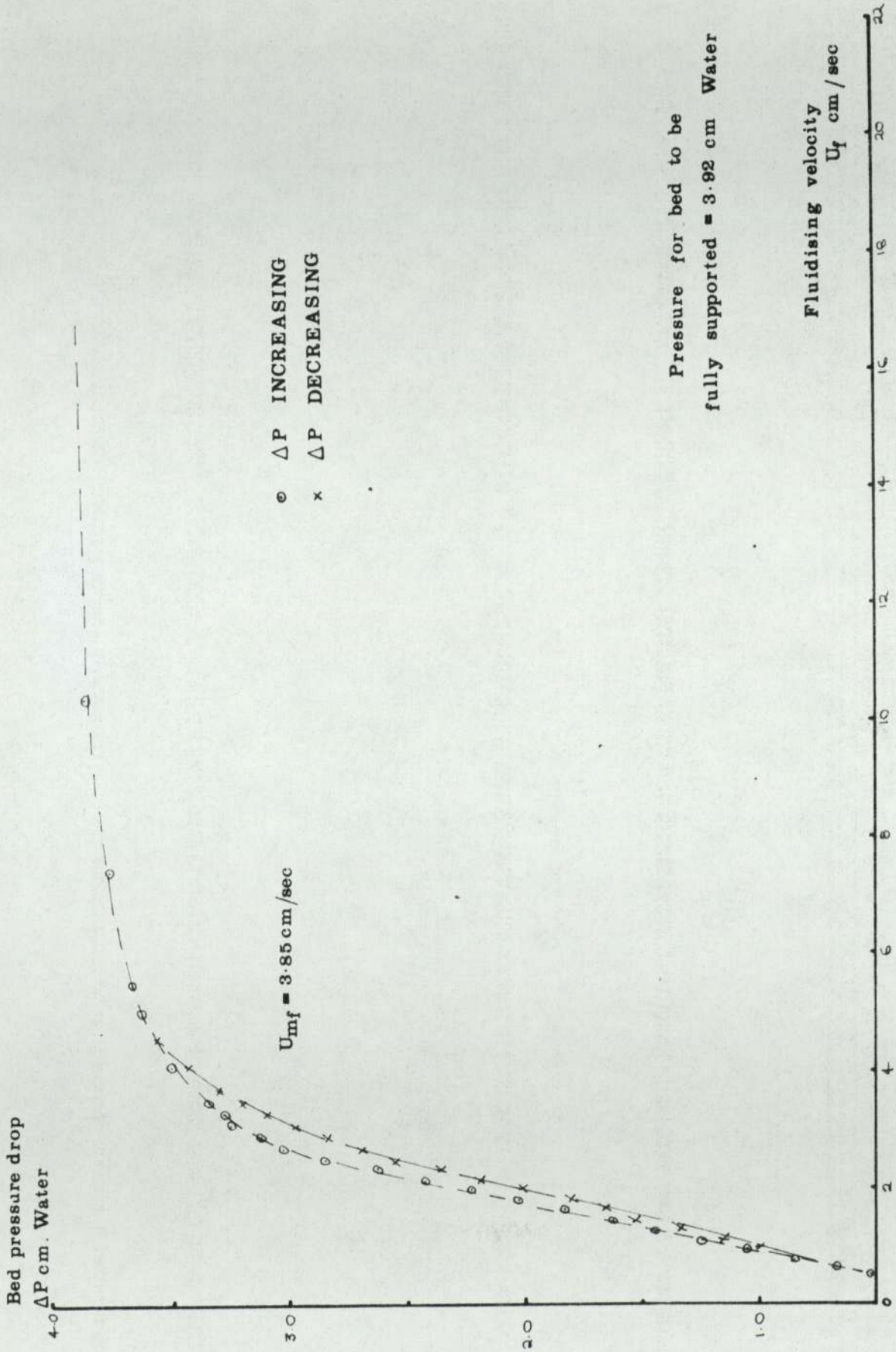

Figure A4.4

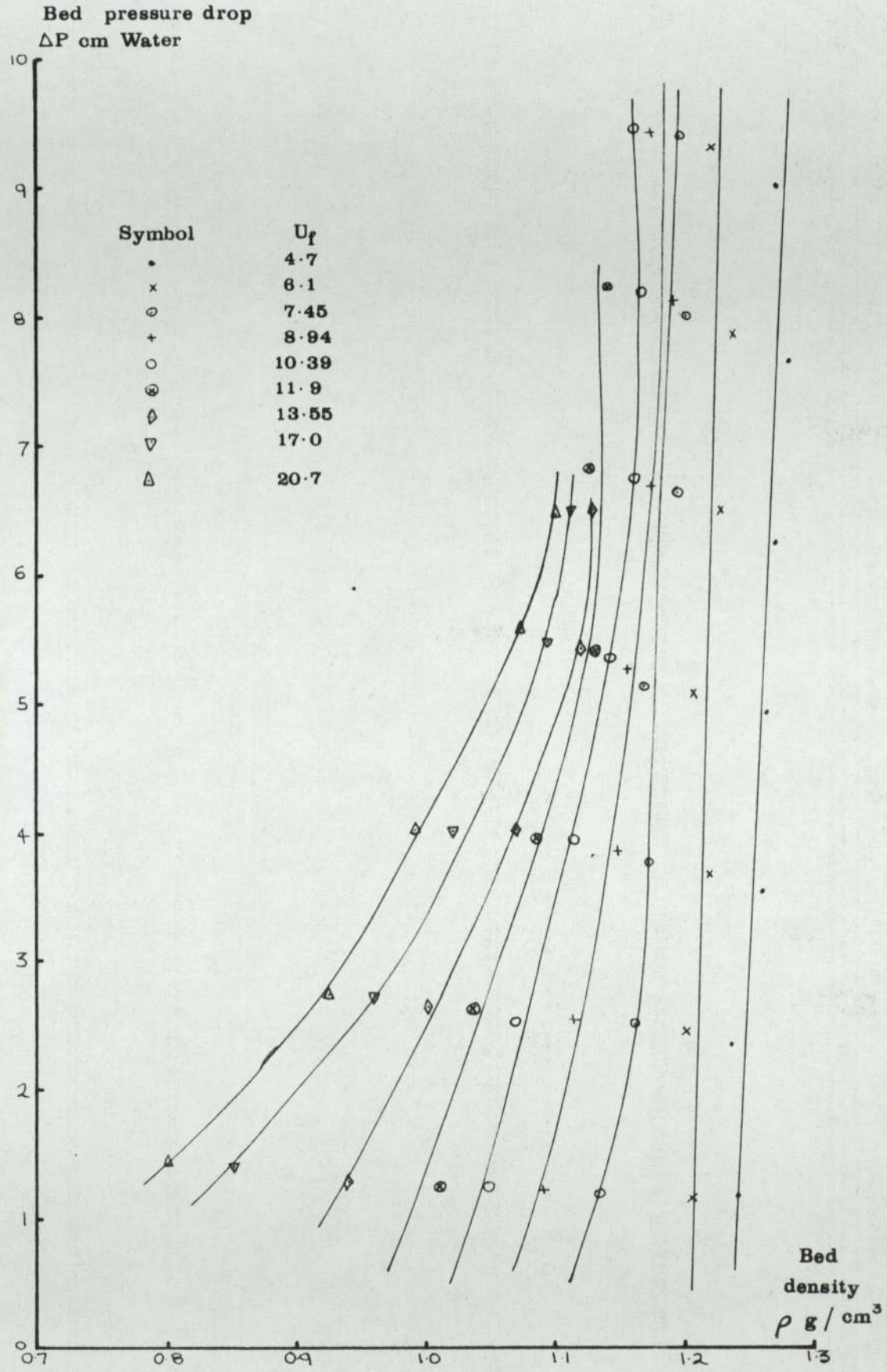

SMALL BED RESULTS — BED PRESSURE DROP AGAINST DENSITY.

Figure A 4.5

HYGROMETER CALIBRATION - NORMAL ELEMENT

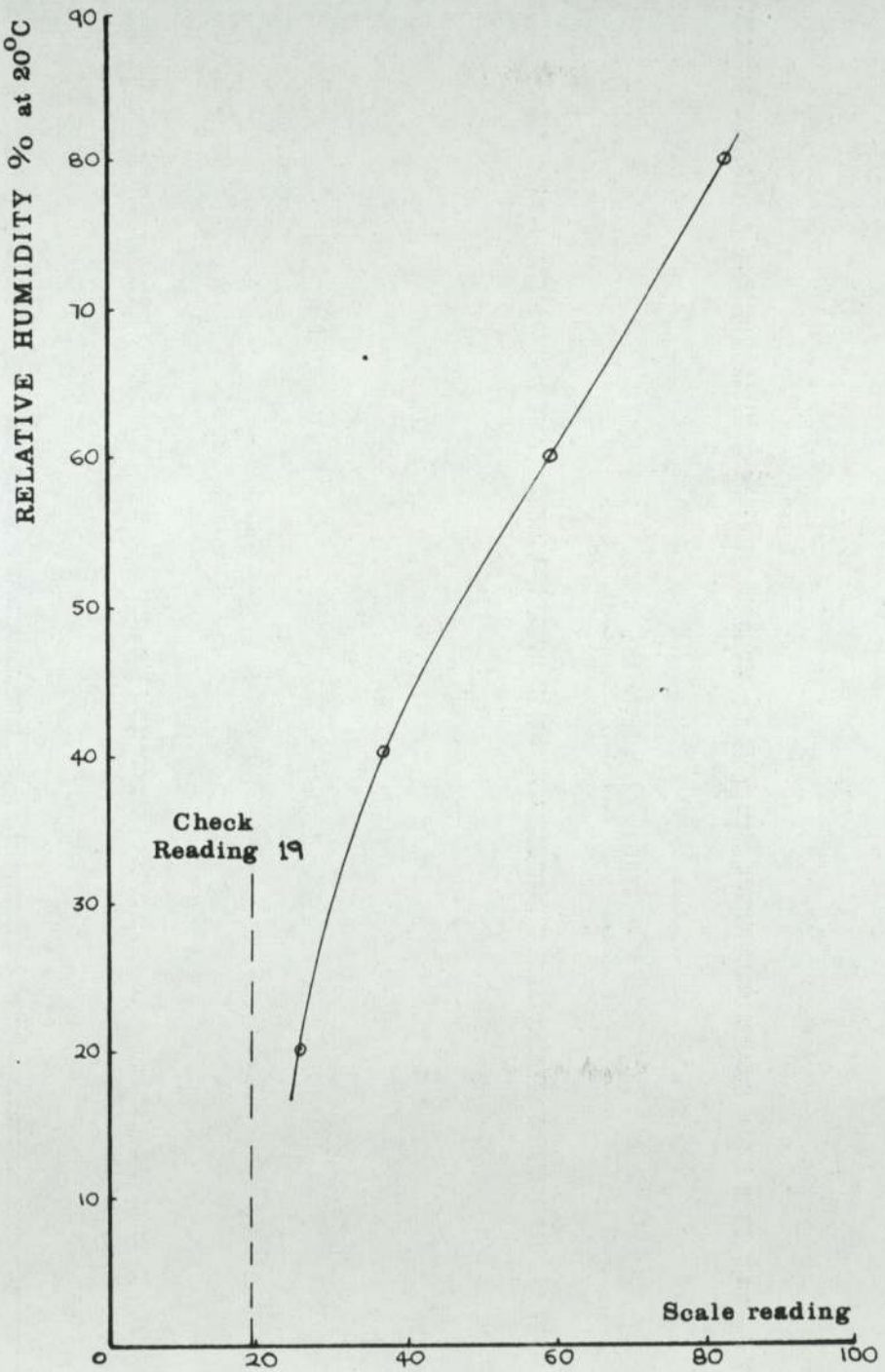

Figure A4.6

HYGROMETER CALIBRATION - GOLD SPOT ELEMENT

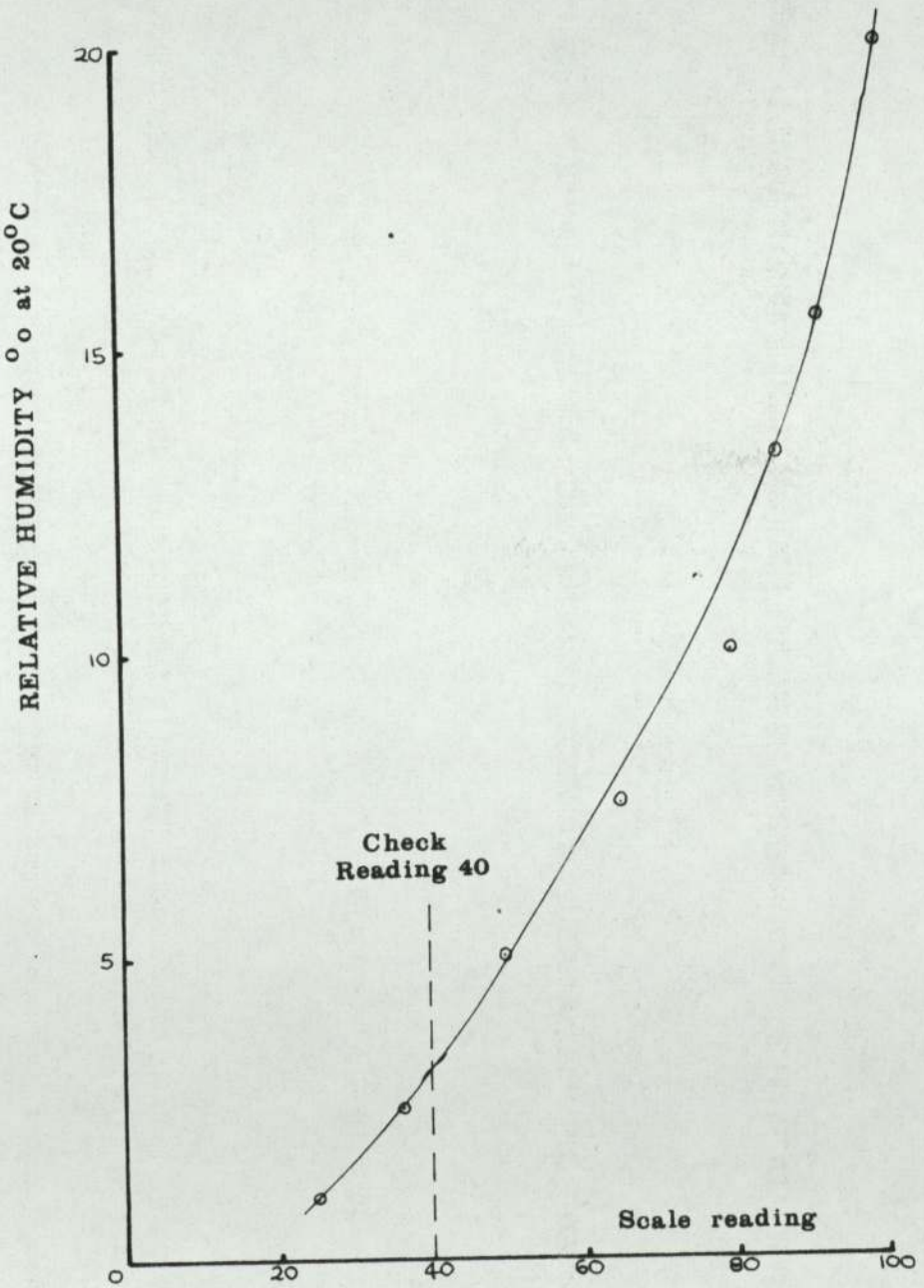

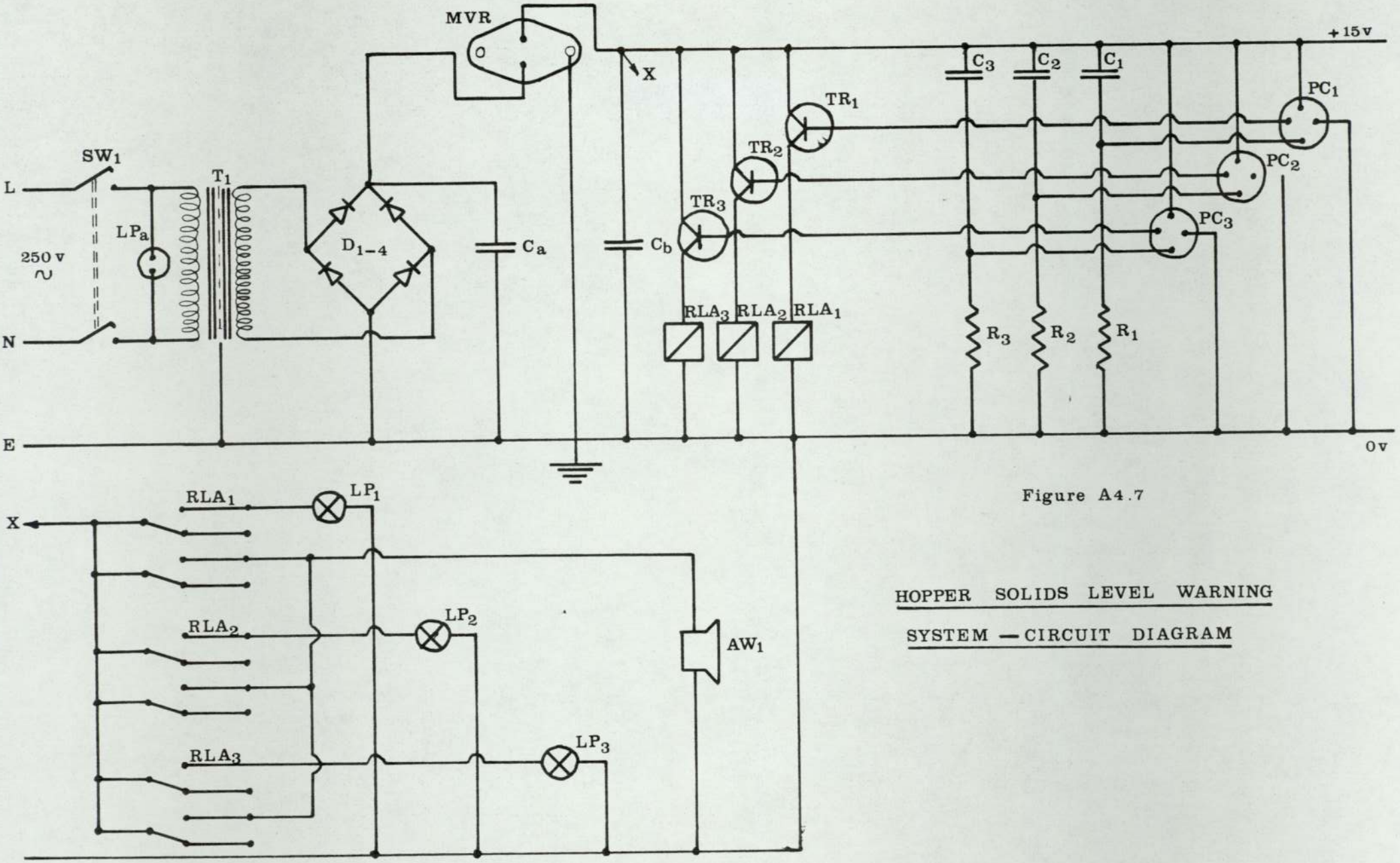

Figure A4.7

HOPPER SOLIDS LEVEL WARNING SYSTEM — CIRCUIT DIAGRAM

KEY TO FIGURE A4.7.

$A.W._1$	Audible warning device R.S.
$C_{a,b}$	680 μF capacitors, 25 v.
$C_{1,2,3}$	100 pF capacitors, polystyrene, 2.5%.
$D_1 - 4$	4 x IN 40001 or R.S. REE 70 diodes.
LP_a	Neon sub-miniaturised indicator.
$LP_{1,2,3}$	Sub-miniature indicators, 12v. R.S.
MVR	15 v. Voltage regulator.
$PC_{1,2,3}$	1 PL PS 12 Photocell.
$R_{1,2,3}$	1 megohm 0.5 W. resistor.
$RLA_{1,2,3}$	Low profile relay, 12v. R.S.
SW_1	Double pole, double throw sub-miniaturised switch.
T_1	Transformer, 17.5 v. R.S. 634.
$TR_{1,2,3}$	Transistor, R.S. 2N. 3053.

APPENDIX 5

EQUIPMENT SUPPLIERS

A list of equipment suppliers, and their products, is given below:

Airflow Developments Ltd. (Manometers)
29, Union Street, Oldham, Lancs.

Bowes Engineering Ltd. (Hydraulic ram)
29, Porchester Road, Nottingham 3.

Buckland Sand and Silica Co. Ltd. (Sand)
Reigate Heath, Reigate, Surrey.

Midland Tank and Ironplate Ltd. (Welded fabrications)
Heneage Street, Birmingham 7.

Mucon Engineering Co. Ltd. ("Mucon" valves)
Winchester Road, Basingstoke, Hants.

Numec Ltd. (Belt conveyor)
New Whittington, Chesterfield, Derbys.

Porvair Ltd. ("Vyon" porous plastic
Estuary Road, Kings Lynn, Norfolk distributor material)

Rotameter Manufacturing Co. Ltd. (Rotameters)
(GEC-Elliott Process Instruments Ltd.)
Croydon, Surrey.

Shaw Moisture Meters (Humidity meter)
Rawson Road, Westgate, Bradford.

Simon-Barron Ltd. (Elevator)
Bristol Road, Gloucester.

APPENDIX 6

SAMPLE SIZE ANALYSES

Sample size analyses

The mean particle diameter in the following table is the surface mean, calculated as described in Chapter 3.

In order to provide a simple measure of the amount of each sample above 250 and 300 μm the symbols 'p' and 'n' are used, derived as follows: The samples of unused sand tested (S_1 - S_6) are very similar, and so their fractions above 250 μm and 300 μm were averaged to provide a representative figure, these being f_1 and f_2 respectively. To compare the fractions in other samples with these figures, 'p' and 'n' are used such that

% of sample above 250 μm = $p.f_1$

% of sample above 300 μm = $n.f_2$

Key to sample designation

C	From channel
CI	Circulating sand, samples taken at weighfeeder exit.
LR	From lower receiver
UR	From upper receiver
S	Unused sand

For clarity, a note on the conditions under which each sample was taken is necessary.

All the channel samples C_1 to C_8 were taken from the flowing bed using the method described in Chapter 3. In all cases the fluidising velocity was low, of the order of 1.6 - 1.8 U_{mf}, and the channel flow velocity was also low, of the order of 0.15 - 0.2 m/s. Bed depths varied slightly, but were within the range used in the experiments.

Samples of circulating sand, CI_1 to CI_6, were all taken at the weighfeeder outlet. Sample CI_1 was taken after a period of running at high fluidising velocity, 4.5 U_{mf}, and sample CI_2 after a corresponding period running at 1.75 U_{mf}. Samples CI_3 to CI_6 were taken after an extended period at

5.0 U_{mf} when the bed was flowing at approximately 1 m/s.

Samples from the lower receiver were taken after completion of a days tests, when the rig had been shut down.

Of the samples taken from the upper receiver, $U.R_1$ was taken using the sampling tube, the others being taken in similar circumstances to those described above for the lower receiver.

Samples of unused sand, S_1 to S_6, were taken from different bags of the new material.

RESULTS OF SAMPLE SIZE ANALYSES

SAMPLE	Mean particle size dp_m /µm	Amount above 250 µm %	Amount above 300 µm %	p	n
C_1	198.6	24.801	5.934	2.835	1.927
C_2	172.2	15.881	3.643	1.815	1.183
C_3	173.9	16.592	3.952	1.897	1.283
C_4	160.6	17.844	4.712	2.04	1.53
C_5	163.7	19.997	5.716	2.286	1.856
C_6	161.2	18.542	5.797	2.12	1.882
C_7	163.6	20.71	5.96	2.367	1.935
C_8	186.0	25.035	7.953	2.862	2.582
CI_1	174.2	14.295	4.043	1.634	1.313
CI_2	170.1	10.54	2.974	1.205	0.966
CI_3	160.4	-	-	-	-
CI_4	158.4	-	-	-	-
CI_5	180.1	-	-	-	-
CI_6	179.8	-	-	-	-
LR_1	213.7	49.527	22.866	5.662	7.424
LR_2	212.7	51.592	23.272	5.898	7.556
LR_3	206.3	48.939	20.839	5.594	6.766
LR_4	214.3	52.455	24.507	5.996	7.957

SAMPLE	Mean particle size d_{p_m} μm	Amount above 250 μm %	Amount above 300 μm %	p	n
UR_1	169.6	19.586	5.741	2.239	1.864
UR_2	378.8	91.421	79.001	10.4	25.6
UR_3	346.4	89.325	72.899	10.2	23.7
UR_4	361.2	87.53	76.0	10.0	24.7
UR_5	360.6	90.82	76.024	10.4	24.7
S_1	148.8	9.004	2.949	-	-
S_2	150.1	8.9	3.276	-	-
S_3	151.7	8.975	3.132	-	-
S_4	149.8	9.787	3.586	-	-
S_5	161.7	9.268	3.424	-	-
S_6	148.6	6.554	2.113	-	-

The average percentage in the above samples, S_1 to S_6, above 250 μm is 8.748, and that above 300 μm is 3.08.

$$f_1 = 8.748$$

$$f_2 = 3.08$$

APPENDIX 7

TABULATED RESULTS

APPENDIX 7

KEY TO TABLES

TABLE NO.	CHANNEL WIDTH	
1 - 6	150 mm.	SET A.
7 - 20	150 mm.	SET B.
21	150 mm.	SET C.
22 & 23	150 mm.	SET D.
24	150 mm.	SET E
25 - 54	100 mm.	
55 - 57	100 mm.	Constant slope tests
57 - 60	150 mm.	Constant slope tests

TABLES 1 - 54

In tables 1 - 54 the following symbols are used:

Symbol	Quantity	Units
Uf	Fluidising velocity	cm/sec.
h	Bed height	mm.
ρ	Bed density x 10^{-3}	kg/m^3.
w	Channel width	mm.
$\dot{M}$	Solids mass flow rate	kg/sec.
U	Linear velocity in channel	m/sec.
τ	Shear stress	N/m^2.
γ	Shear rate	sec^{-1}.
f	Darcy friction factor	-
τ/γ	Apparent viscosity	$Nsec/m^2$.
N_{RE}	Generalised Reynolds Number	-

TABLE 1.

Uf = 17.9 h = 14.9 ρ = 0.845 w = 150

M	U	τ	γ	f	τ/γ	N_{RE}
0.18	0.0953	1.164	15.4	1.2162	0.0756	83.6
0.36	0.1906	2.619	30.74	0.685	0.0852	183.8
0.65	0.344	3.42	55.48	0.2749	0.0616	359.6
0.85	0.455	3.715	73.39	0.1705	0.0506	494.3
1.4	0.7411	4.177	119.5	0.0723	0.035	860.7
1.8	0.9528	5.1	153.68	0.0534	0.0332	1145.3
2.11	1.117	5.58	180.16	0.0424	0.031	1372.1
2.6	1.376	7.1	221.94	0.0356	0.032	1739.4
3.47	1.837	8.97	298.87	0.0252	0.03	2415.9
4.18	2.213	9.62	356.94	0.0186	0.027	2985.6
5.23	2.769	12.67	446.62	0.0157	0.0284	3852.2
5.9	3.123	15.71	503.71	0.0153	0.0312	4416.9
2.3	1.218	5.51	196.45	0.0353	0.028	1514.2
Uf = 17.9	h = 35.0	ρ = 1.02	w = 150			
0.96	0.1793	0.84	15.0	0.204	0.056	178.5
1.2	0.224	1.355	18.74	0.2118	0.0722	231
1.84	0.3436	2.469	28.75	0.1638	0.0859	379.4
2.23	0.4164	2.868	34.85	0.1296	0.0823	475.2
3.0	0.56	3.705	46.86	0.0926	0.0791	669.5
3.63	0.6779	4.94	56.73	0.0843	0.0871	836.3
4.32	0.8067	5.098	67.51	0.0614	0.0755	1022.7
5.31	0.9916	5.736	82.98	0.0457	0.0692	1299.7
6.18	1.154	6.374	96.57	0.0375	0.066	1549.1

TABLE 2.

Uf = 17.9 h = 21.5 ρ = 0.915 w = 150

M	U	τ	γ	f	τ/γ	N_{RE}
0.0725	0.0246	0.25	2.946	3.61	0.0849	14.4
0.1175	0.0398	0.55	4.766	3.03	0.1154	25.3
0.338	0.1146	0.999	13.72	0.66	0.0728	88.2
0.495	0.1678	1.598	20.09	0.49	0.0795	138.5
0.613	0.2078	1.798	24.89	0.36	0.0722	178.3
0.775	0.2627	1.947	31.46	0.25	0.0619	235.1
0.923	0.3129	2.52	37.47	0.23	0.0673	289.1
1.155	0.3915	3.49	46.89	0.199	0.0744	376.7
1.47	0.4983	3.55	59.68	0.125	0.0595	500.8
1.145	0.388	3.17	46.47	0.184	0.0682	372.7
1.61	0.546	3.55	65.39	0.104	0.0543	557.9
1.97	0.668	4.04	80.0	0.079	0.0505	707.9
2.4	0.814	4.79	97.49	0.063	0.0491	894
1.49	0.505	3.696	60.48	0.127	0.0611	508.8
0.175	0.059	0.325	7.066	0.815	0.046	39.9
2.08	0.705	4.319	84.43	0.074	0.0512	754.5
2.66	0.902	5.667	108.0	0.061	0.0525	1009.2
3.43	1.163	6.841	139.3	0.044	0.0491	1362.3
4.79	1.623	10.09	194.4	0.034	0.0519	2020.1
0.93	0.315	2.846	37.7	0.251	0.0755	291.4
0.52	0.176	1.348	21.08	0.394	0.0663	146.5
2.68	0.908	5.418	108.7	0.0572	0.0498	1017.2
4.85	1.644	9.912	196.9	0.0319	0.0503	2050.9
5.4	1.83	12.23	219.2	0.0319	0.0558	2327.9
6.55	2.22	13.93	265.9	0.0246	0.0524	2924.1
7.28	2.468	11.28	295.6	0.0161	0.0382	3312.8

TABLE 3.

Uf = 13.45 h = 27.5 ρ = 1.024 w = 150

M	U	τ	γ	f	τ/γ	N_{RE}
6.1	1.445	10.85	144.5	0.0406	0.0751	1664.3
4.0	0.948	7.04	94.8	0.061	0.0743	1023.8
2.9	0.687	5.23	68.7	0.086	0.0761	706.9
1.77	0.419	3.78	41.9	0.168	0.0902	399.7
0.95	0.225	2.35	22.5	0.362	0.1044	195.0
0.63	0.149	1.81	14.9	0.637	0.1215	100.5
0.133	0.032	0.235	3.15	1.85	0.0746	32.83
Uf = 13.45 h = 40.0		ρ = 1.085	w = 150			
0.86	0.132	0.51	10.11	0.216	0.0504	-
1.06	0.163	1.25	12.49	0.347	0.1	191.2
1.6	0.246	1.95	18.85	0.237	0.1034	240.8
2.21	0.339	3.15	25.98	0.202	0.1212	322.4
2.68	0.412	3.7	31.57	0.161	0.1172	406.5
3.72	0.571	4.91	43.75	0.111	0.1122	599.2
5.1	0.783	6.12	60.0	0.074	0.102	872.5
6.03	0.926	7.09	70.96	0.061	0.0999	1066.4

TABLE 4.

Uf = 9.85 h = 27.5 ρ = 1.11 w = 150

M	U	τ	γ	f	τ/γ	N_{RE}
5.93	1.295	11.05	129.5	0.047	0.0853	1403.5
4.88	1.066	8.65	106.6	0.055	0.0811	1143.7
4.17	0.91	7.56	91.0	0.066	0.0831	968.4
2.95	0.646	6.18	64.6	0.106	0.0957	674.5
2.15	0.469	5.09	46.9	0.166	0.1085	383.0
1.5	0.328	4.43	32.8	0.296	0.1351	221.0
0.8	0.175	3.63	17.5	0.855	0.2074	75.9
0.36	0.079	2.83	7.9	3.27	0.3582	20.4
0.24	0.052	2.18	5.2	5.79	0.4192	11.07
0.08	0.018	0.364	1.75	8.55	0.208	15.0
Uf = 9.85	h = 40.0		ρ = 1.14	w = 150		
0.42	0.061	0.44	4.67	0.825	0.0942	87.5
0.8	0.117	0.92	8.97	0.475	0.1026	111.3
1.13	0.165	1.95	12.64	0.502	0.1543	131.6
2.35	0.344	3.8	26.36	0.225	0.1442	278.0
3.5	0.512	5.06	39.23	0.135	0.129	448.0
4.7	0.687	6.81	52.64	0.101	0.1294	637.0
5.95	0.87	7.88	66.67	0.073	0.1182	846.0

TABLE 5.

Uf = 8.1 h = 27.5 ρ = 1.15 w = 150.

M	U	τ	γ	f	τ/γ	N_{RE}
5.8	1.224	10.65	122.4	0.0496	0.087	
5.32	1.122	4.74	112.2	0.054	0.0868	
4.17	0.88	8.33	88.0	0.075	0.0947	
3.0	0.633	7.72	63.3	0.1345	0.122	
2.4	0.506	6.94	50.6	0.189	0.1372	
1.44	0.304	7.43	30.4	0.561	0.2444	UNOBTAINABLE
2.64	0.557	7.24	55.7	0.163	0.13	
1.73	0.365	8.17	36.5	0.428	0.2238	
1.35	0.285	7.88	28.5	0.675	0.2765	
0.92	0.194	8.03	19.4	1.49	0.4139	
0.75	0.158	7.58	15.8	2.12	0.4797	
0.75	0.158	5.7	15.8	1.59	0.3608	
Uf = 8.1	h = 40	ρ = 1.16	w = 150			
0.47	0.0675	0.395	5.17	0.6	0.0764	
0.5	0.0718	1.684	5.5	2.25	0.3062	
0.65	0.0934	3.17	7.16	2.5	0.4427	
1.07	0.1537	4.8	11.78	1.4	0.4075	
1.65	0.237	5.44	18.16	0.669	0.2996	
2.5	0.359	4.49	27.51	0.294	0.1632	UNOBTAINABLE
3.47	0.4986	4.75	38.21	0.132	0.1243	
4.52	0.6494	6.68	49.76	0.109	0.1342	
5.78	0.8305	7.82	63.64	0.078	0.1229	

TABLE 6.

Uf = 7.2 h = 27.5 ρ = 1.17 w = 150

M	U	τ	γ	f	τ/γ	N_{RE}
0.18	0.037	0.84	3.7	4.025	0.227	12.5
0.24	0.05	1.53	5.0	4.225	0.306	18.0
0.38	0.079	2.33	7.9	2.557	0.2949	30.5
0.65	0.135	3.09	13.5	1.159	0.2289	55.5
1.22	0.253	4.81	25.3	0.515	0.1901	113.8
1.59	0.329	7.1	32.9	0.449	0.2158	153.5
2.34	0.484	9.39	48.4	0.273	0.194	238.5
3.11	0.644	8.17	64.4	0.135	0.1269	474.2
4.1	0.849	9.31	84.9	0.089	0.1097	678.9
5.65	1.17	12.06	117.0	0.0604	0.1031	1028.9
Uf = 7.2	h = 40.0	ρ	= 1.18	w = 150		
4.32	0.61	6.54	46.74	0.119	0.1399	517.2
3.61	0.51	6.19	39.08	0.162	0.1584	420
3.88	0.548	6.24	41.99	0.141	0.1486	456.7
2.63	0.371	4.53	28.43	0.223	0.1593	290.7
1.97	0.278	4.93	21.3	0.433	0.2315	-
1.44	0.203	5.74	15.56	0.944	0.3689	66.3
0.97	0.137	3.52	10.5	1.274	0.3352	43.5
0.7	0.099	3.42	7.59	2.365	0.4506	30.6
0.48	0.068	0.81	5.21	1.184	0.1555	20.6

TABLE 7.

Uf = 17.9 h = 27.5 ρ = 0.961 w = 150

M	U	τ	γ	f	τ/γ	N_{RE}
0.5919	0.1493	2.701	14.93	1.009	0.181	
1.026	0.2588	3.769	25.88	0.4687	0.146	
1.284	0.3239	4.24	32.39	0.3367	0.131	
1.589	0.4008	4.742	40.08	0.2459	0.118	
2.072	0.5227	5.402	52.27	0.1647	0.103	
2.426	0.612	6.721	61.2	0.1495	0.11	
2.972	0.7497	8.228	74.97	0.122	0.11	
3.375	0.8514	8.731	85.14	0.1003	0.103	
3.97	1.001	9.547	100.1	0.0794	0.095	NOT CALCULATED
4.677	1.18	10.992	118.0	0.0658	0.093	
4.05	1.022	10.301	102.2	0.0822	0.101	
3.262	0.8229	8.856	82.29	0.1089	0.108	
2.603	0.6566	6.909	65.66	0.1335	0.105	
1.991	0.5023	5.402	50.23	0.1783	0.108	
1.316	0.332	4.208	33.2	0.3181	0.127	
0.9619	0.2427	2.764	24.27	0.3909	0.114	

TABLE 8.

Uf = 16.1 h = 27.5 ρ = 0.988 w = 150

M	U	τ	γ	f	τ/γ	N_{RE}
0.978	0.24	3.293	24.0	0.4633	0.137	-
1.235	0.303	4.714	30.3	0.416	0.156	-
1.605	0.3938	5.231	39.38	0.2733	0.133	239.6
2.04	0.5006	5.941	50.06	0.1921	0.119	319.3
2.474	0.607	7.168	60.7	0.1576	0.118	402.1
3.053	0.7491	8.653	74.91	0.1249	0.116	517.2
3.648	0.8951	10.01	89.51	0.1012	0.112	640.1
4.275	1.049	11.01	104.9	0.0811	0.105	774.0
4.983	1.223	12.915	122.3	0.07	0.106	930.1
4.388	1.077	11.494	107.7	0.0803	0.107	798.8
3.423	0.8399	9.686	83.99	0.1113	0.115	593.1
2.94	0.7214	8.33	72.14	0.1297	0.115	494.4
2.474	0.607	6.78	60.7	0.1491	0.112	402.1
1.991	0.4885	5.812	48.85	0.1973	0.119	310.0
1.396	0.3425	4.746	34.25	0.3278	0.139	202.7
0.978	0.24	2.518	24.0	0.3543	0.105	-

TABLE 9.

Uf = 16.1 h = 40.0 ρ = 1.063 w = 150

M	U	τ	γ	f	τ/γ	N_{RE}
0.7849	0.1231	1.088	9.433	0.5408	0.115	-
1.171	0.1836	2.448	14.069	0.5469	0.174	-
1.621	0.2542	3.536	19.479	0.4121	0.182	164.2
2.007	0.3147	4.125	24.115	0.3137	0.171	214.4
2.619	0.4106	4.941	31.464	0.2207	0.157	298.9
3.326	0.5215	5.712	39.963	0.1582	0.143	403.1
3.873	0.6072	6.347	46.53	0.1296	0.136	487.5
4.452	0.698	7.253	53.49	0.1121	0.136	580.3
5.257	0.8242	8.613	63.158	0.0955	0.136	714.2
4.018	0.63	6.392	48.277	0.1213	0.132	510.5
3.069	0.4812	5.077	36.874	0.1651	0.138	364.5
2.345	0.3677	4.261	28.177	0.2374	0.151	260.4
1.734	0.2719	3.264	20.836	0.3325	0.157	178.6
1.235	0.1936	1.36	14.836	0.2733	0.092	-

TABLE 10.

U_f = 14.3 h = 27.5 ρ = 1.01 w = 150

M	U	τ	γ	f	τ/γ	N_{RE}
0.4472	0.1073	1.452	10.73	0.9998	0.135	-
0.7528	0.1807	2.409	18.07	0.5848	0.133	-
1.0584	0.254	3.169	25.4	0.3893	0.125	-
1.509	0.3622	4.489	36.22	0.2712	0.124	-
1.911	0.4587	5.149	45.87	0.194	0.112	343.2
2.249	0.5398	5.809	53.98	0.158	0.108	403.8
2.635	0.6325	6.601	63.25	0.1308	0.104	473.2
3.053	0.7328	7.79	73.28	0.115	0.106	548.2
3.568	0.8564	9.11	85.64	0.0984	0.106	640.7
4.211	1.011	10.727	101.1	0.0832	0.106	756.3
4.887	1.173	13.4	117.3	0.0772	0.114	877.5
4.452	1.069	11.684	106.9	0.081	0.109	799.7
4.034	0.9683	10.562	96.83	0.0893	0.109	724.4
3.487	0.837	9.044	83.7	0.1023	0.108	626.2
3.053	0.7328	7.724	73.28	0.114	0.105	548.2
2.635	0.6325	6.601	63.25	0.1308	0.104	473.2
2.217	0.5321	5.743	53.21	0.1608	0.108	398.1
1.863	0.4472	4.984	44.72	0.1975	0.111	334.6
1.477	0.3542	3.565	35.45	0.2248	0.1	-
1.171	0.2811	1.782	28.11	0.1788	0.063	-

TABLE 11.

Uf = 14.3 h = 40.0 ρ = 1.079 w = 150

M	U	τ	γ	f	τ/γ	N_{RE}
0.7045	0.1088	0.2761	8.337	0.173	0.033	-
1.026	0.1585	1.473	12.15	0.4349	0.121	-
1.428	0.2206	2.669	16.9	0.4069	0.158	155.2
1.718	0.2654	3.267	20.34	0.3441	0.161	190.1
2.112	0.3262	4.049	25.0	0.2823	0.162	238.2
2.635	0.407	4.694	31.19	0.2102	0.15	303.8
3.149	0.4864	5.43	37.27	0.1703	0.146	369.3
3.712	0.5734	6.304	43.94	0.1423	0.143	442.3
4.131	0.6381	7.086	48.9	0.1291	0.145	497.2
4.581	0.7076	7.639	54.22	0.1132	0.141	556.9
4.806	0.7424	8.099	56.89	0.109	0.142	587.0
4.581	0.7076	7.915	54.22	0.1173	0.146	556.9
4.187	0.6467	7.225	49.56	0.1282	0.146	504.6
3.68	0.5684	6.35	43.56	0.1458	0.146	438.0
3.182	0.4915	5.522	37.66	0.1696	0.147	373.5
2.643	0.4082	4.878	31.28	0.2172	0.156	304.7
2.265	0.3499	4.233	26.81	0.2566	0.158	257.4
1.798	0.2777	3.313	21.28	0.3188	0.156	199.8
1.557	0.2405	2.761	18.43	0.3542	0.15	170.7
1.203	0.1858	1.38	14.24	0.2967	0.097	-

TABLE 12.

Uf = 11.65 h = 27.5 ρ = 1.062 w = 150

M	U	τ	γ	f	τ/γ	N_{RE}
0.5598	0.1278	2.013	12.78	0.929	0.158	-
0.801	0.1828	2.672	18.28	0.6028	0.146	-
1.123	0.2563	3.887	25.63	0.4461	0.152	-
1.525	0.3481	4.581	34.81	0.285	0.132	-
1.895	0.4326	5.414	43.26	0.2181	0.125	-
2.345	0.5353	6.212	53.53	0.1634	0.116	405.8
2.956	0.6748	7.288	67.48	0.1207	0.108	511.8
3.375	0.7704	8.26	77.04	0.1049	0.107	584.4
3.68	0.84	9.266	84.0	0.099	0.11	637.3
4.131	0.943	10.55	94.3	0.0894	0.112	715.7
5.047	1.152	13.33	115.2	0.0757	0.116	874.6
4.806	1.097	12.494	109.7	0.0783	0.114	832.8
4.549	1.038	12.01	103.8	0.084	0.116	787.9
4.082	0.9318	10.9	93.18	0.0946	0.117	707.1
3.6	0.8218	9.544	82.18	0.1065	0.116	623.5
3.198	0.73	8.191	73.0	0.1159	0.112	553.7
2.699	0.6161	6.802	61.61	0.1351	0.11	467.2
2.281	0.5207	5.692	52.07	0.1582	0.109	394.7
1.959	0.4472	4.928	44.72	0.1858	0.11	338.9
1.686	0.3849	3.54	38.49	0.1801	0.092	-
1.332	0.3041	2.082	30.41	0.1697	0.068	-

TABLE 13.

Uf = 11.65 h = 40.0 ρ = 1.11 w = 150

M	U	τ	γ	f	τ/γ	N_{RE}
0.56	0.084	0.3787	6.437	0.3871	0.059	-
0.8815	0.1324	1.467	10.15	0.6038	0.145	-
1.364	0.2048	2.329	15.69	0.3989	0.148	-
1.654	0.2483	3.077	19.03	0.3599	0.162	177.1
2.04	0.3063	3.787	23.47	0.2911	0.161	221.9
2.393	0.3593	4.355	27.53	0.2433	0.158	263.4
2.651	0.398	4.639	30.5	0.2112	0.152	294.0
3.182	0.4778	5.444	36.61	0.172	0.149	357.7
3.696	0.555	6.391	42.53	0.1496	0.15	420.2
4.308	0.6468	7.479	49.56	0.1289	0.151	495.3
5.047	0.7578	8.805	58.07	0.1106	0.152	587.1
4.565	0.6854	8.047	52.52	0.1235	0.153	527.1
4.179	0.6275	7.385	48.09	0.1353	0.154	479.4
3.359	0.5044	5.965	38.65	0.1691	0.154	379.2
2.956	0.4438	5.349	34.01	0.1959	0.157	330.5
2.651	0.398	4.876	30.5	0.222	0.16	294.0
2.377	0.2569	4.45	27.35	0.252	0.163	261.5
1.927	0.2893	3.598	22.17	0.31	0.162	208.7
1.637	0.2458	2.698	18.84	0.3221	0.143	-
1.155	0.1734	0.9468	13.29	0.174	0.071	-

TABLE 14.

Uf = 9.85 h = 27.5 ρ = 1.11 w = 150

M	U	τ	γ	f	τ/γ	N_{RE}
0.4954	0.1082	2.684	10.82	1.654	0.241	-
0.801	0.1749	4.208	17.49	0.9921	0.241	-
1.123	0.2452	4.5	24.52	0.5396	0.184	-
1.412	0.3083	4.571	30.83	0.3468	0.148	-
1.718	0.3751	5.441	37.51	0.2789	0.145	-
2.072	0.4524	6.167	45.24	0.2173	0.136	-
2.506	0.5472	7.4	54.72	0.1782	0.135	-
2.94	0.6419	8.271	64.19	0.1448	0.129	491.4
3.568	0.779	8.851	77.9	0.1052	0.114	596.3
3.97	0.8668	9.94	86.68	0.0954	0.115	663.5
4.613	1.007	11.753	100.7	0.0836	0.117	770.9
5.112	1.116	12.188	111.6	0.0706	0.109	854.3
4.903	1.071	12.116	107.1	0.0762	0.113	819.9
4.388	0.9581	10.883	95.81	0.0855	0.114	733.4
3.97	0.8668	9.939	86.68	0.0954	0.115	663.5
3.519	0.7683	8.996	76.83	0.1099	0.117	588.1
3.021	0.6596	7.835	65.96	0.1299	0.119	504.9
3.619	0.5718	6.675	57.18	0.1472	0.117	437.7
2.265	0.4945	5.441	49.45	0.1605	0.11	-
1.814	0.3961	4.208	39.61	0.1934	0.106	-
1.573	0.3434	3.265	34.34	0.1997	0.095	-
1.364	0.2978	2.104	29.78	0.1711	0.071	-

TABLE 15.

Uf = 9.85 h = 40.0 ρ = 1.14 w = 150

M	U	τ	γ	f	τ/γ	N_{RE}
0.6241	0.0912	0.6807	6.989	0.5747	0.097	-
0.8654	0.1265	2.1393	9.694	0.9388	0.221	-
1.509	0.2206	2.82	16.905	0.4069	0.167	158.8
1.895	0.277	3.549	21.23	0.3248	0.167	202.5
2.168	0.317	3.987	24.29	0.2786	0.164	234.0
2.442	0.357	4.181	27.36	0.2304	0.153	265.6
2.924	0.4275	5.056	32.76	0.1943	0.154	322.1
3.471	0.5075	6.029	38.89	0.1644	0.155	386.9
3.809	0.5569	6.612	42.68	0.1497	0.155	427.3
4.147	0.6063	7.099	46.46	0.1356	0.153	467.9
4.983	0.7285	8.45	55.82	0.1119	0.152	569.4
4.484	0.6556	7.779	50.24	0.1271	0.155	508.7
4.018	0.5874	7.146	45.01	0.1464	0.16	452.4
3.439	0.5028	6.029	38.53	0.1675	0.156	383.1
3.101	0.4534	5.543	34.74	0.1893	0.16	343.0
2.619	0.3829	4.57	29.34	0.2189	0.156	286.3
2.2	0.3216	4.035	24.64	0.274	0.164	237.6
1.847	0.27	3.306	20.69	0.3185	0.16	197.1
1.461	0.2136	1.993	16.37	0.3068	0.122	-
1.203	0.1759	0.8265	13.48	0.1876	0.061	-

TABLE 16.

Uf = 9.0 h = 27.5 ρ = 1.125 w = 150

M	U	τ	γ	f	τ/γ	N_{RE}
0.447	0.0963	4.706	9.63	3.611	0.489	-
0.785	0.1692	4.927	16.92	1.224	0.291	-
1.235	0.2662	5.147	26.62	0.5169	0.193	-
1.605	0.3459	5.368	34.59	0.3192	0.155	-
1.895	0.4084	6.103	40.84	0.2604	0.149	-
2.586	0.5573	7.611	55.73	0.1744	0.137	397.2
3.326	0.7168	9.118	71.68	0.1263	0.127	542.6
3.922	0.8453	10.074	84.53	0.1003	0.119	665.6
4.5	0.9698	11.324	96.98	0.0857	0.117	789.1
5.208	1.122	11.545	112.2	0.0653	0.103	945.4
4.484	0.9664	10.442	96.64	0.0796	0.108	785.7
4.082	0.8797	9.706	87.97	0.0892	0.11	699.3
3.487	0.7515	9.045	75.15	0.114	0.12	575.3
2.876	0.6198	7.5	61.98	0.1389	0.121	453.2
2.2	0.4741	6.25	47.41	0.1979	0.132	325.1
1.863	0.4015	5.294	40.15	0.2337	0.132	264.6
1.702	0.3668	5.441	36.68	0.2878	0.148	-
1.541	0.3321	4.338	33.21	0.2799	0.131	-
1.219	0.2627	3.088	26.27	0.3184	0.118	-
1.042	0.2246	2.353	22.46	0.3319	0.105	-

TABLE 17.

Uf = 9.0 h = 40.0 ρ = 1.148 w = 150.

M	U	τ	γ	f	τ/γ	N_{RE}
0.624	0.0906	2.252	6.943	1.913	0.324	-
0.914	0.1327	3.525	10.169	1.396	0.347	-
1.251	0.1816	4.504	13.916	0.9525	0.324	-
1.718	0.2493	4.406	19.104	0.4944	0.231	-
1.863	0.2704	4.504	20.721	0.4296	0.217	-
2.426	0.3521	4.896	26.981	0.2754	0.181	-
2.908	0.4221	5.386	32.346	0.2108	0.167	308.3
3.214	0.4665	5.875	35.748	0.1882	0.164	349.4
3.68	0.5341	6.463	40.928	0.158	0.158	413.7
4.115	0.5972	7.05	45.763	0.1378	0.154	475.6
4.645	0.6742	7.834	51.664	0.1202	0.152	553.4
5.16	0.7489	8.421	57.388	0.1047	0.147	631.0
4.581	0.6649	7.442	50.451	0.1174	0.146	543.9
4.34	0.6299	6.854	48.269	0.1205	0.142	508.4
4.05	0.5878	6.659	45.043	0.1344	0.148	466.3
3.552	0.5155	5.973	39.503	0.1567	0.151	395.8
3.117	0.4524	5.288	34.667	0.1802	0.153	336.2
2.667	0.3871	4.602	29.663	0.2142	0.155	-
2.088	0.303	3.525	23.219	0.2677	0.152	-
1.493	0.2167	2.154	16.606	0.3199	0.13	-
1.187	0.1723	0.881	13.203	0.207	0.067	-

TABLE 18.

Uf = 8.1 h = 27.5 ρ = 1.15 w = 150

M	U	τ	γ	f	τ/γ	N_{RE}
0.56	0.12	4.89	12	2.365	0.408	-
0.77	0.162	5.48	16.2	1.454	0.338	-
0.99	0.209	5.8	20.9	0.9234	0.278	-
1.51	0.319	5.64	31.9	0.3856	0.177	-
1.83	0.386	6.16	38.6	0.2875	0.16	-
2.23	0.47	6.7	47	0.211	0.143	-
2.62	0.553	7.96	55.3	0.1812	0.144	-
3.0	0.633	8.57	63.3	0.1489	0.135	-
3.47	0.732	8.73	73.2	0.1134	0.119	586.5
3.99	0.842	9.4	84.2	0.0923	0.112	696.6
4.4	0.928	9.99	92.8	0.0807	0.108	785.0
4.97	1.049	11.21	104.9	0.0675	0.107	912.6
4.69	0.989	10.44	98.9	0.0743	0.106	848.9
4.52	0.954	10.03	95.4	0.0767	0.105	812.1
4.24	0.895	9.54	89.5	0.0829	0.107	750.8
3.66	0.772	8.95	77.2	0.1046	0.116	626.1
3.33	0.703	8.28	70.3	0.1166	0.118	558
2.8	0.591	6.77	59.1	0.1348	0.115	-
2.39	0.504	6.47	50.4	0.1773	0.128	-
1.96	0.414	5.34	41.4	0.217	0.129	-
1.32	0.278	4.8	27.8	0.4326	0.173	-
0.91	0.192	3.9	19.2	0.7366	0.203	-

TABLE 19.

Uf = 8.1 h = 40.0 ρ = 1.16 w = 150

M	U	τ	γ	f	τ/γ	N_{RE}
0.495	0.071	2.88	5.44	3.942	0.529	-
0.978	0.141	3.95	10.8	1.37	0.366	-
1.123	0.161	4.45	12.34	1.185	0.361	-
1.573	0.226	4.75	17.32	0.6417	0.274	-
1.83	0.263	4.96	20.15	0.4946	0.246	-
2.345	0.337	5.73	25.82	0.3481	0.222	-
2.667	0.383	5.85	29.35	0.2751	0.199	-
3.246	0.466	6.14	35.71	0.1953	0.172	335.7
3.857	0.554	6.74	42.45	0.1515	0.159	415.6
4.4	0.632	7.63	48.43	0.1318	0.158	489.0
4.951	0.711	8.4	54.48	0.1147	0.154	565.5
4.597	0.66	7.77	50.58	0.1231	0.154	515.8
4.147	0.596	7.12	45.67	0.1384	0.156	454.8
3.6	0.517	6.03	39.62	0.1556	0.152	-
2.94	0.422	5.25	32.34	0.2036	0.162	-
2.538	0.365	4.9	27.97	0.2537	0.175	-
2.056	0.295	4.45	22.61	0.3531	0.197	-
1.557	0.224	3.77	17.17	0.5185	0.22	-
1.284	0.184	3.12	14.1	0.6352	0.221	-
0.962	0.138	1.63	10.57	0.5916	0.154	-

TABLE 20.

Uf = 7.2 h = 27.5 ρ = 1.17 w = 150

M	U	τ	γ	f	τ/γ	N_{RE}
0.21	0.0435	1.995	4.35	7.194	0.459	
0.35	0.0725	3.22	7.25	4.18	0.444	
0.93	0.1925	4.52	19.25	0.8332	0.235	
1.25	0.259	6.6	25.9	0.6709	0.255	
1.75	0.362	6.37	36.2	0.3314	0.176	
2.0	0.414	6.82	41.4	0.2717	0.165	UNOBTAINABLE
2.7	0.559	6.96	55.9	0.1523	0.125	
3.29	0.68	7.65	68.0	0.113	0.113	
Uf = 7.2	h = 40.0	ρ	= 1.18	w = 150		
3.29	0.464	5.94	35.6	0.1871	0.167	
2.68	0.378	5.03	29.0	0.239	0.173	
2.21	0.312	4.94	23.9	0.3436	0.207	
1.58	0.224	3.42	17.2	0.4625	0.199	
1.22	0.1725	0.957	13.22	0.2182	0.072	UNOBTAINABLE

TABLE 21.

Uf = 7.2 h = 27.5 ρ = 1.17 w = 150

M	U	τ	γ	f	τ/γ	N_{RE}
0.17	0.0352	2.07	3.52	11.398	0.588	
0.51	0.1055	3.14	10.55	1.928	0.298	
0.61	0.1262	3.6	12.62	1.544	0.285	
0.85	0.176	6.44	17.6	1.419	0.366	
1.18	0.244	7.5	24.4	0.8612	0.307	
0.3	0.062	3.06	6.2	5.432	0.494	
0.74	0.153	5.82	15.3	1.698	0.38	
1.4	0.29	6.9	29	0.5599	0.238	
1.72	0.356	5.9	35.6	0.3179	0.166	
2.02	0.418	6.14	41.8	0.2396	0.147	
2.31	0.478	6.51	47.8	0.1946	0.136	
2.69	0.557	6.9	55.7	0.1518	0.124	
3.18	0.658	7.89	65.8	0.1245	0.12	
3.4	0.704	8.5	70.4	0.1172	0.121	
Uf = 7.2	h = 40.0	ρ	= 1.18	w = 150		
3.5	0.494	6.25	37.9	0.1735	0.165	
2.91	0.411	5.14	31.5	0.2061	0.163	
2.53	0.358	4.53	27.4	0.2397	0.165	
2.1	0.297	3.88	22.8	0.2979	0.17	
1.75	0.247	3.02	18.95	0.3357	0.159	
1.5	0.212	2.47	16.25	0.3723	0.152	

UNOBTAINABLE

UNOBTAINABLE

TABLE 22.

Uf = 7.2 h = 27.5 ρ = 1.17 w = 150

M	U	τ	γ	f	τ/γ	N_{RE}
0.45	0.093	3.22	9.3	2.541	0.346	
0.83	0.172	4.37	17.2	1.008	0.254	
1.3	0.269	4.99	26.9	0.4707	0.186	
1.62	0.335	5.29	33.5	0.3217	0.158	
1.9	0.393	6.14	39.3	0.2713	0.156	
2.25	0.466	6.83	46.6	0.2147	0.147	
2.51	0.52	7.43	52	0.1875	0.143	
2.86	0.592	7.43	59.2	0.1447	0.126	
3.33	0.69	8.81	69	0.1263	0.128	
3.95	0.818	9.89	81.8	0.1009	0.121	
4.79	0.99	12.12	99	0.0844	0.122	UNOBTAINABLE
3.63	0.752	8.97	75.2	0.1082	0.119	
2.99	0.619	7.36	61.9	0.1311	0.119	
2.73	0.565	6.6	56.5	0.1411	0.117	
2.31	0.478	6.67	47.8	0.1992	0.14	
2.01	0.416	5.52	41.6	0.2177	0.133	
1.75	0.362	4.67	36.2	0.2431	0.129	
1.53	0.316	4.21	31.6	0.2876	0.133	
1.33	0.275	3.52	27.5	0.3175	0.128	
1.12	0.231	2.23	23.1	0.2853	0.097	

TABLE 23.

Uf = 7.2 h = 40.0 ρ = 1.18 w = 150

M	U	τ	γ	f	τ/γ	N_{RE}
0.56	0.08	1.21	6.1	1.28	0.198	
1.027	0.145	2.42	11.05	0.7743	0.219	
1.188	0.168	3.23	12.8	0.7765	0.252	
1.48	0.21	3.93	16	0.6038	0.246	
1.99	0.28	4.32	21.34	0.3736	0.202	
2.22	0.31	4.44	23.62	0.3133	0.188	
2.65	0.374	5.04	28.5	0.2446	0.177	
3.26	0.46	5.74	35.05	0.1839	0.164	
3.71	0.52	6.25	39.62	0.1568	0.158	
4.23	0.6	6.73	45.72	0.1269	0.147	
5.19	0.73	8.06	55.63	0.1026	0.145	
4.82	0.68	7.55	51.82	0.1107	0.146	UNOBTAINABLE
4.47	0.63	6.86	48	0.1171	0.143	
4.12	0.58	6.64	44.2	0.134	0.15	
3.68	0.52	6.49	39.6	0.1629	0.164	
3.05	0.43	5.53	32.77	0.2027	0.169	
2.49	0.35	4.62	26.67	0.2558	0.173	
2.09	0.295	4.23	22.48	0.3295	0.188	
1.64	0.23	3.41	17.53	0.4375	0.195	
1.3	0.184	2.72	14.02	0.5445	0.194	
0.98	0.138	1.51	10.52	0.5378	0.144	
0.38	0.054	0.39	4.11	0.9133	0.095	

TABLE 24.

Uf = 7.2 h = 27.5 ρ = 1.17 w = 150

M	U	τ	γ	f	τ/γ	N_{RE}
0.174	0.036	1.916	3.6	10.089	0.532	
0.351	0.073	3.059	7.3	3.917	0.419	
0.945	0.196	3.986	19.6	0.7081	0.203	
1.188	0.245	5.214	24.6	0.588	0.212	
1.622	0.336	5.359	33.6	0.3239	0.159	
1.815	0.376	5.635	37.6	0.272	0.15	
2.25	0.466	6.67	46.6	0.2096	0.143	
2.716	0.562	7.054	56.2	0.1524	0.126	
3.086	0.639	7.436	63.9	0.1243	0.116	
2.587	0.536	6.9	53.6	0.1639	0.129	
2.07	0.429	6.286	42.9	0.2331	0.147	
1.654	0.342	5.06	34.2	0.2952	0.148	
1.284	0.266	4.446	26.6	0.4288	0.167	
1.043	0.216	3.45	21.6	0.5046	0.16	
0.866	0.179	2.03	17.9	0.4325	0.113	

UNOBTAINABLE

TABLE 25.

Uf = 21.0 h = 27.5 ρ = 0.931 w = 100

M	U	τ	γ	f	τ/γ	N_{RE}
0.4311	0.168	0.754	18.98	0.23	0.0397	-
0.6241	0.244	1.4	27.57	0.202	0.0508	-
0.8654	0.338	2.262	38.19	0.17	0.0592	401.0
1.284	0.502	3.339	56.73	0.114	0.0589	586.2
1.525	0.596	3.716	67.348	0.09	0.0552	691.2
1.863	0.728	4.685	82.26	0.076	0.057	837.5
2.8	1.094	7.108	123.62	0.051	0.0575	1238.3
3.439	1.343	8.939	151.76	0.043	0.0589	1507.7
3.97	1.551	11.09	175.26	0.04	0.0633	1731.2
3.149	1.23	8.455	138.99	0.048	0.0608	1385.7
2.377	0.928	5.924	104.86	0.059	0.0565	1057.4
1.75	0.6835	4.039	77.24	0.074	0.0523	788.4
1.235	0.482	2.8	54.47	0.104	0.0514	563.8
0.9619	0.376	1.723	42.49	0.105	0.0406	-
0.7689	0.3	0.862	33.9	0.082	0.0254	-

TABLE 26.

Uf = 21.0 h = 40.0 ρ = 1.019 w = 100

M	U	τ	γ	f	τ/γ	N_{RE}
0.8654	0.212	0.806	19.27	0.141	0.0418	-
1.139	0.279	1.832	25.36	0.185	0.0722	-
1.589	0.39	3.223	35.45	0.167	0.0909	388.3
2.136	0.524	4.506	47.64	0.129	0.0946	509.2
2.651	0.65	5.786	59.09	0.108	0.098	620.4
3.037	0.745	6.374	67.73	0.09	0.0941	703.1
3.632	0.891	7.912	81	0.078	0.0977	828.4
4.259	1.044	9.231	94.91	0.067	0.0973	958.0
3.616	0.887	7.619	80.64	0.076	0.0945	825.0
2.973	0.729	6.081	66.27	0.09	0.0918	689.2
2.345	0.575	4.689	52.27	0.111	0.0897	554.4
1.814	0.445	3.517	40.460	0.14	0.0869	438.3
1.412	0.346	1.832	31.45	0.12	0.0583	-
1.107	0.272	0.659	24.73	0.07	0.0266	-

TABLE 27.

Uf = 21.0 h = 55.0 ρ = 1.1 w = 100

M	U	τ	γ	f	τ/γ	N_{RE}
1.316	0.2175	1.036	16.6	0.159	0.0624	-
1.831	0.3026	2.73	23.1	0.217	0.1182	290.4
2.136	0.353	3.77	26.96	0.22	0.1398	303.4
2.731	0.451	5.087	34.46	0.182	0.1476	343.2
3.005	0.497	5.935	37.92	0.175	0.1565	379.2
3.648	0.603	6.877	46.03	0.138	0.1494	462.3
4.147	0.686	7.819	52.33	0.121	0.1494	527.7
4.436	0.733	8.29	55.97	0.112	0.1481	564.9
4.115	0.68	7.724	51.93	0.121	0.1487	523
3.439	0.568	6.594	43.39	0.149	0.152	434.9
2.683	0.444	5.087	33.86	0.188	0.1502	337.8
2.265	0.374	3.956	28.58	0.206	0.1384	308.8
1.782	0.295	2.496	22.48	0.209	0.111	295.8
1.364	0.226	0.754	17.21	0.107	0.0438	-

TABLE 28.

Uf = 18.85 h = 27.5 ρ = 0.955 w = 100

M	U	τ	γ	f	τ/γ	N_{RE}
0.4472	0.17	1.022	19.24	0.296	0.0531	-
0.7206	0.274	1.823	31.01	0.204	0.0588	-
0.9297	0.354	2.403	40	0.161	0.0501	-
1.461	0.556	3.702	62.85	0.1	0.0589	-
1.766	0.673	4.475	75.99	0.083	0.0589	780.3
2.12	0.807	5.857	91.22	0.075	0.0642	884.0
2.715	1.034	8.067	116.83	0.063	0.069	1048.1
3.182	1.212	9.945	136.91	0.057	0.0726	1169.0
3.873	1.475	12.376	166.68	0.048	0.0743	1337.8
4.404	1.677	14.034	189.51	0.042	0.0741	1461.1
3.825	1.457	12.431	164.5	0.049	0.0755	1326.6
3.326	1.267	10.663	143.14	0.056	0.0745	1205.2
2.587	0.985	7.735	111.31	0.067	0.0695	1013.7
2.2	0.838	5.912	94.683	0.071	0.0624	907.2
1.798	0.685	4.31	77.38	0.077	0.0557	789.9
1.461	0.556	3.039	62.85	0.082	0.0484	-
1.268	0.483	2.155	54.57	0.077	0.0395	-
1.075	0.409	1.326	46.24	0.066	0.0287	-

TABLE 29.

Uf = 18.85 h = 40.0 ρ = 1.04 w = 100

M	U	τ	γ	f	τ/γ	N_{RE}
1.107	0.266	0.897	24.18	0.098	0.0371	-
1.203	0.289	1.757	26.29	0.162	0.0668	-
1.444	0.347	2.991	31.56	0.191	0.0948	-
1.702	0.409	3.739	37.19	0.172	0.1005	361.7
2.024	0.486	4.711	44.22	0.154	0.1065	431.4
2.538	0.61	5.907	55.46	0.122	0.1065	544.2
3.214	0.773	6.954	70.23	0.09	0.099	693.3
3.664	0.881	8	80.07	0.079	0.0999	792.4
4.211	1.012	9.309	92.03	0.07	0.1012	913.0
3.391	0.315	7.328	74.1	0.085	0.0989	731.7
2.506	0.602	5.608	54.76	0.119	0.1024	536.9
2.168	0.521	4.86	47.38	0.138	0.1026	463.2
1.847	0.444	4.038	40.35	0.158	0.1001	393.4
1.525	0.367	2.729	33.33	0.156	0.0819	-
1.235	0.297	1.57	26.99	0.137	0.0582	-

TABLE 30.

Uf = 18.85 h = 55.0 ρ = 1.105 w = 100

M	U	τ	γ	f	τ/γ	N_{RE}
1.364	0.224	0.852	17.131	0.123	0.0497	-
1.654	0.272	2.365	20.76	0.231	0.1139	-
2.024	0.333	3.784	25.42	0.247	0.1489	-
2.393	0.394	4.589	30.06	0.214	0.1527	300.0
2.876	0.473	5.44	36.12	0.176	0.1506	365.8
3.423	0.563	6.434	42.99	0.147	0.1497	441.9
3.922	0.645	7.096	49.25	0.123	0.1441	512.1
4.517	0.743	8.231	56.74	0.108	0.1451	597.1
3.986	0.656	7.143	50.06	0.12	0.1427	521.7
3.439	0.566	6.386	43.19	0.144	0.1479	444.5
2.699	0.444	5.109	33.9	0.188	0.1507	341.6
2.056	0.338	3.217	25.82	0.204	0.1246	-
1.654	0.272	1.514	20.76	0.148	0.0729	-
1.509	0.248	0.568	18.95	0.067	0.03	-

TABLE 31.

Uf = 17.9 h = 27.5 ρ = 0.961 w = 100

M	U	τ	γ	f	τ/γ	N_{RE}
0.624	0.236	1.056	26.68	0.158	0.0396	-
0.737	0.279	2.057	31.49	0.22	0.0653	-
0.898	0.34	2.529	38.37	0.182	0.0659	-
1.235	0.467	3.78	52.82	0.144	0.0716	476.0
1.557	0.589	4.336	66.57	0.104	0.0651	598.1
1.847	0.699	5.059	78.94	0.086	0.0641	697.7
2.393	0.906	7.171	102.33	0.073	0.0701	881.3
3.149	1.192	9.784	134.65	0.057	0.0727	1128.1
3.809	1.441	12.675	162.84	0.051	0.0778	1338.0
4.227	1.599	14.34	180.73	0.047	0.0793	1469.3
3.729	1.411	10.284	159.41	0.043	0.0645	1313.0
3.198	1.21	9.2	136.72	0.052	0.0673	1143.4
2.603	0.985	8.505	111.27	0.073	0.0764	950.1
2.007	0.76	5.893	85.82	0.085	0.0687	752.3
1.589	0.601	4.336	67.45	0.1	0.0638	609.1
1.203	0.455	2.613	51.44	0.105	0.0508	-

TABLE 32.

Uf = 17.9 h = 40.0 ρ = 1.048 w = 100

M	U	τ	γ	f	τ/γ	N_{RE}
0.769	0.183	0.8287	16.67	0.189	0.0497	-
0.914	0.218	1.733	19.81	0.279	0.0875	-
1.3	0.31	3.164	28.18	0.252	0.1123	245.7
1.525	0.364	3.842	33.07	0.222	0.1162	292.1
1.879	0.448	4.897	40.75	0.187	0.1202	365.2
2.297	0.548	5.801	49.81	0.148	0.1165	453.6
2.86	0.682	6.63	62.02	0.109	0.1069	574.0
3.536	0.843	8.061	76.67	0.087	0.1051	721.0
3.841	0.916	8.966	83.3	0.082	0.1076	788.4
4.308	1.028	10.096	93.42	0.073	0.1081	892.6
3.986	0.951	9.267	86.44	0.078	0.1072	820.9
3.712	0.886	8.513	80.51	0.083	0.1057	760.7
3.262	0.778	7.534	70.74	0.095	0.1065	661.4
2.86	0.682	6.781	62.02	0.111	0.1093	574.0
2.442	0.583	6.103	52.96	0.137	0.1152	484.9
1.879	0.448	4.671	40.75	0.178	0.1146	365.2
1.493	0.356	3.541	32.37	0.214	0.1094	285.2
1.348	0.322	2.486	29.23	0.183	0.085	-

TABLE 33.

Uf = 17.9 h = 55.0 ρ = 1.11 w = 100

M	U	τ	γ	f	τ/γ	N_{RE}
1.332	0.218	0.618	16.65	0.094	0.0371	-
1.461	0.239	1.616	18.26	0.204	0.0885	-
1.798	0.295	3.184	22.49	0.264	0.1416	-
2.104	0.345	4.467	26.31	0.27	0.1698	237.9
2.619	0.429	5.322	32.74	0.208	0.1626	299.0
3.117	0.511	6.653	38.98	0.184	0.1707	359.2
3.777	0.619	7.603	47.22	0.143	0.161	439.2
4.485	0.735	8.934	56.08	0.119	0.1593	526.0
3.938	0.645	8.173	49.24	0.142	0.166	458.6
3.616	0.592	7.413	45.22	0.152	0.1639	419.2
3.085	0.505	6.653	38.57	0.188	0.1725	354.8
2.554	0.418	5.227	31.94	0.216	0.1637	291.0
2.024	0.331	3.707	25.3	0.244	0.1465	-
1.621	0.266	1.568	20.28	0.16	0.0773	-
1.461	0.239	0.475	18.26	0.06	0.026	-

TABLE 34.

Uf = 16.1 h = 27.5 ρ = 0.988 w = 100

M	U	τ	γ	f	τ/γ	N_{RE}
0.624	0.23	1.715	25.96	0.263	0.0661	-
0.882	0.324	2.629	36.66	0.203	0.0717	-
1.284	0.472	3.886	53.38	0.141	0.0728	-
1.686	0.62	4.658	70.11	0.098	0.0664	691.6
2.12	0.78	6.058	88.17	0.081	0.0687	831.3
2.619	0.964	7.83	108.91	0.068	0.0719	985.3
3.423	1.26	10.744	142.36	0.055	0.0755	1221.4
3.857	1.42	11.944	160.43	0.048	0.0744	1344.2
4.404	1.621	13.888	183.16	0.043	0.0758	1494.8
3.905	1.437	11.944	162.43	0.047	0.0735	1357.2
3.423	1.26	10.344	142.36	0.053	0.0727	1221.4
2.747	1.011	7.744	114.27	0.061	0.0678	1023.7
2.361	0.869	6.287	98.21	0.067	0.064	906.6
2.024	0.745	4.972	84.16	0.073	0.0591	801.3
1.654	0.609	3.972	68.77	0.087	0.0578	-
1.412	0.52	3.029	58.73	0.091	0.0516	-
1.219	0.449	2.286	50.7	0.092	0.0451	-

TABLE 35.

Uf = 16.1 h = 40.0 ρ = 1.063 w = 100

M	U	τ	γ	f	τ/γ	N_{RE}
0.769	0.181	0.7642	16.44	0.176	0.0465	-
0.962	0.226	1.528	20.56	0.226	0.0743	-
1.235	0.291	2.598	26.41	0.231	0.0984	-
1.67	0.393	3.821	35.7	0.186	0.107	340.4
1.863	0.438	4.28	39.83	0.168	0.1075	379.7
2.2	0.518	5.399	47.05	0.15	0.1137	449.8
2.747	0.646	6.19	58.74	0.112	0.1054	562.3
3.166	0.745	7.031	67.68	0.095	0.1039	649.4
3.841	0.903	8.636	82.13	0.08	0.1052	788.6
4.308	1.013	10.011	92.1	0.074	0.1087	885.6
3.809	0.896	8.788	81.44	0.083	0.1079	782.4
3.294	0.775	7.489	70.43	0.094	0.1063	675.8
2.828	0.665	6.61	60.46	0.113	0.1093	579.0
2.249	0.529	5.235	48.08	0.141	0.1089	459.5
1.847	0.434	4.203	39.48	0.168	0.1065	376.2
1.493	0.351	3.133	31.92	0.192	0.0982	-
1.284	0.302	2.063	27.45	0.171	0.0752	-
0.994	0.234	0.917	21.25	0.126	0.0432	-

TABLE 36.

Uf = 16.1 h = 55.0 ρ = 1.115 w = 100

M	U	τ	γ	f	τ/γ	N_{RE}
1.348	0.22	1.48	16.78	0.219	0.0882	-
1.75	0.285	3.055	21.78	0.27	0.1403	-
2.136	0.348	4.296	26.59	0.255	0.1616	-
2.667	0.435	5.442	33.19	0.206	0.164	306.1
3.359	0.548	6.683	41.8	0.16	0.1599	398.5
3.841	0.626	7.733	47.81	0.142	0.1617	464.0
4.436	0.723	8.401	55.22	0.115	0.1521	547.1
3.986	0.65	7.781	49.61	0.132	0.1568	484.4
3.471	0.566	6.922	43.21	0.155	0.1602	413.5
2.956	0.482	6.206	36.8	0.192	0.1686	344.2
2.699	0.44	5.442	33.6	0.202	0.162	310.1
2.088	0.34	4.01	25.99	0.249	0.1543	-
1.686	0.275	2.673	20.99	0.254	0.1273	-
1.316	0.215	1.05	16.37	0.163	0.0641	-

TABLE 37.

Uf = 14.3 h = 27.5 ρ = 1.01 w = 100

M	U	τ	γ	f	τ/γ	N_{RE}
0.302	0.109	1.168	12.31	0.779	0.0949	-
0.544	0.196	1.928	22.11	0.398	0.0872	-
0.801	0.288	2.512	32.58	0.24	0.0771	-
1.042	0.375	3.622	42.4	0.204	0.0854	-
1.493	0.537	4.615	60.71	0.127	0.076	544.7
1.899	0.676	5.579	76.42	0.097	0.073	666.1
2.297	0.827	7.186	93.43	0.083	0.0769	794.4
2.94	1.058	9.289	119.6	0.066	0.0777	985.3
3.6	1.296	11.976	146.43	0.057	0.0818	1176.4
4.259	1.533	13.846	173.25	0.047	0.0799	1362.4
3.841	1.383	12.21	156.25	0.051	0.0781	1245.2
3.536	1.273	11.538	143.82	0.056	0.0802	1158.2
3.037	1.093	9.902	123.53	0.066	0.0802	1013.7
2.426	0.873	7.536	98.66	0.078	0.0764	832.9
1.911	0.688	5.258	77.73	0.088	0.0676	676.4
1.557	0.561	4.382	63.34	0.11	0.0692	565.9
1.219	0.439	3.038	49.6	0.125	0.0613	-
1.107	0.398	2.22	45.01	0.111	0.0493	-

TABLE 38.

Uf = 14.3 h = 40.0 ρ = 1.079 w = 100

M	U	τ	γ	f	τ/γ	N_{RE}
1.075	0.249	0.776	22.64	0.093	0.0343	-
1.235	0.286	1.862	26.02	0.169	0.0716	-
1.348	0.312	2.715	28.39	0.207	0.0956	-
1.686	0.391	4.034	35.51	0.196	0.1136	-
2.136	0.495	5.508	44.99	0.167	0.1224	408.7
2.474	0.573	6.362	52.11	0.144	0.1221	473.1
2.908	0.674	6.788	61.26	0.111	0.1108	556.5
3.584	0.83	8.301	75.48	0.089	0.1098	685.3
4.308	0.998	10.4	90.73	0.077	0.1146	824.0
3.777	0.875	8.805	79.55	0.085	0.1107	722.5
2.94	0.681	7.06	61.94	0.113	0.114	562.3
2.442	0.566	6.168	51.43	0.143	0.1199	476.3
2.136	0.495	5.314	44.99	0.161	0.1181	408.7
1.686	0.391	3.724	35.51	0.181	0.1049	-
1.477	0.342	2.793	31.1	0.177	0.0898	-
1.235	0.286	1.319	26.02	0.12	0.0507	-

TABLE 39.

Uf = 14.3 h = 55.0 ρ = 1.124 w = 100

M	U	τ	γ	f	τ/γ	N_{RE}
1.058	0.171	0.529	13.07	0.129	0.0405	-
1.316	0.213	2.502	16.25	0.393	0.154	-
1.654	0.268	2.887	20.42	0.286	0.1414	-
2.072	0.335	4.138	25.58	0.262	0.1618	-
2.458	0.398	5.101	30.35	0.229	0.1681	277.3
2.892	0.468	5.967	35.71	0.194	0.1671	330.0
3.391	0.549	6.737	41.87	0.159	0.1609	391.6
3.745	0.606	7.603	46.25	0.147	0.1644	435.4
4.275	0.692	8.565	52.8	0.127	0.1622	500.6
3.938	0.637	7.988	48.62	0.14	0.1643	459.4
3.487	0.564	7.122	43.06	0.159	0.1654	401.1
2.973	0.481	6.304	36.7	0.194	0.1718	339.8
2.458	0.398	5.101	30.35	0.229	0.1681	277.3
1.895	0.307	3.272	23.4	0.247	0.1398	-
1.637	0.265	2.117	20.21	0.215	0.1048	-
1.461	0.236	0.818	18.04	0.105	0.0453	-

TABLE 40.

Uf = 13.45 h = 27.5 ρ = 1.024 w = 100

M	U	τ	γ	f	τ/γ	N_{RE}
0.431	0.153	1.363	17.3	0.455	0.0788	-
0.705	0.25	2.518	28.27	0.315	0.0891	-
0.898	0.319	3.11	36.02	0.239	0.0863	-
1.091	0.387	4.028	43.76	0.21	0.092	337.7
1.461	0.519	4.858	58.61	0.141	0.0829	445.8
1.911	0.679	5.983	76.68	0.101	0.078	575.0
2.329	0.827	7.76	93.46	0.089	0.083	693.1
2.892	1.027	10.54	116.05	0.078	0.0908	850.9
3.519	1.25	12.86	141.23	0.064	0.0911	1024.9
4.145	1.49	15.28	168.33	0.054	0.0908	1210.4
3.809	1.353	13.86	152.84	0.059	0.0907	1104.7
3.423	1.216	12.5	137.35	0.066	0.091	998.5
2.908	1.033	10.72	116.69	0.079	0.0919	855.6
2.393	0.85	7.583	96.04	0.082	0.079	711.3
1.943	0.69	5.687	77.97	0.093	0.0729	-
1.573	0.559	4.621	63.13	0.116	0.0732	-
1.155	0.41	2.784	46.34	0.129	0.0601	-

TABLE 41.

Uf = 13.45 h = 40.0 ρ = 1.085 w = 100

M	U	τ	γ	f	τ/γ	N_{RE}
0.576	0.133	1.17	12.07	0.488	0.0969	-
0.721	0.166	1.677	15.1	0.449	0.1111	-
1.042	0.24	2.574	21.83	0.33	0.1179	-
1.396	0.322	3.901	29.24	0.278	0.1334	-
1.686	0.388	4.603	35.32	0.226	0.1303	285.3
2.056	0.474	5.773	43.07	0.19	0.134	354.7
2.635	0.607	6.709	55.2	0.134	0.1215	464.1
3.117	0.718	7.762	65.3	0.111	0.1189	557.0
3.6	0.829	9.361	75.41	0.101	0.1241	651.2
4.34	1.0	11.155	90.91	0.082	0.1227	798.5
3.857	0.889	9.751	80.8	0.091	0.1207	702.6
3.455	0.796	8.737	72.37	0.102	0.1207	623.1
2.94	0.677	7.489	61.59	0.121	0.1216	522.5
2.474	0.57	6.475	51.82	0.147	0.125	433.4
1.879	0.433	4.915	39.35	0.194	0.1249	321.5
1.428	0.329	3.51	29.92	0.239	0.1173	-
1.171	0.27	2.184	24.53	0.221	0.089	-

TABLE 42.

Uf = 13.45 h = 55.0 ρ = 1.13 w = 100

M	U	τ	γ	f	τ/γ	N_{RE}
1.042	0.168	0.532	12.8	0.133	0.0416	-
1.364	0.219	1.838	16.75	0.271	0.1097	-
1.67	0.269	3.144	20.51	0.308	0.1533	-
1.975	0.318	4.354	24.26	0.305	0.1795	-
2.506	0.403	5.515	30.78	0.24	0.1792	260.6
3.278	0.527	7.063	40.27	0.18	0.1754	352.7
3.712	0.597	7.74	45.6	0.154	0.1697	406.0
4.131	0.665	8.708	50.74	0.139	0.1716	458.5
3.745	0.603	8.03	46	0.156	0.1746	410.6
3.278	0.527	7.256	40.27	0.185	0.1802	352.7
2.747	0.442	6.24	33.75	0.226	0.1849	289.2
2.442	0.393	5.515	29.99	0.253	0.1839	253.3
1.991	0.32	4.257	24.46	0.294	0.174	-
1.541	0.248	2.274	18.93	0.262	0.1201	-
1.316	0.212	1.064	16.16	0.168	0.0658	-

TABLE 43.

Uf = 11.65 h = 27.5 ρ = 1.062 w = 100

M	U	τ	γ	f	τ/γ	N_{RE}
0.383	0.131	1.781	14.81	0.782	0.1203	-
0.576	0.197	2.641	22.28	0.513	0.1185	-
0.769	0.263	3.072	29.74	0.335	0.1033	-
1.074	0.368	4.054	41.57	0.226	0.0975	-
1.654	0.566	5.283	63.97	0.124	0.0826	501.1
1.911	0.654	6.266	73.92	0.11	0.0848	562.0
2.281	0.781	8.293	88.24	0.102	0.094	647.1
3.069	1.051	11.242	118.73	0.077	0.0947	819.1
3.68	1.26	13.146	142.37	0.062	0.0923	946.0
4.163	1.425	14.927	161.03	0.055	0.0927	1043.1
4.645	1.59	17.753	179.71	0.053	0.0988	1137.9
4.05	1.387	16.218	156.68	0.064	0.1035	1020.9
3.455	1.183	14.62	133.66	0.079	0.1094	899.8
3.069	1.051	12.839	118.73	0.088	0.1081	819.1
2.474	0.847	8.969	95.7	0.094	0.0937	690.1
2.152	0.737	7.31	83.26	0.101	0.0878	618.0
1.67	0.572	5.222	64.59	0.12	0.0808	505.3
1.461	0.5	4.607	56.5	0.139	0.0815	454.1
1.251	0.428	3.563	48.41	0.147	0.0736	-
1.026	0.351	2.519	39.7	0.154	0.0635	-

TABLE 44.

Uf = 11.65 h = 40.0 ρ = 1.11 w = 100

M	U	τ	γ	f	τ/γ	N_{RE}
0.64	0.144	1.596	13.11	0.556	0.1217	-
0.93	0.209	2.274	19.04	0.375	0.1194	-
1.219	0.275	2.873	24.95	0.274	0.1151	-
1.541	0.347	3.87	31.55	0.232	0.1227	257.2
1.911	0.43	5.147	39.13	0.201	0.1315	324.2
2.393	0.539	6.384	49.01	0.159	0.1303	413.7
3.101	0.698	7.621	63.5	0.113	0.12	546.8
3.728	0.84	9.377	76.34	0.096	0.1228	667.8
4.259	0.959	10.933	87.21	0.086	0.1254	770.4
4.436	0.999	11.411	90.83	0.083	0.1256	805.1
4.082	0.919	10.494	83.59	0.09	0.1255	735.8
3.6	0.811	9.097	73.71	0.1	0.1234	642.9
3.037	0.684	7.541	62.18	0.116	0.1213	535.0
2.474	0.557	6.623	50.65	0.154	0.1308	428.7
1.927	0.434	5.187	39.46	0.199	0.1314	327.5
1.589	0.358	3.99	32.54	0.225	0.1226	266.1
1.284	0.289	2.633	26.28	0.228	0.1002	-

TABLE 45.

Uf = 11.65 h = 55.0 ρ = 1.14 w = 100

M	U	τ	γ	f	τ/γ	N_{RE}
1.284	0.2047	0.781	15.63	0.13	0.05	-
1.493	0.238	2.001	18.17	0.248	0.1101	-
1.911	0.305	4.002	23.27	0.302	0.172	-
2.233	0.356	5.027	27.18	0.278	0.185	232.3
2.779	0.443	6.003	33.84	0.215	0.1774	297.7
3.391	0.541	7.321	41.28	0.176	0.1773	373.5
4.018	0.641	8.297	48.92	0.142	0.1696	452.7
4.259	0.679	8.785	51.86	0.134	0.1694	483.3
4.05	0.646	8.346	49.31	0.14	0.1693	456.7
3.777	0.602	7.76	45.98	0.15	0.1688	421.6
3.262	0.52	6.833	39.72	0.177	0.172	357.0
2.651	0.423	5.71	32.27	0.224	0.1769	282.5
2.184	0.348	4.197	26.5	0.243	0.1578	-
1.766	0.282	2.44	21.5	0.215	0.1135	-
1.541	0.246	0.976	18.76	0.113	0.052	-

TABLE 46.

Uf = 9.85 h = 27.5 ρ = 1.11 w = 100

M	U	τ	γ	f	τ/γ	N_{RE}
0.495	0.162	2.568	18.34	0.706	0.14	-
0.672	0.22	3.275	24.89	0.488	0.1316	-
0.849	0.278	3.853	31.43	0.359	0.1226	-
1.235	0.405	5.008	45.72	0.22	0.1095	-
1.541	0.505	5.811	57.03	0.164	0.1019	407.5
2.007	0.658	7.705	74.3	0.128	0.1037	502.5
2.506	0.821	10.819	92.76	0.116	0.1166	598.8
3.198	1.047	13.548	118.36	0.089	0.1145	725.9
3.809	1.248	15.667	140.98	0.073	0.1111	834.3
4.243	1.39	18.942	157.05	0.071	0.1206	908.6
3.777	1.237	15.924	139.79	0.075	0.1139	828.4
3.166	1.037	13.484	117.16	0.09	0.1151	720.4
2.619	0.858	10.595	96.92	0.104	0.1093	620.0
2.088	0.684	7.673	77.28	0.118	0.0993	518.2
1.702	0.557	5.65	62.99	0.131	0.0897	440.4
1.412	0.463	4.43	52.27	0.149	0.0848	-
1.107	0.362	3.082	40.96	0.17	0.0752	-

TABLE 47.

Uf = 9.85 h = 40.0 ρ = 1.14 w = 100

M	U	τ	γ	f	τ/γ	N_{RE}
0.592	0.13	1.821	11.8	0.716	0.1458	-
0.721	0.158	2.459	14.36	0.692	0.1712	-
1.107	0.243	3.688	22.06	0.439	0.1672	-
1.75	0.384	5.123	34.89	0.244	0.1468	270.7
2.152	0.472	6.516	42.91	0.206	0.1519	339.9
2.972	0.652	8.032	59.26	0.133	0.1355	485.6
3.423	0.751	9.18	68.24	0.114	0.1345	567.6
4.066	0.892	10.53	81.07	0.093	0.1299	686.3
4.484	0.983	11.56	89.4	0.084	0.1293	764.0
4.002	0.878	10.245	74.78	0.093	0.1284	674.4
3.535	0.775	9.098	70.48	0.106	0.1291	587.6
3.037	0.666	7.704	60.54	0.122	0.1273	497.1
2.442	0.535	6.639	48.68	0.163	0.1364	390.3
1.959	0.43	5.245	39.06	0.199	0.1343	306.7
1.493	0.327	3.852	29.76	0.253	0.1294	-
1.139	0.25	2.705	22.7	0.304	0.1192	-

TABLE 48.

Uf = 9.85 h = 55.0 ρ = 1.162 w = 100

M	U	τ	γ	f	τ/γ	N_{RE}
1.203	0.188	0.995	14.37	0.194	0.0692	-
1.348	0.211	2.089	16.1	0.323	0.1298	-
1.637	0.256	3.233	19.56	0.34	0.1653	-
1.975	0.309	4.278	23.59	0.308	0.1813	-
2.619	0.41	5.92	31.28	0.242	0.1893	265.7
3.326	0.52	7.362	39.73	0.187	0.1853	347.1
3.954	0.57	8.556	43.55	0.181	0.1965	384.9
4.324	0.677	8.855	51.65	0.133	0.1714	467.1
3.954	0.619	8.556	47.23	0.154	0.1812	422.3
3.423	0.536	7.661	40.89	0.184	0.1874	359.2
3.101	0.485	6.915	37.04	0.202	0.1867	321.0
2.651	0.415	5.97	31.66	0.239	0.1886	269.3
2.12	0.332	4.378	25.32	0.273	0.1729	-
1.702	0.266	2.686	20.33	0.261	0.1321	-
1.348	0.211	0.846	16.1	0.131	0.0525	-

TABLE 49.

Uf = 9.0 h = 27.5 ρ = 1.125 w = 100

M	U	τ	γ	f	τ/γ	N_{RE}
0.335	0.108	2.99	12.22	1.826	0.2447	-
0.544	0.176	3.676	19.86	0.845	0.1851	-
0.672	0.217	4.099	24.56	0.519	0.1669	-
1.348	0.436	5.53	49.23	0.207	0.1123	324.2
1.702	0.55	7.13	62.15	0.168	0.1147	400.8
2.2	0.711	8.85	80.36	0.125	0.1101	506.5
3.005	0.971	12.75	109.74	0.096	0.1162	673.0
3.632	1.174	15.62	132.65	0.081	0.1178	800.2
4.066	1.314	17.57	148.51	0.072	0.1183	886.8
4.211	1.361	18.54	153.8	0.071	0.1205	915.7
3.873	1.252	16.53	141.46	0.075	0.1169	848.6
3.342	1.08	14.32	122.07	0.087	0.1173	741.6
2.779	0.898	11.39	101.51	0.1	0.1122	626.7
2.233	0.722	8.98	81.54	0.123	0.1101	513.6
1.75	0.566	6.7	63.92	0.149	0.1048	411.4
1.396	0.451	5.27	50.99	0.184	0.1034	334.4
1.171	0.378	3.9	42.77	0.194	0.0912	-

TABLE 50.

Uf = 9.0 h = 40.0 ρ = 1.148 w = 100

M	U	τ	γ	f	τ/γ	N_{RE}
1.171	0.255	2.97	23.18	0.319	0.1281	-
1.235	0.269	3.714	24.46	0.358	0.1518	-
1.541	0.336	5.117	30.51	0.316	0.1677	-
2.023	0.441	6.521	40.06	0.234	0.1628	-
2.603	0.567	7.429	51.52	0.161	0.1442	400.2
3.198	0.696	9.244	63.31	0.133	0.146	493.0
4.002	0.872	11.308	79.23	0.104	0.1427	620.0
4.34	0.945	12.257	85.92	0.096	0.1427	672.9
3.97	0.864	11.225	78.59	0.105	0.1428	614.2
3.535	0.77	9.905	69.99	0.117	0.1415	546.3
3.069	0.668	8.419	60.76	0.132	0.1386	472.8
2.619	0.57	7.387	51.84	0.159	0.1425	402.4
1.991	0.434	5.695	39.42	0.211	0.1445	305.0
1.67	0.364	4.375	33.05	0.23	0.1324	-
1.348	0.294	3.219	26.69	0.26	0.1206	-
1.155	0.252	1.898	22.86	0.209	0.083	-

TABLE 51.

Uf = 9.0 h = 55.0 ρ = 1.169 w = 100

M	U	τ	γ	f	τ/γ	N_{RE}
0.898	0.14	1.201	10.66	0.419	0.1127	-
1.364	0.212	3.053	16.19	0.465	0.1886	-
1.975	0.307	4.805	23.45	0.349	0.2049	183.7
2.329	0.362	5.606	27.65	0.293	0.2027	219.1
3.101	0.482	7.207	36.82	0.212	0.1957	297.9
3.519	0.547	8.208	41.78	0.188	0.1965	341.1
4.131	0.642	9.51	49.04	0.158	0.1939	405
4.42	0.687	9.86	52.48	0.143	0.1879	435.5
3.986	0.62	9.409	47.32	0.168	0.1988	390.1
3.471	0.54	8.208	41.21	0.193	0.1992	336.4
2.747	0.427	6.557	32.62	0.246	0.201	261.6
2.41	0.375	5.956	28.61	0.29	0.2082	227.6
1.911	0.297	4.555	22.69	0.353	0.2007	177.2
1.428	0.222	2.753	16.96	0.382	0.1623	-
1.155	0.18	1.201	13.71	0.254	0.0876	-

TABLE 52.

Uf = 8.1 h = 27.5 ρ = 1.15 w = 100

M	U	τ	γ	f	τ/γ	N_{RE}
0.367	0.116	2.594	13.1	1.342	0.198	47.9
0.576	0.182	3.592	20.57	0.755	0.1746	86.9
0.898	0.284	4.523	32.07	0.39	0.141	156.5
1.348	0.426	6.186	48.16	0.237	0.1284	267.5
1.798	0.569	7.783	64.25	0.167	0.1211	385.8
2.265	0.716	9.978	80.91	0.135	0.1233	473.0
3.166	1.001	15.133	113.09	0.105	0.1338	636.8
3.857	1.219	18.493	137.8	0.087	0.1342	758.4
4.324	1.367	20.821	154.46	0.078	0.1348	839.5
3.873	1.225	17.495	138.37	0.081	0.1264	761.7
3.455	1.092	15.499	123.43	0.09	0.1256	687.9
3.182	1.006	14.202	113.66	0.098	0.125	639.6
2.168	0.686	8.382	77.46	0.124	0.1082	513.9
1.895	0.599	6.652	67.69	0.129	0.0983	470.9
1.557	0.492	5.322	55.63	0.153	0.0957	415.0
1.316	0.416	4.39	47.01	0.177	0.0934	372.5
1.074	0.34	3.293	38.39	0.198	0.0858	327.2

TABLE 53.

Uf = 8.1 h = 40.0 ρ = 1.16 w = 100

M	U	τ	γ	f	τ/γ	N_{RE}
0.318	0.069	1.918	6.24	2.783	0.3074	-
0.528	0.114	2.669	10.34	1.418	0.2581	-
0.721	0.155	3.711	14.12	1.067	0.2628	-
1.428	0.308	5.087	27.99	0.37	0.1817	-
1.83	0.394	5.921	35.86	0.263	0.1651	242.4
2.345	0.505	7.464	45.95	0.202	0.1624	321.4
2.94	0.634	8.59	57.61	0.148	0.1491	416.1
3.423	0.738	10.091	67.06	0.128	0.1505	494.5
4.018	0.866	11.634	78.72	0.107	0.1478	593.0
4.275	0.921	12.927	83.77	0.105	0.1543	636.0
3.857	0.831	11.551	75.57	0.116	0.1529	565.9
3.198	0.689	9.424	62.65	0.137	0.1504	457.4
2.763	0.596	8.215	54.14	0.16	0.1517	387.9
2.313	0.498	7.339	45.32	0.204	0.1619	316.3
1.83	0.394	6.005	35.86	0.267	0.1675	242.4
1.348	0.29	4.42	26.41	0.363	0.1674	-
1.139	0.245	3.419	22.31	0.393	0.1532	-

TABLE 54.

Uf = 8.1 h = 55.0 ρ = 1.179 w = 100

M	U	τ	γ	f	τ/γ	N_{RE}
1.139	0.176	1.211	13.41	0.265	0.0903	-
1.251	0.193	2.321	14.73	0.423	0.1576	-
1.654	0.255	4.036	19.47	0.421	0.2073	-
1.847	0.285	4.843	21.74	0.405	0.2228	155.1
2.297	0.354	6.054	27.04	0.328	0.2239	198.9
3.117	0.481	7.769	36.7	0.228	0.2117	282.7
3.712	0.572	9.283	43.7	0.193	0.2124	344.9
4.115	0.634	9.535	48.44	0.161	0.1968	388.1
4.356	0.672	9.888	51.28	0.149	0.1928	414.9
3.954	0.61	9.586	46.54	0.175	0.206	371.3
3.439	0.53	8.577	40.48	0.207	0.2119	316.0
2.908	0.448	7.265	34.23	0.246	0.2122	260.6
2.57	0.396	6.458	30.25	0.28	0.2135	226.2
1.911	0.295	5.045	22.49	0.394	0.2243	161.4
1.461	0.225	3.077	17.19	0.413	0.179	-
1.155	0.178	1.715	13.6	0.368	0.1261	-

TABLES 55 - 60.

In tables 55 - 60 the following symbols are used:

Symbol	Quantity	Units
Uf	Fluidising velocity	cm/sec.
w	Channel width	mm.
$\dot{M}$	Solids mass flow rate	kg/sec.
h	Bed height	mm.
ρ	Bed density x 10^{-3}	kg/m^3.
$\dot{Q}/w$	Solids volumetric flow rate per unit width of channel x 10^{-2}	$mm^2/sec.$

TABLE 55.

Uf = 11.65 w = 100

M	h	ρ	$\dot{Q}/w$	M	h	ρ	$\dot{Q}/w$
	So = 50.0				So = 150.0		
0.222	16.36	1.011	21.96	0.302	11.24	0.989	30.54
0.512	21.08	1.031	49.66	0.544	13.64	1.0	54.4
0.721	24.2	1.046	68.93	0.688	15.08	1.005	68.46
1.187	32.68	1.081	109.81	1.251	18.44	1.02	122.65
1.605	38.92	1.108	144.86	1.75	22.28	1.038	168.59
1.991	46.84	1.131	176.04	2.104	25.16	1.05	200.38
2.763	56.52	1.14	242.37	2.747	30.44	1.072	256.25
2.522	53.64	1.139	221.42	3.359	33.72	1.086	309.3
2.233	49.48	1.138	196.22	2.828	30.6	1.073	263.56
1.814	42.68	1.12	161.96	1.879	22.68	1.04	180.67
1.396	35.48	1.092	127.84	1.316	18.76	1.021	128.89
1.107	29.64	1.07	103.46	1.01	15.32	1.007	100.3
0.688	21.32	1.033	66.6				
	So = 100.0						
0.302	15.88	1.01	29.9				
0.447	18.44	1.02	43.82				
1.155	22.76	1.04	111.06				
1.605	26.76	1.056	151.99				
2.168	32.2	1.08	200.74				
2.828	38.2	1.104	256.16				
3.359	41.8	1.119	300.18				
2.908	38.52	1.106	262.93				
2.474	33.8	1.086	227.81				
1.847	28.44	1.062	173.92				
1.316	22.44	1.039	126.66				
1.074	18.92	1.022	105.09				

TABLE 56.

Uf = 9.85 w = 100

M	h	ρ	Q/w	M	h	ρ	Q/w
	So = 50.0				So = 150.0		
0.399	19.0	1.079	36.98	0.286	12.44	1.056	27.08
0.479	22.68	1.09	43.94	0.512	14.6	1.064	48.12
0.592	26.2	1.1	53.82	0.785	16.28	1.07	73.36
0.914	33.16	1.119	81.68	1.332	20.68	1.082	123.11
1.686	42.36	1.14	147.89	1.766	24.12	1.093	161.57
2.12	49.8	1.155	183.55	2.265	28.04	1.104	205.16
2.876	60.84	1.168	246.23	3.085	34.04	1.12	275.45
2.458	54.36	1.162	211.53	1.911	24.6	1.095	174.52
1.782	42.6	1.141	156.18	0.978	17.0	1.071	91.32
0.93	27.88	1.103	84.32	0.721	14.6	1.064	67.76
	So = 100.0						
0.335	14.44	1.063	31.51				
0.608	18.12	1.075	56.56				
0.833	20.04	1.081	77.06				
1.026	22.28	1.089	94.21				
1.412	26.28	1.1	128.36				
1.959	31.64	1.114	175.85				
2.715	39.08	1.132	239.8				
1.814	29.24	1.108	163.72				
0.914	20.28	1.082	84.47				
0.656	16.84	1.071	61.25				

TABLE 57.

Uf = 9.0 w = 100

M	h	ρ	$\dot{Q}/w$	M	h	ρ	$\dot{Q}/w$
	So = 50.0				So = 150.0		
0.27	20.44	1.11	24.32	0.335	13.64	1.088	30.79
0.512	25.48	1.122	45.63	0.544	16.04	1.096	49.64
0.592	29.48	1.131	52.34	0.753	16.76	1.099	68.52
1.058	33.88	1.14	92.81	1.3	20.68	1.11	117.12
1.267	37.64	1.149	110.27	1.686	24.04	1.12	150.54
1.686	44.76	1.16	145.34	2.104	27.08	1.128	186.52
2.249	52.68	1.17	192.22	2.892	32.84	1.139	253.91
2.86	62.6	1.179	242.58	2.426	28.6	1.13	214.69
2.345	54.6	1.171	200.26	1.83	23.8	1.119	163.54
1.847	45.72	1.161	159.09	0.898	17.32	1.1	81.64
0.914	30.36	1.134	80.6	0.656	15.08	1.092	60.07
0.576	24.76	1.121	51.38				
	So = 100.0						
0.27	15.72	1.095	24.66				
0.399	18.12	1.102	36.21				
0.769	21.32	1.112	69.15				
1.123	24.92	1.121	100.18				
1.654	29.56	1.132	146.11				
2.168	34.36	1.141	190.01				
2.86	41.08	1.152	248.26				
2.41	36.2	1.145	210.48				
1.702	28.92	1.13	150.62				
0.914	22.28	1.115	81.97				
0.56	18.44	1.103	50.77				

TABLE 58.

Uf = 11.65 w = 150

M	h	ρ	$\dot{Q}/w$	M	h	ρ	$\dot{Q}/w$
	So = 50.0				So = 150.0		
0.495	22.04	1.035	31.89	0.174	10.44	0.983	11.8
0.608	24.04	1.045	38.79	0.318	11.88	0.991	21.39
0.881	27.32	1.06	55.41	0.672	14.28	1.002	44.71
1.316	31.64	1.078	81.39	0.849	15.4	1.006	56.26
1.573	32.84	1.082	96.92	1.235	16.6	1.012	81.36
2.12	37.16	1.1	128.49	1.654	18.12	1.02	108.11
2.747	41.8	1.118	163.81	2.072	20.04	1.027	134.5
3.214	44.84	1.128	189.95	2.876	23.56	1.042	184.0
3.648	47.4	1.135	214.27	3.503	25.48	1.051	222.2
				3.841	27.08	1.059	241.8
	So = 100.0						
0.351	15.4	1.006	23.26				
0.495	17.8	1.018	32.41				
0.914	20.4	1.03	59.16				
1.3	22.6	1.039	83.41				
1.766	23.9	1.044	112.77				
2.184	25.5	1.051	138.53				
3.021	29.2	1.066	188.93				
3.728	32.5	1.081	229.91				

TABLE 59.

Uf = 9.85 w = 150

M	h	ρ	$\dot{Q}/w$	M	h	ρ	$\dot{Q}/w$
	So = 50.0				So = 150.0		
0.335	20.2	1.081	20.66	0.335	12.68	1.058	21.11
0.624	24.36	1.094	38.03	0.56	14.52	1.063	35.12
0.801	26.28	1.1	48.55	0.721	15.88	1.069	44.97
1.284	31.32	1.112	76.98	1.171	17.8	1.073	72.75
1.814	35.88	1.126	107.4	1.541	19.24	1.08	95.13
2.297	39.96	1.135	134.92	2.168	21.08	1.085	133.21
3.021	45.48	1.148	175.43	2.956	24.68	1.095	179.97
3.809	51.88	1.16	218.91	3.648	27.64	1.103	220.49
	So = 100.0						
0.302	15.0	1.065	18.91				
0.56	18.04	1.074	34.76				
0.785	20.12	1.081	48.41				
1.332	24.04	1.091	81.39				
1.782	26.28	1.1	108.0				
2.297	27.32	1.102	138.96				
2.828	29.48	1.109	170.0				
3.519	32.76	1.118	209.84				

TABLE 60.

Uf = 9.0 w = 150

M	h	ρ	$\dot{Q}/w$	M	h	ρ	$\dot{Q}/w$
	So = 50.0				So = 150.0		
0.254	20.04	1.11	15.25	0.351	12.6	1.083	21.61
0.463	24.52	1.121	27.53	0.56	14.68	1.091	34.22
0.785	28.52	1.13	46.31	0.849	16.28	1.096	51.64
1.155	32.36	1.139	67.6	1.267	17.64	1.101	76.72
1.718	37.4	1.148	99.77	1.895	19.88	1.11	113.81
2.49	43.24	1.157	143.47	2.828	23.8	1.12	168.33
3.552	53.08	1.17	202.39	3.761	28.12	1.129	222.09
	So = 100.0						
0.463	16.92	1.1	28.06				
0.737	20.6	1.109	44.31				
1.251	23.48	1.119	74.53				
1.847	26.28	1.125	109.45				
2.635	28.44	1.129	155.6				
3.552	33.0	1.14	207.72				